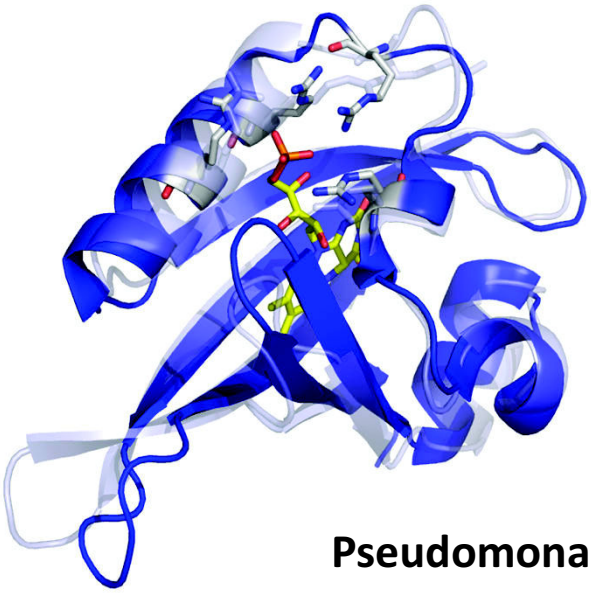

Pseudomonadaceae “short” LOV proteins – structure, function and physiological role

Katrin Jentzsch

Pseudomonadaceae “short” LOV proteins - structure, function and physiological role

Inaugural-Dissertation

zur Erlangung des Doktorgrades
der Mathematisch-Naturwissenschaftlichen Fakultät

der Heinrich-Heine-Universität Düsseldorf

vorgelegt von

Katrin Jentzsch

aus Oberhausen

Düsseldorf, Dezember 2012

Unsere Sache ist es,

den Funken des Lichts festzuhalten,

der aus dem Leben überall da hervorbricht,

wo die Ewigkeit die Zeit berührt.

Johann Christoph Friedrich von Schiller (1759 - 1805)

I Summary

Light, oxygen, voltage (LOV) domains were firstly identified in 1998 by Briggs and co-workers as the blue-light sensitive flavin-binding signaling modules of plant phototropins (phots). Phots control plant photomovement responses and other blue-light dependent phenomena such as chloroplast relocation as well as leaf and stomata opening. More recently, homologous photoreceptor proteins were discovered in a variety of phototrophic and chemotrophic prokaryotes. The LOV domain sensory function hereby strictly depends on the blue-light initiated formation of a covalent bond between the 4a carbon atom of the flavin isoalloxazine ring and a closely positioned conserved cysteine residue in the LOV domain. In the dark this bond is broken within seconds to hours, depending on the LOV protein. In the presented thesis i) two paralogous LOV proteins from *Pseudomonas putida* KT2440 were studied. Both proteins lack a fused effector domain and show drastically different dark recovery kinetics. The presented mutational study suggests a mechanism for the dark recovery process involving stabilization/destabilization of the signaling (adduct) state of the respective protein via distal amino acid residues surrounding the FMN-phosphate. ii) Microsecond transient absorption measurements, homology modeling, as well as the recently published light-state structure of PpSB1-LOV further corroborate this hypothesis. The overall structural arrangement of PpSB1-LOV, together with a complementary phylogenetic analysis, highlights a common ancestry of bacterial LOV photoreceptors and Per-ARNT-Sim (PAS) chemosensors. iii) Additionally, five selected proteins of the *Pseudomonadaceae* "short"-LOV protein family were cloned, expressed, purified and characterized with respect to their photochemistry and dark recovery. The presented data reveal the j of fast and slow-reverting "short" LOV proteins, which points toward conserved blue-light dependent physiological functions in the respective organisms. iv) In light of those findings a physiological study was conducted using *P. putida* KT2440 and a mutant strain in which the PpSB1-LOV encoding gene was disrupted. The presented data hints at the involvement of the PpSB1-LOV photoreceptor in a set of iron-starvation dependent physiological responses, such as growth, motility and production of the iron-scavenger pyoverdin. In conclusion, the in this thesis presented data shed new light on the structure, function and physiological role of a highly conserved family of proteobacterial LOV photoreceptors and thus broadens our understanding of the LOV signaling paradigm.

II Zusammenfassung

Light, Oxygen, Voltage (LOV)-Domänen wurden erstmals 1998 von Briggs und Mitarbeitern als die Blaulicht-sensitiven Flavin-bindenden Signalmodule pflanzlicher Phototropine identifiziert. Als solche kontrollieren sie alle lichtabhängigen Bewegungsreaktionen von Pflanzen (Phototropismus) sowie andere Blaulicht-abhängige Phänomene, wie die Chloroplastenbewegung oder das Öffnen der Spaltöffnungen der Blätter. Erst Jahre später wurden homologe Photorezeptorproteine auch in vielen phototrophen und chemotrophen Prokaryoten entdeckt. Mechanistisch beruht die Sensorfunktion der LOV-Domäne auf der Blaulicht-getriebenen Ausbildung einer kovalenten Bindung zwischen dem 4a-Kohlenstoffatom des Flavin-Isoalloxazinrings und einem konservierten Cystein-Rest in der LOV-Domäne. Im Dunkeln wird diese Bindung thermisch gebrochen. Dieser Vorgang kann, abhängig vom LOV-Protein, zwischen Sekunden bis hin zu mehreren Stunden dauern. In der vorliegenden Arbeit wurden i) zwei sich sehr ähnliche LOV-Proteine aus *Pseudomonas putida* KT2440, welche beide über keine angeschlossene Effektordomäne verfügen, untersucht. Beide Proteine zeigen zudem drastisch unterschiedliche Dunkelrückkehrkinetiken. Eine im Rahmen dieser Arbeit durchgeführte Mutagenesestudie legt nahe, dass im Signalzustand des jeweiligen LOV-Proteins stabilisierende/destabilisierende Wechselwirkungen zwischen der Phosphatgruppe des Flavinmononukleotid-Chromophors und geladenen Aminosäureresten des Proteins ausgebildet werden, welche die Dunkelrückkehr maßgeblich beeinflussen. Diese Hypothese wird des Weiteren durch ii) transiente absorptionsspektroskopische Untersuchungen sowie durch die kürzlich veröffentliche Kristallstruktur des Lichtzustandes von PpSB1-LOV unterstützt. Die Struktur von PpSB1-LOV, zusammen mit einer ergänzenden phylogenetischen Studie, unterstreicht zudem eine gemeinsame Herkunft von bakteriellen LOV-Photorezeptoren und Per-ARNT-Sim (PAS) Chemorezeptoren. iii) Außerdem wurden fünf weitere ausgewählte Proteine der *Pseudomonadaceae* „short“-LOV Proteinfamilie kloniert, gereinigt und bezüglich ihrer Photochemie und Dunkelrückkehr charakterisiert. Diese Untersuchungen deuten auf eine Konservierung unterschiedlicher Dunkelrückkehrkinetiken in verschiedenen Pseudomonaden hin. iv) Zudem legen die in dieser Arbeit vorgestellten Untersuchungen eine Beteiligung des PpSB1-LOV Photorezeptors an einer Reihe durch Eisen-Limitierung hervorgerufener physiologischer Antworten wie Wachstum, Beweglichkeit und Produktion des Eisenchelators Pyoverdin nahe. Zusammenfassend werfen die in dieser Arbeit vorgestellten und diskutierten Daten und Ergebnisse ein neues/erweitertes Licht auf den Zusammenhang von Struktur, Funktion und physiologischer Rolle einer hochkonservierten Familie von proteobakteriellen LOV-Photorezeptoren.

List of publications and poster presentations

a) Peer-reviewed publications (accepted and submitted)

1. **Jentzsch, K.**, Wirtz, A., Circolone, F., Drepper, T., Losi, A., Gärtner, W., Jaeger,K.E., Krauss, U. *Mutual exchange of kinetic properties by extended mutagenesis in two short LOV domain proteins from Pseudomonas putida.* Biochemistry, 2009. **48**: 10321-10333.

2. Circolone, F.,Granzin, J.,**Jentzsch, K**., Drepper, T. ,Jaeger, K. E. Willbold, D., Krauss, U., Batra-Safferling, R. *Structural basis for the slow dark recovery of a full-length LOV protein from Pseudomonas putida.* J Mol Biol, 2012. **417**: 362-374.

3. Rani, R., **Jentzsch, K**., Lecher, J., Hartmann, R., Willbold, D., Jaeger, K.E., Krauss, U. *Conservation of dark recovery kinetic parameters and structural features in the Pseudomonadaceae "short" LOV protein family – implications for the design of LOV-based optogenetic tools.* (to be submitted).

b) Additional manuscripts (in preparation)

Jentzsch K., Kutta J.R., Dick B., Jaeger K.E., Krauss U. *A transient absorption study of the adduct formation kinetics of the twin Pseudomonas putida LOV proteins and selected variants.*

Jentzsch K., Jaeger K.E., Krauss U. *Involvement of the "short" LOV protein PpSB1-LOV in the iron-starvation/motility response of Pseudomonas putida KT2440.*

c) Poster at international scientific conferences

1. **Katrin Jentzsch***, Wolfgang Gärtner, Karl-Erich Jaeger and Ulrich Krauss. *Light Oxygen Voltage (LOV) photoreceptor proteins of Pseudomonas putida – Two Uneven Twins* Jahrestreffen der DFG- Forschergruppe 526 „Blaulicht-sensitive Photorezeptoren", 2009, Staufen im Breisgau, Germany

2. **Katrin Jentzsch*** ,Astrid Wirtz, Franco Circolone, Thomas Drepper, Aba Losi, Wolfgang Gärtner, Karl-Erich Jaeger and Ulrich Krauss. *The twin LOV-proteins of Pseudomonas putida – photochemistry and beyond.* Gordon Research Conference and Seminar on Photosensory Reporters 2010, Il Chiocco, Italien

3. Franco Circolone, Joachim Granzin, **Katrin Jentzsch**, Thomas Drepper, Karl-Erich Jaeger, Dieter Willbold, Renu Batra-Safferling and Ulrich Krauss*. *Structural basis for the slow dark recovery of a full-length LOV protein from Pseudomonas putida.* Gordon Research Conference on Photosensory Receptors and Signal-Transduction, 2012, Galveston, Texas, USA

4. Raj Rani*, Rudolf Hartmann, **Katrin Jentzsch**, Justin Lecher, Dieter Willbold, Karl-Erich Jaeger and Ulrich Krauss. *Conservation of coiled-coil structural motifs in the "short" LOV protein family*. Gordon Research Conference on Photosensory Receptors and Signal-Transduction, 2012, Galveston, Texas, USA

   *presenting author

Table of contents

Abbreviations

In the following, the non-standard abbreviations that were repeatedly used within this thesis are summarized. Excluded from this list are standard English-language abbreviations and SI units. Amino acids were abbreviated using the common one- or three-letter codes.

aa	Amino acid
ADO	ADAGIO
AsLOV2	*Avena sativa* LOV2 domain
ATP	Adenosine 5'-triphosphate
BLUF	Sensor of Blue-light Using FAD Domain
CD	Circular Dichroism
CRY	Chryptochrome
Cry-DASH	*Drosophila, Arabidopsis, Synechocystis* and *Homo* cryptochromes
C-terminal	Carboxy-terminal
DNA	Deoxyribunucleic acid
dNTP	Desoxyribonukleosidtriphosphate
EAL	phosphodiesterase
FAD	Flavin Adenine Dinucleotide (Riboflavin 5'-adenosine diphosphate
FKF1	Flavin-Binding Kelch Repeat F-Box Protein
FMN	Flavin Mononucleotide (Riboflavin 5'-monophosphate)
GAF	cyclic GMP-specific phosphodiesterases, adenylyl cyclases
GGDEF	diguanylate cyclase
HK	Histidine Kinase Domain
HPLC	High Performance Liquid Chromatography
HTH	Helix-Turn-Helix DNA binding domain
IMAC	Immobilized Metal Affinity Chromatography
IPTG	Isopropyl-β-D-thiogalactopyranosid
LOV	Light, Oxygen, Voltage domain
LOV390	LOV signaling state
LOV447	LOV dark state
LOV660	LOV excited triplete state
LOV-HK	LOV-Histidine Kinase
LOV-HK-RR	Hybrid LOV-Histidine Kinase Response Regulator
LKP2 LOV	Kelch Protein2
N-cap	Amino-terminal cap
NMR	Nuclear Magnetic Resonance
NTA	Nitriloacetic acid
N-terminal	Amino-terminal
PCR	Polymerase Chain Reaction

PAS	Per, Arnt, Sim domain
Phot	Phototropin
PVD	Pyoverdine
PYP	Photoactive Yellow Protein
RF	Riboflavin
ROS	Reactive Oxygen Species
RR	Responsive Regulator
SDS	Sodium Dodecyl Sulfate
STAS	Sulfate Transporter Anti-Sigma factor antagonist domain
TR	Transcriptional regulator
UV	Ultra-Violet
Vis	Visible (light fraction)
WC-1	White-Collar-1
ZTL	Zeitlupe

1. Introduction

1.1 The conserved photosensing paradigm-classification distribution and physiological role

1.1.1 A historical perspective on the properties of light

The earliest civilizations on our planet knew about the light's inherent powers, worshipped the sun itself as god and feared the darkness as evil (*1*). In Christianity; light was the first of Gods creations; as he/she separated the light from the darkness (*2*).

Far into modern age, the nature of light remained largely elusive. Different believes and opinions dominated the ancient scholarly world. Initially, in the fifth century BC scholars believed that brightness fills a room without delay in time and that "beams" emanate from the eyes, scanning the environment during the actual procedure of seeing (*3*). This believe, in modified forms, was widespread in ancient greek and roman times (*3, 4*).

It was Titus Lucretius Carus, a Roman poet and philosopher in 55 BC, who carried on the ideas of earlier Greek atomists, that wrote:

"*The light & heat of the sun; these are composed of minute atoms which, when they are shoved off, lose no time in shooting right across the interspace of air in the direction imparted by the shove.*" *– On the nature of the Universe (5)*

Although being similar to later modern particle theories, Lucretius's views were not generally accepted back then.

Famous Galileo Galilei (1564–1642) was one of the first trying to measure the propagation speed of light, however without much success since the instruments he used were far too crude (*6*). Supposedly the first scientist who obtained a valid estimate, although with a deviation of 30 %, was Ole Rømer who used observation-data from the moons of Jupiter in 1676-78 (*7*) to estimate the speed of light. The true nature of light though remained unknown. Sir Isaac Newton (1643-1727) used his emission theory to test and explain the propagation of light through movement of small particles. His attempts enabled the explanation of the phenomenon of reflection, but could not account for other phenomena such as diffraction, which could only be explained by

describing light as a wave (*8*). Christiaan Huygens (1629–1695) and others thus founded the wave-theory of light, which became more and more established through the experiments of Thomas Young (1773–1829) (*9*). James Clerk Maxwell (1831–1879) was the first to postulate that light itself is an electromagnetic wave (*10*).

Thus, in the late 19th century, the wave theory of light dominated the scientific world and all questions regarding the nature of light seemed to be answered. Based on the observations of Phillip von Lenard describing the photoelectric effect a radically new understanding emerged, when Max Planck (1858–1947) and Albert Einstein (1879–1955) introduced their quantum hypothesis (*11, 12*). This theory represents the foundation of our current understanding of the inherent properties of light. Freely translated, Albert Einstein stated the following in his seminal paper about the properties of light.

[Light consists of] … "*a limited number of spatially localized energy quanta, which move without being divided and can only be absorbed and emitted as a whole*."

Today the dual nature of light which stems from the observation that in certain experiments light can neither be strictly described as a wave, nor as a particle, is widely accepted (*13, 14*). Given this early fascination for the phenomenon light and later on its interplay with (biological) matter, it is not surprising that we know today a great deal about (biological) systems that allow a wide range of organisms to respond to light stimuli over the whole visible spectral range.

1.1.2 The importance of (blue)-light

Prior to providing a more detailed overview over the different photoreceptor families in general as well as blue-light photoreceptors in particular, it seems necessary to mention the significance of the blue range of the visible-light spectrum. Light of short wavelengths (UVA/blue light: 320 nm – 500 nm) can trigger a variety of responses in living organisms (*15-18*)(and references therein). Of all wavelengths blue light most deeply penetrates the water column (*19*) e.g. in marine microbial habitats, providing an obvious environmental stimulus to most organisms dwelling there. Thus for most photosynthetic organisms, which directly use light as energy

source, such as plants, alga and phototrophic microbes, blue light represents an important stimulus for optimization of their photosynthesis yield (*20*).

Likewise, radiation with such an inherent energy as blue light (430 – 500 nm, energy content approximately 239 to 280 kJ/mol) does not only pose beneficial effects on organisms. Blue light is e.g. absorbed by porphyrins, which are produced by bacteria and plants for the synthesis of heme- or chlorophyll precursors (*21, 22*). Excited porphyrins, however, are photo-converted with a high yield to the corresponding excited triplet state, which in the presence of oxygen can result in the generation of singlet oxygen (and other reactive oxygen species (ROS)) (*23*). Singlet oxygen is extremely harmful due to its high reactivity. Severe DNA-damage and damage to a wide range of tissues e.g. lipids and proteins that lead to lethal lesions and eventually to cell death are known (*23, 24*).

Thus, it is not surprising that a plethora of photoreceptors responding to wavelengths of the visible (380nm-780nm) (Figure 1); and in particular the blue spectral range (430 nm - 500 nm), are ubiquitously distributed in most living beings (Figure 2 and 3).

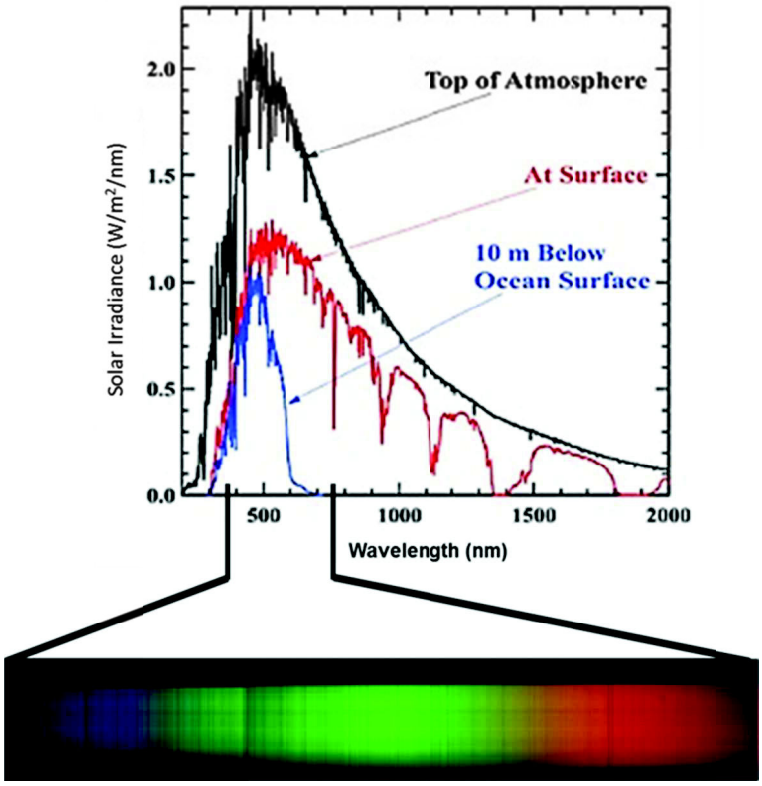

Fig. 1: Solar radiation and absorption spectrum of light. At the top of the atmosphere, approximately 7 % of the radiation is in the ultraviolet, 41 % in the visible, and 52 % in the infrared spectral range. The intensity of electromagnetic radiation that reaches the surface of our planet is considerably less than that at the top of the

atmosphere. The highest energy light is most effectively filtered out. This is very important because high energy light (gamma rays, x-rays, UV-radiation) penetrates the cells of living beings, causing damage. The lower panel depicts the visible portion of sunlight from blue to red (approx. 380nm-780nm). Adapted from Department of Chemistry, Prof. Patricia Shapley, University of Illinois and Astronomy Department, Boston University.

1.1.3 The classification and distribution of photoreceptors in the three kingdoms of life

The capability to react upon any signal (e.g. light) of course needs a precondition: organisms must have the ability to perceive it. In other words, they need to possess certain kinds of light-absorbing biomacromolecules. Those so-called photoreceptors are integrated protein-ligand complexes designed to sense and relay the biological signal to initiate a biological response in order to provide the organism with the means to adapt to changing light conditions. Those photoreceptors enable the organisms not only to pick up the direction of the light source but also enables them to integrate its spectral properties, intensities and duration. At the molecular level, the ability of photoreceptor proteins to sense or absorb visible light, is usually directly linked to a small protein-bound ligand called the chromophore. Derived from the Greek word *chromos*, meaning color, this chromophore, as the light absorbing moiety gives the photoreceptor protein its color and at the same time enables protein photosensitivity.

Over various evolutionary steps, nature has invented several different kinds of photoreceptors to facilitate the adaption to changing light conditions in different habitats or niches. Since the visible fraction of the spectrum (ca. 380 – 780 nm) is the one with the strongest influence on earth, most so far identified and described photoreceptor proteins allow responses to very discrete wavelengths of the visible light fraction. So far, only one photoreceptor has been identified to respond to wavelengths outside the visible spectrum, in the UV-B range. The plant photoreceptor UVR8 (UV-B resistance locus 8) was recently structurally characterized (*25, 26*). The findings of those studies will be described in more detail below.

1.1.4 The eight known photoreceptor families with distinct photochemistry

To current knowledge, eight sensory photoreceptor families, each possessing a distinct photochemistry, are identified in the three kingdoms of life (Figure 2). These are: phytochromes (Phy) (*27*), and xanthopsins (*28*), rhodopsins (*29*), cyanobacterial orange carotenoid proteins (OCP) (*30*), plant UV photoreceptors such as UVR8, as well as the blue-light responsive

cryptochromes (*31*), BLUFs (sensor of Blue-Light using FAD) (*32, 33*), and light, oxygen, voltage (LOV) domain containing photoreceptors (*34*) (Figure 2 and 3).

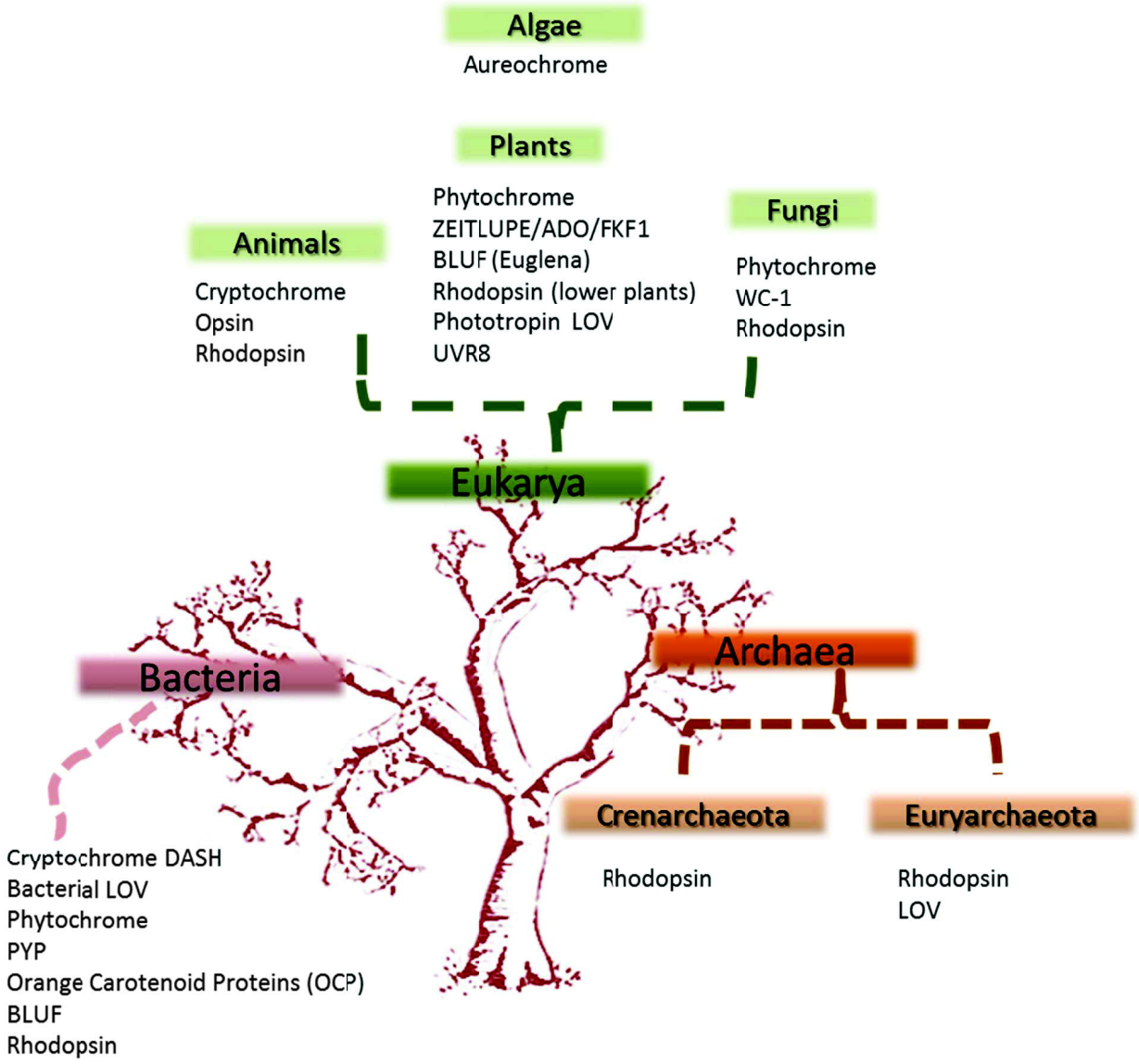

Fig. 2: Distribution of photoreceptor proteins in the three kingdoms of life. Photoreceptor proteins of most families are ubiquitiously distributed throughout all three kingdoms of life. The LOV-domain containing photoreceptor proteins can be found in Bacteria, Archaea and Eukaryotes (except animals). Equally dispersed are cryptochromes, phytochromes and rhodopsins. Abbreviations: LOV: light, oxygen, voltage domain family of photoreceptors including plant phots and ZEITLUPE/ADAGIO(ADO)/Flavin Binding Kelch Repeat F-Box proteins (FKF1), BLUF: Sensor of blue-light using FAD domain, PYP: photoactive yellow protein, Cryptochrome DASH: cryptochrome family, in relation with cryptochromes found in *Drosophila, Arabidopsis, Synechocystis* and *Homo*, OCP: orange carotenoid protein, UVR8: UV-B resistance locus 8

Figure 3 provides a schematic overview over the detected wavelength-range of all so far described photoreceptors systems.

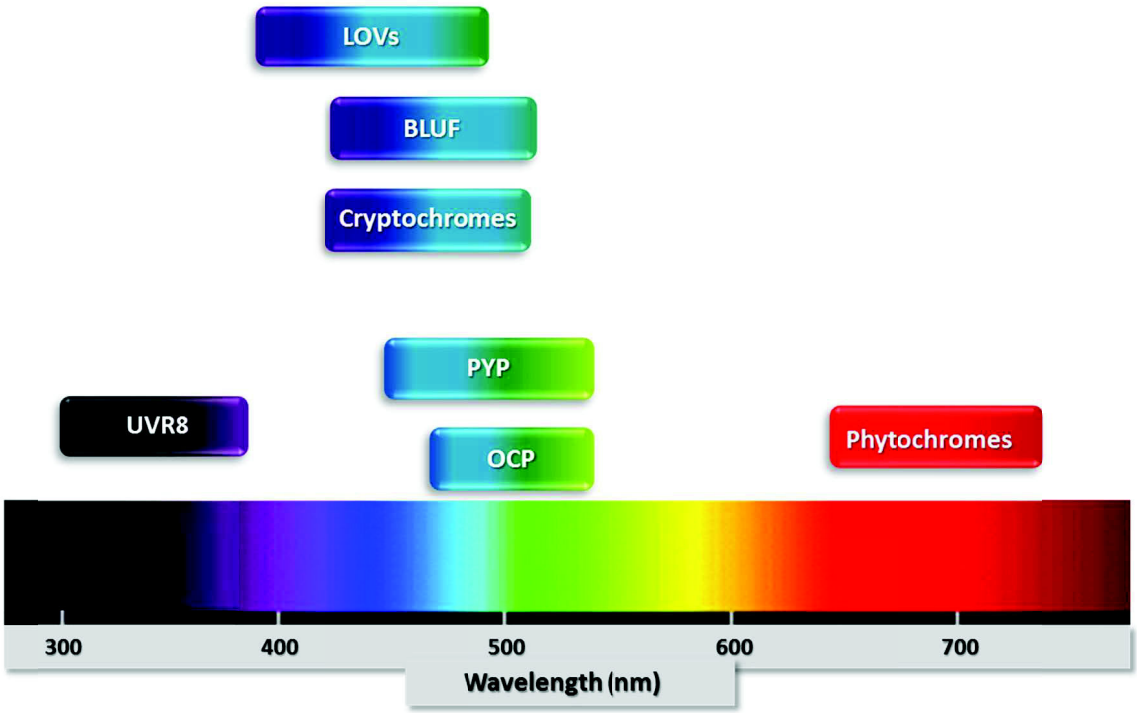

Fig. 3: Spectral range detected by the so far known photoreceptor systems. Abbreviations as in Fig. 2:LOV: light, oxygen, voltage domain family of photoreceptors including plant phots and ZEITLUPE/ADAGIO(ADO)/Flavin Binding Kelch Repeat F-Box proteins (FKF1), BLUF: Sensor of blue-light using FAD domain, PYP: photoactive yellow protein, Cryptochrome DASH: cryptochrome family, in relation with cryptochromes found in *Drosophila, Arabidopsis, Synechocystis* and *Homo*,OCP: Orange Carotenoid Protein, UVR8: UV-B resistance locus 8

1.1.4.1 Plant, cyanobacterial and proteobacterial phytochromes

The effect of red and far-red light sensing tetrapyrrole ligand-binding phytochromes on plant growth and flowering were first observed by Sterling Hendricks and Harry Borthwick at the USDA-ARS Beltsville Agricultural Research Center in Maryland during a period from the late

1940s to the early 1960s (*35*). They used a spectrograph built from borrowed and war-surplus parts and subsequently observed that red light was very effective in promoting germination or triggering flowering responses (*35*). Furthermore, they saw that the observed red light responses were reversible by far-red light, which for them indicated the presence of a photoreversible pigment (*35*). In 1959, Butler and Siegelman firstly identified the pigment using a spectrophotometer. Butler also proposed the name phytochrome for the red light/far-red light photoreversible pigment (*36*). Their structural properties and biochemistry have been thoroughly studied in the past two to three decades (e.g. (*37-41*)). Phytochromes are involved in plant cellular responses and tropisms such as chloroplast movement, cytoplasmic motility, endoreduplication and nyctinastic movement of leaves, as well as other tropic responses such as gravitropism, polarotropism and phototropism (*41*). Phytochromes can be (photo)converted between a red- and far-red-light absorbing form, out of which, the far-red absorbing form was suggested to be the active species (*37*). They contain linear tetrapyrrols such as bilins as chromophore, which undergo a light-dependent reversible *cis/trans* isomerization around one double bond in the chromophore, which in turn triggers the physiological response (*42*). From the first discovery it took almost half of a century, until first hints emerged that phytochromes are not only present in plants, but also in prokaryotes. In 1996 in the genome of the cyanobacterium *Synechocystis* a gene was found, which seemed to be a homologue of the plant phytochrome. In 1997 it was described as the first prokaryotic phytochrome (*43*). Successively more phytochromes have been found in other prokaryotic organisms e.g., *Agrobacterium tumefaciens,* a gram-negative, plant pathogenic soil bacterium (*44*) or *Deinococcus radiodurans*, an extremophile bacterium highly resistant against ionizing radiation (*45*). Apart from cyanobacteria, were phytochromes mediate complementary chromatic adaptation responses (*43, 46*), little is known about the physiological role of prokaryotic phytochromes (*47*).

1.1.4.2 Photoactive yellow protein (PYP) and the xanthopsin photoreceptor family

In the late 1960's and 70's, *Halorhodospira halophila*, formerly called *Ectothiorhodospira halophila* was firstly isolated from extremely saline lakes in the USA and Egypt (*48, 49*). *H. halophila* is a unicellular phototrophic purple sulfur bacterium that deposits sulfur extracellularly. It was not until 1985, when T.E. Meyer first reported the isolation of a series of

colored proteins from the halophilic bacterium (*50*). Later, in 1986 one of these proteins was baptized photoactive yellow protein (PYP), due to its color and photoreactivity (*51*). Today, PYP represents the archetype within the Xanthopsin family (*28*). After the first discoveries, southern hybridizations and PCR experiments led to the discovery of more PYPs in six other purple bacterial species (*28*). Xanthopsins covalently bind *trans p*-coumaric acid as isomerizable chromophore. They seem to be much less widespread than other photoreceptor proteins. Although being photochemically and structurally well characterized (*52*), no conclusive biological role could be assigned to those photoreceptor modules to date, although it was proposed, that *H. halophila* PYP regulates negative phototaxis, i.e. the movement away from blue light, and harmful UV light (*53*).

1.1.4.3 Microbial rhodopsins

Another family of photoreceptors present in microorganisms are the rhodopsins (*29*). Pristine (bacterial) rhodopsins, initially isolated from Haloarchaeal lineages, typically bind an isomerisable retinal chromophore (*54-56*). Microorganisms containing rhodopsin genes inhabit the most miscellaneous environments including salt flats, soil, fresh water, surface and deep sea water, glacial sea habitats, and human and plant tissues as fungal pathogens (*57*). Subsequently, starting in 1999, previously unknown archaeal rhodopsin homologues were identified in several organisms from the kingdoms of Eukarya and Bacteria. Rhodopsins are present in an incredibly vast phylogenetic range, including haloarchaea, proteobacteria *(52, 58)*, cyanobacteria (*59*), fungi *(60)*, dinoflagellates, and green algae (*61*). Interestingly, up to now, no rhodopsin homolog could be identified in higher plants. Proton/ion pump related functions (*62*), and phototaxis in positive or negative fashion (*63, 64*) are the most common phenomena associated to bacterial rhodopsins to date.

1.1.4.4 Cyanobacterial orange carotenoid proteins

Only very recently, Wilson and co-workers identified a novel family of photoreceptors which they termed orange photoactive carotenoid proteins (OCP) (*65*). They could demonstrate that the

OCP of *Synechocystis* PCC 6803 (*22*) is a member of a larger, uniquely cyanobacterial, family of photoactive proteins, binding a carotenoid (3′-hydroxyechinenone (hECN)) as chromophore. In plants, carotenoids play an essential role in photoprotection within the chlorophyll-membrane antenna of photosystem II by participating in the conversion of potentially harmful excess light energy into heat (*66*). In contrast, the photoprotective mechanism in cyanobacteria remained widely elusive (*65*) until the discovery of OCP. According to Wilson and co-workers (*65*), blue-green light initiates the photocycle of OCP, in which a reversible conversion from its dark stable orange form to a red "active" form occurs. Hereby formation of the red form is essential for OCPs photoprotective mechanism. The detailed photophysics of the OCP photocycle were revealed in 2012 (*30*), but will not be discussed in detail here.

1.1.4.5 Plant UVR8 – the first genuine photoreceptor without a ligand chromophore

All above described photoreceptors contain small molecule ligands as light-absorbing chromophores. A remarkable exception is the above briefly mentioned *A. thaliana* protein UVR8, which is a UV-B sensing (280 nm - 315 nm) photoreceptor (*67*). It was originally identified as a regulatory protein involved in UV-B dependent plant responses (*68*) and was only very recently shown to be a true photoreceptor for UV-B (*67*). The recently published structure revealed, that the protein has a β-propeller fold and is dimeric in the absence of UV-B light, upon UV-B irradiation it undergoes an immediate switch from its homodimeric form to a monomer, triggering a signaling pathway for ultraviolet protection in *A. thaliana* (*25, 26*). Although it remains unclear, how exactly UV-B perception triggers dissociation of the UVR8 homodimer, there are some informations, that could be gathered in the recent past. A set of arginine residues that stabilize the homodimeric interface make intramolecular interactions with surrounding tryptophan residues, two of which collectively serve as the UV-B chromophore (*26*). Furthermore, UVR8 shares sequence homology with mammalian proteins involved in regulating chromatin condensation, for example the human RCC1 gene product, and has been shown to localize to the nucleus when the plant is exposed to UV-B light and subsequently interacts with chromatin (*69*).

1.1.4.6 Flavin-binding blue-light photoreceptors

In the past two decades, several blue-light photoreceptor families, that all rely on the blue-light sensitivity of different flavin-type chromophores bound within the respective proteins, were described. Among plants, algae and fungi eight main classes can be distinguished: the cryptochromes (*31*), the BLUF-domain containing proteins (*32*), phototropins (phots) (*70*), neochromes (*71*), aureochromes (*72*), proteins of the ZTL/ADO/FKF1 family ((*73*) and citations therein) as well as the fungal VVD (*74*) and white-collar1 proteins (*75*). Hereby, the latter six families rely on LOV-sensor domains for signal perception.

1.1.4.7 Cryptochromes

Cryptochromes (*31*) operating in the UV-A and blue-light spectral region, regulate similar processes as the previously mentioned red/far-red light responsive phytochromes. Cryptochromes usually bind flavin adenine dinucleotide (FAD) and 5,10-methenyl-tetrahydrofolyl-polyglutamate (MTHF) as chromophores, while the latter one probably acts as an antenna pigment for the FAD chromophore. Regulated processes include phototropism, light-induced stomatal opening, and chloroplast movement in response to changes in light intensity (*76-81*). Furthermore, cryptochromes are found in higher eukaryotes, including mammals, (*Homo sapiens*), insects (*Drosophila*), plants (*Arabidopsis*) and algae (*Chlamydomonas*) (*31, 82*). Classically, plant or animal cryptochromes are characterized by their high sequence similarity to DNA photolyases, interestingly, though, they lack intrinsic DNA-photolyase activity (*79, 83, 84*). Recently, a new family of cryptochromes, referred to as CRY-DASH, was discovered in several photosynthetic and non-photosynthetic prokaryotes (*85-87*). The name was given to highlight the relationship with the cryptochromes found in *Drosophila, Arabidopsis*, *Synechocystis* and *Homo (88)*. Based on recent experimental evidence, demonstrating that members of this cryptochrome family possess DNA-photolyase activity towards cyclobutane pyrimidine dimers in single stranded DNA, the placement of Cry-DASH proteins in the cryptochrome blue-light photoreceptor family has been challenged (*89*).

1.1.4.8 BLUFs – unique photochemistry and much debate

A younger family of photoreceptor proteins is called the BLUF family (Blue Light Sensing Using FAD) (*32*). In anoxygenic phototrophic bacteria such as *Rhodobacter sphaeroides* BLUF proteins control the blue-light dependent expression of photosynthesis genes (*90*). In the unicellular alga *Euglena gracilis* a BLUF domain containing adenylyl cyclase (PAC) apparently controls the blue-light dependent photoavoidance response (*91*). While the primary photochemical processes occurring in the BLUF domain flavin chromophore after blue-light excitation have been studied in great detail using ultra-fast spectroscopic methods, the structural consequences of photoactivation are still a matter of controversial debate (*33, 92-96*).

1.1.4.9 LOV photoreceptors - the most versatile blue-light photoreceptor family known to date

The phototropins (phot1 and phot2) are flavoprotein LOV domain containing photoreceptors that mediate a large number of photo-responses in *A. thaliana*, as well as in other plants. (Figure 4). Plant phototropins are membrane associated serine/threonine kinases that contain two light sensing LOV domains (LOV1 and LOV2) N-terminally attached to the Ser/Thr kinase domain (*97*). The most prominent effect mediated by plant phototropins is the bending of the growing plant hypocotyls towards a unidirectal source of blue light (*34, 38*). Further, plant blue-light responses include amongst others: chloroplast photoaccumulation/photoavoidance (*38, 98*) stomatal opening at dawn when the blue-light portion is enriched in sunlight (*99*); floral induction (*100*) as well as cotyledon/leaf expansion and leaf movement responses (*101, 102*).

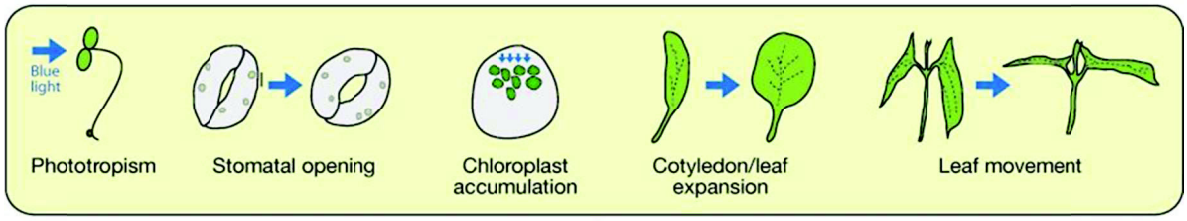

Fig. 4: Diagram illustrating the range of phototropin-induced responses in higher plants. Phot1 and phot2 are activated by blue light and overlap in function to mediate several responses. These are enclosed in the yellow rectangle and include phototropism, stomatal opening, chloroplast accumulation movement, and cotyledon and leaf expansion. (adapted from (*103*)).

Fern neochromes are chimeric photoreceptors containing both LOV domains as well as phytochrome bilin binding sensory modules. Neochrome1 mediates nuclear movement in the fern *Adiantum capillus-veneris* (*104*), moreover, the green alga *Mougeotia scalaris* harbours two neochromes that are functionally equivalent to the fern genes (*71*), these are examples for a convergent evolution of photosensing units (*71*). Aureochromes are LOV domain dependent blue-light receptors in photosynthetic stramenopiles, like the yellow-green algae *Vaucheria frigida* or the brown algae *Fucus distichus* (*105*). To current knowledge, there are two types of aureochromes, aureochrome-1 and aureochrome-2 (*106*). RNA interference experiments demonstrated that AUREO1 controls branch development, whereas AUREO2 allows development of the alga sex organ (*105*). Another LOV photoreceptor-family is the ZTL/FKF1/LKP2 (Zeitlupe/ Flavin-binding Kelch-repeat, LOV F-box Protein2) family (*107*). This family comprises a range of positively acting factors, playing a crucial role as transcriptional activators by regulation of protein turnover of oscillator components that control circadian timekeeping in plants (*108-110*).

In the fungal kindom, a LOV-domain containing family of photoreceptor proteins, the so-called white-collar1 (WC-1) photoreceptors mediate the setting of the circadian clock (e.g. in *N. crassa*) (*111*). The flavoprotein VVD serves as fungal blue light photoreceptor for photoadaption (*112*). In *N. crassa* VVD is localized in the cytoplasm and, as a second fungal blue-light photoreceptor besides WC-1, enables the organism to perceive and respond to daily changes in light intensity (*112*).

1.1.5 Bacterial LOV photoreceptors – a versatile family of structurally diverse photoreceptors

When genome mining and several initial biophysical and biochemical studies suggested the conservation of the LOV domain photosensing paradigm between different taxa (*21, 32, 40, 59, 83, 113, 114*), it was not very surprising that phototropin-like LOV-domain containing proteins were found in photosynthetic prokaryotes such as cyanobacteria and some phototrophic proteobacteria such as e.g. *R. sphaeroides* or *Erhythrobacter litoralis* (*21*). Strikingly, putative LOV proteins were also identified in organisms that cannot directly benefit from sensing a blue-light stimulus such non-photosynthetic chemotrophic bacteria (*21*). Such in most cases putative, LOV domain containing photoreceptors are found a variety of non-photosynthetic prokaryotes, like as plant pathogen species (e.g. *Pseudomonas syringae*), plant root colonizing species (e.g. *P. putida*) and in human/mammalian pathogens (e.g. *Brucella* and *Listeria* species), but also among common soil and leaf-associated bacteria (e.g. *Bacillus* spp.) (*21*). Apparently, they are even more widespread in chemotrophic microbes than in phototrophic ones (*115*). However, a bias of current databases towards chemotrophic microorganisms cannot be ruled out since members of those genera contain common mammalian/human pathogens or biotechnologically interesting organisms and are thus likely the ones to be sequenced first. With respect to the biological function of bacterial LOV proteins, our understanding is much more limited compared to the plant and fungal LOV-domain containing proteins. Only recently first hints emerged, demonstrating that some of the bacterial LOV-domain containing proteins mediate blue-light dependent physiological responses *in vivo.* Those examples will be discussed in the following paragraph. From a general perspective, it was recently proposed that bacterial blue-light photoreceptors (including BLUF and LOV proteins) might help bacteria "make important lifestyle decisions" i.e. by enabling a light dependent control of surface attachment, multicellularity, biofilm formation or virulence and pathogenicity (*17*). All so far known LOV-protein dependent physiological responses in prokaryotes are illustrated in Figure 5.

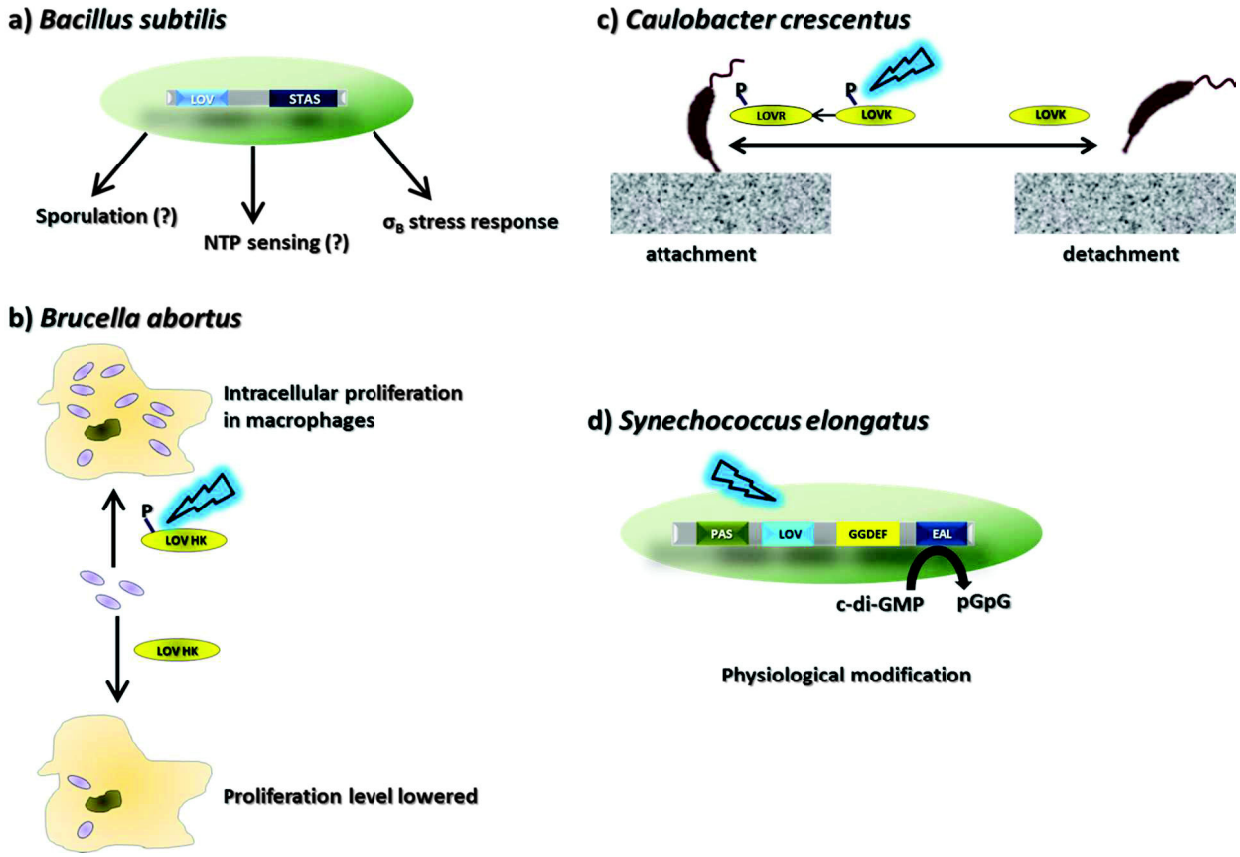

Fig. 5: Light-dependent bacterial physiological responses. a) ***Bacillus subtilis***: Under stress conditions, illumination of the LOV domain of the *Bacillus subtilis* YtvA protein results in activation of the RNA polymerase σB dependent gene expression ensuing stress response of the organism. b) ***Brucella abortus*****:** a LOV histidine kinase (HK) is phosphorylated in a blue-light dependent manner and positively regulates intracellular proliferation in a macrophage model. c) ***Caulobacter crescentus:*** Light activation of the LovK protein (containing a histidine kinase effector domain) induces autophosphorylation. LovK, together with LovR, regulate cell adhesion through a yet unknown mechanism. d) ***Synechococcus elongatus*****:** Regulation of the phosphodiesterase activity of the EAL domain in the LOV-GGDEF–EAL protein of the organism is controlled by the LOV domain. Thus, light exposure is predicted to control the cellular level of cyclic di-GMP, an important second messenger involved in the regulation of biofilm formation. Abbreviations: NTP, nucleoside 5′-triphosphate; PAS, Per–Arnt–Sim; pGpG, acyclic di-GMP. ;adapted from (*116*).

The first identified bacterial LOV protein, YtvA of *B. subtilis*, was found to act in the general stress response pathway of the organism (*117-119*). YtvA up-regulates the alternative transcription factor σ^B through a cascade of Rsb proteins in a blue-light regulated way via the stressosome. The stressosome is the large MDa multi-component stress-dependent regulatory complex of *B. subtilis* (*117-119*). The non-phototrophic Gram-positive pathogenic bacterium *Listeria monocytogenes* responds to blue light, by the action of an YtvA-homolog (Lmo0799) supposedly via similar mechanisms as suggested for *B. subtilis* YtvA. Furthermore, invasiveness and swimming motility are apparently affected in a blue-light dependent manner (*120*).

A LOV histidine-kinase (LOV-HK) identified in the mammalian pathogen *B. abortus*, regulates host persistence and virulence of the strain in a blue-light dependent manner (*121*). Data obtained using a macrophage infection model suggested a blue-light and LOV-HK dependent positive regulation of intracellular proliferation.

In the marine bacterium *C. crescentus*, a similar protein, namely a LOV histdine-kinase regulates cellular attachment (*122*). The histidine-kinase LovK binds a flavin cofactor, undergoing the typical LOV-photocycle. Within the same operon a response regulator, LovR is found, which represents the second component of the LovK/LovR two-component signaling system. LovK displays increased ATPase and autophosphorylation activity in response to blue light. When *C. crescentus* is grown in the presence of blue light, cell-cell attachment is dramatically enhanced, furthermore it was found that absence of the response regulator LovR results in severe attenuation of cell attachment to a glass surface under laminar flow (*122*).

In *S. elongatus* a LOV-GGDEEF-EAL domain-containing protein exhibits blue-light inducible phosphodiesterase activity catalyzing the hydrolysis of the secondary messenger cyclic di-GMP (c-di-GMP) (*123*). c-di-GMP is involved in the regulation of biofilm formation, cell motility and virulence (*116*).

Although more and more data are brought forward which directly links LOV photoreceptor encoding genes with bacterial physiological responses, a detailed structural understanding as to how a single structurally highly conserved sensory module is able to control a broad variety of different associated effector domains, is still missing. In order to provide the structural basis for the understanding of LOV signal-transduction mechanisms, photochemistry, structure and LOV domain dynamic properties will be discussed in the following chapters.

1.2 LOV domains as the conserved sensory modules of architecturally diverse photoreceptors

Like plant phototropins, bacterial LOV photoreceptor proteins are organized in a modular fashion typical for bacterial signaling proteins (*124*). Usually one N-terminally localized sensor LOV domain is connecting to a C-terminal effector or output domain via interdomain linker sequences (*113, 124*).

To date, several architectural sub-classes of LOV-domain / effector-domain combinations have been recognized (*21, 73, 113*). Among this structurally diverse set of architectures (Figure 6), several sub-groups emerge: The largest set of architectures contain histidine-kinase effector domains fused to the LOV sensor core (LOV-HKs). Those sequences make up approximately 50 % of all so far identified bacterial LOV proteins (*116*). Examples include putative photoreceptor proteins found in plant pathogen species (e.g. *Xanthomonas spp*. or *P. syringae)* as well as other proteobacterial lineages like *Sphingomonas spp*, *Novosphingobium* or the aquatically dwelling *C. crescentus*. Furthermore, as also outlined above, LOV-HKs can be found in a set of human/animal pathogens such as *Brucella* spp.. In a subset of LOV-HKs the histidine kinase is followed by an N -or C-terminally attached response regulator domain (RR). All so far characterized LOV-HKs exhibit the conserved phot-like photocycle. Concomitantly illumination triggers HK autophosphorylation (*122, 123, 125-127*). In cases where a cognate RR has been identified subsequent phosphor-relay to the RR has been observed (*128*). This suggests the presence of fully functional light-dependent two-component systems, which eventually control gene expression via a LOV-HK / RR phosphor-relay, in many chemotrophic bacteria (*129*) for most of which no light-dependent physiological functions have been reported.

The second largest group is constituted by LOV proteins containing GGDEF and EAL domains (approx. 20 % of bacterial LOV proteins (*116*)). GGDEF and EAL domains are enzymatically active protein modules showing diguanylate cyclase and phosphodiesterase activity, respectively (*130, 131*). They commonly act on cyclic-di-GMP, an important secondary messenger molecule, either facilitating synthesis (GGDEF, cyclase activity) or hydrolysis (EAL, phosphodiesterase activity) of the molecule (*132*).

Another large group of bacterial LOV proteins includes the previously described YtvA-like LOV-STAS architectures (approx. 10 % of all bacterial LOV proteins). Less common are LOV-SpoIIE (sporulation stage II protein E) proteins (*133*) (approx. 2 %) (*116*) and LOV-HTH (helix–turn–helix) proteins (approx. 3.5 %) (*134*). The latter one, represents a sensor system were blue-light illumination directly controls DNA-binding via the HTH domain (*135, 136*). Although not yet shown experimentally, this in turn would enable direct transcriptional control and hence regulation of gene expression.

More scattered in nature are LOV proteins associated with additional putative sensor domains such GAF (cyclic GMP-specific phosphodiesterases, adenylyl cyclases) (*137*) and/or other PAS (Per, Arnt, Sim) domains (*138*).

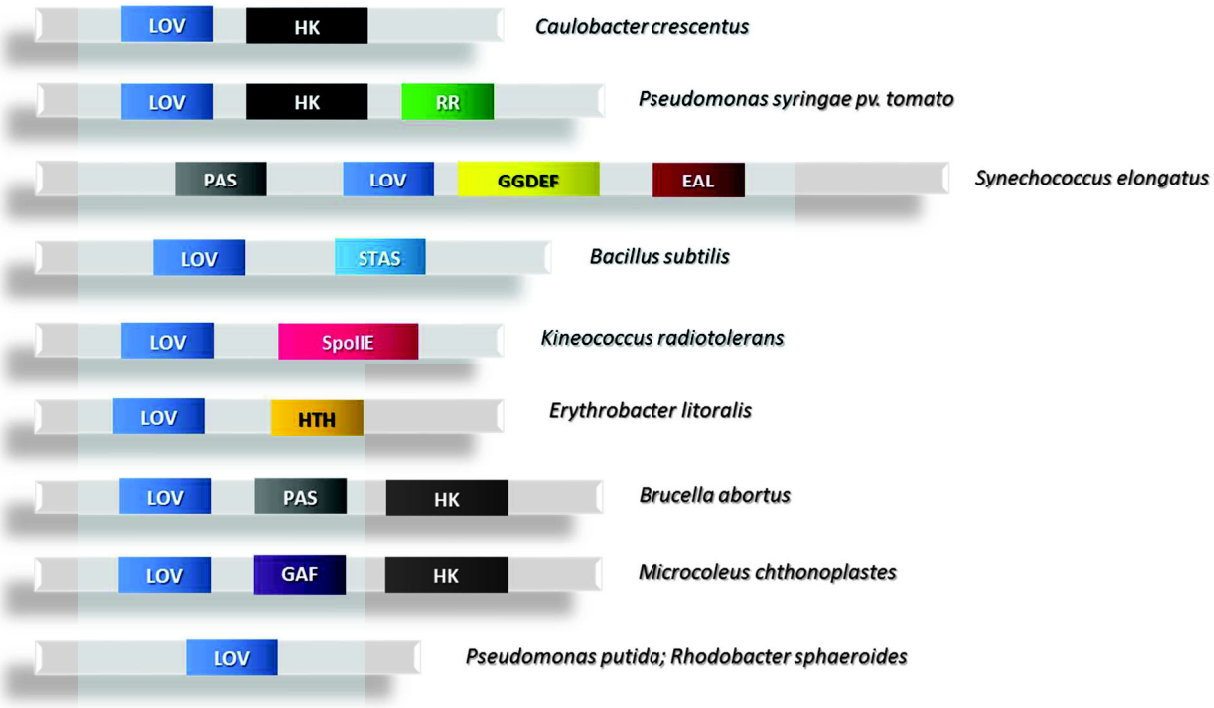

Fig. 6: Domain architecture of selected LOV proteins. This cartoon presents just a few examples of the hundreds of LOV (light, oxygen or voltage) domain-containing proteins. Abbreviations: LOV: light, oxygen, voltage domain; STAS: sulphate-transporter antisigmafactor antagonist domain; SpoIIE: sporulation stage II protein E;HTH: helix-turn-helix; HK: histidine kinase domain; RR: response regulator domain; PAS: Per, Arnt, Sim domain; GGDEF: diguanylate cyclase; EAL: phosphodiesterase, GAF: cyclic GMP-specific phosphodiesterases, adenylyl cyclases.

The third largest bacterial LOV protein sub-class (approx. 13 % of all bacterial LOV proteins), is constituted by unusual LOV photoreceptors which lack fused effector domains (*42, 115*). Those "short" LOV proteins, conserved among saprotrophic fluorescent Pseudomonads such as *P. putida* and *P. fluorescens,* will be the main focus of the present thesis.

1.2 The LOV signaling paradigm – conserved core structure and photochemistry

In the early years of the new millennium, X-ray crystallographic studies of the isolated *C. reinhardtii* phototropin LOV1 (*139*) and *Adiantum* phy3 LOV2 domain (*140*) revealed that LOV domains exhibit a prototypical PAS fold (*141*). The name PAS, was hereby derived from the name of the three proteins, where it was first observed: the protein Period (Per), the human aryl hydrocarbon receptor nuclear translocator protein (ARNT) and the *Drosophila* single minded protein (SIM) (*142*). PAS domains possess a general α/β fold, consisting of a five-stranded antiparallel β-sheet flanked by α-helices with the following arrangement of the secondary structural elements: Aβ-Bβ-Cα-Dα-Eα-Fα-Gβ-Hβ-Iβ. The general PAS fold represents an ubiquitary structural motif that is shared by a huge number of sensor proteins. Currently, the SMART domain content database (http://smart.embl-heidelberg.de/) lists 29383 sequences containing a PAS domain. Many times, PAS domains bind small ligands which enable signal perception by the sensor domain (*141, 143-145*). Prominent examples include: the light-sensitive photoactive yellow protein (PYP) that binds *p*-coumaric acid as chromophore (*144*), the heme-binding, oxygen-sensing FixL (*145*) as well as with the FAD-binding redox-sensing NifL protein (*143*).

Most LOV domains bind flavin mononucleotide (FMN) within a pocket formed by the anti-parallel β-scaffold and a helical connector constituted by Cα-Dα-Eα-Fα. In the dark, the FMN chromophore is non-covalently bound within the sensor core domain. Hereby, the 3-10 helix Eα, that contains the conserved LOV sequence motif GXNCRFLQ, harbours the photoactive cysteine residue essential for the LOV photoreaction mechanism (see below).

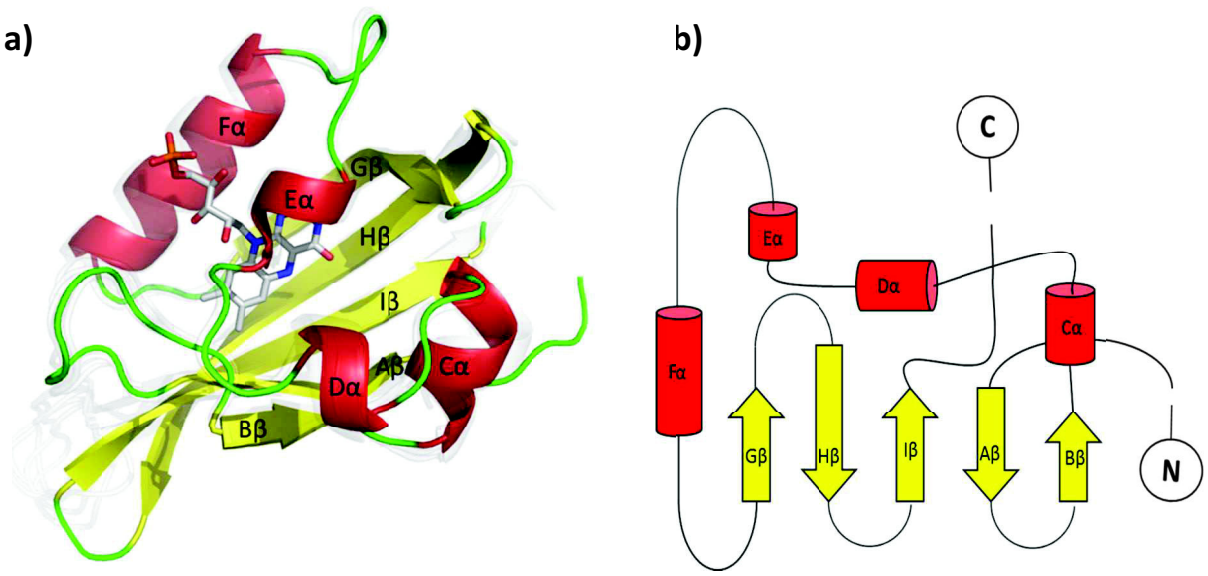

Fig. 7: X-ray structure of the canonical LOV-core domain. a) The superposition of several LOV core domain structures. Selected light state structures of *Adiantum capillus veneris* Phy3 LOV2 (PDB ID: 1G28), *A. sativa* LOV2 (PDB ID: 2V1A), *A. thalliana* phot1-LOV1 (PDB ID: 2Z6C), *A. thaliana* phot2-LOV1 (PDB ID: 2Z6D), *B. subtilis* YtvA (PDB ID: 2PR5) and *C. reinhardtii* LOV1 (PDB ID: 1N9L) were superimposed. The CrLOV1 structure is colored according to secondary structure. α-helices are shown in red, β-strands in yellow and random-coils are highlighted in green. b) Topology representation of the general LOV-fold . α-helices and β-strands are color coded as in a).

1.3 The photocycle of LOV domains

The LOV photocycle basically comprises two reaction branches: i) a photochemical reaction which is initiated by excitation of the FMN chromophore with blue light, resulting in the formation of a meta-stable signaling state and ii) a dark reaction resulting in the recovery of the protein (and its chromophore) from the signaling state to the dark (ground) state when light is switched off after excitation. The complete photocycle is illustrated in Figure 8 (forward photochemical reaction in blue, dark recovery in black). As both reactions are of primary importance in the present thesis both pathways will be discussed in detail in the following:

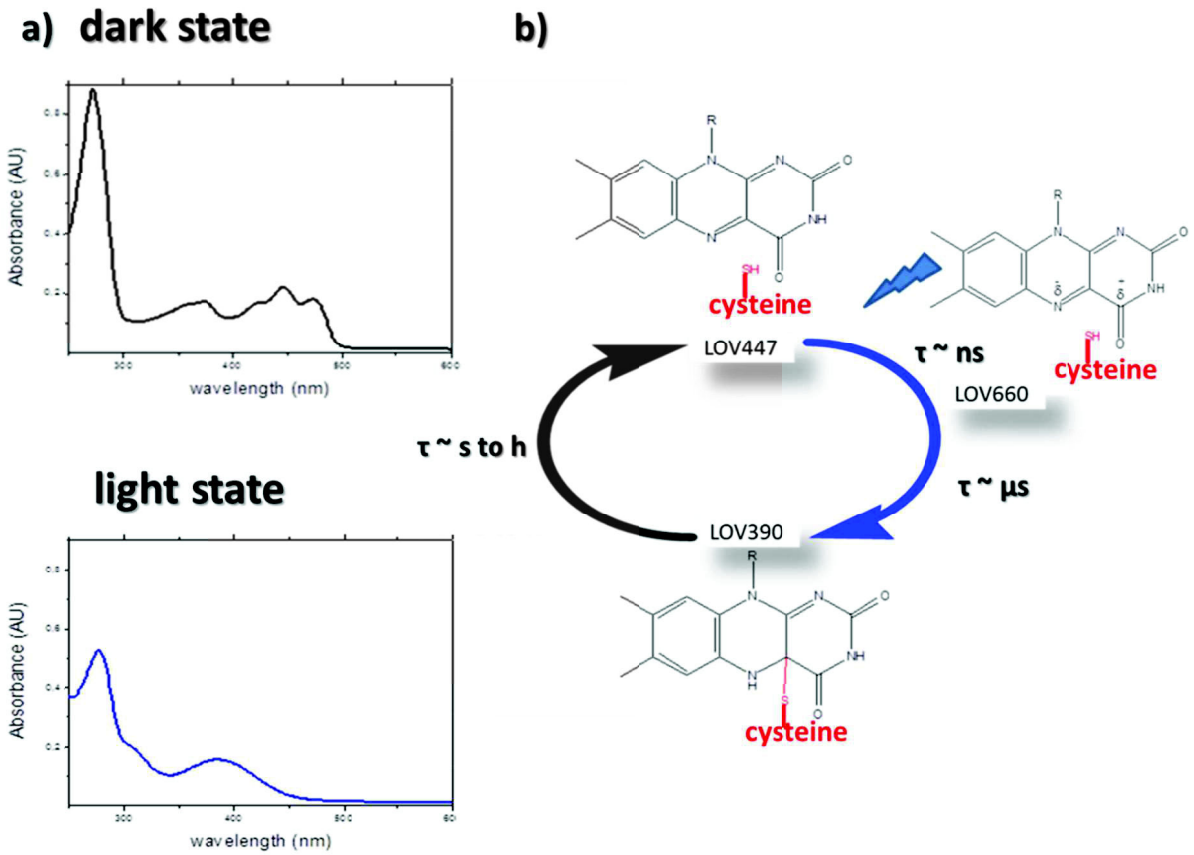

Fig. 8: The LOV photocycle. a) Spectral changes associated with LOV photoexcitation as seen in steady-state UV/Vis spectra. b) Illustration of the LOV photocycle. In the dark state (LOV447) blue-light illumination induces the transient formation of the singlet excited state of FMN which decays within nanoseconds to a spectrally red-shift triplet-state intermediate (LOV660) (*146*). From the triplet state the LOV signaling state, or light state, (LOV390) is formed within microseconds (*146*). In this state a covalent bond is formed between the 4a carbon atom of the flavin isoalloxazine ring and a totally conserved cysteine residue (photoadduct). Dark state recovery occurs thermally within seconds, hours or even days, depending on the LOV protein (*113*).

Forward reaction: blue-light excitation and adduct formation

Photon absorption in the FMN molecule that is in the dark non-covalently bound within the LOV domain (LOV447, numbers refer the absorption maximum of the intermediate), excites the FMN molecule on a ps-time scale (*97*) to its excited singlet state ^{1}[FMN]. Intersystem crossing results in a rapid population of the FMN triplet state (^{3}[FMN], LOV660) which represents the first LOV photocycle intermediate detectable by transient absorption spectroscopy (*97*). From the triplet state, signaling state formation usually occurs within 1-2 µs and results in the formation of a covalent bond between the C4a atom of the FMN isoalloxazine ring and the completely conserved photoactive cysteine residue (photoadduct) located within the Eα-helix of the LOV domain (*126, 147*).

Dark recovery: breaking the photoadduct

In the dark, the photoadduct will be broken resulting in the formation of the initial non-covalent parent (dark) state (LOV447), thus completing the photocycle (*148*). Depending on the LOV protein this dark recovery reaction can take seconds to hours (*73*). For example, the time constants for the dark recovery of phototropin LOV domains are in the order of 10 to 100 seconds (*149*). Much longer (or even irreversible) dark recovery reactions were observed for the isolated LOV domain of *A. thaliana* FKF1 (*150*) and in a LOV histidine kinase from *Brucella melitensis* (*151, 152*). Hereby, the structural or mechanistic basis resulting in such different dark reaction kinetics is not well understood.

However, several hypotheses have been brought forward: A study by Alexandre and co-workers pointed towards a general base-catalyzed recovery reaction, probably driven from two surface exposed histidine residues in the *A. sativa* phot1-LOV2-domain (*153*). This proposal would confirm an earlier hypothesis by Swartz *et. al* that suggested a base catalysed driven dark recovery in LOV-domains (*154*). Another hypothesis suggested an additional mechanism, driven mainly by steric interactions in the FMN binding pocket of the LOV-domain. Christie and coworkers (*155*) conducted a random mutagenesis study on the LOV2-domain of *A. sativa* phot1. They found that an isoleucine residue located within van der Waals distance from the highly conserved photoactive cysteine influences the dark recovery reaction. It was suggested that this isoleucine probably makes contact with its methyl-group to the sulfhydryl group of the cysteine (*103*) thus creating constrain in the protein to stabilize the light-state intermediate (*155*). Thus generally, the thermal recovery to the dark state can be strongly influenced by mutations (*156-158*) and the chemical environment of the chromophore (i.e. avaibility of a proton-abstracting base).

1.4 LOV signal-transduction - from photon absorption to physiological output

One question of primary importance common for all LOV proteins is how the signal received by photon absorption in the FMN molecule is translated first of all into a structural signal within the LOV domain and secondly how the signal relay between the sensor LOV domain and associated effector domains is realized in the full-length photoreceptor. Initially, these aspects were studied

using X-ray crystallography. X-ray diffraction data were recorded on LOV protein crystals grown in the dark. After recording dark state data, the same LOV protein crystals were illuminated and light-state data were recorded. While photoadduct formation could be observed in those crystals (FMN-C4a sp^3 hybridization, covalent bond between FMN-C4a and Cys-Sγ), large scale conformational changes were apparently absent (*126, 140, 159*). This suggests that either conformational motions are impaired by the crystal lattice or can only occur in context of the full-length photoreceptor protein.

An early hypothesis regarding the LOV domain signal transduction mechanism was based on solution NMR data, performed on a C-terminally extended LOV2 construct of *A. sativa* phot1 (*160, 161*). This construct contained, apart from the sensor LOV domain, 20 additional C-terminal amino acids. The authors provided evidence that this additional segment forms an α-helix in solution (*160*). Therefore, in this study and in all later work that used extended LOV domain constructs, this segment was termed Jα-helix. NMR experiments revealed a tight interaction between the Jα-helix and the LOV core β-scaffold in the dark. Upon illumination the Jα-helix apparently dissociates from the core and eventually becomes disordered (*160*). In a subsequent study, the dark state Jα-helix / LOV core interaction was destabilized by mutation resulting in constitutively active full-length phot (*161*). This latter data, along with more recent experiments (*162, 163*) provides strong evidence for the validity of this mechanism for plant phot1 activation. Given the sequence similarity between plant and bacterial LOV domains, immediate questions arise regarding the conservation of this structural relay mechanism in the three kingdoms of life.

In light of recent data obtained for several plant, fungal and bacterial LOV proteins variable signal relay mechanisms seem to be realized in different LOV photoreceptor classes. Prominent examples will be discussed in the following:

A good example, illustrating the dynamic nature of the LOV signaling process is seen for the *N. crassa* protein VVD. Here, as for all LOV domains, illumination induces the formation of a flavin-cysteinylthio adduct. Photo adduct formation eventually results in an altered hydrogen bonding network centered around the N-terminal cap of VVD. This subsequently triggers the release of the N-terminal cap from the protein core and results in a restructured acceptor pocket for the N-terminal cap of the opposite subunit to allow light-dependent dimer formation (*164*).

Substitution of residues critical for the switch between the monomeric and the dimeric states of the protein had profound effects on light adaptation in *Neurospora* (*164*).

Another, very recent example from the bacterial kingdom is the *B. subtilis* YtvA protein (*165*). In the X-ray structure of an extended YtvA-LOV construct the C-terminal Jα-helix extends into the solvent. Illumination of dark grown YtvA-LOV crystals was shown to cause photoadduct formation, which triggers slight rearrangements throughout the LOV domain. Concomitantly, in the dark and light structures, the two subunits of the dimeric protein rotate relative to each other by 5°. This small quaternary structural change is presumably a component of the mechanism by which the activity of YtvA is regulated in response to light (*165*).

For their artificial LOV histidine kinase, YF1, Möglich and co-workers suggested a model, where signals are transmitted from the LOV sensor domain to the histidine kinase domain via a 40°– 60° rotational movement within an α-helical coiled-coil linker, suggesting that light is acting as a rotary switch (*166*) in case of YF1 and potentially also YtvA and related bacterial LOV photoreceptors. Their data suggest that the major effect of light is to induce relative rotational motion between the LOV sensor and histidine kinase effector domains, probably through perturbation of the coiled coil interaction (*166*).

In one very recent study, Nash and colleagues reported the structural basis of photosensitivity in the bacterial LOV-HTH DNA-binding protein EL222 of *E. litoralis* HTCC2594 (*136*). The dark-state crystal structure revealed interactions between the EL222 LOV- and HTH domains. In EL222 it appears that the Jα-helix serves solely as an interdomain linker and associates with the HTH effector domain rather than docking onto the LOV β-scaffold as in AsLOV2 or protruding from the LOV-core as seen for YtvA (*165*). The observed LOV / HTH interaction could hereby account for inhibition of DNA-binding in the dark, as observed in accompanying gel-shift experiments (*136*). When illuminated, the authors proposed that this interaction is broken and both, the LOV and HTH-domains are freed from each other, which allows dimerization of EL222 via the LOV and HTH domains thus enabling target DNA-binding. The latter hypothesis was based on limited proteolysis experiments as well as solution NMR data for the full-length EL222 protein (*136*).

1.5 The saprotrophic fluorescent Pseudomonad *P. putida* KT2440 possesses two LOV domain containing proteins

P. putida KT2440 is a rod shaped, flagellated, gram-negative metabolically versatile saprophytic bacterium that is found in most soil and water habitats. It belongs to the γ-subclass of the Proteobacteria (*167*) and has been certified as a biosafety host for the cloning of foreign genes. Its optimal growth temperature is around 25-30 °C. The genus *P. putida* comprises several strains (including KT2440) that colonize plant roots establishing a mutually beneficial relationship between the plant and bacteria (plant commensal lifestyle). The surface of the root rhizosphere allows the bacteria to thrive from the root nutrients. In turn, *P. putida* induces plant growth and protects the plants from pathogens. Because *P. putida* assist in promoting plant development, researchers use it in bioengineering research to develop biopesticides and to improve plant health (*168*). Due to its metabolic versatility, the bacterium also has considerable potential for biotechnological applications. For example, the organism is able to degrade aromatic or aliphatic hydrocarbons i.e. organic solvents such as toluene and is able to convert styrene oil to biodegradable plastic polyhydroxyalkanoates (PHA) (*168*). It has thus been employed for the bioremediation of polystyrene foam waste which was thought to be non-biodegradable (*169-171*). Due to the bacteria's ability to decompose organic pollutants, researchers are attracted to using *P. putida* for soil bioremediation purposes (see e.g. (*172-174*)). In the late 1990s, the genome of *P. putida* KT2440 was sequenced, revealing 6.18 Mb of genomic information which provides the genetic basis for its versatile metabolic activities (*168, 175-177*). While KT2440 shares 85 % of the predicted coding regions with the facultative human pathogen *Pseudomonas aeruginosa* PAO1(*172*), key virulence factors including exotoxin A and type III secretion systems are missing. In conclusion the analysis of the KT2440 genome provided important insight into the non-pathogenic nature of the strain and pointed to potential new applications in agriculture, biocatalysis and bioplastic production (*172*).

Interestingly, the *P. putida* KT2440 genome encodes two genes with significant similarity to plant LOV photoreceptors. The two ORFs are annotated as sensory-box proteins and are therefore in the following termed PpSB1-LOV (UniProt-ID: Q88E39) and PpSB2-LOV (UniProt-ID: Q88JB0) (*178*). Both proteins consist of a LOV-core domain flanked by short N-

and C-terminal segments but lack a fused effector domain. They are thus members of the "short" LOV protein family. In fact, they were the first bacterial "short" LOV proteins to be characterized (*178, 179*). The two LOV domains are very similar in sequence (about 66 % identical amino acid positions), but display significantly different photochemical characteristics i.e. with respect to dark-state recovery. While PpSB1-LOV is one of the slowest reverting LOV proteins with a dark recovery time constant τ_{REC} of about 37 hours (at 25°C), its counterpart PpSB2-LOV reverts very fast (τ_{REC} = 120 seconds) (*178*). The fact, that *P. putida* KT2440 possesses two highly conserved LOV-domain containing proteins, which moreover exhibit significantly different dark state recovery kinetics, renders the system an ideal starting point to address the structural and mechanistic basis that determines LOV protein dark reaction kinetics. While both *P. putida* KT2440 LOV proteins have previously been characterized with respect to photochemistry, little is known about their physiological importance for the organisms. Preliminary studies hinted towards blue-light dependent regulation of siderophore (pyoverdine) synthesis under iron limiting conditions and pointed at the involvement of the only blue-light photoreceptors encoded in the *P. putida* KT2440 genome, namely PpSB1-LOV and PpSB2-LOV(*178*).

1.6 Scope and outline of this thesis

In recent years more and more information has been gathered regarding the structure, function and physiological role of bacterial LOV photoreceptor proteins. Open key questions relate to mechanistic aspects of the photocycle including the excact mechanism of adduct formation and dark-recovery, signal-relay mechanisms within the LOV sensor domain and signal-transduction mechanisms between sensor and effector domains in multidomain photoreceptors. Given the peculiarity of the *P. putida* KT2440 PpSB1-LOV / PpSB2-LOV photoreceptor system outlined above, several important questions arise, which will be addressed in this thesis:

i) What is the structural and/or mechanistic basis of the different dark reaction kinetics observed for the two sequence-wise highly conserved proteins?

ii) Are fast and slow reverting dark recovery reactions conserved in other "short" LOV proteins found widespread in the genus *Pseudomonas*?

iii) What is the structural and functional role of the N- and C-terminal extensions found outside of the conserved LOV core domain in the two proteins?

iv) How is the light-signal being communicated in *P. putida* KT2440 and what physiological functions do the two potential photoreceptors serve?

The main part of the presented thesis consists of attached publications and is additionally completed by so far unpublished experimental data to substantiate the arguments in the published work. The combined contents accentuates the same general theme, namely the study of the structure-function relationship in bacterial blue-light photoreceptor proteins of the "short" LOV-family.

2. The LOV-proteins of *P. putida* KT2440 - two uneven twins

2.1 Mutual exchange of kinetic properties by extended mutagenesis in two short LOV domain proteins from *Pseudomonas putida*

Katrin Jentzsch, Astrid Wirtz, Franco Circolone, Thomas Drepper, Aba Losi, Wolfgang Gärtner, Karl-Erich Jaeger and Ulrich Krauss

Biochemistry **48:** 10321-10333

2.2 A transient absorption study of the adduct formation kinetics of the twin *Pseudomonas putida* LOV proteins and selected variants

Katrin Jentzsch, Roger-Jan Kutta, Bernhard Dick, Karl-Erich Jaeger and Ulrich Krauss

Unpublished supplementary data to chapter 2.1

BIOCHEMISTRY
including biophysical chemistry & molecular biology
Article

Biochemistry **2009,** *48,* 10321–10333 10321
DOI: 10.1021/bi901115z

Mutual Exchange of Kinetic Properties by Extended Mutagenesis in Two Short LOV Domain Proteins from *Pseudomonas putida*[†]

Katrin Jentzsch,[‡] Astrid Wirtz,[‡] Franco Circolone,[‡] Thomas Drepper,[‡] Aba Losi,[§] Wolfgang Gärtner,[∥] Karl-Erich Jaeger,[‡] and Ulrich Krauss*[,‡]

[‡]*Institut für Molekulare Enzymtechnologie, Heinrich-Heine Universität Düsseldorf, FZ-Jülich, Stetternicher Forst D-52426 Jülich, Germany,* [§]*Department of Physics, University of Parma, Parma, Italy, and* [∥]*Max-Planck-Institute for Bioinorganic Chemistry, Mülheim, Germany*

Received July 1, 2009; Revised Manuscript Received September 21, 2009

ABSTRACT: We previously characterized a LOV protein PpSB2-LOV, present in the common soil bacterium *Pseudomonas putida*, that exhibits a plant phototropin LOV-like photochemistry [Krauss, U., Losi, A., Gärtner, W., Jaeger, K. E., and Eggert, T. (2005) *Phys. Chem. Chem. Phys. 7*, 2804−2811]. Now, we have identified a second LOV homologue, PpSB1-LOV, found in the same organism with approximately 66% identical amino acids. Both proteins consist of a conserved LOV core flanked by short N- and C-terminal extensions but lack a fused effector domain. Although both proteins are highly similar in sequence, they display drastically different dark recovery kinetics. At 20 °C, PpSB2-LOV reverts with an average time constant of 137 s from the photoequilibrium to the dark state, whereas PpSB1-LOV exhibits an average dark recovery time constant of 1.48×10^5 s. Irrespective of the significant differences in their dark recovery behavior, both proteins showed nearly identical kinetics for the photochemically induced adduct formation. In order to elucidate the structural and mechanistic basis of these extremely different dark recovery time constants, we performed a mutational analysis. Six amino acids in a distance of up to 6 Å from the flavin chromophore, which differ between the two proteins, were identified and interchanged by site-directed mutagenesis. The amino acid substitution R66I located near the FMN phosphate in LOV domains was identified in PpSB1-LOV to accelerate the dark recovery by 2 orders of magnitude. *Vice versa*, the corresponding substitution I66R slowed down the dark recovery in PpSB2-LOV by a factor of 10. Interestingly, the interchange of the C-terminal extensions between the two proteins also had a pronounced effect on the dark recovery time constants, thus highlighting a coupling of these protein regions to the chromophore binding pocket.

Many organisms depend on the ability to sense the quality and quantity of the incoming radiation in order to optimally respond to changing light environments by optimizing the yield of photosynthesis, fine-tuning their metabolism to environmental/nutritional conditions, or avoiding harmful irradiation. Detection of physical parameters, such as wavelength distribution or intensity and duration of light exposure, needs to be integrated in order to produce a balanced physiological response. One class of photoreceptor sensor modules are the so-called light, oxygen, voltage (LOV)[1] domains (*1*). LOV domains show an absorption in the blue spectral region due to a noncovalently bound flavin chromophore (FMN (flavin mononucleotide), λ_{max} around 447 nm). They were initially identified as the light-sensing part of plant phototropins (phot), the primary blue light photoreceptors for plant phototropism (*2*), chloroplast movement, leaf expansion, and stomata opening (*3*).

In the past decade, genome mining revealed that LOV signaling modules are equally widespread in the prokaryotic world (*4*). The first prokaryotic LOV domain-containing protein that was biochemically and biophysically characterized was YtvA from *Bacillus subtilis* (*5*). Subsequently, LOV domain homologous sequences were identified in a variety of phototrophic and chemotrophic prokaryotes. Consequently, biochemical studies on various prokaryotic LOV proteins were conducted and revealed that the LOV-signaling paradigm is conserved between eu- and prokaryotes (*5*−*7*). Studies on light-dependent physiological effects in prokaryotes are still sparse; a regulation of the general stress response, cell−cell attachment, and the regulation of virulence have been reported so far (*8*−*10*).

Despite their origin from pro- or eukaryotic organisms, the photochemistry and the following (thermally) driven reactions of LOV domains are principally the same and differ mainly in the kinetic time constants for the respective reactions. Absorption of light by the protein in the dark state, that maximally absorbs at 447 nm (LOV447), generates the singlet excited state of FMN that undergoes on a nanosecond time scale an intersystem crossing process to form the corresponding triplet state, that shows a red-shifted absorption maximum at 660 nm (LOV660) (*11*). In turn, LOV660 decays within a few microseconds to give rise to a covalent adduct between the C4a carbon atom of the flavin isoalloxazine ring and the thiol group of a closely positioned cysteine residue, which results in a shift of the absorption maximum to 390 nm (LOV390). This blue-shifted absorbing species is considered the signaling state of LOV domains (*12*−*14*). Although the nature of the distinguishable

[†]This work was supported by the Deutsche Forschungsgemeinschaft (Forschergruppe FOR526).

*Corresponding author: phone, ++492461612939; fax, ++492461612490; e-mail, u.krauss@fz-juelich.de.

[1]Abbreviations: LOV, light, oxygen, voltage; FMN, flavin mononucleotide; phot, phototropin; FKF1, flavin-binding Kelch-repeat F-box protein 1.

Published on Web 09/22/2009

intermediates of the LOV photocycle is well established, the exact mechanism by which the covalent bond is formed is yet under discussion. In brief, two reaction mechanisms for covalent adduct formation have been suggested: (i) an ionic model and (ii) a radical pair mechanism (*15*). Recent FT-IR studies (*16*, *17*) as well as theoretical (quantum mechanical) considerations (*18*, *19*) disfavor an ionic mechanism but, however, cannot rule it out completely (*16*). In the dark, the covalent bond formation is reversible, whereas the bond reopens within minutes or hours for various LOV proteins (*5*, *6*, *20*−*22*). For some proteins, e.g., the flavin-binding Kelch-repeat F-box protein (FKF1) of *Arabidopsis*, the recovery can take up to several days (*21*). While the primary events in the LOV photocycle are mechanistically relatively well understood, the molecular basis of the dark recovery kinetics is far from being resolved.

Early on, the dark recovery of plant phototropin LOV domains was suggested to be base-catalyzed due to an observed pH dependence of the process with a suggested p*K* value between 5 and 6 (*12*, *13*). However, no basic amino acids are found in close proximity to the FMN chromophore in the different available plant LOV domain structures (*23*, *24*). Therefore, it was speculated that general base catalysis occurs from surface-exposed histidine residues located distantly from the FMN chromophore via a network formed by the base, the chromophore, and intraprotein water molecules (*13*). This suggestion recently found support in a study by Alexandre and co-workers that demonstrated (i) that imidazole can act as an efficient enhancer of the dark recovery rate and (ii) that blocking of histidines by diethyl pyrocarbonate slows down the recovery (*25*).

In a detailed study, Christie and co-workers employed a random mutagenesis approach to identify residues in the LOV2 domain of *Avena sativa* phot1 (As-phot1 LOV2), which influence the dark recovery kinetics and the LOV photochemistry. They identified one amino acid residue (I427, As-phot1 numbering) with an outstanding functional effect in van der Waals contact with the sulfur atom of the photoreactive cysteine residue that upon exchange to valine accelerated the dark recovery 10-fold. The authors thus concluded that steric interactions in the protein around the FMN chromophore can influence the dark recovery process (*26*). Moreover, LOV1−LOV2 tandem constructs showed altered dark recovery rates, implying that protein−protein interactions also contribute to the process (*27*).

We recently reported the photochemical and biochemical characterization of a LOV blue light signaling module (termed PpSB2-LOV) (*6*), identified in the plant-root colonizing proteobacterium *Pseudonomas putida* KT2440. Here we present evidence that the same microorganism possesses a second LOV protein (termed PpSB1-LOV) that is highly conserved in sequence to PpSB2-LOV (66% identical amino acid positions) but displays significantly different photochemical behavior with respect to dark state recovery kinetics. The respective dark recovery time constants observed for the two proteins differ by 3 orders of magnitude, being much faster for PpSB2-LOV. Both proteins consist of a conserved LOV core flanked by N- and C-terminal extensions but lack a fused effector domain.

The mechanistic and structural reasons for these drastically different dark recovery kinetics were studied by an extensive mutational analysis. Several amino acids that are localized in close proximity to the FMN chromophore and differ between the two proteins were interchanged. Furthermore, we interchanged the C-terminal, putatively helical extension between the two proteins. Using this approach we have identified one amino acid position, located in close proximity to the FMN phosphate on helix Fα that is a major determinant for the velocity of the photocycle. Remarkably, the interchange of the C-terminal extension had a pronounced effect on the dark recovery. Besides influencing the kinetics of the dark recovery process, a change in selectivity of the incorporated chromophore was caused by the mutation.

MATERIALS AND METHODS

Bacterial Strains and Plasmids. All bacterial strains used in this study were grown either in Luria−Bertani (LB) broth or in autoinduction (AI) media (adapted from ref *28*) for heterologous expression of recombinant proteins. In brief, the media consisted of 12 g/L casein hydrolysate, 24 g/L yeast extract, and 5 g/L glycerol, in 100 mM potassium phosphate buffer, pH 7.0. The media were supplemented for induction with 0.5 g/L glucose and 2 g/L lactose, respectively. The genes coding for the two LOV proteins, PpSB1-LOV (Swiss Prot: Q88E39) and PpSB2-LOV (Swiss Prot: Q88JB0), were cloned in a similar manner as described previously for PpSB2-LOV (*6*). In this study, we used a construct of PpSB2-LOV that, in contrast to the formerly described one (*6*), lacks the first three N-terminal amino acids. All constructs were expressed as N-terminal hexahistidine tagged fusion proteins (tag sequence: MGSSHHHHHHSSGLVPRGSH) in *Escherichia coli* BL21(DE3). Overexpression was carried out either in 50 mL cultures (for the prescreening) or in 1 L AI media cultures for 3 h at 37 °C after which the cultures were shifted to 30 °C. Subsequently, the cells were incubated for 48 h (prescreening) or 72 h (large-scale overexpression) at constant agitation (120 rpm) in the dark.

General Molecular Biological Techniques. Isolation of recombinant plasmids, gel extraction of DNA fragments, DNA ligation, and transformation into *E. coli* strains were carried out according to standard laboratory protocols (*29*).

Site-Directed Mutagenesis and Construction of Variants. The genes encoding full-length PpSB1-LOV and PpSB2-LOV in pET28a were used as template DNA for PCR mutagenesis. Site-directed mutagenesis was carried out using the QuikChange mutagenesis technique according to the instructions given by the manufacturer (Stratagene, La Jolla, CA). In most cases, Turbo-*Pfu* DNA polymerase (Stratagene) was used for amplification. The oligonucleotide primer sequences used throughout this study are summarized in Supporting Information Table 1.

Overall, six point mutations were introduced into each protein. The mutations introduced into PpSB1-LOV were A13H, K23Q, E47D, R61H, R66I, and K71E. Correspondingly, the mutations generated for PpSB2-LOV were H13A, Q23K, D47E, H61R, I66R, and E71K.

In order to generate mutants with interchanged C-terminal extensions, we introduced a *Zra*I restriction site by QuikChange mutagenesis into the PpSB2-LOV gene at the immediate end of the LOV core domain (following D118 in the translated PpSB2-LOV core gene). PpSB1-LOV already possesses a *Zra*I site at the respective position in the gene. This allowed for the straightforward interchange of the C-terminal extensions between PpSB1-LOV and the PpSB2-LOV mutant with the introduced *Zra*I site by subcloning. All generated mutants were verified by sequencing.

Small-Scale Prescreening of PpSB1-LOV and PpSB2-LOV Variants. After overexpression in small scale (see above),

the cultures were harvested by centrifugation for 30 min at 5000 rpm at 4 °C. The resulting cell pellet was resuspended in 5 mL of 10 mM sodium phosphate buffer (pH 8.0) supplemented with 10 mM NaCl. Cells were broken by sonication for 2 min on ice. The procedure was repeated four to five times until complete cell lysis was observed. Cell debris and unbroken cells were removed by centrifugation for 10 min at 14000 rpm at 4 °C. The crude cell extract was transferred into fresh Eppendorf tubes and stored in the dark at 4 °C until further processing.

A first evaluation of the kinetic behavior of the generated PpSB1-LOV and PpSB2-LOV variants was achieved using crude cell extracts (prepared as described above) in a microtiter plate (MTP) based prescreening approach. In brief, the respective dark recovery kinetics were measured by recording a kinetic trace at 480 nm absorbance after illumination of all samples in the MTP wells for 30 s using a custom-made 96-well LED illuminator (Fa. Seltsam, Aachen, Germany). All measurements were performed using a SpectraMax 250 MTP photometer (Molecular Devices, Ramsey, MN) thermostated to 30 °C. Each MTP well contained 150 μL of cell crude cell extracts of the respective overexpressing strain. For each variant the kinetic measurement was performed in triplicate. A 10 mM sodium phosphate buffer (pH 8.0) supplemented with 10 mM NaCl was used as reference. Crude cell extracts from a strain harboring only the empty pET28a plasmid and the crude cell extracts of cultures expressing the respective wild-type PpSB1-LOV and PpSB2-LOV proteins were used as controls.

Large-Scale Protein Overexpression and Purification. The wild-type and selected mutant LOV proteins were expressed in large scale as described above and purified using immobilized metal affinity chromatropgraphy (IMAC) as described previously (*6*). After elution from the IMAC column, the pooled LOV protein containing fractions were desalted using a VivaSpin concentrator unit (10 kDa MWCO). The final buffer was 10 mM sodium phosphate buffer (pH 8.0) supplemented with 10 mM of NaCl. All purified proteins were stored at 4 °C in the dark until further use.

Spectroscopic Techniques. All spectroscopic work was carried out under dim red safety light. Measurement of the light-dependent absorption changes in the UV/vis region (200−600 nm) was carried out using a UV-2401PC UV/vis spectrophotometer with temperature control set to 20 °C (Shimadzu, Duisburg, Germany). Protein samples were diluted in 10 mM sodium phosphate buffer supplemented with 10 mM NaCl (pH 8.0) to a final absorbance at 450 nm of about 0.2. The same buffer was used as a reference. After recording of the protein dark state spectra, the samples were illuminated for 30 s using a blue light emitting Led-Lensers V8 lamp (Zweibrüder Optoelectronics, Solingen, Germany). Subsequently, the light state spectrum was recorded.

The dark state recovery was measured from illuminated samples by recording the absorption recovery at 480 nm for 1.5 h in the case of the PpSB2-LOV variants and over a total time period of 30 h for PpSB1-LOV, respectively. All measurements were carried out at 20 °C. All recovery kinetics of PpSB2-LOV variants were measured at least three times for two independent protein preparations. Due to the very slow recovery of the PpSB1-LOV proteins, the samples were only measured twice for two independent protein preparations of each variant and wild-type protein.

Tryptophan fluorescence spectra for the proteins in their dark-adapted state were recorded as described previously (*6*). Circular dichroism (CD) spectra were accumulated for all mutant and wild-type proteins using a JASCO J-810 spectropolarimeter, temperature controlled to 20 °C. CD spectra were evaluated and deconvoluted using convex constraint analysis (CCA) by employing a data set of five pure components as described by Buttani et al. (*30*). Other CD deconvolution tools using the DichroWeb server (http://dichroweb.cryst.bbk.ac.uk/) (*31*) were tested as well as were other data sets of pure components. However, in all cases, the predicted curves deviated much more from the experimental ones as for the deconvolution using the CCA algorithm.

Chromatographic Techniques. Separation and quantification of FAD (flavin adenine dinucleotide), FMN (flavin mononucleotide), and riboflavin was achieved as described previously (*32*).

The determination of the native molecular weights of proteins was achieved by using a BioSep-SEC-S3000 HPLC column in the dimension 300/7.8 (Phenomenex, Aschaffenburg, Germany). A sodium phosphate buffer (200 mM, pH 7.5) containing 150 mM sodium chloride was used as eluent under isocratic conditions (1 mL/min). The elution of the proteins was followed by UV detection at 220 and 280 nm. Calibration and estimation of protein molecular weights were achieved by employing a standard mixture of proteins of known molecular weight (Aqueous Sec 1; Phenomenex, Aschaffenburg, Germany). Prior to injection, equal amounts of the respective LOV protein were dialyzed against 200 mM sodium phosphate buffer, pH 7.5, supplemented with 150 mM sodium chloride. Each sample was injected twice, and at least two independent protein preparations were used for the analysis. The identity of the respective elution peak was verified by its typical LOV (flavin) spectrum.

Homology Modeling and Bioinformatic Analysis. Homology models for the LOV-core domains of PpSB1-LOV and PpSB2-LOV were generated based on the *Chlamydomonas reinhardtii* LOV1 dark state crystal structure (1N9L) (best template according to SwissModel (*24*)). All models were energy minimized by using either the GROMOS96 (*33*) force field implemented in SwissPDB-Viewer (*34*) or the MAB all-atom force field implemented in the MOLOC modeling package (*35*). Evaluation of amino acid side-chain rotamers was performed using WinCoot version 0.1.2 (*36*). The quality of the models was evaluated using the SAVS (structure analysis and validation) server (http://nihserver.mbi.ucla.edu/SAVES/) as described previously (*6*). Sequence alignments were generated using the AlignX tool, implemented in the VectorNTI sequence analysis package. Alignments were visualized and edited manually using the GeneDoc tool (*37*). Phylogenetic analyses were performed using either PhyML (*38*), MultiPhyl (*39*), or IQPNNI (*40*). Bootstrapped maximum-likelihood trees with 100 replicates for each run were generated using the PhyML server and the MultiPhyl server, respectively. Next-neighbor interchange and subtree pruning and recrafting tree searches using 100 bootstrap replicates were performed using MultiPhyl server. Additionally, bayesian posterior probability support values were added to each branch of the ML tree using BEAST v1.4.5 (*41*).

RESULTS

Protein Expression and Biochemical Characterization of the Wild-Type (WT) PpSB1- and PpSB2-LOV Proteins. In contrast to the previously characterized PpSB2-LOV construct (*6*), the PpSB2-LOV construct used in this study lacked the

first three amino acids at the N-terminus of the protein rendering the amino acid numbering for both proteins identical. This short truncation did not alter the spectral properties of the protein nor did it affect the dark recovery rate constant in comparison to the previously reported value.

Both proteins could be expressed in soluble form as N-terminal hexahistidine-tagged fusion proteins. The IMAC purified proteins had a yellow color indicative for the presence of a flavin cofactor. Analytical HPLC-based size-exclusion chromatography revealed an apparent molecular mass of 37.1 kDa for PpSB1-LOV and 39.7 kDa for PpSB2-LOV, which suggests a dimeric organization for both proteins. The calculated molecular masses of the respective monomers are 18.6 kDa for PpSB1-LOV and 19.2 kDa for PpSB2-LOV, both in good agreement with the monomer band observed in denaturing SDS−PAGE analysis (not shown). The chromophore content of purified PpSB1-LOV and PpSB2-LOV was determined by protein denaturation, extraction, and HPLC analysis. The HPLC analysis revealed that PpSB1-LOV binds predominately FMN (96 ± 4%) with minor traces of FAD (4 ± 0%). Contrarily, PpSB2-LOV contains a mixture of FMN (70 ± 3%), riboflavin (26 ± 8%), and traces of FAD (4 ± 0%).

Spectroscopic Studies and Recovery Kinetics of Wild-Type PpSB1/2-LOV Proteins. In the dark, both proteins exhibit the typical LOV-like UV/vis spectra (Figure 1) with very similar absorption maxima in the blue region around 450 nm indicative of a noncovalently bound flavin species (LOV447). In the UVA region, the spectrum of PpSB1-LOV shows a maximum at 376 nm (Figure 1A, upper panel) much like isolated YtvA-LOV (*42*), whereas the band for PpSB2-LOV is slightly blue shifted and broader with a double peak structure at 350 and 370 nm (Figure 1B, upper panel). Upon blue light illumination the absorption band in the visible region decreases for both proteins, although for PpSB2-LOV the photoproduct (LOV390) cannot be accumulated to 100%. The recovery of the dark state (LOV447) for both proteins was recorded at 480 nm after blue light illumination (Figure 1). The experimental data can best be fitted using a double exponential decay function, yielding two time constants, $\tau_1 = 113 \pm 7$ min ($A_1 = 2.2 \pm 0.1\%$) and $\tau_2 = 2525 \pm 22$ min ($A_2 = 97.8 \pm 0.5\%$) for PpSB1-LOV. Double exponential fitting of the kinetic trace for PpSB2-LOV resulted in $\tau_1 = 28 \pm 2$ s ($A_1 = 29.5 \pm 2\%$) and $\tau_2 = 184 \pm 15$ s ($A_2 = 70.5 \pm 1\%$). According to the formula $\tau_{rec} = \sum A_i \tau_i /100$, this results in average dark recovery time constants of $\tau_{rec} = 2471 \pm 22$ min for PpSB1-LOV and $\tau_{rec} = 137 \pm 11$ s for PpSB2-LOV (at 20 °C). The latter value is well in accordance with the previously reported value for PpSB2-LOV of $\tau_{rec} = 114$ s (*6*). All measurements were at least performed twice for two independent protein preparations of PpSB1-LOV and three times each for two independent preparations of PpSB2-LOV. The experimental error associated with τ_{rec} was about 10%.

Sequence Analysis and Mutational Strategy To Modifiy Dark Recovery Kinetics. The two proteins are highly similar in sequence (about 66% identity). Both possess short N- and C-terminal extensions of the LOV-core domain. To address the mechanistic reason for the drastically different dark recovery kinetics, a mutational analysis was carried out. A multiple sequence alignment of PpSB1-LOV and PpSB2-LOV highlighting the introduced mutations together with the sequences of YtvA-LOV and AsLOV2 is shown in Figure 2.

The selection of amino acid positions that were mutated in this study was based on a sequence alignment that included both PpSB1-LOV and PpSB2-LOV sequences and a selection of fast reverting phototropin LOV2 domains as well as sequences of the slow reverting FKF1/LKP2/ZTL LOV family (*21*) (Supporting Information Figure 1). Based on this alignment, amino acid positions were chosen that differ between PpSB1-LOV and PpSB2-LOV and, moreover, are different in the fast reverting phototropin LOV domains and the slow reverting FKF1/LKP2/ZTL LOV proteins. From a homology model generated for PpSB2-LOV (*6*), which is based on the *C. reinhardtii* LOV1 structure (PDB entry 1N9L), amino acid positions in a distance of 6 Å from the FMN chromophore were chosen for mutual interchange between PpSB1-LOV and PpSB2-LOV (highlighted in Figure 2). Hence, when the mutation A13H was generated in PpSB1-LOV, the corresponding H13A mutation was generated in PpSB2-LOV. Six mutations were generated for each of the two proteins: A13H, K23Q, E47D, R61H, R66I, and K71E for PpSB1-LOV and the respective exchanges in PpSB2-LOV. The most pronounced sequence differences between PpSB1-LOV and PpSB2-LOV are found in the extensions C-terminal to the LOV-core domain (Figure 2). Accordingly, the C-terminal portions were interchanged between both proteins. The respective variant termed cSB1/αSB2 contains the PpSB1-LOV core domain (residues 1−118) and the extension of PpSB2-LOV, and *vice versa* the variant cSB2/αSB1 consists of the LOV-core domain of PpSB2-LOV (residues 1−118) and the C-terminal extension of PpSB1-LOV. In summary, this strategy resulted in 12 different constructs, each carrying a single specific amino acid exchange and two mutants with interchanged C-terminal extensions.

Small-Scale Prescreening of PpSB1-LOV and PpSB2-LOV Mutants. Small-scale expression cultures were grown as described in Materials and Methods. The crude cell extracts of mutants together with the respective wild-type proteins were initially analyzed for changes in their dark recovery kinetics using a microtiter plate based assay. The recovery for the wild-type PpSB2-LOV protein was determined under these conditions as 106 ± 4 s, in good agreement with the time constant previously observed for the purified protein (*6*). For three mutants, a strong deviation from the WT behavior was found: PpSB2-H61R (731 ± 20 s), -I66R (1760 ± 16 s), and cSB2/αSB1 (338 ± 8 s). All other PpSB2-LOV mutants showed negligible to minor changes with respect to the WT protein (-H13A, -Q23K, -D47E, -E71K). Due to the slow recovery of PpSB1-LOV ($\tau_{rec} = 2471$ min at 20 °C), it was difficult to record dark recovery time traces for the respective mutant proteins as well as for the wild-type using our prescreening approach in microtiter plates. The dark recovery for the PpSB1-LOV mutants was therefore monitored for 3 h only. In this way it was possible to identify three faster reverting mutants, which showed exponential kinetics within 3 h of measuring time (Table 1). Interestingly, the variants identified carried the mutations at the same amino acid positions which were previously identified for PpSB2-LOV to slow down the recovery. Mutants identified were PpSB1-R61H (109 ± 4 min), -R66I (5.9 ± 0.1 min), and cSB1/αSB2 (263 ± 12 min). Therefore, these three PpSB1-LOV mutants and the three corresponding PpSB2-LOV mutants were chosen for purification and further characterization.

Purification and Characterization of PpSB1-LOV and PpSB2-LOV Mutant Proteins. All mutant proteins were expressed and purified as described for the respective wild-type proteins. All proteins exhibited typical LOV-like UV/vis spectra (see Supporting Information Figure 2). Spectral changes between mutated and wild-type proteins were minor, and the protein-to-chromophore ratio was in most cases close to 1. The

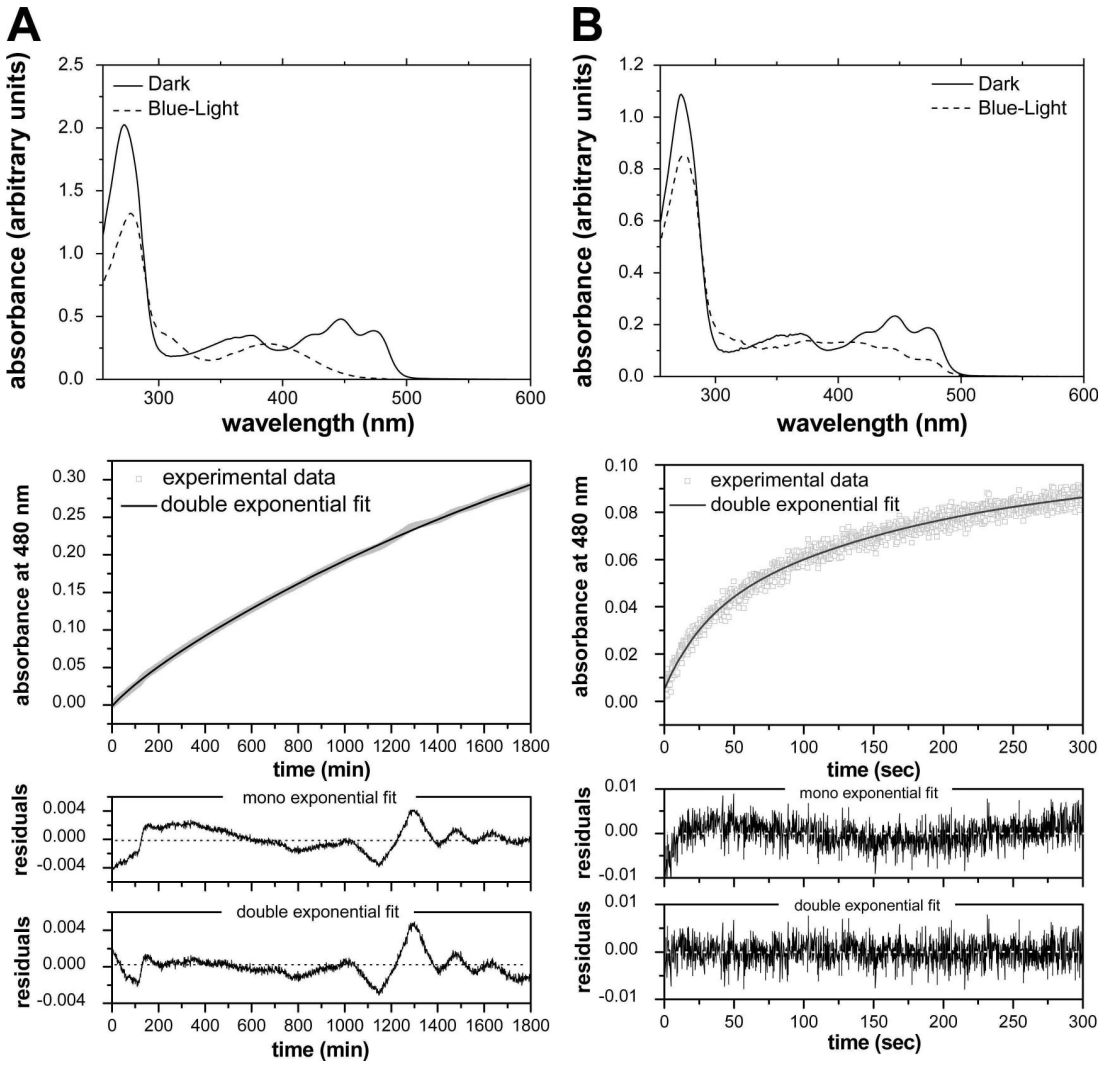

FIGURE 1: Blue light sensitivity and photochemistry of wild-type PpSB1-LOV (A) and PpSB2-LOV (B). The UV/vis absorbance spectra for the dark state of both proteins are shown as a solid line, and the corresponding absorbance spectra after illumination with blue light are depicted as a dashed line (upper panel). Below the UV/vis spectra the dark recovery time traces recorded at 480 nm absorbance for the respective protein after blue light illumination for 30 s are shown. The experimental data are depicted with open squares (in gray); solid lines (in black) indicate the double exponential fit of the data. The two lower panels give the residual distribution for a single and double exponential fit of the experimental data, respectively. Residuals are better distributed for the double exponential fit, especially in the shorter time region; thus, the dark recovery time traces were fitted using a double exponential decay curve.

chromophore content was assessed from the UV/vis spectra (absorption ratio 272 nm/447 nm) as described previously (*43*). The kinetics of the dark state recovery for all mutant proteins were determined in triplicate for at least two independent preparations (Table 2).

For both proteins, the mutation at position 66 has the strongest influence on dark recovery (PpSB1-R66I, PpSB2-I66R), accelerating the lifetime from 2471 ± 22 min (41.2 h) for PpSB1-LOV to about 23 ± 1 min in the case of PpSB1-R66I. This represents an acceleration of the dark recovery by roughly 2 orders of magnitude. Conversely, the corresponding I66R mutation in PpSB2-LOV shows the strongest effect of all analyzed PpSB2-LOV mutants. The dark recovery in the latter case is slowed down by a factor of about 7 from 137 ± 11 s (PpSB2-LOV) to 975 ± 363 s (PpSB2-I66R).

The mutation R61H in PpSB1-LOV accelerates the dark recovery by a factor of about 3 (from 2471 ± 22 min to 765 ± 589 min), whereas the corresponding H61R mutation in PpSB2-LOV slows the recovery down to 581 ± 237 s (by a factor of about 4).

The mutual exchange of the C-terminal extensions of PpSB1-LOV and PpSB2-LOV, resulting in cSB1/αSB2 and cSB2/αSB1, also had a pronounced effect on the dark recovery of the two proteins. The recovery time constant of cSB1/αSB2 was about 2 times faster (1330 ± 448 min) compared to PpSB1-LOV (2471 ± 22 min). Conversely, the recovery of cSB2/αSB1 was slowed down by a factor of 3 from 137 ± 11 s for the WT protein to 444 ± 39 s for cSB2/αSB1. It should be noted here that the dark recovery time constants determined for the purified proteins (Table 2) differed quantitatively (but not qualitatively) from the values obtained with measurements using crude cell extracts (Table 1). For example, the mutant PpSB1-R66I displayed a 369-fold acceleration in crude cell extracts. In contrast, the purified mutant protein only showed a 107-fold acceleration of the dark recovery. The same holds true for all analyzed variants with the kinetic effects being more pronounced in crude extracts.

Chromophore Acceptance and Oligomerization of PpSB1-LOV and PpSB2-LOV Proteins. The flavin chromophore content and composition were analyzed for all mutant

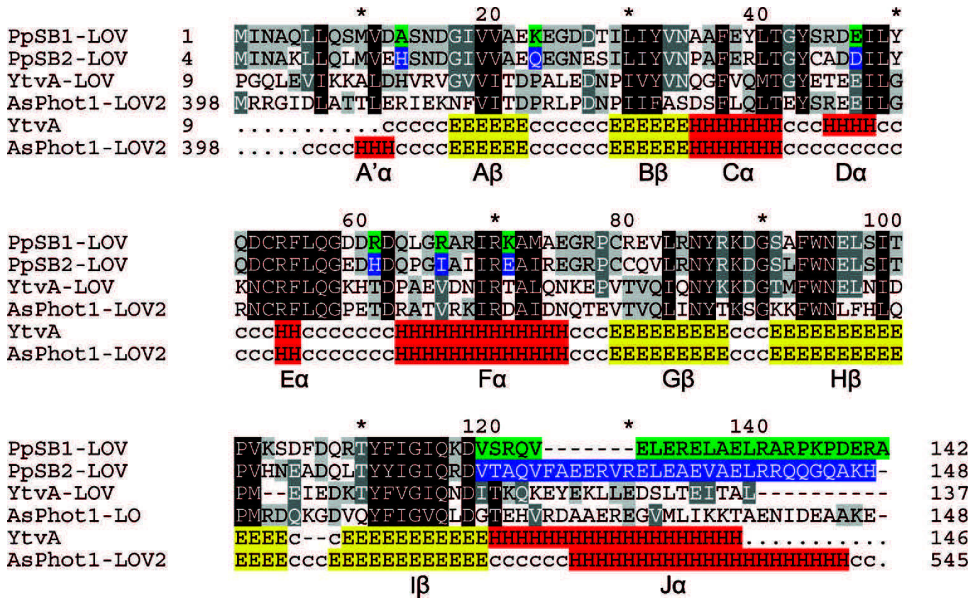

FIGURE 2: Sequence alignment of PpSB1-LOV, PpSB2-LOV, *B. subtilis* YtvA-LOV, and *A. sativa* phot1-LOV2. The PpSB2-LOV construct used throughout this study lacked the first three amino acids compared to the previously described construct and the sequence in the database (Q88JB0). Introduced point mutations are highlighted in green for PpSB1-LOV and blue for PpSB2-LOV. The mutually exchanged C-terminal extensions are highlighted in both sequences. Identical amino acids are shaded in black; similar amino acids are shaded in dark (above 80% conservation) and light gray (under 60% conservation). Below the alignment the assignment of secondary structure elements is shown for AsLOV2 and YtvA using the numbering according to the YtvA-LOV crystal structure. α-Helices (H) are marked in red, β-strand structures (E) are highlighted in yellow, and random coil elements (c) are depicted in white.

Table 1: Dark Recovery Time Constants Observed in the Small-Scale Prescreening Using Crude Cell Extracts of All PpSB2-LOV and PpSB1-LOV Proteins

protein	τ_{rec} (min)[b]	protein	τ_{rec} (s)[a]	*x*-fold change
PpSB1-LOV	nd	PpSB2-LOV	106 ± 4	
PpSB1-A13H	nd	PpSB2-H13A	189 ± 4	+1.8
PpSB1-K23Q	nd	PpSB2-Q23K	355 ± 7	+3.3
PpSB1-E47D	nd	PpSB2-D47E	153 ± 5	+1.5
PpSB1-R61H	109 ± 4	PpSB2-H61R	731 ± 20	+7
PpSB1-R66I	6 ± 0	PpSB2-I66R	1760 ± 16	+16
PpSB1-K71E	nd	PpSB2-E71K	293 ± 4	+2.7
cSB1/αSB2	263 ± 12	cSB2/αSB1	388 ± 8	3.6

[a]Values derive from triplicate measurements for the same crude cell extract. [b]For PpSB1-LOV wild type and certain slow reverting variants the dark recovery kinetics could not be determined (nd) in crude cell extracts because the recovery time traces did not obey a monoexponential decay over a measuring time of 3 h. In particular, for the wild-type PpSB1-LOV protein it was impossible to assess the dark recovery time constant using small-scale prescreening. Therefore, no values for the change in the respective time constant (*x*-fold change) could be derived for the PpSB1-LOV mutant proteins. For comparison, the purified wild-type PpSB1-LOV proteins show a dark recovery time constant of 2212 min at 20 °C.

and wild-type proteins (Table 2). All PpSB1-LOV proteins bound predominately FMN as chromophore. Whereas most mutant proteins did not exhibit any change in their chromophore preference, the PpSB2-I66R mutant exhibited a PpSB1-LOV-like chromophore content, binding only FMN. In contrast, PpSB2-LOV accepts both FMN and riboflavin in a ratio of 70/30. Conversely, the corresponding PpSB1-R66I mutant did not exhibit any change in chromophore composition, binding only FMN, like all other PpSB1-LOV preparations.

Size-exclusion chromatography was performed to elucidate the native oligomerization state of the respective mutant proteins. In all cases, the analysis revealed a dimeric organization with a retention time (within the uncertainty of the method) identical to the values observed for the respective wild-type proteins.

Tryptophan Fluorescence Measurements To Probe Local Structural Changes Due to Introduction of the Mutations. Both proteins possess a single tryptophan (W94) residue localized on the LOV core and conserved among most LOV proteins. Therefore, W94 in both proteins represents a sensitive probe for local structural changes that might be introduced by the mutation. Tryptophan fluorescence spectra were recorded after excitation at 295 nm and were normalized for the amount of absorbed energy at the excitation wavelength (Figure 3). The Trp emission maximum of PpSB2-LOV (338 nm) is red shifted by about 3 nm compared to PpSB1-LOV (341 nm). Interestingly, the interchange of the C-terminal extensions between the two proteins results in a correlated shift of the Trp fluorescence maxima. In cSB2/αSB1 the emission maximum is red shifted by about 4 to 342 nm. *Vice versa*, cSB1/αSB2 has a Trp emission maximum (337 nm) which is blue shifted by about 3 nm compared to PpSB1-LOV (341 nm).

Whereas the R66I mutation in PpSB1-LOV had practically no effect on the Trp emission maximum (340 nm compared to 341 nm in the wild-type protein), the corresponding I66R mutation in PpSB2-LOV resulted in a red shift of the emission maximum to 341.5 nm in comparison to the wild type (338 nm). The H61R (PpSB2-LOV) and the respective R61H (PpSB1-LOV) mutation had no effect on the emission maximum of W94.

CD Spectroscopy of WT and Mutant Proteins. For all proteins used in this study, CD spectra were recorded in the dark and after 30 s of blue light illumination. CD spectra of the two wild-type LOV proteins and the mutants possessing interchanged C-terminal extensions are shown in Figure 4.

Spectra were smoothened and used for deconvolution applying the CCA (convex constraint analysis) algorithm implemented in the CCA$^+$ tool (*25*). For deconvolution we used the data set

Table 2: Dark Recovery Time Constants and Observed Chromophore Acceptance for Mutant and Wild-Type LOV Proteins

	dark recovery kinetics		chromophore acceptance		
protein	τ_{rec}[a]	x-fold change	FMN (%)[b]	riboflavin (%)[b]	FAD (%)[b]
PpSB1-LOV	2471 ± 22 min		96.0 ± 4.0	nd	3.5 ± 0
PpSB1-R66I	23 ± 1 min	−107	100 ± 0	nd	nd
PpSB1-R61H	765 ± 589 min	−3	99.1 ± 1.2	0.9 ± 0	nd
cSB1/αSB2	1330 ± 448 min	−2	100 ± 0	nd	nd
PpSB2-LOV	137 ± 11 s		70.3 ± 3.0	26.0 ± 8.0	3.7 ± 0
PpSB2-I66R	975 ± 363 s	+7	100 ± 0	nd	nd
PpSB2-H61R	581 ± 237 s	+4	22.2 ± 3.0	53.9 ± 5.3	23.6 ± 2.1
cSB2/αSB1	444 ± 39 s	+3	65.4 ± 1.9	26.7 ± 1.0	7.9 ± 2.7

[a]Values derive from triplicate measurements on at least two independent preparations. In most cases a double exponential decay curve best fitted the kinetic data. The reported average τ_{rec} values were derived from the sum of the two exponential time constants τ_1 and τ_2 according to the formula $\tau_{rec} = \sum A_i\tau_i/100$. For certain preparations the standard deviation resulting from the measurement of two independent preparations is exceeding 10%. This is apparently due to a variation between the different preparations for the same mutant protein. However, the overall trend regarding the acceleration or deceleration remains the same even within the large associated error. [b]Values derive from triplicate measurements on at least two independent preparations. nd: not detectable. A standard deviation of 0% results when one of the flavin species (e.g., FAD) could only be detected in one of the two independent preparations.

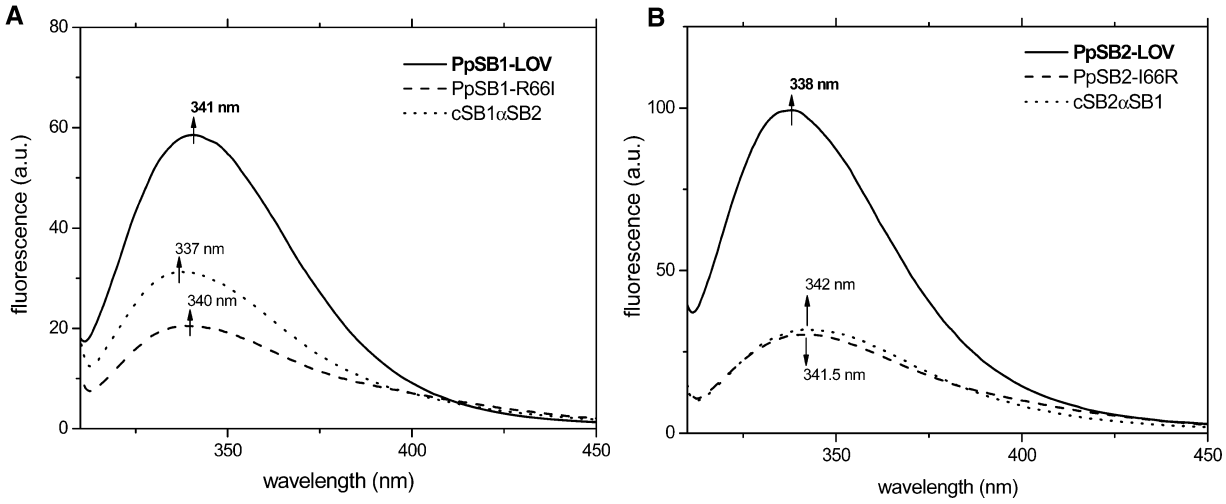

FIGURE 3: Fluorescence emission spectra of W94 for PpSB1-LOV (A) and PpSB2-LOV (B) and in the respective mutant proteins after excitation at 295 nm. The Trp emission spectra for the wild-type proteins are shown with solid lines. PpSB1-R66I and PpSB2-I66R are drawn in dashed lines. The spectra for the mutants with interchanged C-terminal extensions (cSB1αSB2 and cSB2αSB1) are depicted with dotted lines. In all cases the emission maxima are marked by an arrow.

employed by Buttani et al. (*30*) that assumes five pure components: (i) α-helices, (ii) turns and other structures, (iii) parallel/twisted β-sheets, (iv) random coils, and (v) antiparallel β-sheets. For all proteins the obtained CD spectra could be fitted well with the theoretically CCA-predicted curves. The total average rmsd between the calculated and experimental spectrum was in all cases well below 5%. All variants (even the mutants with the interchanged C-terminal extensions) (Figure 4) exhibit very similar CD spectra to the respective wild-type proteins (see Supporting Information Figure 3). For the two wild-type proteins, Table 3 summarizes the CCA analysis derived percentages for the five pure components. Table 4 shows a comparison between the theoretically expected secondary structure composition and the CD-derived values for the two wild-type LOV proteins. For both wild-type proteins and all mutants the differences between dark and light state CD spectra were small.

We compared the CD-derived secondary structural predictions for the two full-length *Pseudomonas* LOV proteins to known LOV domains by analyzing a set of currently available LOV domain crystal structures with respect to their content of α-helices, β-strands, and coil/turn structures (Table 4). On average, LOV-core domains (consisting of about 105 aa) contain about 27 amino acids in helical conformation, consist of about 40 aa β-strands, and contain 38 aa coils/turns and other structures.

As evident from Table 4, the CD-derived content of α-helices with about 45−47 aa for the two proteins clearly exceeds the theoretically expected value of 27 amino acids. The number of amino acids that in both *Pseudomonas* proteins constitute the β-scaffold closely matches the expected values. In both proteins, the number of amino acids in coil/turn structures exceeds the expected value by about 20, which is readily accounted for by the 20 amino acid long N-terminal tag and the introduced thrombin site (sequence: MGSSHHHHHH-SSGLVPRGSH).

DISCUSSION

Site-Directed Mutagenesis Combined with Microtiter Plate Prescreening Readily Identified Amino Acids Influencing the Dark Recovery. Our mutagenesis and prescreening strategy readily identified a number of PpSB1-LOV and PpSB2-LOV variants with altered dark recovery kinetics. Prescreening in microtiter plates allows for a fast and easy evaluation of the dark

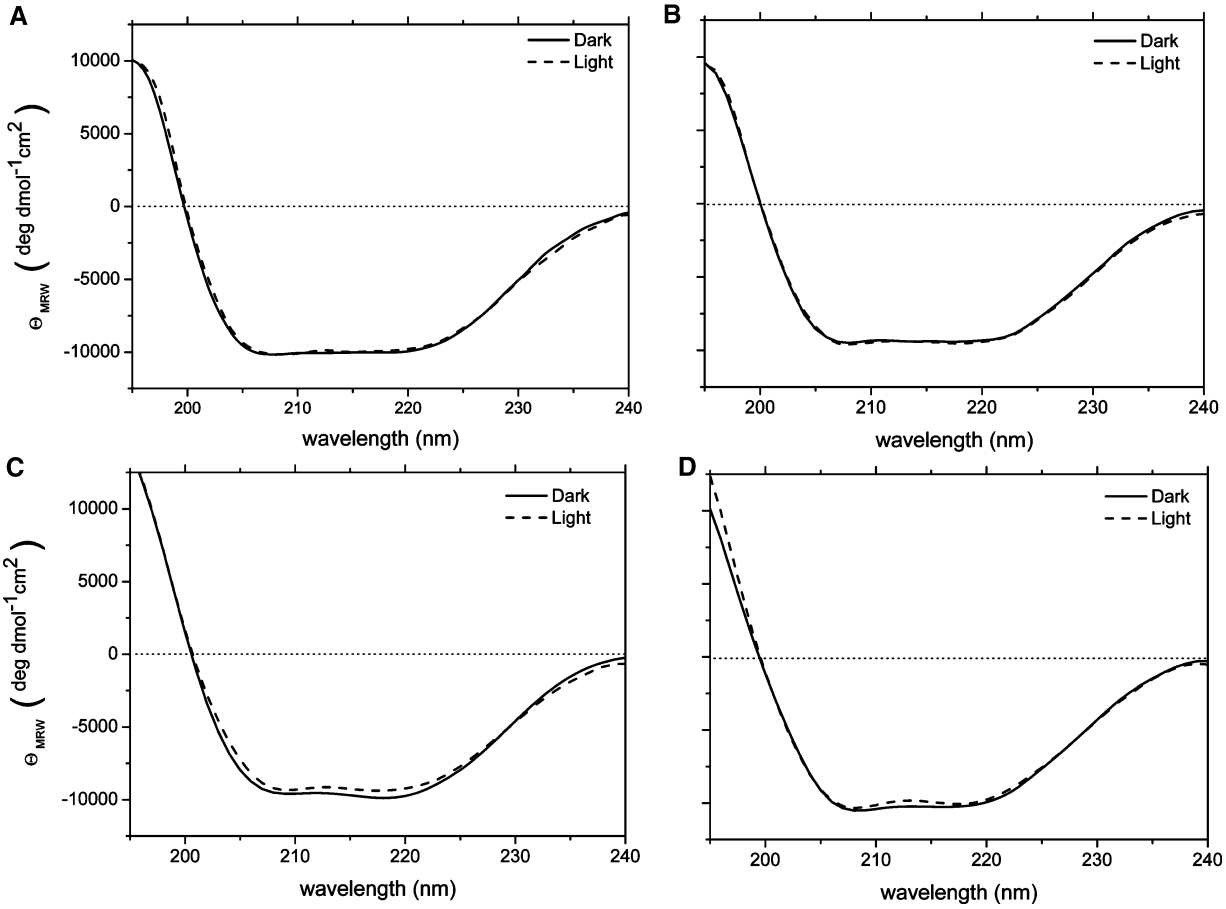

FIGURE 4: Far-UV CD spectra recorded for wild-type PpSB1-LOV (A) and PpSB2-LOV (B) as well as for cSB1/αSB2 (C) and cSB2/αSB1 (D). The depicted spectra represent the mean of two independent measurements on two different preparations. Spectra for the dark-adapted proteins are shown in solid lines whereas the corresponding spectra after 30 s of blue light illumination are depicted with dashed lines.

Table 3: Results of the CCA Analysis on CD Spectra

protein	α-helix (%)	turn and others (%)	twisted or parallel β-sheets (%)	random coil (%)	antiparallel β-sheets (%)
PpSB1 dark	29.0 ± 1.8	22.7 ± 1.6	13.5 ± 0	21.4 ± 2.6	13.5 ± 2.8
PpSB1 light	29.6 ± 1.0	22.5 ± 1.6	14.5 ± 0.3	20.9 ± 1.9	12.6 ± 1.0
PpSB2 dark	26.5 ± 0.7	23.0 ± 3.3	15.7 ± 0.5	19.3 ± 2.1	15.6 ± 1.1
PpSB2 light	26.5 ± 0.7	22.5 ± 2.6	16.2 ± 0.4	19.3 ± 1.3	15.6 ± 1.1

recovery kinetics of mutated LOV proteins without the need for protein purification. This strategy should be amenable to even higher throughput by cultivating mutant LOV protein expressing clones, e.g., derived from a mutant library (*26*), in 96-well deep-well plates. However, care has to be taken when interpreting the dark recovery time constants derived using such crude cell extracts. We observed quantitative but not qualitative differences between the values obtained with crude cell extracts and those with purified proteins. A similar effect has previously been observed for mutants of *B. subtilis* YtvA protein (A. Losi, personal communication). Thus, it appears that certain components in the *E. coli* crude extracts influence the dark recovery of LOV proteins. Nevertheless, such a prescreening approach, in particular when combined with microtiter plate cultivation, enables a fast and efficient selection of LOV mutants with altered photochemical reactivities. UV/vis spectroscopy (Supporting Information Figure 2) and CD spectroscopy (Figure 4 and Supporting Information Figure 3) performed on the respective purified wild-type and mutant proteins revealed proper folding of all constructs used throughout this study.

Protein−Chromophore Interactions around the FMN Phosphate Stabilize the Adduct State of LOV Domains. The amino acid in position 66 strongly influences the dark recovery in both proteins in a correlated manner. Moreover, in PpSB2-LOV, this mutation also affects the chromophore preference toward a PpSB1-LOV-like behavior (accepting only FMN) whereas the wild-type protein accepts both FMN and riboflavin in a ratio of 70/30. This in fact implies a physical interaction between R66 in PpSB1-LOV and the FMN phosphate. Whereas the mutation R66I in PpSB1-LOV accelerates the dark recovery of the mutant by 2 orders of magnitude, the corresponding mutation in PpSB2-LOV (I66R) slows down the recovery by roughly 1 order of magnitude. Interestingly, the corresponding mutation in PpSB1-LOV (R66I) does not result in a change of chromophore acceptance. This suggests additional structural components adding to the very slow dark

Table 4: Comparison between Expected and CD Predicted Secondary Structure Composition

protein	no. of amino acids		
	α-helix	β-strands	coils/turns/ others
consensus LOV core[a] (105 residues)	27 ± 1.8	40 ± 2.6	38 ± 4
PpSB1-LOV[b] (162 residues)	47 ± 3	44 ± 4	71 ± 3
PpSB2-LOV[b] (168 residues)	45 ± 1	54 ± 1	71 ± 5

[a]The expected secondary structure content for LOV domains was inferred from the available dark state structures. All crystal structures were truncated for the consensus LOV-core domain. Secondary structure content was predicted by using the DSSP algorithm. PDB coordinates: 1G28, 1N9O, 2PR5, 2V1A, 2Z6C, and 2Z6D. [b]For the full-length proteins PpSB1-LOV and PpSB2-LOV the number of amino acids in a given conformation are derived from two sets of CD measurements on two different preparations.

recovery time constant of PpSB1-LOV as well as to the strong preference for FMN.

The inspection of the homology models generated for the two LOV-core domains (for details see Materials and Methods) revealed that R66 in PpSB1-LOV is readily brought within hydrogen-bonding distance to the FMN phosphate by simply adjusting favorable rotamers (Figure 5A). The corresponding side chain, I66 in PpSB2-LOV, is apparently not able to contact the FMN phosphate in a similar manner (Figure 5B).

Laser-induced optoacoustic spectroscopy (LIOAS) on LOV domains and proteins revealed a high energy content of the photoadduct LOV390, e.g., 180 kJ/mol for *C. reinhardtii* LOV1 (CrLOV1) and 136 kJ/mol for *B. subtilis* YtvA indicating that the photoproduct stores more than 55% of the 0-0 energy (246.5 kJ/mol) (*44*). This high energy content of LOV390 ensures the enthalpic driving force for completion of the photocycle. In the dark state of LOV domains and in CrLOV1, the FMN phosphate is stabilized by hydrogen bonds and/or salt bridges with amino acids R58 and R74 corresponding to R54 and R70 in PpSB1-LOV and PpSB2-LOV, respectively (see Figure 5). Upon formation of the adduct state, the lateral chain of R58 in CrLOV1 moves slightly away from the FMN ribityl chain, resulting in a distance change between the FMN phosphate and R58. Concomitantly, the weak interactions between R74 and the FMN phosphate are strengthened. These movements help in stabilizing the adduct state and must be reversed for completion of the photocycle in the dark. Furthermore, Losi and co-workers demonstrated that the mutation of one of the two arginines that coordinate the FMN phosphate (R58, in CrLOV1) to lysine accelerated the dark recovery about 3-fold (*44*). A similar effect was observed for the corresponding mutation R63K in YtvA, where the recovery is accelerated 8-fold from 3900 to about 480 s at 20 °C (A. Losi, personal communication; Y. Tang, Z. Cao, E. Livoti, U. Krauss, K.-E. Jaeger, W. Gärtner, and A. Losi, submitted for publication). For CrLOV1 and YtvA, it was thus concluded that the substitution R58K hinders the conformational rearrangements around the FMN phosphate, as confirmed also by LIOAS data, destabilizing the adduct state and inducing the faster recovery of the respective mutant proteins. In PpSB1-LOV, residue R66 is located close to the second arginine coordinating the FMN phosphate (R74 on helix Fα in CrLOV1, R70 in PpSB1-LOV) and is thus located opposite to the photoactive cysteine and R54 (on helix Eα, corresponding to R58 in CrLOV1 and R63 in YtvA). In light of our data, one can speculate that in the adduct state of PpSB1-LOV, not only the

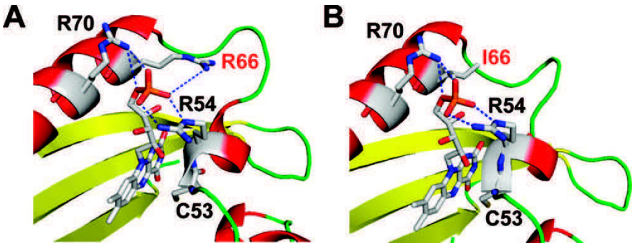

FIGURE 5: View of the FMN-binding pocket and the protein region surrounding the FMN phosphate for PpSB1-LOV and PpSB2-LOV, respectively. Both figures are derived from homology models of the PpSB1-LOV (A) and the PpSB2-LOV (B) LOV-core structures. The *C. reinhardtii* LOV1 structure (1n9O) was selected as template. The two highly conserved arginine residues (R54 and R70 in both proteins) that coordinate the FMN phosphate are labeled and shown in stick representation. The photoactive cysteine residue (C53 in both proteins) involved in the light-dependent adduct formation between the protein and the flavin-isoalloxazine ring is included for orientation. Additionally, the amino acid in position 66 in both *Pseudomonas* LOV proteins (R66 in PpSB1-LOV and I66 in PpSB2-LOV) is highlighted.

interaction with R70 (R74 in CrLOV1) is strengthened but also the interaction with R66. These rearrangements might further stabilize the adduct, e.g., by relieving some of the strain imposed on the protein/chromophore assembly present in the adduct state that results from the covalent linkage of the flavin isoalloxazine ring to the photoactive cysteine. This in turn results in a very slow dark recovery of the PpSB1-LOV protein. *Vice versa*, the absence of the stabilizing interaction in PpSB2-LOV and PpSB1-R66I results in a faster dark recovery much like in phot LOV domains. Studies on PpSB1-LOV and PpSB2-LOV using optoacoustics and the determination of the energy content of LOV390 in the two proteins would help to understand the peculiar features of the photocycle of two *P. putida* proteins and advance our understanding of the photochemistry of bacterial LOV proteins.

Notably, in the vast majority of LOV domains this position on helix Fα is occupied by a hydrophobic amino acid, which does not influence the recovery kinetics (e.g., V75 in YtvA, V462 in As-phot1 LOV2). The only other very slow reverting LOV domains of the FKF1/LKP2/ZTL LOV family (τ_{rec} = 62.5 h at room temperature) (*21*) contain a valine at the position corresponding to R66 in PpSB1-LOV; thus the very slow recovery of the FKF1 LOV proteins must result from a different mechanism as suggested here for the *P. putida* LOV proteins. Zikihara and co-workers speculated that the slow reversion may derive from the nine amino acid insertion to the LOV-core amino acid sequence between helix Eα and Fα. Notably, the latter two helices harbor the two arginines discussed above that in all LOV domains coordinate the FMN phsophate. Thus, it is tempting to speculate that the orientation of amino acids around the FMN phosphate, e.g., influenced by the insertion found in FKF1 LOV between Eα and Fα, might result in a stabilization of the adduct state and hence result in a very slow dark recovery reaction. In conclusion, the dependency of the dark recovery on the amino acid in position 66 in PpSB1-LOV and PpSB2-LOV must be a peculiar feature of the two *Pseudomonas* LOV proteins. However, the general mechanism of tuning the dark recovery by an intricate network of amino acids surrounding the FMN phosphate might well be a conserved mechanism present in all LOV domain systems.

In PpSB1-LOV and PpSB2-LOV the Dark Recovery Is Not Driven by Steric Constraint. Recently, Christie and co-workers could show that steric constraint can tune the dark

recovery kinetics in LOV domains, although mechanistically acting from the opposite side of the FMN-binding pocket (*26*). They identified one amino acid residue (I427, As-phot1 numbering) located in van der Waals contact with the sulfur atom of the photoreactive cysteine (C450). An exchange of this residue by valine accelerates the dark recovery 10-fold and slows down the adduct formation by a factor of 2 as revealed by laser flash photolysis measurements. The authors thus concluded that steric interactions in the protein around the FMN chromophore, specifically close to the photoreactive cysteine residue, can influence the dark recovery process either by stabilizing the adduct or by facilitating its decay. To address the latter issue for PpSB1-LOV and PpSB2-LOV, we have performed an investigation of the adduct formation kinetics of the two wild-type LOV proteins by time-resolved laser flash photolysis (Supporting Information Figure 6). The measurement did not reveal any major difference in the adduct formation kinetics for the two wild-type proteins. In PpSB1-LOV and PpSB2-LOV the FMN triplet (LOV660) decays to the adduct state with a time constant of 1.5 and 1.6 μs, respectively. Thus, we can rule out the involvement of a similar recovery-driving mechanism based on steric constraint in the FMN-binding pocket of the two *P. putida* LOV proteins. More likely, the adduct seems to be stabilized by the strengthened interaction of R66 and the FMN phosphate in PpSB1-LOV and PpSB2-I66R and destabilized in PpSB2-LOV and PpSB1-R66I. This stabilization versus destabilization then results in slow versus fast dark recovery reactions.

The Role of Histidines in the Dark Recovery. The effect of the mutation at position 61 (located about 6 Å from the FMN N5 in a loop connecting Eα and Fα helices) in both proteins would argue for a mechanism as proposed by Alexandre and co-workers (*25*). The authors suggested histidine-driven base catalysis from a surface-exposed His residue in quite some distance to the FMN chromophore via a hydrogen-bonding network. The kinetic effect (3−4-fold change) observed for the R61H mutation in PpSB1-LOV and the H61R mutation in PpSB2-LOV, respectively, showed about the same order of magnitude as reported by Alexandre et al. (2-fold change). Here, the authors blocked the histidines of AsLOV2 with diethyl pyrocarbonate (DEPC), a histidine-specific modifying agent resulting in a slowed dark recovery. However, this putative mechanism seems to be much less effective in the two *Pseudomonas* LOV proteins, compared to the tuning of the dark recovery by the FMN phosphate/protein interaction. Thus, at least H61 in PpSB2-LOV is not solely responsible for the fast dark recovery of the protein. It should be noted here that PpSB2-LOV possesses four histidines (one in the N-terminal extension (H13), two in the LOV core (H61, H103), and one in the C-terminal extension (H148)) whereas PpSB1-LOV contains none. The mutation of the second His residue in PpSB2-LOV (H13) had no apparent effect on the recovery of PpSB2-LOV whereas the corresponding mutation A13H in PpSB1-LOV renders the recovery even slower compared to the wild-type protein (data not shown). The two other histidines H103 and H148 were not considered for mutation due to their large distance to the FMN molecule.

The Partially Helical LOV-Core Extensions Influence the Recovery of Both Pseudomonas LOV Proteins but Do Not Undergo Pronounced Conformational Changes. In the far-UV region both wild-type proteins possess typical CD spectra of proteins rich in α-helical and β-sheet content (*45*) much like other LOV proteins for which CD data are available (*30*, *46*−*48*). We are aware that CD spectroscopy is not a precise method for the determination of secondary structure content. In particular, the spectra of pure α-helices and antiparallel β-sheet structures are very similar and thus sometimes difficult to separate during deconvolution. Nevertheless, based on previous data and component curve assignments (*30*), our CD spectra suggest that in PpSB1-LOV and PpSB2-LOV about 20 amino acids in the N- and C-terminal extensions should be in a helical conformation. Under the assumption of a canonical LOV fold, the N- and C-terminal extensions account for about 40 residues which may thus adopt a partial helical structure. In comparison, the N- and C-terminal extensions of the monomeric LOV construct of *A. sativa* phot1-LOV2 that was recently crystallized (PDB access code 2v1a) contain in sum about 24 amino acids in a helical conformation. In the dimeric *B. subtilis* YtvA-LOV crystal structure (2pr5), which is so far the only structure available for a bacterial LOV protein, the C-terminal extension to the LOV core contains about 18 amino acids in a helical conformation. Thus, despite the lack of sequence similarity between the corresponding protein regions, similar structural elements, namely, an N-terminal helical cap structure and a C-terminal Jα helix, appear to be present outside of the conserved LOV core in different plant and bacterial LOV proteins. However, the orientation of the C-terminal Jα helix in the two *Pseudomonas* LOV proteins cannot be resolved without additional structural information. For plant phototropins, the LOV2 associated Jα helix was suggested to promote signaling from the LOV2 domain to the phot kinase (*49*). This notion was based on solution NMR studies (*49*−*51*), indicating that light triggers the displacement or unfolding of the C-terminal Jα helix that connects the LOV2 domain to the kinase in full-length phot. This in turn results in the autophosphorylation of the phot kinase and might allow for downstream signaling and initiation the phototrophic response. For plant LOV2 systems, this model has also found support through CD spectroscopy (*47*, *48*) and time-resolved thermal grating and thermal lens experiments (*52*). However, for bacterial LOV systems, so far no light-dependent loss of helical content could be observed using CD spectroscopy (*30*). Similar to those latter observations, we did not observe any significant light-dependent loss of helicity for the two *P. putida* LOV proteins. However, on the basis of CD data alone we cannot rule out that a structural rearrangement takes place which is not accompanied by a loss of secondary structure, e.g., involving a movement or the rotation of the helices.

Influence and Orientation of the C-Terminal Extension. In this study, only the C-terminal (Jα helix) extensions of PpSB1-LOV and PpSB2-LOV were interchanged between the two proteins as the extensions N-terminal to the LOV core did not differ significantly in their amino acid sequence. This exchange had a pronounced effect on the recovery of PpSB1-LOV and PpSB2-LOV, accelerating the recovery of cSB1/αSB2 by a factor of 2 and slowing down the recovery of cSB2/αSB1 by a factor of 3 with respect to the wild-type proteins. The kinetic effect of interchanging the C-terminal extensions on the dark recovery process, as well as the influence of the interchange on the spectral properties of the sole Trp residue (W94), is clear evidence for an interaction of the C-terminal extension with residues that directly or indirectly interact with the FMN chromophore. The latter result moreover indicated that the respective extensions are located close to W94 in both proteins. A "helix-out" orientation, as in the crystal structure of YtvA-LOV (*53*) (Supporting Information Figure 5C), would nicely account for the observed phenomena, since W103 in YtvA-LOV and the corresponding

W94 in both *Pseudomonas* LOV proteins are in close proximity to the Jα extension in a "helix-out" conformation. Still, in the AsLOV2 structure, where the Jα helix packs against the LOV-core β-scaffold in a "helix-in" conformation, the sole Trp (W491, As-phot1 numbering) similarly contacts the Jα helix in a hinge region that connects the AsLOV2 core to the Jα helix (Supporting Information Figure 5D) (*54*). When we align the respective C-terminal extensions of PpSB1-LOV and PpSB2-LOV to the corresponding Jα helix in either YtvA-LOV or AsLOV2 (not shown), a higher similarity to the Jα helix of YtvA-LOV (about 20% identical and 40% similar positions) compared to AsLOV2 (15% identical and 21% similar positions) is detected. This, together with the dimeric organization of the two proteins (YtvA LOV is dimeric and AsLOV2 forms a monomer), might point toward a similar ("helix-out") orientation of the C-terminal extension in the two *Pseudomonas* LOV proteins and the truncated YtvA-LOV construct of the crystal structure. However, without further structural data, no unequivocal conclusions can be made as to the orientation both N- and C-terminal extensions as well as to the mode of dimerization.

Functional Significance and Phylogenetic Conservation of PpSB1-LOV- and PpSB2-LOV-like Proteins in Different Pseudomonas Strains. The lack of a fused effector domain in both *Pseudomonas* proteins suggests that protein−protein interactions must play a role in signaling by the two LOV proteins. The observation of a blue light effect in *P. putida*, such that selectively blue light irradiation results in an increased excretion of the iron scavenger pyoverdine under iron-limiting conditions (Krauss, Ph.D. Thesis, 2008), suggests that either PpSB1-LOV and/or PpSB2-LOV, as the only blue light receptors in the completely sequenced *P. putida* genome, could be involved in this physiological response. The presence of two highly similar LOV proteins with very different kinetic properties in the same organism raises the question whether these differences bear any functional importance or, more generally, whether the velocity of the dark recovery influences the biological sensor function of these LOV proteins. In such case, evolution should have retained those different velocities over time, and certain functional classes of LOV photoreceptors should show similar dark recovery kinetics. A recent review revealed that about 13% of the up to now identified bacterial LOV proteins are so-called "short" LOV's lacking a fused effector domain (*4*) but probably contain N- and C-terminal extensions of varying length. Thus, the two LOV proteins of *P. putida* KT2440 constitute the first two characterized examples of a structurally conserved family of bacterial LOV proteins whose biological function(s) remain(s) yet elusive. This family is largely restricted to proteobacterial lineages with members present in different Pseudomonads as well as in a few phototrophic α-Proteobacteria such as *Rhodobacter sphaeroides* (*4*). In several *Pseudomonas* strains like *P. putida* F1, *P. putida* W619, and *P. putida* KT2440, from which the two LOV proteins of this study have been cloned, invariably two "short" LOV proteins are present. A phylogenetic tree generated for several "short" *Pseudomonas* LOV proteins supports a classification into PpSB1-LOV and PpSB2-LOV-like clades (see Supporting Information Figure 4) and thus highlights the possibility of retaining fast (PpSB2-LOV) and slow reverting (PpSB1-LOV) proteins in one organism at a time. Moreover, in all LOV proteins affiliated with the PpSB1-LOV- like clade, invariably an arginine is present in the position corresponding to R66 in PpSB1-LOV. *Vice versa*, all proteins of the PpSB2-LOV-like clade possess an isoleucine corresponding to I66 in PpSB2-LOV (alignment not shown). This observation points toward an evolutionary (and maybe functional) conservation of LOV photochemical properties and implies the conservation of slow (PpSB1-LOV-like) and fast (PpSB2-LOV-like) recovering sensor proteins within one organism. Physiological studies currently underway in our laboratory will provide insights into this peculiar genetic feature of the genus *P. putida*.

CONCLUSIONS

Our study, performed on two highly similar bacterial LOV proteins, highlights the importance of residues in the FMN-binding pocket that form an intricate network to tune the dark recovery in LOV proteins. This effect can be drastic, since apparently a single mutation, namely, R66I in PpSB1-LOV, is sufficient to accelerate the dark recovery process by 2 orders of magnitude. The opposite mutation in PpSB2-LOV decelerates the kinetics significantly. Thus, our study indicates that strain, presumably imposed on the chromophore in the adduct state, effectively tunes the dark recovery in LOV proteins. Most importantly, stabilization versus destabilization of the adduct state seems to occur from amino acids surrounding the FMN phosphate. This mechanism, albeit realized differently in different proteins, might well represent a general mechanism for tuning the dark recovery in all LOV domain systems. An additional kinetic effect driven from surface-exposed histidine residues, suggested to be in place in plant LOV domains, cannot be ruled out to influence the dark recovery. However, based on our mutational analysis, this effect should be much less efficient as compared to tuning of the dark recovery caused by the R66−FMN phosphate interaction. While this report was under revision, a comprehensive study identified additional amino acid positions that effectively tune the dark recovery in different plant and bacterial LOV systems (*55*). Although the identified residues and the observed kinetic effects are different from those described here, the study further highlights the importance of the intricate network of amino acids surrounding the FMN chromophore that effectively tunes the dark recovery in LOV domains. CD experimental data led us to conclude that N- and C-terminal extensions to the LOV core in the two *Pseudomonas* proteins are at least partially helical. The absence of significant light-dependent secondary structural changes, mainly the absence of the loss of helical content, highlights the hypothesis that the signal-propagation mechanisms might not be conserved between plant and bacterial LOV systems. Nevertheless, conserved structural elements like the C-terminal (Jα) helical extensions could play a role in the signal propagation from the flavin chromophore in LOV domains to fused or interacting effector domains via LOV-associated structural elements.

ACKNOWLEDGMENT

The authors thank Björn Zorn (Max-Planck-Institute for Bioinorganic Chemistry, Muelheim an der Ruhr, Germany) for laser flash photolysis measurements.

SUPPORTING INFORMATION AVAILABLE

Table 1, oligonucleotides used throughout this study; Figure 1, multiple sequence alignment of LOV domains aiding mutation selection; Figure 2, UV/vis spectra of mutant LOV proteins; Figure 3, CD spectra of mutant LOV proteins; Figure 4, phylogenetic tree generated for selected *Pseudomonas* "short" LOV proteins; Figure 5, Jα helix orientations observed in

bacterial and plant LOV domain structures; Figure 6, laser flash photolysis measurements on PpSB1-LOV and PpSB2-LOV. This material is available free of charge via the Internet at http://pubs.acs.org.

REFERENCES

1. Christie, J. M., Salomon, M., Nozue, K., Wada, M., and Briggs, W. R. (1999) LOV (light, oxygen, or voltage) domains of the blue-light photoreceptor phototropin (nph1): binding sites for the chromophore flavin mononucleotide. *Proc. Natl. Acad. Sci. U.S.A. 96*, 8779–8783.
2. Briggs, W. R., and Christie, J. M. (2002) Phototropins 1 and 2: versatile plant blue-light receptors. *Trends Plant Sci. 7*, 204–210.
3. Ohgishi, M., Saji, K., Okada, K., and Sakai, T. (2004) Functional analysis of each blue light receptor, cry1, cry2, phot1, and phot2, by using combinatorial multiple mutants in *Arabidopsis*. *Proc. Natl. Acad. Sci. U.S.A. 101*, 2223–2228.
4. Losi, A., and Gärtner, W. (2008) Bacterial bilin- and flavin-binding photoreceptors. *Photochem. Photobiol. Sci. 7*, 1168–1178.
5. Losi, A., Polverini, E., Quest, B., and Gärtner, W. (2002) First evidence for phototropin-related blue-light receptors in prokaryotes. *Biophys. J. 82*, 2627–2634.
6. Krauss, U., Losi, A., Gärtner, W., Jaeger, K. E., and Eggert, T. (2005) Initial characterization of a blue-light sensing, phototropin-related protein from *Pseudomonas putida*: a paradigm for an extended LOV construct. *Phys. Chem. Chem. Phys. 7*, 2804–2811.
7. Losi, A. (2006) Flavin-based photoreceptors in bacteria, in Flavins: Photochemistry and Photobiology (Silva, E., and Edwards, A. M., Eds.) The Royal Society of Chemistry, Cambridge, U.K.
8. Avila-Perez, M., Hellingwerf, K. J., and Kort, R. (2006) Blue light activates the sigmaB-dependent stress response of *Bacillus subtilis* via YtvA. *J. Bacteriol. 188*, 6411–6414.
9. Purcell, E. B., Siegal-Gaskins, D., Rawling, D. C., Fiebig, A., and Crosson, S. (2007) A photosensory two-component system regulates bacterial cell attachment. *Proc. Natl. Acad. Sci. U.S.A. 104*, 18241–18246.
10. Swartz, T. E., Tseng, T. S., Frederickson, M. A., Paris, G., Comerci, D. J., Rajashekara, G., Kim, J. G., Mudgett, M. B., Splitter, G. A., Ugalde, R. A., Goldbaum, F. A., Briggs, W. R., and Bogomolni, R. A. (2007) Blue-light-activated histidine kinases: two-component sensors in bacteria. *Science 317*, 1090–1093.
11. Kennis, J. T., Crosson, S., Gauden, M., van Stokkum, I. H., Moffat, K., and van Grondelle, R. (2003) Primary reactions of the LOV2 domain of phototropin, a plant blue-light photoreceptor. *Biochemistry 42*, 3385–3392.
12. Kottke, T., Heberle, J., Hehn, D., Dick, B., and Hegemann, P. (2003) Phot-LOV1: photocycle of a blue-light receptor domain from the green alga *Chlamydomonas reinhardtii*. *Biophys. J. 84*, 1192–1201.
13. Swartz, T. E., Corchnoy, S. B., Christie, J. M., Lewis, J. W., Szundi, I., Briggs, W. R., and Bogomolni, R. A. (2001) The photocycle of a flavin-binding domain of the blue light photoreceptor phototropin. *J. Biol. Chem. 276*, 36493–36500.
14. Pfeifer, A., Majerus, T., Zikihara, K., Matsuoka, D., Tokutomi, S., Heberle, J., and Kottke, T. (2009) Time-resolved Fourier transform infrared study on photoadduct formation and secondary structural changes within the phototropin LOV domain. *Biophys. J. 96*, 1462–1470.
15. Kennis, J. T. M., and Akexandre, M. T. A. (2006) Mechanisms of light activation in flavin-binding photoreceptors, in Flavins: Photochemistry and Photobiology (Silva, E., and Edwards, A. M., Eds.) pp 287−319, Royal Society for Chemistry, Cambridge, U.K.
16. Alexandre, M. T., Domratcheva, T., Bonetti, C., van Wilderen, L. J., van Grondelle, R., Groot, M. L., Hellingwerf, K. J., and Kennis, J. T. (2009) Primary reactions of the LOV2 domain of phototropin studied with ultrafast mid-infrared spectroscopy and quantum chemistry. *Biophys. J. 97*, 227–237.
17. Pfeifer, A., Majerus, T., Zikihara, K., Matsuoka, D., Tokutomi, S., Heberle, J., and Kottke, T. (2009) Time-resolved Fourier transform infrared study on photoadduct formation and secondary structural changes within the phototropin LOV domain. *Biophys. J. 96*, 1462–1470.
18. Neiss, C., and Saalfrank, P. (2007) Ab initio quantum chemical investigation of the first steps of the photocycle of phototropin: a model study. *Photochem. Photobiol. 77*, 101–109.
19. Domratcheva, T., Fedorov, R., and Schlichting, I. (2006) Analysis of the primary photocycle reactions occurring in the light-oxygen-voltage blue-light receptor by multiconfigurational quantum-chemical methods. *J. Chem. Theory Comput. 2*, 1565–1574.
20. Losi, A. (2004) The bacterial counterparts of plants phototropins. *Photochem. Photobiol. Sci. 3*, 566–574.
21. Zikihara, K., Iwata, T., Matsuoka, D., Kandori, H., Todo, T., and Tokutomi, S. (2006) Photoreaction cycle of the light, oxygen, and voltage domain in FKF1 determined by low-temperature absorption spectroscopy. *Biochemistry 45*, 10828–10837.
22. Zoltowski, B. D., Schwerdtfeger, C., Widom, J., Loros, J. J., Bilwes, A. M., Dunlap, J. C., and Crane, B. R. (2007) Conformational switching in the fungal light sensor Vivid. *Science 316*, 1054–1057.
23. Crosson, S., and Moffat, K. (2001) Structure of a flavin-binding plant photoreceptor domain: insights into light-mediated signal transduction. *Proc. Natl. Acad. Sci. U.S.A. 98*, 2995–3000.
24. Fedorov, R., Schlichting, I., Hartmann, E., Domratcheva, T., Fuhrmann, M., and Hegemann, P. (2003) Crystal structures and molecular mechanism of a light-induced signaling switch: the Phot-LOV1 domain from *Chlamydomonas reinhardtii*. *Biophys. J. 84*, 2474–2482.
25. Alexandre, M. T., Arents, J. C., van Grondelle, R., Hellingwerf, K. J., and Kennis, J. T. (2007) A base-catalyzed mechanism for dark state recovery in the *Avena sativa* phototropin-1 LOV2 domain. *Biochemistry 46*, 3129–3137.
26. Christie, J. M., Corchnoy, S. B., Swartz, T. E., Hokenson, M., Han, I. S., Briggs, W. R., and Bogomolni, R. A. (2007) Steric interactions stabilize the signaling state of the LOV2 domain of phototropin 1. *Biochemistry 46*, 9310–9319.
27. Guo, H., Kottke, T., Hegemann, P., and Dick, B. (2005) The phot LOV2 domain and its interaction with LOV1. *Biophys. J. 89*, 402–412.
28. Studier, F. W. (2005) Protein production by auto-induction in high density shaking cultures. *Protein Expression Purif. 41*, 207–234.
29. Sambrook, J., and Russell, D. (2001) Molecular cloning: a laboratory manual, 3rd ed., Cold Spring Harbor Laboratory Press, Cold Spring Harbor, NY.
30. Buttani, V., Losi, A., Eggert, T., Krauss, U., Jaeger, K. E., Cao, Z., and Gärtner, W. (2007) Conformational analysis of the blue-light sensing protein YtvA reveals a competitive interface for LOV-LOV dimerization and interdomain interactions. *Photochem. Photobiol. Sci. 6*, 41–49.
31. Whitmore, L., and Wallace, B. A. (2004) DICHROWEB, an online server for protein secondary structure analyses from circular dichroism spectroscopic data. *Nucleic Acids Res. 32*, W668–W673.
32. Cao, Z., Buttani, V., Losi, A., and Gärtner, W. (2007) A blue light inducible two component signal transduction system in the plant pathogen *Pseudomonas syringae* pv. tomato. *Biophys. J. 94*, 897–905.
33. Schuler, L. D., Daura, X., and Van Gunsteren, W. F. (2001) An improved GROMOS96 force field for aliphatic hydrocarbons in the condensed phase. *J. Comput. Chem. 22*, 1205–1218.
34. Guex, N., and Peitsch, M. C. (1997) SWISS-MODEL and the Swiss-PdbViewer: an environment for comparative protein modeling. *Electrophoresis 18*, 2714–2723.
35. Gerber, P. R., and Muller, K. (1995) Mab, a generally applicable molecular-force field for structure modeling in medicinal chemistry. *J. Comput.-Aided Mol. Des. 9*, 251–268.
36. Emsley, P., and Cowtan, K. (2004) Coot: model-building tools for molecular graphics. *Acta Crystallogr. D 60*, 2126–2132.
37. Nicholas, K., Nicholas, H. J., and Deerfield, D. (1997) GeneDoc: analysis and visualization of genetic variation. *EMBNEWS 4*, 14.
38. Guindon, S., Lethiec, F., Duroux, P., and Gascuel, O. (2005) PHYML Online—a web server for fast maximum likelihood-based phylogenetic inference. *Nucleic Acids Res. 33*, W557–W559.
39. Keane, T. M., Naughton, T. J., and McInerney, J. O. (2007) MultiPhyl: a high-throughput phylogenomics webserver using distributed computing. *Nucleic Acids Res. 35*, W33–37.
40. Vinh le, S., and von Haeseler, A. (2004) IQPNNI: moving fast through tree space and stopping in time. *Mol. Biol. Evol. 21*, 1565–1571.
41. Drummond, A. J., and Rambaut, A. (2006) BEAST v1.4 , available from http://beast.bio.ed.ac.uk/.
42. Losi, A., Quest, B., and Gärtner, W. (2003) Listening to the blue: the time-resolved thermodynamics of the bacterial blue-light receptor YtvA and its isolated LOV domain. *Photochem. Photobiol. Sci. 2*, 759–766.
43. Losi, A., Ghiraldelli, E., Jansen, S., and Gärtner, W. (2005) Mutational effects on protein structural changes and interdomain interactions in the blue-light sensing LOV protein YtvA. *Photochem. Photobiol. 81*, 1145–1152.
44. Losi, A., Kottke, T., and Hegemann, P. (2004) Recording of blue light-induced energy and volume changes within the wild-type and mutated phot-LOV1 domain from *Chlamydomonas reinhardtii*. *Biophys. J. 86*, 1051–1060.

45. Fasman, G. D. (1996) Circular dichroism and the conformational analysis of biomolecules, Plenum Press, New York, NY.
46. Katsura, H., Zikihara, K., Okajima, K., Yoshihara, S., and Tokutomi, S. (2009) Oligomeric structure of LOV domains in *Arabidopsis* phototropin. *FEBS Lett. 583*, 526–530.
47. Nash, A. I., Ko, W. H., Harper, S. M., and Gardner, K. H. (2008) A conserved glutamine plays a central role in LOV domain signal transmission and its duration. *Biochemistry 47*, 13842–13849.
48. Corchnoy, S. B., Swartz, T. E., Lewis, J. W., Szundi, I., Briggs, W. R., and Bogomolni, R. A. (2003) Intramolecular proton transfers and structural changes during the photocycle of the LOV2 domain of phototropin 1. *J. Biol. Chem. 278*, 724–731.
49. Harper, S. M., Christie, J. M., and Gardner, K. H. (2004) Disruption of the LOV-Jalpha helix interaction activates phototropin kinase activity. *Biochemistry 43*, 16184–16192.
50. Harper, S. M., Neil, L. C., and Gardner, K. H. (2003) Structural basis of a phototropin light switch. *Science 301*, 1541–1544.
51. Yao, X., Rosen, M. K., and Gardner, K. H. (2008) Estimation of the available free energy in a LOV2-J alpha photoswitch. *Nat. Chem. Biol. 4*, 491–497.
52. Nakasone, Y., Eitoku, T., Matsuoka, D., Tokutomi, S., and Terazima, M. (2007) Dynamics of conformational changes of *Arabidopsis* phototropin 1 LOV2 with the linker domain. *J. Mol. Biol. 367*, 432–442.
53. Möglich, A., and Moffat, K. (2007) Structural basis for light-dependent signaling in the dimeric LOV domain of the photosensor YtvA. *J. Mol. Biol. 373*, 112–126.
54. Halavaty, A. S., and Moffat, K. (2007) N- and C-terminal flanking regions modulate light-induced signal transduction in the LOV2 domain of the blue light sensor phototropin 1 from *Avena sativa*. *Biochemistry 46*, 14001–14009.
55. Zoltowski, B. D., Vaccaro, B., and Crane, B. R. (2009) Mechanism-based tuning of a LOV domain photoreceptor, Nat. Chem. Biol. (Epub ahead of print doi:10.1038/nchembio.210).

Unpublished supplementary data to chapter 2.1

A transient absorption study of the adduct formation kinetics of the twin *Pseudomonas putida* LOV proteins and selected variants

Katrin Jentzsch[1], Roger-Jan Kutta[2], Bernhard Dick[2], Karl-Erich Jaeger[1] and Ulrich Krauss[1]

1: Institut für Molekulare Enzymtechnologie, Heinrich-Heine-Universität Düsseldorf, Forschungszentrum Jülich,

2: Lehrstuhl für Physikalische Chemie, Institut für Physikalische und Theoretische Chemie, Universität Regensburg

Abstract

In order to address whether the mutations described in 2.1 that drastically alter the dark recovery kinetics of PpSB1-LOV and PpSB2-LOV (*1*) also influence the forward kinetic process (here measured as triplet decay), we carried out transient absorption measurements in the microsecond time-range for the two wild-type proteins as well as for a set of four variants. In comparison to previous laser-flash photolysis experiments performed for the two wild-type proteins (see chapter 2.1, (*1*)) similar triplet decay times are obtained. None of the introduced mutations had a significant impact on the triplet decay and thus adduct formation kinetics. The presented data thus essentially rules out that structural differences in the FMN binding-pocket realized selectively in the dark state of PpSB1-LOV and PpSB2-LOV are the driving force behind the drastically different dark recovery reactions.

Introduction

Time resolved and transient absorption spectroscopy

In physics and physical chemistry, spectroscopic techniques are being used widely to study dynamic processes in materials, chemical compounds or solutions. One of these techniques is called time resolved spectroscopy. It is mostly used to study processes that occur after illumination by a light pulse, but in principle, this technique can be applied to any process that leads to a change in properties of a material or solution.

In transient-absorption spectroscopy, which poses an extension of absorption spectroscopy, the absorbance at a particular wavelength or range of wavelengths of a sample is detected as a function of time after excitation by a flash of light. Typically, both the excitation light (”pump”) and the light for measuring the absorbance (”probe”) are generated by a pulsed laser. In transient absorption spectroscopy, a fraction of the molecules is promoted to an electronically excited state by means of an excitation (or pump) pulse. A weak probe pulse (i.e., a pulse that has such a low intensity that multiphoton/multistep processes are avoided during probing) is sent through the sample with a delay τ with respect to the pump pulse. A difference absorption spectrum is then calculated, i.e., the absorption spectrum of the excited sample minus the absorption spectrum of the sample in the ground state (DA). By changing the time delay τ between the pump and the probe and recording a DA spectrum at each time delay, a DA profile as a function of τ and wavelength λ, i.e., a DA (λ, τ) is obtained. DA (λ, τ) contains information on the dynamic processes that occur in the system under study, such as excited state energy migration, electron and/or proton transfer processes, isomerization, and intersystem crossing. In order to extract this information, global analysis procedures may be applied (see below). One advantage of time-resolved absorption spectroscopy over for example time-resolved fluorescence is that with the former, the evolution of non-emissive states and dark states can be investigated (*2*). Some examples for processes that can be studied using this technique are optical gain spectroscopy of semiconductor laser materials (*3, 4*), the behavior of electrons that are freed from a molecule or crystalline material (*5*), the transfer of excitation energy between molecules, parts of molecules, or molecules and their environment (*6, 7*) or, as in the here presented case chemical reactions that are initiated by light or so called photoinduced chemical reactions (*8, 9*).

Photocycle and reaction kinetics of LOV photoreceptors

Among all currently photochemically characterized LOV proteins, the light-signalling mechanism mediated by them is accepted to be highly conserved. In brief, the LOV domain bound flavin mononucleotide (FMN) molecule is excited from the dark or ground state to its excited singlet state on a ps-to ns-time scale

(*10*). From the singlet excited state radiative (fluorescence) and non-radiative decay processes in part result in recovery of the ground-state. For a fraction of the excited FMN molecules intersystem crossing occurs within ns resulting in the population of the FMN triplet state (*10*). From the triplet state, the signalling state is formed within µs to give rise to a covalent bond between the 4a-carbon of the flavin chromophore and the SH-group of a crucial, fully conserved, cysteine in the canonical sequence motif (GXN**C**RFLQ, Cysteine shown in bold) (*11*, *12*). The latter mentioned signalling state is known to be the longest living species of the LOV photocycle, it reverts back into the ground state thermally within seconds to days for plant and bacterial LOV domains (*1, 13-15*). Whereas many mutational studies have been carried out to assess the mechanism of the LOV domain dark-recovery reaction (*1, 14, 16-19*), mechanistic aspects of the forward reaction resulting in adduct formation are far from understood, presumably mostly due to the short lifetime of potential intermediates and species therein. Christie and co-workers, demonstrated in a mutational study using the *A. sativa* phototropin1 LOV2 domain, that steric interactions responsible for accelerating the dark-recovery process (*16*), also influenced adduct formation reaction kinetics. In an earlier study (see chapter 2.1 of this dissertation) (*1*), laser-flash photolysis (another time-resolved spectroscopic technique) was used to address this issue by measuring adduct formation kinetics for the slow and fast reverting PpSB1-LOV and PpSB2-LOV proteins. For the two wild-type proteins no major differences in the adduct formation kinetics were observed essentially ruling out a similar adduct stabilizing mechanism as suggest by Christie and co-workers (*16*). In order to address whether the mutation that drastically alter dark recovery kinetics of PpSB1-LOV and PpSB2-LOV also influence the forward kinetic process, we here carried out transient absorption measurements for a set of four variants. For PpSB1-LOV R66I and PpSB1-LOV R61H the dark recovery reaction was accelerated about 100- or 3-fold, respectively (see, chapter 2.1 (*1*)). The mutual exchange of the corresponding amino acid positions in PpSB2-LOV (I66R or H61R) resulted in an about 7 or 4-fold slower dark recovery process (see chapter 2.1 (*1*). As reference, the respective wild-type proteins were studied. All experimental work was carried out during a lab-visit at the chair of Prof. Bernhard Dick (Lehrstuhl für Physikalische Chemie, Institut für Physikalische und Theoretische Chemie, Universität Regensburg) by Dr. Roger-Jan Kutta.

Material and Methods

Protein overexpression and purification

PpSB1-LOV, PpSB2-LOV as well as the corresponding R66I, R61H and I66R, H61R mutants were expressed and purified as described in Jentzsch et al. 2009 (see chapter 2.1, (*1*)). All proteins were freshly prepared for this study and stored at 4 °C in the dark in 10 mM sodium-phosphate buffer pH 8 supplemented with 10 mM NaCl.

Time-resolved UV/Vis absorption measurements

For the measurements a quartz flow cuvette with 2 mm optical path length for excitation and 10 mm for probe light was used. This cuvette was connected via flexible Teflon tubes with a storage vessel. A peristaltic pump was employed to pump the sample through the cuvette during the measurement. The overall sample volume was about 10 mL. The sample was excited at 450 nm by an Optical Parametric Oscillator (OPO, Continuum Inc., Santa Clara, CA, USA) pumped by the third harmonic of a Nd:YAG laser (Surelite II, Continuum Inc,, Santa Clara, CA, USA) with a pulse width of 8-10 ns.

The setup of the transient absorption spectrometer with streak camera has been described elsewhere (*20*). All measurements were carried out during a 2-week lab-visit at the chair of Prof. Bernhard Dick, Lehrstuhl für Physikalische Chemie, Molecular Spectroscopy and Photochemistry, (University of Regensburg, Germany) in close cooperation with Dr. Jan-Roger Kutta.

Results

Figure 2 depicts the decay associated spectra (DAS) in three dimensions (time/µs, wavelength, ΔO.D) of all measurements, accumulated over 100 laser shots, each recorded over a time-window of 5 µs at pH 8. On the x-axis the time in µs is depicted, on the y-axis the wavelength in the relevant range from ~ 350 to 720 nm is shown. Hereby the color code used in the Figure and shown on the right hand of each graph visualizes ΔO.D values, ranging from black (zero opitical density change), red to yellow (positive values) and from green to blue (negative values).

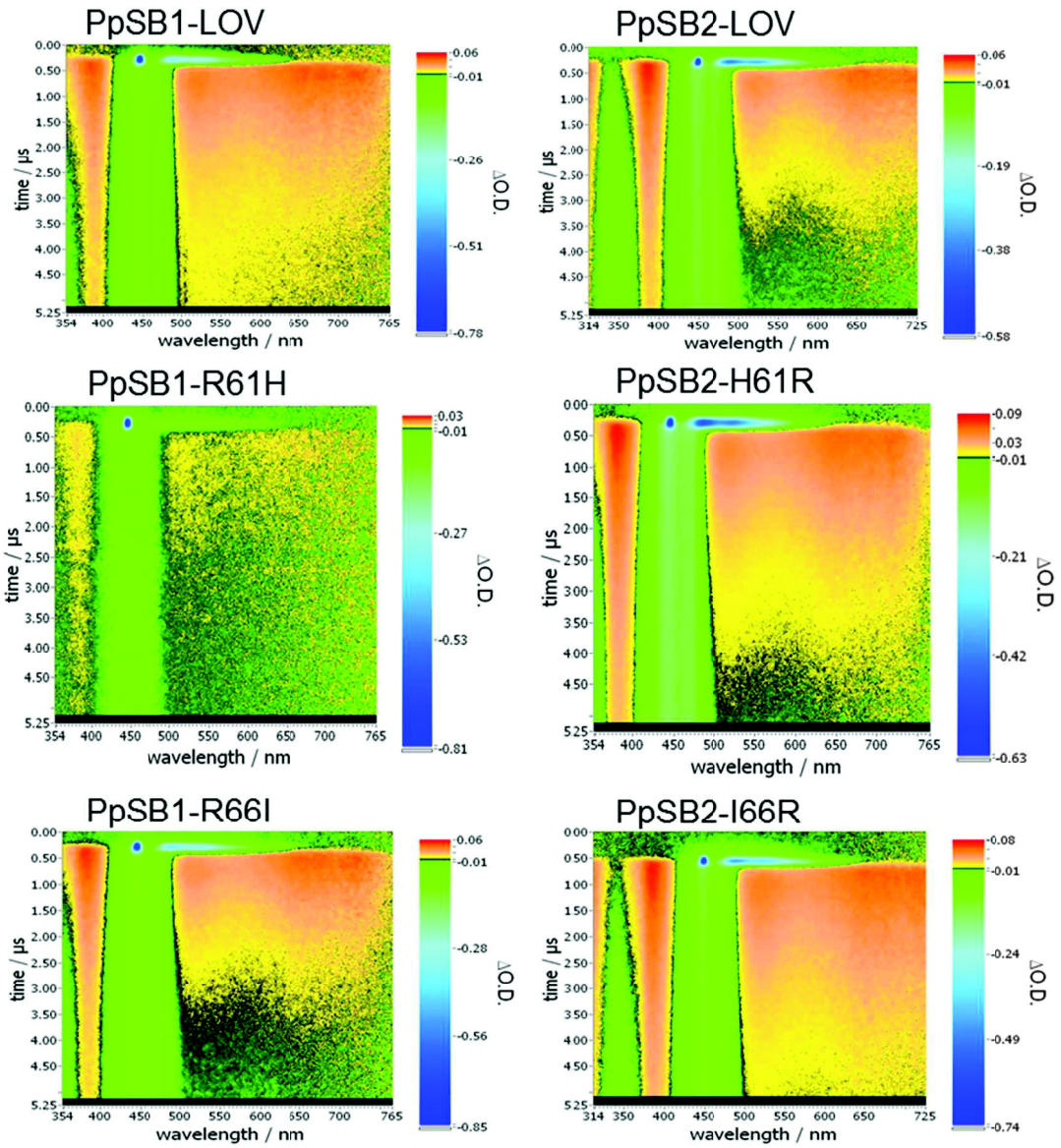

Fig. 2: Visualized data matrices of all measured samples. Axis of abscissae is the wavelength in nm, axis of ordinates holds the time in µs, red to yellow colors denote positive values of optical density, black areas resemble zero values and green to blue areas resemble negative values.

For all measured samples the visualized data matrizes presented in Figure 2 look similar. The excitation laser pulse at 450 nm is visible after 0,25 µs as blue spot in the uppermost section of all graphs, next to it, a slightly red-shifted (480-550 nm) blue area occurring at about the same time corresponds to fluorescence emitted by the sample upon excitation. Another event taking place within the same time is the adduct formation, visible as red area at 390 nm, fading over orange back to yellow. In the red spectral region around 700 nm triplet formation and decay can be seen (red area fading to orange and yellow). The broad green signal (400-500 nm) is the afterglow of the laser-pulse. Of all measured samples solely PpSB1-LOV R61H gave a very poor signal. This was due to the fact that this mutant protein lost significant amounts of

chromophore (FMN) during purification, concentration and storage.

In order to calculate triplet-decay constants (corresponding to the time-constant of adduct formation) and thus to draw conclusions as to whether forward kinetic processes are influenced by the structural differences introduced by mutation, single spectra at a wavelength of about 700 nm were derived from the set of data and decay constants were calculated using Origin 7G and a pulse decay equation of the third order (set up by Roger-Jan Kutta). Figure 3 shows the decay curves of all mutants and wild-type proteins.

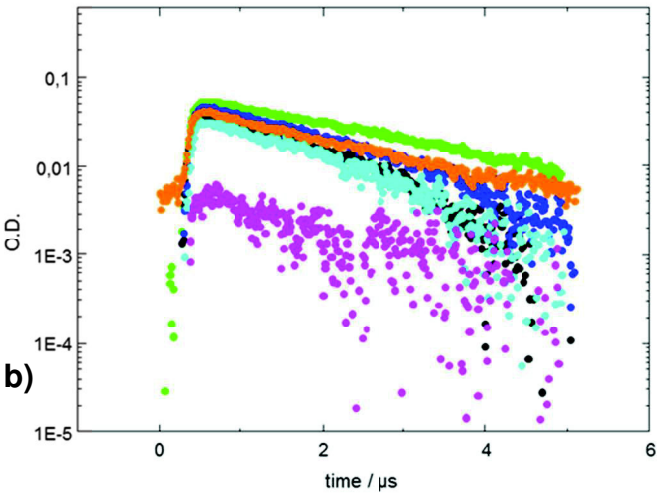

Protein	τ (decay time in µs)
PpSB1-LOV	**1,62**
PpSB1-LOV R61H	1,80
PpSB1-LOV R66I	**1,80**
PpSB2-LOV	**1,80**
PpSB2-LOV H61R	**2,10**
PpSB2-LOV I66R	2,50

Fig. 3: Decay curves of mutant and wildtype proteins. a) Triplet decay of PpSB1-LOV, PpSB2-LOV and the respective mutant proteins derived from the time trace at about 700 nm (triplet state of FMN) as O.D. versus time in µs. PpSB1-LOV: green dots; PpSB2-LOV: black dots; PpSB1-R61H:pink dots; PpSB2-H61R: dark blue dots; PpSB1-R66I: cyan dots; PpSB2-I66R: green dots. b) Calculated triplet decay times of the PpSB1-LOV, PpSB2-LOV and the respective mutant proteins. Single spectra were derived from the data sets at ~ 700 nm and resemble raw data.

As reported previously based on laser-flash photolysis data, the difference in triplet decay between the two wild-type proteins is not as large as the difference in their dark recovery. Here, transient absorption measurements corroborate previous laser flash photolysis data, were triplet decay times of 1.5 and 1.6 µs were estimated for PpSB1-LOV and PpSB2-LOV (see chapter 2.1, (*1*)). Overall all values are quite close to each other, the only two mutants that appear to have a somewhat slower triplet-decay are the PpSB2-LOV H61R and I66R variants. The dark recovery of both was slowed down by the mutations (3 and 7-fold) compared to the respective wild-type PpSB2-LOV protein (see chapter 2.1, (*1*)). Yet the triplet decay, meaning part of the light-initiated forward kinetic process is only marginally slowed down (1.2 and 1.4-fold).

Discussion

Using transient absorption measurements we were able to derive adduct formation kinetics (measured as triplet decay) for all PpSB1-LOV and PpSB2-LOV variants (R61H, R66I, H61R, I66R). From single wavelength decay curves, derived from the data matrix, triplet-decay constants could be determined. Hereby, none of the introduced mutations had any significant impact on the forward kinetic process (adduct formation kinetics). For AsLOV2 it was previously shown that steric support imposed on the photoactive cystein residue (Cys39 in AsLOV2) by nearby residues such as Ile16 impact on both forward light-initiated and dark recovery reactions (*16*). While mutation of Ile16 to valine accelerated the dark recovery reaction 10-fold, adduct formation was slowed down by a factor of 2 (*16*). For the two *P. putida* proteins, solely the two PpSB2-LOV variants (H61R and I66R) showed a 1.2 and 1.5-fold slower triplet decay. However, in contrast to the study of Christie *et. al* (*16*) the respective variants showed slowed dark recovery kinetics. Moreover, the corresponding mutations that drastically accelerated the dark recover of PpSB1-LOV did not have any significant impact on the triplet decay. Thus, based on the here presented data for both wild-type proteins as well as for all studied variants a similar structural mechanism as suggested by Christie *et. al* for AsLOV2 can essentially be ruled out for PpSB1-LOV and PpSB2-LOV

Conclusions

Because for both PpSB1-LOV and PpSB2-LOV forward reactions resulting in adduct state formation are equally efficient it seems likely that structural differences realized in the respective dark state of PpSB1-LOV and PpSB2-LOV are not the driving force behind the drastically different dark recovery reactions. In conclusion it seems more likely that adduct state stability is differently tuned in the two proteins i.e. by the strain imposed by adduct formation and anchoring of the FMN phosphate at the proximal end of the flavin ribityl chain (by R66 and R61 in PpSB1-LOV). This adduct state stability is then influenced by introducing the respective mutations that influence the anchoring of the FMN phosphate in the LOV domain of the respective protein, which in turn results in drastically altered dark recovery reactions (see chapter 2.1 and 3.1) (*1, 21*)).

References

1. Jentzsch, K., Wirtz, A., Circolone, F., Drepper, T., Losi, A., GaÌˆrtner, W., Jaeger, K.-E., and Krauss, U. (2009) Mutual Exchange of Kinetic Properties by Extended Mutagenesis in Two Short LOV Domain Proteins from *Pseudomonas putida*, *Biochemistry 48*, 10321-10333.

2. Berera, R., van Grondelle, R., and Kennis, J. (2009) Ultrafast transient absorption spectroscopy: principles and application to photosynthetic systems, *Photosynthesis Research 101*, 105-118.

3. Klimov, V. I., Mikhailovsky, A. A., Xu, S., Malko, A., Hollingsworth, J. A., Leatherdale, C. A., Eisler, H.-J., and Bawendi, M. G. (2000) Optical Gain and Stimulated Emission in Nanocrystal Quantum Dots, *Science 290*, 314-317.

4. Klimov, V. I., Ivanov, S. A., Nanda, J., Achermann, M., Bezel, I., McGuire, J. A., and Piryatinski, A. (2007) Single-exciton optical gain in semiconductor nanocrystals, *Nature 447*, 441-446.

5. Wang, Y., Hang, K., Anderson, N. A., and Lian, T. (2003) Comparison of Electron Transfer Dynamics in Molecule-to-Nanoparticle and Intramolecular Charge Transfer Complexes, *The Journal of Physical Chemistry B 107*, 9434-9440.

6. Gust, D., Moore, T. A., and Moore, A. L. (1993) Molecular mimicry of photosynthetic energy and electron transfer, *Accounts of Chemical Research 26*, 198-205.

7. Nguyen, T.-Q., Wu, J., Doan, V., Schwartz, B. J., and Tolbert, S. H. (2000) Control of Energy Transfer in Oriented Conjugated Polymer-Mesoporous Silica Composites, *Science 288*, 652-656.

8. Miller, S. E., Lukas, A. S., Marsh, E., Bushard, P., and Wasielewski, M. R. (2000) Photoinduced Charge Separation Involving an Unusual Double Electron Transfer Mechanism in a Donor−Bridge−Acceptor Molecule, *Journal of the American Chemical Society 122*, 7802-7810.

9. Kubo, M., Mori, Y., Otani, M., Murakami, M., Ishibashi, Y., Yasuda, M., Hosomizu, K., Miyasaka, H., Imahori, H., and Nakashima, S. (2007) Ultrafast Photoinduced Electron Transfer in Directly Linked Porphyrin−Ferrocene Dyads, *The Journal of Physical Chemistry A 111*, 5136-5143.

10. Kennis, J. T. M., Crosson, S., Gauden, M., van Stokkum, I. H. M., Moffat, K., and van Grondelle, R. (2003) Primary Reactions of the LOV2 Domain of Phototropin, a Plant Blue-Light Photoreceptor *Biochemistry 42*, 3385-3392.

11. Kottke, T., Heberle, J., Hehn, D., Dick, B., and Hegemann, P. (2003) Phot-LOV1: Photocycle of a Blue-Light Receptor Domain from the Green Alga *Chlamydomonas reinhardtii*, *Biophysical Journal 84*, 1192-1201.

12. Swartz, T. E., Corchnoy, S. B., Christie, J. M., Lewis, J. W., Szundi, I., Briggs, W. R., and Bogomolni, R. A. (2001) The photocycle of a flavin-binding domain of the blue light photoreceptor phototropin, *J Biol Chem 276*, 36493-36500.

13. Krauss, U., Losi, A., Gärtner, W., Jaeger, K.-E., and Eggert, T. (2005) Initial characterization of a blue-light sensing, phototropin-related protein from *Pseudomonas putida*: a paradigm for an extended LOV construct, *Physical Chemistry Chemical Physics 7*, 2804-2811.

14. Zikihara, K., Iwata, T., Matsuoka, D., Kandori, H., Todo, T., and Tokutomi, S. (2006) Photoreaction Cycle of the Light, Oxygen, and Voltage Domain in FKF1 Determined by Low-Temperature Absorption Spectroscopy *Biochemistry 45*, 10828-10837.

15. Losi, A., Polverini, E., Quest, B., and Gärtner, W. (2002) First Evidence for Phototropin-Related Blue-Light Receptors in Prokaryotes, *Biophysical Journal 82*, 2627-2634.

16. Christie, J. M., Corchnoy, S. B., Swartz, T. E., Hokenson, M., Han, I.-S., Briggs, W. R., and Bogomolni, R. A. (2007) Steric Interactions Stabilize the Signaling State of the LOV2 Domain of

Phototropin 1 *Biochemistry 46*, 9310-9319.

17. Losi, A., Kottke, T., and Hegemann, P. (2004) Recording of Blue Light-Induced Energy and Volume Changes within the Wild-Type and Mutated Phot-LOV1 Domain from *Chlamydomonas reinhardtii*, *Biophysical Journal 86*, 1051-1060.

18. Cao, Z., Buttani, V., Losi, A., and Gärtner, W. (2008) A Blue Light Inducible Two-Component Signal Transduction System in the Plant Pathogen *Pseudomonas syringae* pv. tomato, *Biophysical Journal 94*, 897-905.

19. Alexandre, M. T. A., Arents, J. C., van Grondelle, R., Hellingwerf, K. J., and Kennis, J. T. M. (2007) A Base-Catalyzed Mechanism for Dark State Recovery in the *Avena sativa* Phototropin-1 LOV2 Domain, *Biochemistry 46*, 3129-3137.

20. Langenbacher, T., Immeln, D., Dick, B., and Kottke, T. (2009) Microsecond Light-Induced Proton Transfer to Flavin in the Blue Light Sensor Plant Cryptochrome, *Journal of the American Chemical Society 131*, 14274-14280.

21. Circolone, F., Granzin, J., Jentzsch, K., Drepper, T., Jaeger, K. E., Willbold, D., Krauss, U., and Batra-Safferling, R. (2012) Structural basis for the slow dark recovery of a full-length LOV protein from *Pseudomonas putida*, *J Mol Biol 417*, 362-374.

3. From kinetics to structure

3.1 Structural basis for the slow dark recovery of a full-length LOV protein from *Pseudomonas putida*

Franco Circolone , Joachim Granzin , Katrin Jentzsch , Thomas Drepper , Karl-Erich Jaeger , Dieter Willbold , Ulrich Krauss and Renu Batra-Safferling

J Mol Biol **417:** 362-374

doi:10.1016/j.jmb.2012.01.056 J. Mol. Biol. (2012) 417, 362–374

Contents lists available at www.sciencedirect.com

Journal of Molecular Biology

journal homepage: http://ees.elsevier.com.jmb

Structural Basis for the Slow Dark Recovery of a Full-Length LOV Protein from *Pseudomonas putida*

Franco Circolone[1]†, Joachim Granzin[2]†, Katrin Jentzsch[1], Thomas Drepper[1], Karl-Erich Jaeger[1], Dieter Willbold[2,3], Ulrich Krauss[1]* and Renu Batra-Safferling[2]*

[1]*Institut für Molekulare Enzymtechnologie, Heinrich-Heine-Universität Düsseldorf, D-52426 Jülich, Germany*
[2]*Institute of Complex Systems, ICS-6: Structural Biochemistry, Research Centre Jülich, D-52425 Jülich, Germany*
[3]*Institut für Physikalische Biologie, Heinrich-Heine-Universität Düsseldorf, 40225 Düsseldorf, Germany*

Received 6 September 2011; received in revised form 15 December 2011; accepted 31 January 2012
Available online 7 February 2012

Edited by F. Schmid

Keywords:
photoreceptor;
LOV domain;
PAS domain;
crystal structure;
photocycle

Blue-light photoreceptors containing light–oxygen–voltage (LOV) domains regulate a myriad of different physiological responses in both eukaryotes and prokaryotes. Their light sensitivity is intricately linked to the photochemistry of the non-covalently bound flavin mononucleotide (FMN) chromophore that forms a covalent adduct with a conserved cysteine residue in the LOV domain upon illumination with blue light. All LOV domains undergo the same primary photochemistry leading to adduct formation; however, considerable variation is found in the lifetime of the adduct state that varies from seconds to several hours. The molecular mechanism underlying this variation among the structurally conserved LOV protein family is not well understood. Here, we describe the structural characterization of PpSB1-LOV, a very slow cycling full-length LOV protein from the Gram-negative bacterium *Pseudomonas putida* KT2440. Its crystal structure reveals a novel dimer interface that is mediated by N- and C-terminal auxiliary structural elements and a unique cluster of four arginine residues coordinating with the FMN-phosphate moiety. Site-directed mutagenesis of two arginines (R61 and R66) in PpSB1-LOV resulted in acceleration of the dark recovery reaction approximately by a factor of 280. The presented structural and biochemical data suggest a direct link between structural features and the slow dark recovery observed for PpSB1-LOV. The overall structural arrangement of PpSB1-LOV, together with a complementary phylogenetic analysis, highlights a common ancestry of bacterial LOV photoreceptors and Per-ARNT-Sim chemosensors.

Introduction

Light is a ubiquitous environmental stimulus for nearly all organisms, triggering various physiological processes. Thus, many organisms possess dedicated photoreceptors that bind different chromophores allowing them to respond to different wavelengths of the visible spectrum.[1] One such class of photoreceptor proteins, enabling living beings to sense and respond to blue-light irradiation, is the family of light–oxygen–voltage (LOV) photoreceptors.[2–4] The sensor modules of LOV photoreceptors are small photosensitive protein domains that bind oxidized flavin mononucleotide (FMN) as light-absorbing chromophore.[5] LOV domains are usually part of multidomain proteins, where at least one LOV

*Corresponding authors. E-mail addresses: u.krauss@fz-juelich.de; r.batra-safferling@fz-juelich.de.

† F.C. and J.G. contributed equally to this work.

Abbreviations used: LOV, light–oxygen–voltage; PAS, Per-ARNT-Sim; FMN, flavin mononucleotide; PDB, Protein Data Bank; ESRF, European Synchrotron Radiation Facility.

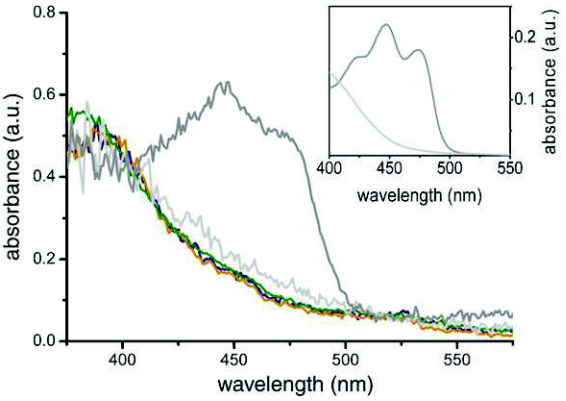

Fig. 1. Single crystal microspectrometry. The spectrum recorded immediately after transferring the light-grown crystal to the instrument is shown as blue line. To verify that no further spectral changes do occur, we illuminated the loop with mounted crystal for 30 s with blue light. Subsequently, a second absorbance spectrum was recorded (orange line). The green line depicts the absorbance spectra of a light-grown crystal after incubation in dark for 4 days at room temperature. For comparison, 20 µl of PpSB1-LOV protein solution with the protein concentration as used in the crystallization setup [20 mg/ml in 10 mM Tris–HCl buffer (pH 7.5)] was placed in a 1-mm-quartz cuvette. Absorbance spectra were recorded for the dark-adapted protein (dark-gray line) and after 30 s of blue-light illumination (light-gray line) using the same microspectrometer setup as employed for the crystal measurements. The corresponding section of conventional UV/Vis spectra recorded for the PpSB1-LOV protein in both dark (dark-gray line) and light (light-gray line) states in solution is shown as inset. The reference spectra were recorded using a UV/Vis spectrophotometer.

Table 1. Data collection and refinement statistics

Data collection	
Space group	$P6_1$
Cell dimensions (Å) (T = 100 K)	
a, *b*	55.1
c	222.0
Resolution (Å)	2.63
Beamline	ESRF ID23-2 (Grenoble)
Detector	MarCCD
Wavelength (Å)	0.873
Unique reflections	11,307
Average redundancy	6.1 (4.1)
Completeness (%)	99.8 (95.9)[a]
R_{merge} (%)	6.4 (46.1)[a]
Wilson *B*-factor (Å^2)	63.1
$I/\sigma(I)$	15.4 (2.6)[a]
Refinement	
Resolution range (Å)	55.5–2.63
R_{work} (%)	22.4
R_{free} (%)	26.9
Number of protein atoms	2115 (two molecules per asymmetric unit)
Number of FMN atoms	62
Number of water molecules	15
Average *B*-factor (Å^2)	
Protein	67.2
FMN	51.0
Water	48.3
r.m.s.d.	
Bonds (Å)	0.01
Angles (°)	1.316

[a] Indicates the value for the outermost shell (2.68–2.63 Å). For calculation of R_{free}, 4.82% of the reflections were reserved.

domain is required for sensing the light signal.[2,6,7] Light absorption in the flavin chromophore initiates a photocycle in which a metastable covalent adduct (in the following, referred to as light state) is formed between the FMN-C4a atom and a closely positioned conserved cysteine residue in the LOV domain.[7] Mechanistically, the adduct formation step is assumed to be accompanied by a conformational rearrangement in the surrounding protein with the signal being relayed from the site of photon capture in the LOV sensor domain to fused effector domains.[7] In turn, the light-initiated change in effector domain "activity" enables the organism to respond to the signal with a change in its behavior or physiology.[2,8] Consequently, the transient flavin-cysteinyl thiol adduct is broken in the dark, thus completing the photocycle. The time of dark recovery can vary from seconds to hours depending on the LOV protein.[9,10]

In eukaryotes such as plants, fungi and algae, a limited set of conserved LOV photoreceptor architectures have been identified. Those include plant phototropins, plant neochromes, proteins of the FKF1/ZTL/ADO family, algal aureochromes, fungal WC-1 and VVD proteins, [2,11,12] as well as the recently identified algal LOV histidine kinases.[13] In contrast, bacteria possess a broad spectrum of different LOV photoreceptor proteins with variable multidomain architectures that, at times, are not even conserved within a distinct phylogenetic group.[4,6]

Fig. 2. PpSB1-LOV crystal structure. (a) Ribbon diagram of the light state of PpSB1-LOV (1–134) colored according to secondary structure elements (helices, light blue; β strands, light green; loops, yellow). The FMN in the chromophore binding pocket is shown as stick model and is colored by element: carbon, yellow; nitrogen, blue; oxygen, red; phosphorus, purple. (b) Topological representation of the backbone fold of PpSB1-LOV. The secondary structure elements' helices and β strands are labeled with the color codes as in (a). (c) The dimer of PpSB1-LOV. Monomer subunits are colored blue and green, respectively. The FMN cofactors are shown as space-filled model colored as in (a). (d) Close-up view of the dimer interface showing intersubunit hydrogen bonds and salt bridges shown as broken lines between the residues shown as stick models colored by element as in (a). The residues involved in the hydrophobic interactions are colored dark blue in the ribbon representation. The view in this figure is parallel with the 2-fold dimer axis, roughly $y + 90°$ around the horizontal axis. 2-Fold axis in (c) runs from top to bottom.

Bacterial proteins usually contain a single LOV domain fused N-terminally to a set of different effector domains such as phosphodiesterases, histidine kinases, anti-σ-factor antagonists and helix–turn–helix DNA binding domains.[6] In both eukaryotes and prokaryotes, LOV photoreceptors exist, which lack a fused effector domain.[14,15] In bacteria, those so-called "short" LOV proteins constitute about 13% of the third largest bacterial LOV protein family.[6] While the physiological role of eukaryotic

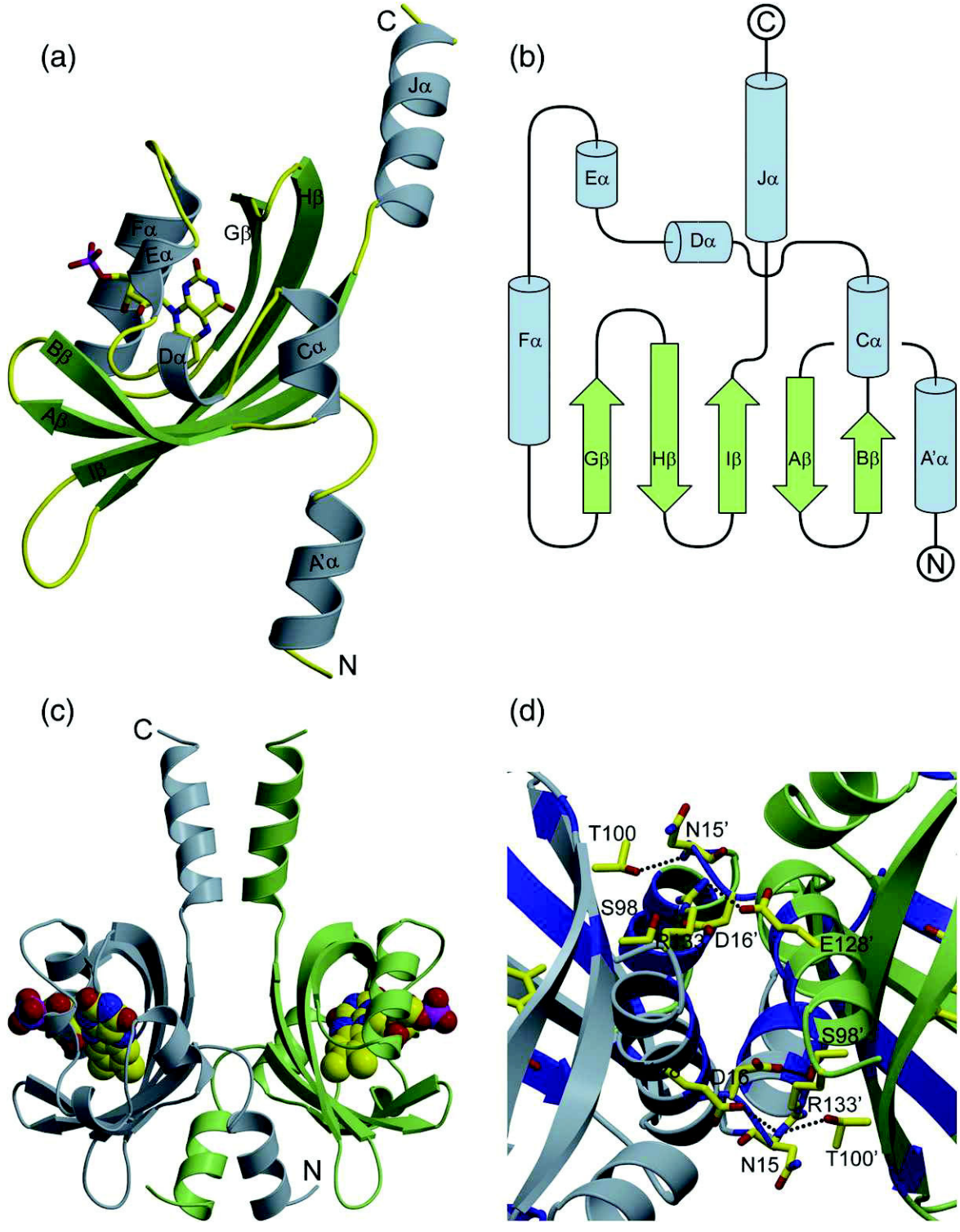

Fig. 2 (*legend on previous page*)

LOV photoreceptors is well studied,[2,12,16] the function of bacterial LOV photoreceptors has remained elusive for a long time. However, several recent studies demonstrate an integral role for LOV photoreceptor proteins in the physiology of a number of different chemotrophic microorganisms (reviewed in Ref. 8). LOV-mediated responses include light-dependent tuning of the general stress response,[17] regulation of virulence and infectivity[18] and cell–cell and cell-surface attachment responses.[19]

Due to the broad variety of structurally distinct effector domains fused to the LOV sensory domain in eukaryotic and prokaryotic photoreceptors, immediate questions about the conservation of the inherent signal-transduction mechanism arise. Previous X-ray crystallographic studies of LOV domain conformational dynamics reveal only minor overall structural changes after photoexcitation of dark-grown crystals[15,20–24] (also reviewed in Refs. 7 and 25). Hereby, in most cases, either isolated LOV domains[20–22] or constructs containing short N- and C-terminal helical extensions were studied.[15,23,24] This implies that (i) the light-induced structural changes within the core LOV domain are only minor, (ii) large structural rearrangements are impaired by the crystal packing or (iii) the signal relay is mediated by a pronounced structural rearrangement outside the LOV core domain or is only possible in full-length photoreceptor proteins. Thus, our atomic-level understanding about the light-induced signal-transmission process in LOV photoreceptor systems is presently based on the extrapolation of minor structural changes observed in protein crystals grown in the dark.[7] In contrast, nuclear magnetic resonance (NMR) spectroscopic studies performed in solution on an N- and a C-terminally extended LOV domain construct[26] and on one bacterial two-domain LOV photoreceptor[27] revealed widespread structural changes but failed to provide structural information at atomic resolution. These observations stress the importance of further structural studies on full-length LOV photoreceptor proteins by NMR spectroscopy and X-ray crystallography.

In the presented work, we report the light state structure of the full-length LOV photoreceptor protein PpSB1-LOV from *Pseudomonas putida* KT2440 obtained from crystals grown under constant illumination. The dimeric PpSB1-LOV protein, as a member of the "short" LOV family, lacks a fused effector domain and shows an unusually slow dark recovery ($\tau_{REC} \approx 40$ h at 20 °C).[9] In the crystal, a novel mode of LOV–LOV interaction is observed, that is mediated by N- and C-terminal auxiliary structural elements. Moreover, the combination of structural and biochemical analyses of the PpSB1-LOV protein, together with the characterization of the PpSB1-LOV R61H/R66I double mutant, provides a structural understanding of the very slow dark recovery reaction of the protein. Structural similarities between the PpSB1-LOV protein and other bacterial LOV and Per-ARNT-Sim (PAS) sensor domain structures hereby extend beyond the sensor core domain. Complementary phylogenetic analysis highlights an evolutionary relationship between bacterial LOV photoreceptors and oxygen/redox-sensing PAS chemosensors.

Results

Crystallization and single crystal microspectrometry

Initial crystallization trials were conducted both in the dark and under continuous low-level white-light illumination. Remarkably, PpSB1-LOV crystals only grew under continuous illumination. In order to elucidate the nature of the conformational state of PpSB1-LOV present in the light-grown crystals, we used single crystal microspectrometry. The method allows monitoring of the visible-light absorption of the FMN chromophore within the crystal, which in turn provides spectroscopic evidence for the crystallized photocycle intermediate prior to cryo-cooling. In order to test the microspectrometry setup, we recorded dark state (Fig. 1; absorbance maxima at 447 nm, dark-gray line) and light state spectra (Fig. 1; absorbance maxima at 390 nm, light-gray line) for the PpSB1-LOV protein in solution. In comparison, microspectrometry data recorded on several PpSB1-LOV crystals grown under constant illumination reveal typical light state absorbance spectra (Fig. 1; absorbance maxima at 390 nm, blue line) indicative of adduct formation within the crystal prior to cryo-cooling. Subsequently, light-grown crystals were kept at room temperature in the dark for 4 days to allow dark adaptation. For the protein in solution, this time period is sufficient for a complete recovery to the dark state. Interstingly, dark adaption of the crystals did not result in any spectral recovery with respect to the FMN absorbance at 447 nm (green line in Fig. 1). This suggests trapping of the light state intermediate in the crystal.

Crystal structure of the PpSB1-LOV protein in the light state

The crystal structure of the PpSB1-LOV protein in the light state has been determined at 2.6 Å resolution (Table 1 and Fig. 2). The final atomic model in one asymmetric unit is a dimer, where the monomer subunits (Fig. 2a and b) are related by a 2-fold non-crystallographic symmetry (Fig. 2c). Each monomer is composed of residues 1–134 of the protein and an FMN cofactor (Fig. 2a). The C-terminal residues 135–142 of both molecules could not be traced in the electron density maps and are thus likely to be disordered. Additionally, no electron density was observed for the first 20

amino acids of the recombinant LOV protein, which comprises the N-terminal His tag and the thrombin protease cleavage site derived from the expression vector pET28a. According to Ramachandran plots generated with MolProbity (PHENIX),[28] the model exhibited good geometry with none of the residues in disallowed regions.

Three-dimensional structures for the LOV proteins have been determined previously.[15,20–24,27,29,30] The residues 17–118 make up the conserved LOV core domain, comprising the characteristic α/β-fold PAS topology (Fig. 2a and b). The antiparallel β-scaffold consists of the strands Aβ (residues 17–24), Bβ (residues 27–33), Gβ (residues 79–86), Hβ (residues 92–103) and Iβ (residues 110–118), flanked by four α-helices [Cα (residues 35–41), Dα (residues 45–48), Eα (residues 53–56) and Fα (residues 64–75)]. The residues located on the β-scaffold and helices Eα and Fα form the cavity with tightly bound FMN chromophore. In addition, two noncanonical structural elements, an N-terminal helix (A′α, residues 4–12) and a C-terminal helical element (termed Jα-helix, residues 120–132), are also present in the PpSB1-LOV structure. Both helices protrude away from the LOV core domain (Fig. 2a and c). The N-terminal A′α-helix is part of an N-terminal cap (residues 1–16), which partly covers the adjacent LOV core β-scaffold.

Structural comparison with other LOV domains

We compared the PpSB1-LOV core domain structure with other known LOV structures including several eukaryotic and one bacterial LOV domain (Supplementary Information, Table I). In summary, a comparison between the PpSB1-LOV and the available LOV core domain structures in either their dark or their light state reveals the highest structural similarity with the light state structure of *Chlamydomonas reinhardtii* phot-LOV1 domain [Protein Data Bank (PDB) ID: 1N9O] and *Bacillus subtilis* YtvA-LOV (PDB ID: 2PR6), reminiscent of the microbial origin of the PpSB1-LOV protein.

A superimposition of the PpSB1-LOV core domain with reported LOV domain structures in the light state is shown in Fig. 3. Among the LOV protein family, the largest deviations are found in the loop connecting the Hβ and Iβ strands. The PpSB1-LOV core shows additional structural differences in both loop segments and in the core secondary structure elements. In particular, the loop between the helices Eα and Fα bends toward the FMN-phosphate moiety, with its orientation being mainly stabilized by the directional pull of the FMN-phosphate on the charged side chain of residue R61 located within this loop. A second structural difference between the PpSB1-LOV domain and all other LOV structures is found in the β-scaffold, where the two β-sheets (Aβ and Bβ) are

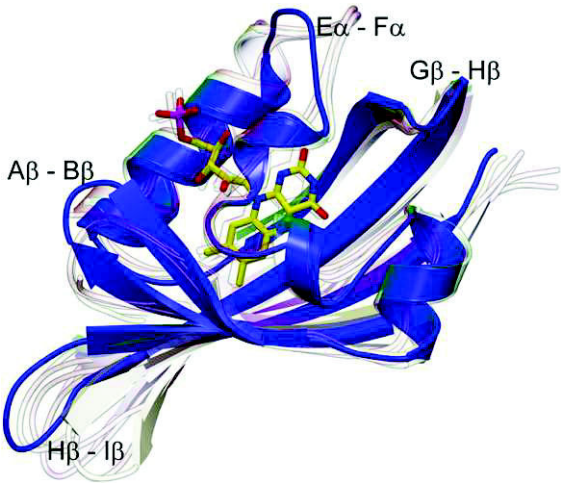

Fig. 3. The superposition of the LOV core domains. The selected light state structures PpSB1-LOV (colored dark blue), *Adiantum capillus veneris* Phy3 LOV2 (PDB ID: 1JNU; light coral, $Q=0.5476$), *A. sativa* phot1-LOV2 (PDB ID: 2V0W; magenta, $Q=0.4107$), *B. subtilis* YtvA (PDB ID: 2PR6; yellow, $Q=0.5433$) and *C. reinhardtii* LOV1 (PDB ID: 1N9N; green, $Q=0.554$) were included in the analysis using the secondary structure matching program[48] with residues from one protein chain in each case. Note: a higher Q score indicates a better alignment (see Q values above in parentheses). For clarity, ribbon diagram of the PpSB1-LOV structure is shown in full color with the FMN as stick model colored by element as in Fig. 2a, whereas all other structures are made highly transparent. Differences are seen in the loop regions labeled in this figure.

extended by three and four residues, respectively. Compared to other LOV core structures, this unusual structural property results in an extended antiparallel arrangement of Aβ and Bβ, which is mutually stabilized by hydrogen bonding between the backbone amide nitrogen and backbone carbonyl oxygen atoms of residues E24 and D27, respectively (Supplementary Information). A similar interaction is absent in all other light- or dark state LOV structures, which possess an extended and well-ordered loop segment in this region (Fig. 3).

The PpSB1-LOV dimer interface is largely formed by two auxiliary structural elements found outside of the canonical LOV domain

PISA analysis‡ revealed an extensive dimer interface involving a buried surface area of 3732 Å^2.[31] The interface is constituted largely by hydrophobic residues from the two structural elements A′α and Jα located outside the LOV core domain, as well as between the central part of the LOV domain (Fig. 2c and d). Specifically, the

‡http://www.ebi.ac.uk/msd-srv/prot_int/pistart.html

interchain interactions are found in the following three regions of the dimer structure: (i) between the N-terminal cap (including helix A′α) and its counterpart from the other subunit, (ii) between hydrophobic residues in the N-terminal cap and the β-scaffold of the opposite subunit (Aβ, Bβ, Hβ and Iβ; see Fig. 2c and d) and (iii) between the Jα-helices protruding from the LOV core (Fig. 2c and d).

Moreover, the dimer interface constituted by residues in the central β-scaffold involves a set of interactions between charged residues and hydrogen-bonding interactions between polar side chains. The OD2 atom of D16 forms an interchain hydrogen bond with the OG atom of residue S98 of the opposite subunit. Likewise, the OG1 atom of T100 forms an interchain hydrogen bond with the backbone amide of N15 (Fig. 2d). Additionally, NH1 and NH2 atoms of residue R80 are found in close proximity to the OD2 atoms of residue D16 (3.3 Å) of the opposite subunit (not shown in Fig. 2d).

Interactions between the Jα-helices in the dimeric PpSB1-LOV protein is mediated by a canonical coiled-coil interaction via hydrophobic residues (L125, L129 and L132), occupying the positions d, a, d in two subsequent heptad repeats (see Supplementary Fig. S1). A further stabilization of the interchain helix–helix interaction is seen as a result of the presence of salt bridges between the OE2 atom of residue E128 and the NH2 atom of residue R133 in the respective opposite subunits (Fig. 2d).

Protein chromophore contacts—flavin binding pocket

The difference electron density map clearly shows the presence of one FMN molecule in each monomer. The majority of the residues forming the FMN binding cavity is conserved as compared to other bacterial and plant LOV domains (Fig. 4).[22,24] Residues directly interacting with the FMN chromophore are found mainly on the β-sheets G, H and I and on helices Eα and Fα. The FMN isoalloxazine ring is coordinated by hydrogen bonding with residues N85, N95 and Q116. The FMN ribityl chain in turn is hydrogen bonded to D52 and Q57. Four arginine residues R54, R61, R66 and R70 form salt bridges with the terminal phosphate group of FMN molecule (Fig. 4a; Supplementary Table II). Additionally, a cluster of hydrophobic residues contributes to the rigid coordination of the FMN chromophore within the binding pocket (Fig. 4a). The residues lining the dimethyl benzene ring of the flavin are V19, A21, F37, L56, I69, M73, L83, L97, I99, F112, I113 and G114. Figure 4b depicts the σ-A weighted electron density ($2mF_o - DF_c$ map) around the C53-S$^\gamma$ FMN-C4a region. The continuous density in the area is indicative of the presence of interaction between residue C53 and flavin C4a. No negative or positive differences were observed during the refinement around FMN-C4a in *sp3* geometry. The interatomic distance between C53-

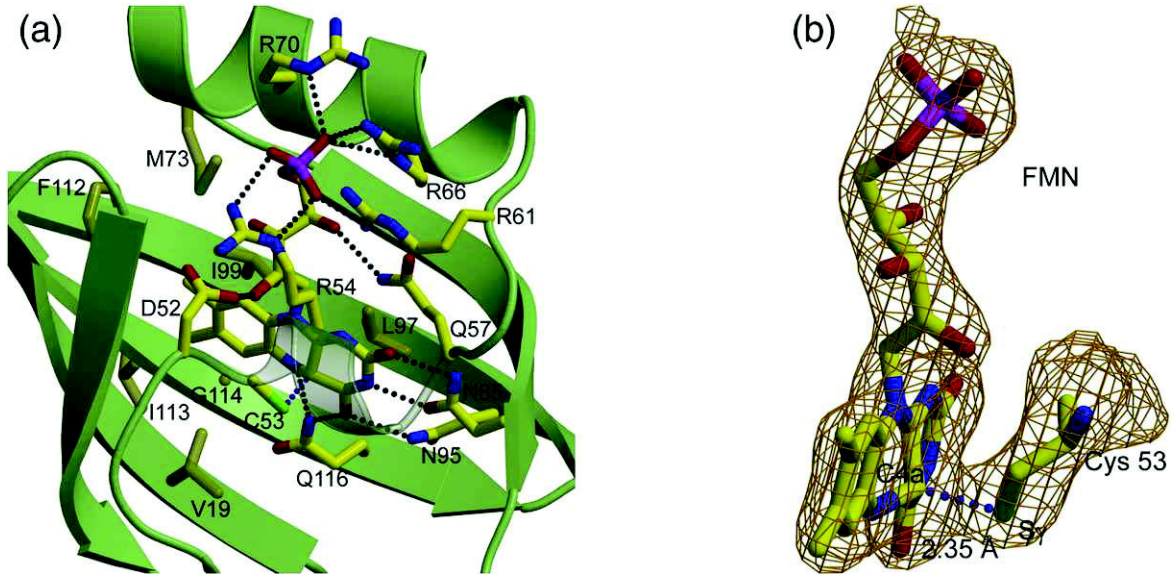

Fig. 4. The FMN binding pocket of PpSB1-LOV. (a) Ribbon diagram of PpSB1-LOV (green) with FMN cofactor and the interacting amino acid residues shown as stick models colored by element: carbon, yellow; nitrogen, blue; oxygen, red; sulfur, green; phosphorus, purple. The broken lines represent the hydrogen bonds between the FMN and the protein amino acids. For clarity, the 3_{10} helix Eα is made transparent. Note: the arginine cluster (R54, R61, R66 and R70) interacting with the phosphate moiety of the FMN; the nonplanar geometry of the FMN ring where the FMN-C4a is *sp3* hybridized. (b) The σ-A weighted $2mF_o - DF_c$ electron density map of the FMN and residue cysteine 53 contoured at 1.3 σ. The density (orange) between the C53-S$^\gamma$ and FMN-C4a is continuous, with the bond distance of 2.35 Å.

S^{γ} and FMN-C4a is 2.35 Å, which is too long for a covalent bond and too short for van der Waals contacts. Nevertheless, our electron density map of the PpSB1-LOV crystal favors the FMN-C4a as *sp3* hybridized and not as planar flavin ring seen in case of the dark structures (verified by $mF_o - DF_c$ map). The interatomic distance between C53-S^{γ} and FMN-C4a in previously reported dark state structures of LOV domains is ≥4.4 Å, which allows us to reason that, despite the absence of a thioether covalent bonding, our structure is closer to the light state than to the dark state (note that crystal growth took place under continuous illumination).

One of the significant differences between previously reported light- and dark state structures is found in the orientation of one glutamine residue in the FMN binding pocket. Residues Q123 and Q513 in YtvA-LOV and in *Avena sativa* phot1-LOV2 form a hydrogen bond with the O4 atom of the FMN isoalloxazine ring in the dark. Upon illumination, this glutamine undergoes a conformational rearrangement possibly involving the flipping of its side chain to form a new hydrogen bond with the newly protonated N5 atom of the flavin ring.[21,22,24] In the PpSB1-LOV structure, the corresponding Q116 forms two hydrogen bonds with the FMN isoalloxazine ring—O4…NE2–Q116 (2.75 Å) and N5…NE2–Q116 (2.87 Å) (Fig. 4a). Unlike in the previously reported light state structures described above, the side chain of residue Q116 does not require any flipping and is hydrogen bonded to both, the N5 atom and the O4 atom of the FMN isoalloxazine ring.

Within the FMN binding pocket, the most prominent structural difference between PpSB1-LOV and other LOV domains is the presence of two additional arginines (R61 and R66) that, in PpSB1-LOV, form salt bridges with the FMN-phosphate. In all other known LOV structures, the amino acids corresponding to R61 and R66 are polar or hydrophobic (Supplementary Fig. S1). Residue R61 is present in the loop connecting Eα and Fα, and residue R66 is located in the Fα-helix. The salt bridge between R61 and the FMN-phosphate results in a directional pull imposed on the Eα–Fα loop, causing an unusual "bent-in" conformation. Residues R61 and R66 together with the two conserved arginines in LOV proteins, namely, R54 (on Eα) and R70 (on Fα), form a unique cluster of charged residues that tightly coordinate the FMN-phosphate group (Fig. 4a). This highly organized network, in particular, involving the two additional arginines R61 and R66, is a peculiar feature of the PpSB1-LOV protein.

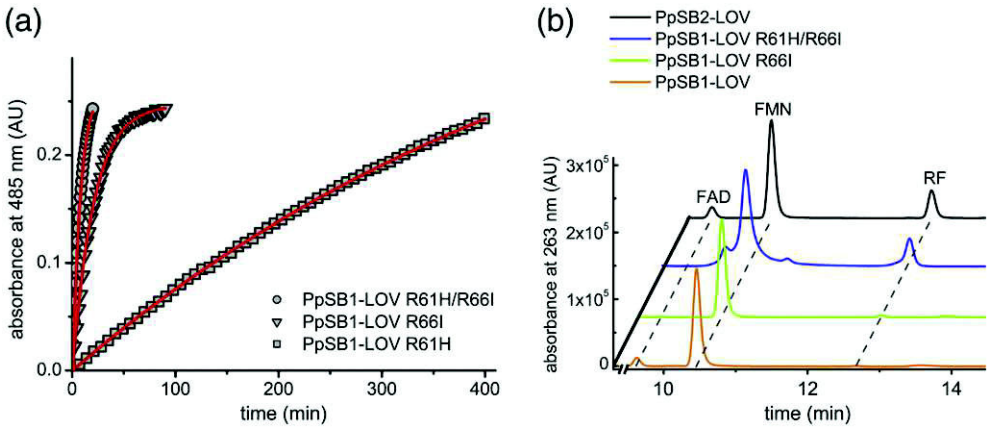

Fig. 5. Dark recovery and HPLC analysis of the flavin content for several PpSB1-LOV and PpSB2-LOV constructs. (a) Dark recovery time traces recorded at 485 nm absorbance for the respective protein construct after illumination for 30 s with blue light. All measurements were performed at 20 °C. Interpolated curves (shown as red line) obtained by single exponential fitting of the data are superimposed on the experimental data. Presented time constants are derived from two independent measurements. Representative curves are depicted for PpSB1-LOV R61H (rectangles; $\tau_{REC} = 765 \pm 589$ min), PpSB1-LOV R66I (triangles; $\tau_{REC} = 23 \pm 1$ min)[9] and the respective double mutant PpSB1-LOV R61H/R66I (circles; $\tau_{REC} = 9 \pm 2$ min). Under identical conditions, the corresponding PpSB1-LOV wild-type protein shows a dark recovery time constant of τ_{REC} of 2471 ± 22 min.[9] Please note that, due to the instability of the PpSB1-LOV R61H mutant protein, the error associated with the dark recovery time constant clearly exceeds 10%. (b) HPLC analysis of the flavin content of PpSB1-LOV (orange), PpSB2-LOV (black), PpSB1-LOV R66I (green) and the double mutant PpSB1-LOV R66I/R61H (blue). Whereas the PpSB1-LOV wild-type protein predominately binds FMN as chromophore, the homologous PpSB2-LOV protein accepts FMN and riboflavin (RF) in a ratio of 70:30.[9] Independent substitution of R61 for histidine and R66 for isoleucine, the corresponding residues in PpSB2-LOV, does not affect chromophore acceptance.[9] In contrast, the double mutant of PpSB1-LOV, bearing both R61H and R66I substitutions, shows a PpSB2-LOV-like chromophore acceptance binding FMN and RF in a ratio of about 70:30.

Residues R61 and R66 cooperatively affect the dark recovery process and the chromophore acceptance in PpSB1-LOV

Using site-directed mutagenesis, we previously identified R61 and R66 as two key amino acids contributing to the slow recovery of PpSB1-LOV (τ_{REC} = 2471 min at 20 °C).[9] The interchange of R66 to isoleucine, the corresponding residue in the fast reverting PpSB1-LOV paralog PpSB2-LOV (τ_{REC} = 2.3 min at 20 °C), resulted in a roughly 100-fold acceleration of the dark recovery reaction (PpSB1-LOV R66I, τ_{REC} = 23 min at 20 °C).[9] Notably, both the fast reverting R66I mutant of PpSB1-LOV and the PpSB2-LOV protein fail to crystallize under the same conditions as the PpSB1-LOV wild-type protein. The corresponding exchange of R61 to histidine had moderate impact on the dark recovery time constant, accelerating the reaction by a factor of about 5 (PpSB1-LOV R61H, τ_{REC} = 765 min at 20 °C).[9] Here, we have constructed the corresponding double mutant of the PpSB1-LOV protein (PpSB1-LOV R66I/R61H). This mutant shows further acceleration with a time constant for the dark recovery process of τ_{REC} = 9 min at 20 °C (Fig. 5a). This corresponds to an approximately 280-fold acceleration compared to the corresponding wild-type protein. Previously, HPLC analysis of the chromophore content revealed that the R61H and the R66I single mutations in PpSB1-LOV were insufficient to change the chromophore acceptance from binding only FMN (PpSB1-LOV) to a PpSB2-LOV-like behavior, which accepts mixture of FMN and riboflavin (RF) at a ratio of 70:30.[9] Interestingly, the double mutant PpSB1-LOV R66I/R61H exhibits a PpSB2-LOV-like chromophore acceptance binding both FMN and riboflavin at a ratio of 70:30 (Fig. 5b).

Discussion

A conserved arginine cluster in PpSB1-LOV determines dark recovery kinetics and chromophore acceptance

The presented results demonstrate that the unique arginine residues R61 and R66 of PpSB1-LOV act in a cooperative manner in determining the slow dark recovery and the chromophore binding specificity of this blue-light photoreceptor. In the crystal structure, these residues are part of a unique network of four arginine residues tightly coordinating the FMN-phosphate moiety (Fig. 4a). The tight coordination between R61 and the FMN-phosphate group results in a bending of the Eα–Fα loop toward the FMN chromophore hence forming a distinct conformation (Fig. 3a). Mechanistically, this could result in a direct stabilization of the light state conformation, for example, by constraining the orientation of the phosphate moiety and possibly of the whole FMN molecule in the light state geometry. This in turn would reduce possible thermal fluctuations that drive the dark recovery process. A tighter binding of the FMN molecule in our structure is also indicated by smaller interatomic distances between residues N95 and Q116 and the FMN isoalloxazine ring (see Supplementary Table III for a comparative analysis among deposited LOV structures). The other two arginine residues in the cluster, namely, R54 and R70, are well conserved in the LOV family (Supplementary Fig. S1). Substitution of one of the conserved arginines within different LOV proteins (R63 in YtvA; R58 in CrLOV1) to lysine accelerates the dark recovery of these proteins 3- to 10-fold.[32] This latter observation, together with our mutagenesis data for PpSB1-LOV, stresses the importance of the arginine cluster coordinating FMN-phosphate in the recovery process in LOV domains.

Protein chromophore contacts in light state PpSB1-LOV crystals

Based on microspectrometry data recorded for light-grown PpSB1-LOV crystals, we assign the conformational state present in the crystal prior to cryo-trapping and data collection as light state (see Fig. 1). Nevertheless, we do not observe a Cys53-S$^{\gamma}$ FMN-C4a covalent linkage (Fig. 4b) in the electron density map. The latter observation is most likely due to radiolysis of the Cys53–FMN thioether bond caused by the high-energy X-ray beam, as has been previously observed for other LOV proteins.[15,22,23] Close inspection of the electron density around the FMN-C4a atom in PpSB1-LOV structure suggests a *sp3* hybridization of the respective carbon atom, in contrast to a planar conformation seen in the dark-state structures. Thus, with respect to the Cys53–FMN thioether linkage, our structure represents a "mixed state" much like the photoexcited-state structure of CrLOV1 (1N9N), which was determined from a single crystal after illumination.[22]

Interestingly, microspectrometry data of the dark-adapted PpSB1-LOV crystals suggest that the protein is trapped in the light state within the crystal. The conformational motions in the LOV core domain and the peripheral protein regions such as, the N-terminal cap and the C-terminal Jα-helix, are likely to be structurally coupled to influence the dark recovery process in the crystal. This notion is supported by different biochemical studies, where removal[33] or swapping of the C-terminal Jα-helix[9] had a significant impact on the efficiency of the dark recovery process. Likewise, crystal packing effects, which inhibit large-scale conformational rearrangements, for example, of peripheral protein regions, could result in trapping of the protein in a spectral and structural light state. In contrast, previous

reports have shown that, for dark-grown crystals, photoexcitation and consequently adduct formation is possible. This might be the case because photochemical reaction steps of the FMN molecule, that is, the formation of the singlet excited state of FMN, the intersystem crossing to the FMN triplet state and subsequent cysteinyl adduct formation,[5] will inevitably occur independent of the conformational changes in the protein. Population of the light state (adduct formation) would thus be detectable spectroscopically, even though larger-scale protein conformational changes, in particular, in peripheral protein regions, could yet be severly impaired. Thus, the most likely explanation for the lack of larger-scale conformational changes in photoexcited LOV domain structures is structural constrains imposed by crystal packing forces on the mobility of the protein in the crystal.[30,34]

A novel mode of LOV–LOV dimerization is mediated by a structurally conserved N-terminal capping motif and protruding C-terminal Jα-helices

The PpSB1-LOV protein forms a dimer in the crystal where the two subunits are related by a 2-fold symmetry. The extensive dimer interface involves residues from three major regions of each subunit, namely, the N-terminal cap (including the A′α-helix), the central LOV domain β-scaffold and the C-terminal Jα-helix. Involvement of all three structural motifs has not been observed so far in dimers of other LOV protein structures. In the PpSB1-LOV dimeric structure, the N-terminal cap packs against the hydrophobic central part of the β-scaffold surface localized on the opposite monomer and interacts with its counterpart of the opposite subunit and the central LOV core domain. The protruding C-terminal Jα-helix packs against its respective counterpart (Fig. 2c and d). In addition, the dimer interaction is facilitated by a set of hydrogen-bonding interactions between polar side chains (D16, S98 and T100) and salt bridges between charged residues (D16 and R80) that protrude from the LOV core into the interface to contact the opposite subunit. Globally, this mode of interaction resembles the head-to-head dimeric organization found in the crystal structure of *B. subtilis* YtvA-LOV,[24] which is the closest bacterial homolog of PpSB1-LOV among all previously determined LOV structures. Position T100 (in Hβ) that forms an interchain hydrogen bond to N15 (in the N-terminal cap of the opposite subunit) in PpSB1-LOV is occupied by an aspartic acid residue (D109) in YtvA-LOV. In full-length YtvA, mutation of D109 to leucine fully abolishes the light-induced physiological response.[35] In the structure of the YtvA-LOV domain, the OD2 atom of D109 is hydrogen bonded to the OH group of Y41 (located in the Bβ strand) on the opposite subunit within the dimer. Thus, the mode of interaction with regard to this residue seems different between YtvA-LOV and PpSB1-LOV. Although the crystallized YtvA-LOV construct lacks the structural feature corresponding to the N-terminal cap of PpSB1-LOV, comparative sequence analysis (see Supplementary Fig. S1), CD spectroscopy data[36] and recent NMR studies[37] strongly suggest its presence in the full-length protein. It is thus plausible that, in the full-length YtvA protein (containing an N-terminal cap), the dimer–dimer interaction is different from the one observed in the crystal structure of YtvA-LOV domain. Moreover, comparative sequence and secondary structure analysis of different LOV sensory systems (Supplementary Fig. S1) reveal the conservation of potentially helical segments localized N- and C-terminally to the LOV core domain (corresponding to the N-terminal cap and the Jα-helix of PpSB1-LOV). Thus, although the orientation of both auxiliary elements is qualitatively different in different prokaryotic and eukaryotic LOV structures, the corresponding structural elements appear to be an integral part in most of the full-length LOV photoreceptors.

The mode of PpSB1-LOV dimerization shows high structural similarities to non-light-sensing dimeric PAS sensor systems. Structures with very similar dimeric arrangement include the heme-binding *Escherichia coli* PAS oxygen sensor EcDOS (PDB ID: 1S67[38]), the heme-binding *Rhizobium meliloti* PAS domain of RmFixL (PDB ID: 1EW0[39]), the *Azotobacter vinelandii* FAD (*f*lavin *a*denine *d*inucleotide)-binding PAS domain of the redox sensor AvNifL (PDB ID: 2GJ3[40]) and a *Nostoc punctiforme* PAS domain (NpPAS) of a signal transduction histidine kinase, crystallized in ligand-free form (PDB ID: 2P04[41]) (Supplementary Fig. S3). In particular, the orientation of the N-terminal capping helix (A′α) is very similar between PpSB1-LOV and the four compared PAS sensor systems. Moreover, sequence-based phylogenetic analysis (Supplementary Fig. S3) highlights a common evolutionary ancestry of bacterial LOV and PAS sensors and implies the presence of related signal-propagation mechanisms within the wider PAS family including eukaryotic PAS sensor domains.

Concluding remarks

The presented structure of the PpSB1-LOV protein represents the first wild-type full-length LOV photoreceptor structure obtained from crystals grown under constant illumination. The structure reveals a unique cluster of arginine residues lining the FMN-phosphate moiety thereby providing the structural basis for the very slow dark recovery of the *P. putida* photoreceptor. Apparently, the stable flavin-cysteinyl adduct in PpSB1-LOV, resulting in a very long lifetime of the light state, enables

crystallization under continuous low-level illumination. This notion is further supported by the observation that the fast reverting PpSB1-LOV mutant R66I, as well as its fast reverting paralogous twin PpSB2-LOV, fails to crystallize under the same light conditions. Recent mutational studies aiming to tune LOV photocycle dynamics[9,10] could thus pave the way toward slow reverting LOV proteins, which in turn would allow protein crystallization to be performed under constant illumination to obtain "true" light state structures. During the preparation of the manuscript, the structure of a VVD mutant (M135I, M165I) with a similarly slow photocycle ($\tau_{REC} \approx 3000$ min)[10] was determined from crystals grown after white-light exposure.[30] Here, significant structural changes were also observed when compared to the previously determined structure of the photoexcited state obtained by illumination of dark-grown crystals. Interestingly, the largest structural differences between the previously determined VVD dark state structure and the newly determined light-state structure are seen in the N-terminal cap of the protein. This observation and our own results clearly highlight the importance of auxiliary N- and C-terminal structural elements for photoreceptor activation. Furthermore, their broad conservation also in evolutionary related bacterial PAS chemosensors suggests a general role for PAS signalling responses, which has yet to be addressed experimentally.

Materials and Methods

Site-directed mutagenesis and generation of variants

The gene encoding full-length PpSB1-LOV in pET28a cloned as described previously[9] was used as template DNA for PCR mutagenesis. Site-directed mutagenesis was carried out using the QuikChange mutagenesis technique according to the instructions given by the manufacturer (Stratagene, La Jolla, CA). Turbo-Pfu DNA polymerase (Stratagene) was used for amplification. Oligonucleotide primers for the introduction of the respective R61H and R66I amino acid substitutions were as follows: PpSB1_R61H_fw: 5′-GCAGGGTGACGACCATGACCAGCTTGG-3′ and PpSB1_R61H_rev: 5′-CCAAGCTGGTCATGGTCGTCACCCTGC-3′ and PpSB1_R66I_fw: 5′-CGTGACCAGCTTGGCATTGCACGCATCCGCAAGG-3′ and PpSB1_R66I_rev: 5′-CCTTGCGGATGCGTGCAATGCCAAGCTGGTCACG-3′.

Protein expression and purification

The PpSB1-LOV protein was expressed in *E. coli* BL21 (DE3) as described previously.[9] The cell pellet (5 g cells, wet weight) was dissolved in 30 ml lysis buffer [50 mM NaH_2PO_4, 300 mM NaCl and 10 mM imidazole (pH 8.0)]. Cells were lysed by passing the cell suspension four times through a French pressure cell (Thermo Scientific, Waltham, MA) at a constant pressure of 1100 bar. The soluble fraction and pellet were separated by centrifugation at 4 °C, 9200*g*, with a SLC-4000 rotor for 30 min. The lysate was purified by metal affinity chromatography using a Superflow Ni-NTA resin (QIAGEN, Hilden, Germany). All purification steps employing an ÄKTAexplorer FPLC system (GE Healthcare, Buckinghamshire, UK) were carried out at 4 °C. Elution was performed with a gradient between washing buffer [50 mM NaH_2PO_4, 300 mM NaCl and 20 mM imidazole (pH 8.0)] and elution buffer [50 mM NaH_2PO_4, 300 mM NaCl and 250 mM imidazole (pH 8.0)]. The purity of the eluted fractions was evaluated by SDS-PAGE. Pure fractions were pooled, and the elution buffer was exchanged to 10 mM Tris–HCl (pH 7.0) and 10 mM NaCl by spin filtration using Vivaspin concentrator units (molecular mass cutoff: 10 kDa) (Sigma-Aldrich, St. Louis, MO). The final protein concentration used for crystallization trials was 40 mg/ml as determined using the Bradford assay.

Spectroscopic techniques

All spectroscopic analysis were carried out under dim red safety light. Measurement of light-dependent absorption changes in the UV/Vis region (200–600 nm) was carried out using a Beckman DU-650 spectrophotometer. All measurements were performed at 20 °C. Protein samples were stored and diluted in 10 mM sodium phosphate buffer supplemented with 10 mM NaCl (pH 8.0). In order to generate the LOV proteins light state, we illuminated the samples for 30 s using a blue-light (450 nm)-emitting LED Lenser V8 lamp (Zweibrüder Optoelectronics GmbH, Solingen, Germany). The dark-state recovery was measured from illuminated samples by recording the absorption recovery at 485 nm until the baseline was reached.

Single crystal microspectrometry

PpSB1-LOV crystals grown in light were mounted in a 200-μm loop. Absorbance spectra in the wavelength range 350–700 nm were recorded using an IR/Vis microscope equipped with a 100-W Hg lamp, as described previously.[42] Absorbance spectra were recorded for the light-grown crystals, for the same crystals illuminated for 30 s with blue light using a 450-nm LED Lenser V8 lamp and for the light-grown crystals kept in dark for up to 4 days at room temperature.

Chromatographic techniques

Separation and quantification of FAD, FMN and riboflavin was achieved using HPLC as described previously.[9]

Protein crystallization

The purified protein was concentrated to 40 mg/ml, and crystallization setups were performed using the vapor-diffusion method. Crystals were grown in 2-μl sitting drops (1 μl purified protein + 1 μl reservoir solution) against 100 mM Tris (pH 7.5) and 8–18% (w/v) polyethylene glycol 3350 at 19 °C either under continuous

white-light illumination using one neon tube Lumilux Plus 18W 21-840 (Osram, Munich, Germany) or in the dark. Usually, the crystals appeared within 3 days under light conditions.

Data collection

An X-ray diffraction data set was collected at 100 K. Prior to cryo-cooling, the crystal was soaked stepwise in reservoir solution containing up to 20% (v/v) glycerol. Native data were recorded at the micro-focus beamline ID23-2 of the European Synchrotron Radiation Facility (ESRF) (Grenoble, France) tuned to a wavelength of 0.8726 Å on a MarCCD detector (Marresearch). Radiation damage was taken into account in the data collection strategy based on calculations using the program BEST.[43] Data processing including reflections up to 2.63 Å resolution was carried out using MOSFLM[44] and SCALA (CCP4).

Structure determination

The crystals obtained for PpSB1-LOV belonged to space group $P6_1$. The structure was determined by molecular replacement using MOLREP (CCP4)[45] with a single native data set. The search model was created from the crystal structure of the phot-LOV1 domain from *C. reinhardtii* (PDB ID: 1N9L[22]) by replacing amino acid side chains with the software Chainsaw (CCP4). Crystals were found to contain two molecules per asymmetric unit, corresponding to a Matthews coefficient of 2.97 $Å^3$/Da and a solvent content of 58.6%. Following rigid-body refinement using the PHENIX package,[28] the model was improved in an iterative manner, including several cycles of non-crystallographic-symmetry-restrained positional and isotropic temperature factor refinement with PHENIX and manual rebuilding using the program COOT.[46] For statistics on data collection and refinement, refer to Table 1.

Graphical representation

Unless otherwise indicated, figures were generated with MOLSCRIPT[47] and Raster3D[48] using secondary structure assignments as given by the DSSP program.[49]

PDB accession code

The atomic coordinates and structure factors for PpSB1-LOV (ID: 3SW1) have been deposited in the PDB§.

Acknowledgements

The authors wish to thank Georg Büldt for continuous generous support and the scientists at beamline ID23-2 at the ESRF (Grenoble, France). Part of this work has been funded by the Deutsche Forschungsgemeinschaft within the GRK1166 "Biocatalysis in Non-Conventional Media".

§ http://rutgers.rcsb.org/pdb

Supplementary Data

Supplementary data associated with this article can be found, in the online version, at doi:10.1016/j.jmb.2012.01.056

References

1. van der Horst, M. A. & Hellingwerf, K. J. (2004). Photoreceptor proteins, "star actors of modern times": a review of the functional dynamics in the structure of representative members of six different photoreceptor families. *Acc. Chem. Res.* **37**, 13–20.
2. Demarsy, E. & Frankhauser, C. (2009). Higher plants use LOV to perceive blue light. *Curr. Opin. Plant Biol.* **12**, 69–74.
3. Losi, A. (2006). Flavin-based photoreceptors in bacteria. In *Flavins Photochemistry and Photobiology* (Silva, E. & Edwards, A. M., eds), 6, pp. The Royal Soceity of Chemistry, Cambridge, UK.
4. Krauss, U., Minh, B. Q., Losi, A., Gärtner, W., Eggert, T., von Haeseler, A. & Jaeger, K. E. (2009). Distribution and phylogeny of light-oxygen-voltage-blue-light-signaling proteins in the three kingdoms of life. *J. Bacteriol.* **191**, 7234–7242.
5. Losi, A. (2007). Flavin-based blue-light photosensors: a photobiophysics update. *Photochem. Photobiol.* **83**, 1283–1300.
6. Losi, A. & Gärtner, W. (2008). Bacterial bilin- and flavin-binding photoreceptors. *Photochem. Photobiol. Sci.* **7**, 1168–1178.
7. Zoltowski, B. D. & Gardner, K. H. (2011). Tripping the light fantastic: blue-light photoreceptors as examples of environmentally modulated protein–protein interactions. *Biochemistry*, **50**, 4–16.
8. Purcell, E. B. & Crosson, S. (2008). Photoregulation in prokaryotes. *Curr. Opin. Microbiol.* **11**, 168–178.
9. Jentzsch, K., Wirtz, A., Circolone, F., Drepper, T., Losi, A., Gärtner, W. *et al.* (2009). Mutual exchange of kinetic properties by extended mutagenesis in two short LOV domain proteins from *Pseudomonas putida*. *Biochemistry*, **48**, 10321–10333.
10. Zoltowski, B. D., Vaccaro, B. & Crane, B. R. (2009). Mechanism-based tuning of a LOV domain photoreceptor. *Nat. Chem. Biol.* **5**, 827–834.
11. Ishikawa, M., Takahashi, F., Nozaki, H., Nagasato, C., Motomura, T. & Kataoka, H. (2009). Distribution and phylogeny of the blue light receptors aureochromes in eukaryotes. *Planta*, **230**, 543–552.
12. Chen, C. H., Dunlap, J. C. & Loros, J. J. (2010). Neurospora illuminates fungal photoreception. *Fungal Genet. Biol.* **47**, 922–929.
13. Djouani-Tahri el, B., Christie, J. M., Sanchez-Ferandin, S., Sanchez, F., Bouget, F. Y. & Corellou, F. (2011). A eukaryotic LOV-histidine kinase with circadian clock

function in the picoalga *Ostreococcus*. *Plant J.* **65**, 578–588.
14. Krauss, U., Losi, A., Gärtner, W., Jaeger, K. E. & Eggert, T. (2005). Initial characterization of a blue-light sensing, phototropin-related protein from *Pseudomonas putida*: a paradigm for an extended LOV construct. *Phys. Chem. Chem. Phys.* **7**, 2804–2811.
15. Zoltowski, B. D., Schwerdtfeger, C., Widom, J., Loros, J. J., Bilwes, A. M., Dunlap, J. C. & Crane, B. R. (2007). Conformational switching in the fungal light sensor Vivid. *Science*, **316**, 1054–1057.
16. Takahashi, F., Yamagata, D., Ishikawa, M., Fukamatsu, Y., Ogura, Y., Kasahara, M. *et al.* (2007). AUREOCHROME, a photoreceptor required for photomorphogenesis in stramenopiles. *Proc. Natl Acad. Sci. USA*, **104**, 19625–19630.
17. Avila-Pérez, M., Hellingwerf, K. J. & Kort, R. (2006). Blue light activates the σB-dependent stress response of *Bacillus subtilis* via YtvA. *J. Bacteriol.* **188**, 6411–6414.
18. Swartz, T. E., Tseng, T. S., Frederickson, M. A., Paris, G., Comerci, D. J., Rajashekara, G. *et al.* (2007). Blue-light-activated histidine kinases: two-component sensors in bacteria. *Science*, **317**, 1090–1093.
19. Purcell, E. B., Siegal-Gaskins, D., Rawling, D. C., Fiebig, A. & Crosson, S. (2007). A photosensory two-component system regulates bacterial cell attachment. *Proc. Natl Acad. Sci. USA*, **104**, 18241–18246.
20. Crosson, S. & Moffat, K. (2001). Structure of a flavin-binding plant photoreceptor domain: insights into light-mediated signal transduction. *Proc. Natl Acad. Sci. USA*, **98**, 2995–3000.
21. Crosson, S. & Moffat, K. (2002). Photoexcited structure of a plant photoreceptor domain reveals a light-driven molecular switch. *Plant Cell*, **14**, 1067–1075.
22. Fedorov, R., Schlichting, I., Hartmann, E., Domratcheva, T., Fuhrmann, M. & Hegemann, P. (2003). Crystal structures and molecular mechanism of a light-induced signaling switch: the Phot-LOV1 domain from *Chlamydomonas reinhardtii*. *Biophys. J.* **84**, 2474–2482.
23. Halavaty, A. S. & Moffat, K. (2007). N- and C-terminal flanking regions modulate light-induced signal transduction in the LOV2 domain of the blue light sensor phototropin 1 from *Avena sativa*. *Biochemistry*, **46**, 14001–14009.
24. Möglich, A. & Moffat, K. (2007). Structural basis for light-dependent signaling in the dimeric LOV domain of the photosensor YtvA. *J. Mol. Biol.* **373**, 112–126.
25. Möglich, A., Ayers, R. A. & Moffat, K. (2009). Structure and signaling mechanism of Per-ARNT-Sim domains. *Structure*, **17**, 1282–1294.
26. Harper, S. M., Neil, L. C. & Gardner, K. H. (2003). Structural basis of a phototropin light switch. *Science*, **301**, 1541–1544.
27. Nash, A. I., McNulty, R., Shillito, M. E., Swartz, T. E., Bogomolni, R. A., Luecke, H. & Gardner, K. H. (2011). Structural basis of photosensitivity in a bacterial light–oxygen–voltage/helix–turn–helix (LOV–HTH) DNA-binding protein. *Proc. Natl Acad. Sci. USA*, **108**, 9449–9454.
28. Adams, P. D., Grosse-Kunstleve, R. W., Hung, L. W., Ioerger, T. R., McCoy, A. J., Moriarty, N. W. *et al.* (2002). PHENIX: building new software for automated crystallographic structure determination. *Acta Crystallogr., Sect. D: Biol. Crystallogr.* **58**, 1948–1954.
29. Nakasako, M., Zikihara, K., Matsuoka, D., Katsura, H. & Tokutomi, S. (2008). Structural basis of the LOV1 dimerization of *Arabidopsis* phototropins 1 and 2. *J. Mol. Biol.* **381**, 718–733.
30. Vaidya, A. T., Chen, C. H., Dunlap, J. C., Loros, J. J. & Crane, B. R. (2011). Structure of a light-activated LOV protein dimer that regulates transcription. *Sci. Signal.* **4**, ra50, doi:10.1126/scisignal.2001945.
31. Krissinel, E. & Henrick, K. (2007). Inference of macromolecular assemblies from crystalline state. *J. Mol. Biol.* **372**, 774–797.
32. Tang, Y., Cao, Z., Livoti, E., Krauss, U., Jaeger, K. E., Gärtner, W. & Losi, A. (2010). Interdomain signalling in the blue-light sensing and GTP-binding protein YtvA: a mutagenesis study uncovering the importance of specific protein sites. *Photochem. Photobiol. Sci.* **9**, 47–56.
33. Purcell, E. B., McDonald, C. A., Palfey, B. A. & Crosson, S. (2010). An analysis of the solution structure and signaling mechanism of LovK, a sensor histidine kinase integrating light and redox signals. *Biochemistry*, **49**, 6761–6770.
34. Phillips, G. N., Jr (1990). Comparison of the dynamics of myoglobin in different crystal forms. *Biophys. J.* **57**, 381–383.
35. Avila-Pérez, M., Vreede, J., Tang, Y., Bende, O., Losi, A., Gärtner, W. & Hellingwerf, K. (2009). *In vivo* mutational analysis of YtvA from *Bacillus subtilis*: mechanism of light activation of the general stress response. *J. Biol. Chem.* **284**, 24958–24964.
36. Buttani, V., Losi, A., Eggert, T., Krauss, U., Jaeger, K. E., Cao, Z. & Gärtner, W. (2007). Conformational analysis of the blue-light sensing protein YtvA reveals a competitive interface for LOV–LOV dimerization and interdomain interactions. *Photochem. Photobiol. Sci.* **6**, 41–49.
37. Jurk, M., Dorn, M. & Schmieder, P. (2011). Blue flickers of hope: secondary structure, dynamics and putative dimerisation interface of the blue-light receptor YtvA from *Bacillus subtilis*. *Biochemistry*, **50**, 8163–8171.
38. Park, H., Suquet, C., Satterlee, J. D. & Kang, C. (2004). Insights into signal transduction involving PAS domain oxygen-sensing heme proteins from the X-ray crystal structure of *Escherichia coli* Dos heme domain (*Ec* DosH). *Biochemistry*, **43**, 2738–2746.
39. Miyatake, H., Mukai, M., Park, S. Y., Adachi, S., Tamura, K., Nakamura, H. *et al.* (2000). Sensory mechanism of oxygen sensor FixL from *Rhizobium meliloti*: crystallographic, mutagenesis and resonance Raman spectroscopic studies. *J. Mol. Biol.* **301**, 415–431.
40. Key, J., Hefti, M., Purcell, E. B. & Moffat, K. (2007). Structure of the redox sensor domain of *Azotobacter vinelandii* NifL at atomic resolution: signaling, dimerization, and mechanism. *Biochemistry*, **46**, 3614–3623.
41. Ma, X., Sayed, N., Baskaran, P., Beuve, A. & van den Akker, F. (2008). PAS-mediated dimerization of soluble guanylyl cyclase revealed by signal transduction histidine kinase domain crystal structure. *J. Biol. Chem.* **283**, 1167–1178.
42. Efremov, R., Gordeliy, V. I., Heberle, J. & Büldt, G. (2006). Time-resolved microspectroscopy on a single crystal of bacteriorhodopsin reveals lattice-induced differences in the photocycle kinetics. *Biophys. J.* **91**, 1441–1451.

43. Bourenkov, G. P. & Popov, A. N. (2010). Optimization of data collection taking radiation damage into account. *Acta Crystallogr., Sect. D: Biol. Crystallogr.* **66**, 409–419.
44. Leslie, A. G. W. (1992). Recent changes to the MOSFLM package for processing film and image plate data. *Joint CCP4 and ESF-EAMCB Newsletter on Protein Crystallography*, **26**.
45. Winn, M. D., Ballard, C. C., Cowtan, K. D., Dodson, E. J., Emsley, P., Evans, P. R. *et al.* (2011). Overview of the CCP4 suite and current developments. *Acta Crystallogr., Sect. D: Biol. Crystallogr.* **67**, 235–242.
46. Emsley, P. & Cowtan, K. (2004). Coot: model-building tools for molecular graphics. *Acta Crystallogr., Sect. D: Biol. Crystallogr.* **60**, 2126–2132.
47. Kraulis, P. J. (1991). MOLSCRIPT: a program to produce both detailed and schematic plots of protein structures. *J. Appl. Crystallogr.* **24**, 946–950.
48. Merritt, E. A. & Bacon, D. J. (1997). Raster3D: photorealistic molecular graphics. *Methods Enzymol.* **277**, 505–524.
49. Kabsch, W. & Sander, C. (1983). Dictionary of protein secondary structure: pattern recognition of hydrogen-bonded and geometrical features. *Biopolymers*, **22**, 2577–2637.

4. *Pseudomonadaceae* "short" LOV proteins

4.1 Conservation of dark recovery kinetic parameters and structural features in the *Pseudomonadaceae* "short" LOV protein family – implications for the design of LOV-based optogenetic tools

Raj Rani*, Katrin Jentzsch*, Justin Lecher, Rudolf Hartman, Dieter Willbold, Karl-Erich Jaeger and Ulrich Krauss

* Contributed equally

Biochemistry **52**, 4460-4473

BIOCHEMISTRY
including biophysical chemistry & molecular biology

Article

pubs.acs.org/biochemistry

Conservation of Dark Recovery Kinetic Parameters and Structural Features in the Pseudomonadaceae "Short" Light, Oxygen, Voltage (LOV) Protein Family: Implications for the Design of LOV-Based Optogenetic Tools

Raj Rani,[†] Katrin Jentzsch,[†] Justin Lecher,[‡] Rudolf Hartmann,[‡] Dieter Willbold,[‡,§] Karl-Erich Jaeger,[†] and Ulrich Krauss*[,†]

[†]Institut für Molekulare Enzymtechnologie, Heinrich-Heine-Universität Düsseldorf, Forschungszentrum Jülich, Stetternicher Forst, D-52426 Jülich, Germany

[‡]Institute of Complex Systems, ICS-6, Forschungszentrum Jülich, Jülich, Germany

[§]Institut für Physikalische Biologie, Heinrich-Heine-Universität Düsseldorf, Düsseldorf, Germany

Supporting Information

ABSTRACT: In bacteria and fungi, various light, oxygen, voltage (LOV) sensory systems that lack a fused effector domain but instead contain only short N- and C-terminal extensions flanking the LOV core exist. In the prokaryotic kingdom, this so-called "short" LOV protein family represents the third largest LOV photoreceptor family. This observation prompted us to study their distribution and phylogeny as well as their photochemical and structural properties in more detail. We recently described the slow and fast reverting "short" LOV proteins PpSB1-LOV and PpSB2-LOV from *Pseudomonas putida* KT2440 whose adduct state lifetimes varied by 3 orders of magnitude [Jentzsch, K., Wirtz, A., Circolone, F., Drepper, T., Losi, A., Gärtner, W., Jaeger, K. E., and Krauss, U. (2009) *Biochemistry 48*, 10321−10333]. We now present evidence of the conservation of similar fast and slow-reverting "short" LOV proteins in different *Pseudomonas* species. Truncation studies conducted with PpSB1-LOV and PpSB2-LOV suggested that the short N- and C-terminal extensions outside of the LOV core domain are essential for the structural integrity and folding of the two proteins. While circular dichroism and solution nuclear magnetic resonance experiments verify that the two short C-terminal extensions of PpSB1-LOV and PpSB2-LOV form independently folding helical structures in solution, bioinformatic analyses imply the formation of coiled coils of the respective structural elements in the context of the dimeric full-length proteins. Given their prototypic architecture, conserved in most more complex LOV photoreceptor systems, "short" LOV proteins could represent ideally suited building blocks for the design of genetically encoded photoswitches (i.e., LOV-based optogenetic tools).

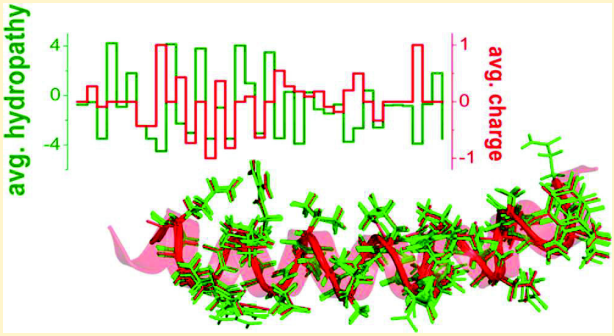

Light, oxygen, voltage (LOV) photoreceptors are ubiquitously distributed, functionally versatile, multidomain sensory systems,[1,2] whose blue light-sensitive LOV domains show a conserved Per-Arnt-Sim (PAS) fold.[3] Like other PAS domains,[3] LOV domains bind a small molecule ligand [i.e., flavin mononucleotide (FMN)] that mediates initial signal perception.[4] Hereby, LOV domains undergo a blue light-dependent photocycle, which intricately links flavin photochemistry and protein structural rearrangements in the vicinity of the FMN molecule to larger scale conformational changes of N- and C-terminally located structural elements outside of the conserved sensor core domain.[4] In multidomain LOV photoreceptors, those latter structural elements link the sensor domain with a variety of different effector domain modules such as kinases, phosphodiesterases, DNA-binding domains, and transcription factors.[1,5,6] In most recent studies, those auxiliary elements are termed the N-terminal cap (N-cap) and C-terminal Jα-helix.[7−11] For many of the previously studied LOV photoreceptor proteins, removal of those elements is possible without impairing folding and photocycling. In fact, most LOV domain X-ray structures were initially obtained for truncated constructs consisting only of the conserved sensor core domain.[12−14] More recently, it became evident that, for example, the interaction of those linker elements with the sensor core domain can be modulated by blue light, eventually facilitating the biological response.[4,6] In the rapidly growing field of LOV-based optogenetics, this relay mechanism is exploited to confer light-dependent control to non-photo-

Received: March 11, 2013
Revised: May 27, 2013
Published: June 7, 2013

dx.doi.org/10.1021/bi400311r | *Biochemistry* 2013, 52, 4460−4473

sensitive enzymes and proteins.[15−21] In conclusion, the orientation and structure of the N- and C-terminal elements outside the conserved sensor core is of primary importance for understanding LOV- and PAS-based signaling responses[4,6,7] and can provide a rational basis for the design of LOV-based optogenetic switches.[16] While those N- and C-terminal elements apparently make up a conserved part of most LOV photoreceptors,[4,6,7] their sequence as well as the mode and degree of interaction between them and the sensory core domain varies from system to system.[4,18]

In bacteria and fungi, a subset of LOV photoreceptors that lack fused effector domains exist. Those proteins either possess only an N-cap (*Neurospora crassa* VVD[22]) or contain both N-cap and Jα structural elements (*Pseudomonas putida* PpSB1-LOV and PpSB2-LOV[7] and RsLOV of *Rhodobacter sphaeroides* 2.4.1[23,24]). In bacteria, "short" LOV proteins are present in approximately 11−13% of fully sequenced bacterial genomes.[5] This renders them the third largest LOV protein family in the prokaryotic kingdom.[5] Although "short" LOV proteins lack associated effector domains, a physiological function has been attributed to *N. crassa* VVD and recently also to RsLOV.[23,24] While VVD modulates gating of the circadian clock via interaction with the White-Collar Complex (WCC), the central transcription factor of the circadian clock in *N. crassa*,[22] RsLOV, was suggested to act as a repressor of photosynthesis gene expression and was linked to photooxidative damage responses, carbohydrate metabolism, and chemotaxis.[24]

We recently described a set of two "short" LOV proteins, PpSB1-LOV and PpSB2-LOV, from the saprotrophic microbe *P. putida* KT2440.[25,26] The two proteins are highly similar with respect to their amino acid sequence (approximately 66% identical amino acids) but display drastically different photocycle kinetic properties.[25,26] The light state X-ray structure determined for the slow-cycling PpSB1-LOV protein revealed a canonical LOV core domain with short helical N- and C-terminal extensions (N-cap and Jα-helix, respectively).[7] Both of the latter structural elements facilitate assembly of the parallel homodimer in the crystal. Hereby, the C-terminal Jα-helices, which protrude from the subunit core, contribute to dimer stability by supporting subunit assembly via a coiled-coil-like interaction promoted by hydrophobic residues buried in the Jα dimer interface.[7] Thus, it is of considerable interest whether variable dark recovery kinetic properties as well as the respective auxiliary structural features are conserved among the family of "short" LOV proteins. Although the recent X-ray structure provides the first insights into the structural role of both N- and C-terminal extensions, their role for folding of the full-length "short" LOV proteins in solution is yet ill defined.

To address evolutionary conservation of "short" LOV proteins, we here study the distribution and phylogeny as well as photochemical and structural properties of a set of bacterial "short" LOV proteins. Specifically, we present evidence of a subclassification of bacterial "short" LOV proteins with respect to conserved sequence features and phylogeny. Five "short" LOV proteins of the Pseudomonadaceae group were spectroscopically characterized, suggesting an evolutionary conservation of fast- and slow-reverting "short" LOV proteins in Pseudomonadaceae. The conservation of N- and C-terminal auxiliary structural elements (Jα-helix and N-cap, respectively) was studied by CD and solution nuclear magnetic resonance (NMR) spectroscopy. Truncation studies conducted with PpSB1-LOV and PpSB2-LOV proteins, as the structural prototypes of the here identified Pseudomonadaceae "short" LOV protein family, suggested that both structural elements contribute to proper protein folding in solution. While bioinformatic sequence analyses of the C-terminal Jα-helix extensions imply the presence of coiled-coil interaction motifs in all Pseudomonadaceae "short" LOV proteins, CD and NMR spectroscopic studies revealed that the respective Jα-helix extensions of PpSB1-LOV and PpSB2-LOV can form independently folding helical structures, but not coiled coils when studied as synthetic peptides in isolated form. Implications for the role of the respective extensions in "short" LOV signaling and for the design of LOV-based optogenetic tools are discussed.

MATERIALS AND METHODS

Bacterial Strains and Plasmids. All bacterial strains used in this study were grown either in Luria-Bertani (LB) broth or in autoinduction (AI) medium[27] as described previously.[25,26] Synthetic genes encoding five Pseudomonadaceae "short" LOV proteins were obtained from Eurofins MWG operon GmbH (Ebersberg, Germany). The respective UniProt entries were as follows: Q3KHW7 for *Pseudomonas fluorescens* Pf0-1-LOV, Q4KI48 for *P. fluorescens* Pf5-LOV, C3K1W0 for *P. fluorescens* SBW25-LOV, B1JAC4 for *P. putida* W619_1-LOV, and B1J385 for *P. putida* W619_2-LOV. The latter organism, like *P. putida* KT2440, possesses two "short" LOV paralogs. All other *Pseudomonas* strains contain only one "short" LOV protein-encoding gene. All genes were custom synthesized carrying 5′-*Nde*I and 3′-*Xho*I restriction endonuclease sites. During gene synthesis, codon usage was not optimized, retaining the original DNA sequence as found in the UniProt and NCBI GenBank databases. *Nde*I and *Xho*I restriction sites were used to subclone the synthetic genes (supplied in a pCR2.1 vector) into pET28a vectors (Novagen/Merck, Darmstadt, Germany) for heterologous expression in *Escherichia coli*. Truncated PpSB1-LOV and PpSB2-LOV constructs were amplified via polymerase chain reaction (PCR) as described below and similarly cloned into the pET28a vector system for expression. All constructs were expressed as N-terminal hexahistidine-tagged fusion proteins (tag sequence, MGSSHHHHHHSSGLVPRGSH) in *E. coli* BL21(DE3). Please note that in this study a PpSB2-LOV construct was used, which in contrast to the database entry (Swiss-Prot entry Q88JB0) lacks the first three N-terminal amino acids.[28] The sequences of all synthetic genes as well as of the truncated PpSB1-LOV and PpSB2-LOV variants were verified by sequencing (SeqLab GmbH, Göttingen, Germany).

General Molecular Biology Techniques. Isolation of recombinant plasmids, gel extraction of DNA fragments, DNA ligation, and transformation of *E. coli* strains were conducted according to standard laboratory protocols.[29]

Construction of Truncated PpSB1-LOV and PpSB2-LOV Variants. The truncated PpSB1-LOV and PpSB2-LOV variants were amplified by PCR from pET28a vectors containing the full-length PpSB1-LOV and PpSB2-LOV coding genes[25,26] by using gene specific primers (Table 1 of the Supporting Information), designed to allow directional cloning of the respective truncated variant into the pET28a vector system by employing 5′-*Nde*I and 3′-*Xho*I restriction endonuclease sites. At the 3′-end of the respective gene fragment, a TAA stop codon was added. The truncated constructs consisted of the following protein segments: PpSB1-ΔNcap (residues 17−142), PpSB1-ΔJα (residues 1−119), PpSB1-ΔNcapΔJα (residues 17−119), PpSB2-ΔNcap (resi-

dues 17−148), PpSB2-ΔJα (residues 1−119), and PpSB2-ΔNcapΔJα (residues 17−119).

Protein Overexpression and Purification. All LOV proteins were expressed and purified using immobilized metal affinity chromatography (IMAC) as described previously.[26] After elution from the IMAC column, the pooled LOV protein-containing fractions were desalted using a Sephadex G25 column. Samples were concentrated employing a VivaSpin concentrator unit (10 kDa molecular mass cutoff) (Sigma-Aldrich, St. Louis, MO). The final buffer was 10 mM sodium phosphate buffer (pH 8.0) supplemented with 10 mM NaCl. All purified proteins were stored at 4 °C in the dark until further use.

Sodium Dodecyl Sulfate−Polyacrylamide Gel Electrophoresis (SDS−PAGE) and Immunoblot Analysis. SDS−PAGE was performed by using 15% polyacrylamide Tris/glycine gels as described by Laemmli,[30] in a vertical MiniProteanII gel apparatus (Bio-Rad Laboratories, Munich, Germany), or by using precast Novex Tris/glycine gels (4−12% polyacrylamide) in an XCell SureLock mini-cell electrophoresis system (Novagen/Merck, Darmstadt, Germany). For SDS−PAGE analyses of soluble and insoluble cell fractions, equal amounts of cells were resuspended [10% (w/v) wet cells] in 10 mM sodium phosphate buffer (pH 8.0) supplemented with 10 mM NaCl. Cells were lysed by being passed three times through a chilled 40K French pressure cell (Thermo Scientific, Waltham, MA) at a constant pressure of 5.5×10^7 Pa. The soluble protein was separated from cell debris and insoluble aggregates by centrifugation at 12000 rpm for 20 min at 4 °C. The resulting supernatant is termed the soluble protein fraction. The insoluble pellet was resuspended in the initial volume of buffer and designated as the insoluble fraction. The protein concentration of the soluble fraction was determined using the Bradford assay.[31] For SDS−PAGE analyses, approximately 20 μg of soluble protein as well as the corresponding volume of the insoluble fraction was loaded per lane.

For Western blot analyses, SDS−PAGE-separated proteins were electro-transferred onto a polyvinylidene fluoride (PVDF) membrane (Bio-Rad Laboratories, Hercules, CA). For the detection of membrane-bound PpSB1-LOV and PpSB2-LOV proteins, polyclonal PpSB1-LOV and PpSB2-LOV antisera (rabbit) (Eurogentec, Seraing, Belgium) were used. For hybridization, antisera were diluted 1:40000 with TBS-T buffer [25 mM Tris-HCl, 3 mM KCl (pH 8.0), and 140 mM NaCl supplemented with 0.2% Tween 20]. As a loading control, T7 RNA polymerase was detected using monoclonal T7 RNA polymerase antibodies (Novagen/Merck) at a 1:20000 dilution in TBS-T. As secondary antibodies, either a goat anti-rabbit horseradish peroxidase (HRP) conjugate (PpSB1-LOV and PpSB2-LOV detection) or a goat anti-mouse HRP conjugate (T7 detection) (Bio-Rad Laboratories, Munich, Germany) was used. Both secondary antibodies allow the detection of the PVDF membrane-bound target antigen by chemiluminescence. Chemiluminescence signals were detected using the Amersham ECL Western Blotting Detection Reagents (GE Healthcare, Uppsala, Sweden) by photographing the blot membrane using a Stella camera system (raytest GmbH, Straubenhardt, Germany).

Peptide Synthesis. PpSB1-Jα (residues 120−142 of the full-length protein) and PpSB2-Jα peptides (residues 120−148 of the full-length protein) were purchased in N-acetylated custom-synthesized form (98% pure) from Peptide 2.0 Inc. (Chantilly, VA): PpSB1-Jα (ACE-S_{120}-RQVELERELAELRAR-PKPDERA$_{142}$) and PpSB2-Jα (ACE-T_{120}AQVFAEERVRELE-AEVAELRRQQGQAKH$_{148}$). For NMR or CD analyses, the respective peptides were resuspended to a final concentration of 1 mM in either 100 mM sodium phosphate buffer (pH 6.3) supplemented with 50 mM NaCl or 20 mM sodium phosphate buffer (pH 7.5) supplemented with 1 mM NaCl, respectively.

UV−Vis Absorbance Spectroscopy. All spectroscopic work was conducted under dim red safety light. Light-dependent absorption changes in the UV−vis region (200−600 nm) were recorded using a Beckmann UV650 spectrophotometer (Beckmann Coulter, Krefeld, Germany) with the temperature control set to 37 °C. Protein samples were diluted in 10 mM sodium phosphate buffer supplemented with 10 mM NaCl (pH 8.0). The same buffer was used as a reference. LOV protein light state UV−vis spectra were recorded after illuminating the sample for 30 s using a blue light-emitting Led-Lensers V8 lamp (Zweibrüder Optoelectronics, Solingen, Germany). Dark state recovery was measured from illuminated samples by monitoring the absorption recovery at 480 nm. All dark recovery kinetic measurements were taken three times using three independent protein preparations. Dark recovery time traces were fit using a single-exponential decay function by employing Origin 7G (OriginLab Corp., Northampton, MA).

Circular Dichroism (CD) Experiments. Far-UV circular dichroism (CD) spectra were recorded using a temperature-controlled JASCO J-810 spectropolarimeter. For secondary structure composition analyses, all LOV protein samples [diluted in 10 mM sodium phosphate buffer (pH 8.0) supplemented with 10 mM NaCl] were incubated for 10 min at 20 or 1 °C in the spectropolarimeter. CD spectra were collected between 190 and 250 nm in 0.5 nm intervals with a scan speed of 100 nm/min. Three spectra were averaged to obtain the final CD spectrum of the respective protein. All protein CD spectra were evaluated and deconvoluted using the Convex-Constraint Analysis (CCA) tool by employing a data set of five pure components for the *Pseudomonas* LOV proteins as described previously.[32]

CD Spectroscopic Analysis of Peptide Unfolding and/or Refolding. To monitor the temperature-dependent unfolding of the PpSB1-Jα and PpSB2-Jα peptides, far-UV CD spectra were recorded sequentially while the temperature of the sample was increased from 1 to 65 °C using a constant ramp rate of 1 °C/min. Refolding of the respective peptide was followed in a similar manner by cooling the completely unfolded peptide sample to 1 °C using the same ramp rate. Jα-peptide CD spectra were analyzed as described for the protein samples, but assuming the presence of only two pure components (random coil and α-helix). Melting temperatures were obtained from the plot of the ellipticity at 222 nm (Θ_{222}) versus temperature (Figure 5) by fitting the experimental data to eq 1. The same fit was used to estimate the maximal and minimal ellipticity values for the fully folded peptides, $[\Theta]_{folded}$, and the completely unfolded peptides, $[\Theta]_{unfolded}$. Those latter values were used to quantitatively describe α-helix melting in terms of the α-helical fraction (f_α) under the premise of a two-state transition (eq 2).

$$\Theta_{222}(T) = \frac{[\Theta]_{folded} - [\Theta]_{unfolded}}{1 + e^{(T-T_m)/dx}} + [\Theta]_{unfolded} \quad (1)$$

$$f_\alpha = \frac{[\Theta] - [\Theta]_{unfolded}}{[\Theta]_{folded} - [\Theta]_{unfolded}} \quad (2)$$

Thermodynamic parameters were obtained by fitting the calculated equilibrium α-helix fraction (f_α) to eq 3

$$\ln(K_{eq}) = \ln\left(\frac{f_\alpha}{1-f_\alpha}\right) = \frac{-\Delta H}{R}\left(\frac{1}{T}\right) + \frac{\Delta S}{R} \quad (3)$$

The fits of $\ln(K_{eq})$ versus $1/T$ were highly linear with R values of >0.999. From this fit, values for enthalpy ΔH and entropy ΔS were obtained. The relation $\Delta G = \Delta H - T\Delta S$ was used to obtain the Gibbs free energy of unfolding (ΔG) at a given temperature.

NMR Experiments. All NMR measurements were taken in 100 mM sodium phosphate buffer (pH 6.3) supplemented with 50 mM NaCl, deuterated 2,2,2-trifluoroethanol (TFE) with a final concentration of 10% (v/v) (PpSB1-Jα) or 25% (v/v) (PpSB2-Jα), and 10% (v/v) D_2O. Lyophilized peptide samples were dissolved in the buffer described above to a final concentration of ~1 mM. All NMR experiments were conducted at 25 °C using 5 mm Shigemi NMR tubes on a Varian VNMRS 900 MHz NMR spectrometer equipped with a Z-axis pulsed-field-gradient triple-resonance cryo-probe. Experimental data were collected in phase-sensitive mode using quadrature detection in ω_1 by time-proportional phase incrementation. The water signal was suppressed by the WATERGATE method. Resonance assignment for both peptide samples was accomplished using two-dimensional (2D) (^{1}H−^{1}H) TOCSY and (^{1}H−^{1}H) NOESY experiments. A mixing time of 60 ms and a B1 field of 9000 Hz were used for 2D ^{1}H−^{1}H TOCSY experiments. 2D ^{1}H−^{1}H NOESY experiments were performed with a mixing time of 350 ms. All 2D spectra were collected acquiring 256 increments in the F_1 dimension each consisting of 80 scans. ^{1}H chemical shifts were referenced externally to 2,2-dimethyl-2-silapentane sulfonate at 0 ppm.

Structure Calculations and Structure Analysis. Time domain NMR data were processed and converted into the frequency domain with the aid of NMRPipe.[33] Spectral evaluation and proton resonance assignment were conducted using CcpNmr Analysis.[34] NOESY cross-peak assignment and structure calculations were performed using the combination of Aria version 2.3.1[32] and CNS version 1.21[35,36](including the Aria patchset) with the PARALLHDG version 5.3 force field. All MD parameters were used in the default configuration, but the numbers of steps were increased to 8000 during refinement and 20000 in each cooling phase. The 10 lowest-energy structures of the 250 calculated were further refined in explicit water as a final step in the Aria procedure. Geometrical parameters of the derived structural models and the corresponding secondary structure distribution were analyzed and visualized using MOLMOL,[37] PyMOL,[38] WHAT-IF,[39] and MolProbity.[40] The residue-wise secondary structure propensity (SSP) for the peptide samples was estimated from NMR chemical shift data using the SSP tool developed by Marsh and co-workers.[41] For the superposition and analysis of structures, either PyMOL (Schrödinger LLC, Cambridge, MA)[38] or the Yasara structure suite[42] was employed.

Bioinformatic Analysis. Initially, protein sequences that were significantly similar to the two "short" LOV proteins of *P. putida* KT2440 were obtained from the NCBI database by using the PSI-BLAST tool[43] employing the PpSB1-LOV and PpSB2-LOV amino acid sequences as a query. To verify coverage of all Pseudomonadaceae genome sequences, the same search was conducted using the NCBI genomic group BLAST tool (http://www.ncbi.nlm.nih.gov/sutils/genom_table.cgi), restricting the search to the group of Pseudomonadaceae. Domain content analyses were performed using the SMART tool.[44] Amino acid sequence alignments were generated with T-COFFEE.[45] Alignments were visualized and edited manually using GeneDoc.[46] Bootstrapped maximum-likelihood trees with 100 replicates for each run were generated using the RaxML webserver.[47] Sequence IDs as well as accession numbers for the respective protein sequences can be found in Table 2 of the Supporting Information. The multiple-sequence alignment used for phylogenetic tree computations is shown in Figure 1 of the Supporting Information. The PCOILS webserver[48] was used to analyze Jα-helix sequences for the presence of a coiled-coil heptad repeat pattern. Residue-wise charges and average hydropathies (according to the Kyte−Doolittle scale[49]) were inferred from sequence alignments using custom Perl scripts.

RESULTS

Distribution and Phylogeny of "Short" LOV Proteins in Prokaryotes. To elucidate the "short" LOV protein distribution and phylogeny in more detail, we obtained sequences that were significantly similar to PpSB1-LOV and PpSB2-LOV from GenBank. To verify all obtained sequences are part of the "short" LOV protein family, we performed domain content analyses using the SMART webserver.[44] In this way, we obtained 61 sequences from 53 different bacteria (Table 2 of the Supporting Information). With the exception of one sequence from the actinobacterium *Nakamurella multipartita* Y-104, "short" LOV protein sequences are apparently present only in proteobacteria. In proteobacteria, they are predominant in the γ-subclass (38 sequences) and α-subclass (18 sequences) and can be found in a limited subset of β-proteobacteria (4 sequences). The corresponding phylogentic tree suggested the separation into γ-proteobacterial "short" LOV proteins (Figure 1, colored dark blue, green, light blue, and black) and "short" LOV proteins of other proteobacteria (Figure 1, colored gray). A closer look into the sequence diversity present in the respective alignment (Figure 1 of the Supporting Information) further supports this subdivision by revealing a previously noted noncanonical FMN-binding motif, Y(Q/R)D**C**RFLQG, for most γ-proteobacterial "short" LOV sequences (Figure 1 of the Supporting Information). The remaining "short" LOV proteins contained the classical G(X)N**C**RFLQG motif present in all other prokaryotic and eukaryotic LOV proteins (Figure 1 of the Supporting Information).

In particular, all "short" LOV sequences of the Pseudomonadaceae group (24 sequences) contain the noncanonical Y(Q/R)DCRFLQG sequence motif. Among those, 12 organisms possess only one "short" LOV homologue, whereas six organisms that contain, like *P. putida* KT2440, two genes encoding "short" LOV proteins can be identified. Currently, the Pseudomonadaceae group comprises 181 unique strains for which the genome is completely sequenced. Given this number, "short" LOV proteins with a high level of sequence similarity and thus probably structural and functional similarity to the two *P. putida* KT2440 "short" LOV proteins can be found in ~10% of the sequenced Pseudomonadaceae. The only other γ-proteobacterial orders in which "short" LOV protein sequences, comprising the Y(Q/R)DCRFLQG signature motif, can be identified are Oceanospirillales, Chromatiales, and Thiotrichales.

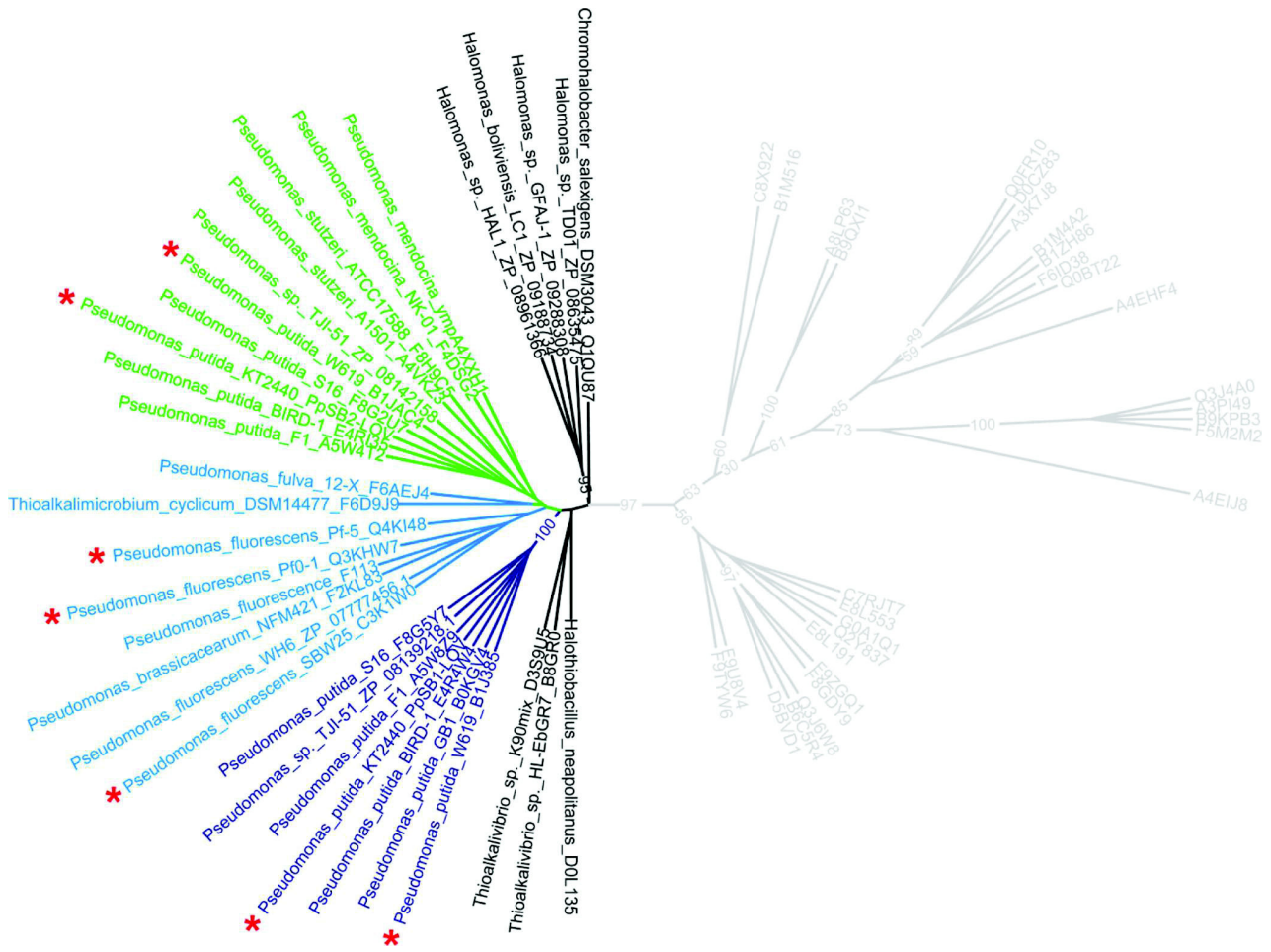

Figure 1. Unrooted phylogentic tree illustrating the distribution and evolutionary divergence of "short" LOV proteins. The tree can globally be divided into two parts: (i) sequences of γ-proteobacterial origin comprising the noncanonical Y(Q/R)DCRFLQG FMN-binding motif (colored black, dark blue, light blue, and green) and (ii) sequences of other proteobacterial subclasses comprising the canonical LOV protein motif G(X)NCRFLQG (colored gray). In the γ-proteobacterial branch, the two *P. putida* KT2240 "short" LOV proteins, PpSB1-LOV and PpSB2-LOV, are found on two distinct clades. The PpSB1-LOV clade is colored dark blue and the PpSB2-LOV clade green. Whereas the PpSB1-LOV clade (dark blue) is comprised solely of *P. putida* sequences, sequences of *P. mendocina* and *P. stutzeri* strains can be found in the PpSB2-LOV clade (green). A third clade (light blue) is formed by sequences from *P. fluorescens*, *P. cyclicum*, and *P. fulva* strains. "Short" LOV sequences from organisms outside the Pseudomonadaceae group are found in orders Oceanospirillales, Chromatiales (black), and Thiotrichales (*T. cyclicum* strain DSM14477, light blue). The Pseudomonadaceae "short" LOV proteins that were characterized in this study are denoted with red asterisks.

In the γ-proteobacterial branch, the two *P. putida* KT2240 "short" LOV proteins, PpSB1-LOV and PpSB2-LOV, are found on three distinct clades (Figure 1). Whereas the PpSB1-LOV clade (Figure 1, dark blue) is comprised solely of *P. putida* sequences, sequences of *Pseudomonas mendocina* and *Pseudomonas stutzeri* strains can be found in the PpSB2-LOV clade (Figure 1, green). A third clade (Figure 1, light blue) is formed by "short" LOV sequences from *P. fluorescens*, *Pseudomonas cyclicum*, *Pseudomonas fulva*, and *Thioalkalimicrobium cyclicum*. The latter sequence represents an exception as it, as a sequence of Thiotrichales origin, clusters within the Pseudomonadaceae clade. Please note that this grouping is incongruent with general organismal phylogeny as reconstructed from 16s rRNA sequences and thus highlights the possibility of "short" LOV inheritance via horizontal gene transfer. Two additional distinct clades are formed by sequences originating from Oceanospirillales (e.g., *Chromohalobacter salexigens* DSM 3043) and Chromatiales (e.g., *Halothiobacillus neapolitanus*) (Figure 1, black).

UV−Vis Spectroscopic and Biochemical Characterization of an Exemplary Set of Pseudomonadaceae "Short" LOV Proteins. The clear separation of the fast-reverting PpSB2-LOV protein sequence from its slow-reverting PpSB1-LOV counterpart on two distinct clades in the phylogentic tree suggests an evolutionary conservation of fast- and slow-reverting "short" LOV proteins in the Pseudomonadaceae group. To study the conservation of structural features and recovery kinetic properties, we cloned, expressed, purified, and characterized a set of five different "short" LOV proteins found in the three distinct Pseudomonadaceae clades. The following "short" LOV proteins were selected as representative sequences: *P. fluorescens* Pf01-LOV (Q3KHW7), *P. fluorescens* Pf5-LOV (Q4KI48), *P. fluorescens* SBW25-LOV (C3K1W0), *P. putida* W619_1-LOV (B1JAC4), and *P. putida* W619_2-LOV (B1J385). All five sequences show the classical features of the Pseudomonadaceae "short" LOV protein family, i.e., Y(Q/R)D<u>C</u>RFLQG motif, conserved N-cap, and C-terminal Jα-extension. All proteins could be expressed in soluble form in *E.*

dx.doi.org/10.1021/bi400311r | *Biochemistry* 2013, 52, 4460−4473

coli and were purified to homogeneity as described previously for PpSB1-LOV and PpSB2-LOV.[25] After equilibration for 2 days at 4 °C in the dark, all protein samples were visibly yellow, indicating the presence of a noncovalently bound flavin chromophore. All five proteins appeared to be dimeric in high-performance liquid chromatography (HPLC)-based size-exclusion chromatographic studies (Table 3 of the Supporting Information). HPLC analyses of the chromophore content revealed that all proteins bound predominately FMN as well as a certain amount of riboflavin as a chromophore (Table 3 of the Supporting Information). With respect to quaternary structure and flavin chromophore content, all of the studied proteins were thus highly similar to the two previously characterized *P. putida* KT2440 LOV proteins.[25] Dark state and photoequilibrium (30 s of blue light illumination) UV−vis spectra are depicted in Figure 2. All proteins displayed typical phototropin LOV-like UV−vis spectral characteristics as well as blue light sensitivity (Figure 2).

Much to our surprise, for two of the five proteins, namely, Pf01-LOV and SBW25-LOV, no recovery was observed from photoequilibrium to the dark state after illumination with blue light. Hereby, when measured at 25 °C, next to no spectral recovery of the flavin specific absorption band in the blue region of the spectrum (400−500 nm) was visible over 16 h of measuring time (data not shown). One possible explanation to account for such a behavior would be a very slow dark recovery reaction, even beyond that of the already slow-reverting PpSB1-LOV protein (τ_{rec} of ~2400 min at 25 °C[25]). Consequently, we attempted to accelerate the thermal breaking of the covalent FMN-C4a-cysteinyl-thiol adduct by conducting measurements at 37 °C. At this temperature, full recovery could be achieved for the two very-slow-reverting proteins. For comparison, we also recorded dark recovery time traces for the two previously studied *P. putida* KT2440 "short" LOV proteins at 37 °C. The adduct state lifetimes (τ_{rec}) of the four *P. putida* (strains KT2440 and W619) proteins were as follows: 109 ± 18 min for PpSB1-LOV, 0.5 ± 0.1 min for PpSB2-LOV, 53 ± 4 min for W619_1-LOV, and 0.9 ± 0.1 min for W619_2-LOV. Even at this elevated temperature, both *P. fluorescens* proteins displayed a very slow dark recovery with τ_{rec} values of 810 ± 72 min for Pf01-LOV and 1470 ± 100 min for SBW25-LOV. Please note that for the latter protein dark recovery time traces could not be measured until reversion was complete because of the inherent instability of the protein over the extended measuring times at 37 °C. During the measurement, SBW25-LOV partially precipitates and loses the FMN chromophore, complicating interpretation of the data. Thus, the presented adduct state lifetime represents only a lower bound estimate. Compared to the slow-reverting PpSB1-LOV protein, Pf0-1-LOV and SBW25-LOV revert 7 and 13 times slower, respectively. Surprisingly, Pf5-LOV displayed an adduct state lifetime (τ_{rec}) of ~3.6 ± 1.5 min and is thus rather fast-reverting.

Bioinformatic Analysis of N- and C-Terminal Extension of the Pseudomonadaceae "Short" LOV Protein Family. The N-terminal region, corresponding to the N-cap (helix A′α) of PpSB1-LOV, is conserved in sequence in all γ-proteobacterial "short" LOV proteins (Figure 1 of the Supporting Information). In contrast, the C-terminal extension (Jα-helix) is much more variable in both length and sequence. The recently determined crystal structure of PpSB1-LOV [Protein Data Bank (PDB) entry 3SW1][7] revealed that both auxiliary structural elements are part of the subunit interface stabilizing the formation of the parallel homodimer in the

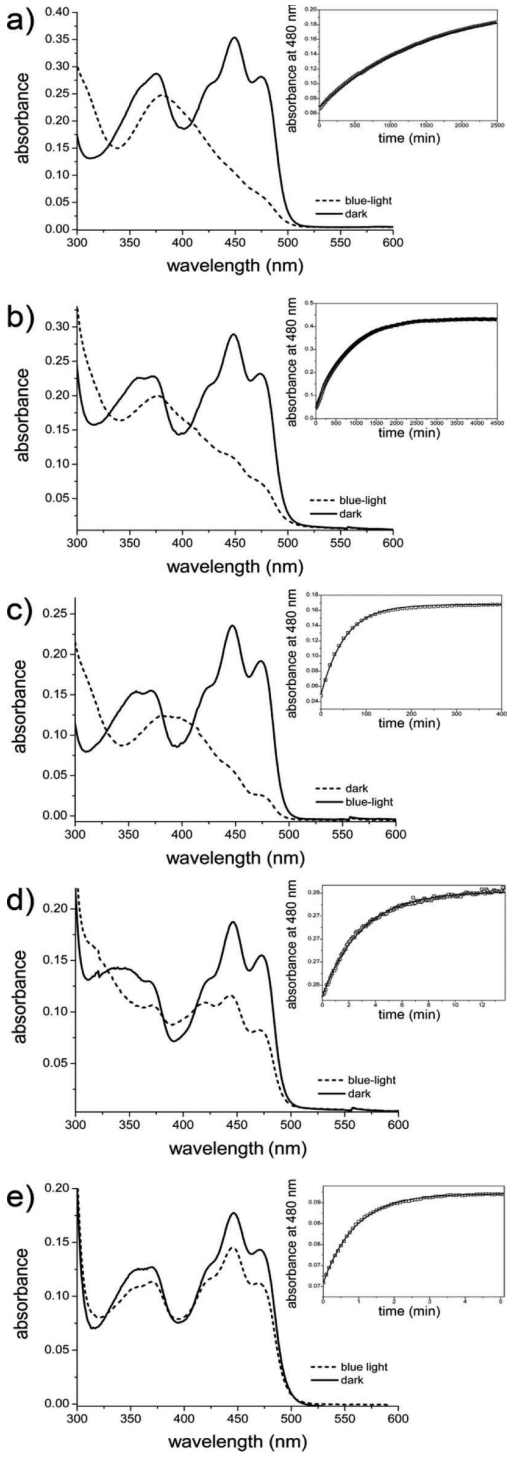

Figure 2. Blue light sensitivity of Pseudomonadaceae "short" LOV proteins. UV−vis absorbance spectra of the dark state (—) and the respective photoequillibrium state recorded after illumination with blue light for 30 s (---). The inset shows the respective dark recovery time traces recorded at 480 nm absorbance. All measurements were performed at 37 °C. The adduct state lifetimes (τ_{rec}), determined from single-exponential fits of the experimental data, were as follows: (a) 1470 ± 100 min for SBW25-LOV, (b) 810 ± 72 min for Pf01-LOV, (c) 53 ± 4 min for W619_1-LOV, (d) 3.6 ± 1.5 min for Pf5-LOV, and (e) 0.9 ± 0.1 min for W619_2-LOV.

dx.doi.org/10.1021/bi400311r | *Biochemistry* 2013, 52, 4460−4473

crystal mostly via hydrophobic interchain contacts. The C-terminal Jα-helix, which protrudes from the LOV core, hereby supports subunit association via a coiled-coil-like arrangement of interface-buried hydrophobic residues. To verify whether this structural feature might be conserved in all Pseudomonadaceae "short" LOV proteins, we analyzed the respective protein sequences for the presence the canonical *abcdefg* heptad repeat pattern characteristic of coiled-coil structures (Figure 3).

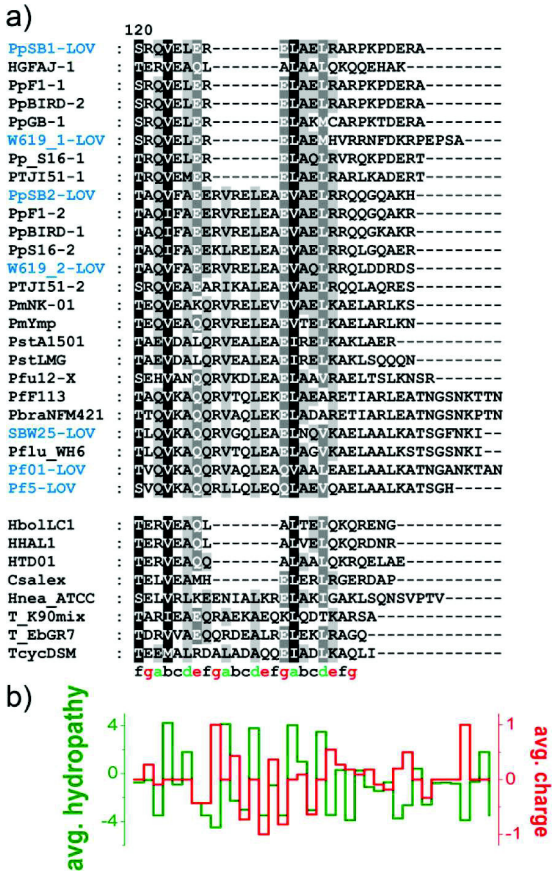

Figure 3. Sequence alignment of the C-terminal Jα-helix extensions of Pseudomonadaceae "short" LOV proteins (a) and average hydropathies as well as average charges inferred from the alignment (b). Average residue-wise hydropathies were assigned according to the Kyte–Doolittle scale.[49] Jα-helix sequences highlighted in blue denote "short" LOV proteins that were experimentally characterized in this study.

For all sequences, the coiled-coil prediction tool PCOILS[48] predicts the presence of either two or three heptad repeats (Figure 3a). This is also apparent in the alignment (Figure 3a) where two distinct sequence length patterns can be identified. In a subset of sequences, a conserved seven-amino acid insertion is present after the first heptad repeat, accounting for two helical turns in structure. Moreover, the structural interaction pattern typical for coiled coils, featuring hydrophobic interactions via residues *a*–*d* and salt bridge contacts via residues *e*–*g* of the heptad, is conserved in all sequences (Figure 3b). Thus, bioinformatic analyses for sequences of the Pseudomonadaceae "short" LOV family suggest the presence of a well-defined N-cap as well as C-terminal Jα-helix elements prone to mediating subunit association via coiled-coil interactions, much like in the PpSB1-LOV crystal structure.

CD Spectroscopic Studies of the Pseudomonadaceae "Short" LOV Proteins. To assess the global secondary structure content of the five new Pseudomonadaceae "short" LOV proteins, we conducted CD spectroscopic studies in a manner similar to that described for PpSB1-LOV and PpSB2-LOV.[25] Far-UV CD spectra recorded at 20 °C were used to estimate the secondary structure content of the five LOV proteins. CD spectra were deconvoluted using the convex constraint analysis tool (CCA+)[50] applying a data set of five pure components: (i) α-helices, (ii) turns and other structures, (iii) parallel and twisted β-sheets, (iv) random coils, and (v) antiparallel β-sheets.[25,51] Table 1 summarizes the CCA-derived secondary structure content of the five Pseudomonadaceae "short" LOV proteins in comparison to that of PpSB1-LOV and PpSB2-LOV.[25]

Table 1. Results of the CCA Analysis of CD Spectra

protein	no. of residues/length of Jα-helix	CD-derived secondary structure content,[a] no. of amino acids		
		α-helix	β-strands	coil, turn, other
PpSB1-LOV	162/23	47 ± 3	44 ± 4	71 ± 3
W619_1-LOV	166/27	44 ± 1	45 ± 4	77 ± 5
Pf01-LOV	178/38	57 ± 7	41 ± 2	80 ± 9
SBW25-LOV	175/36	69 ± 7	35 ± 8	71 ± 1
PpSB2-LOV	168/29	45 ± 1	54 ± 1	71 ± 5
W619_2-LOV	168/29	44 ± 2	54 ± 4	70 ± 2
Pf5-LOV	172/33	60 ± 1	42 ± 1	70 ± 1
PDB entry 3SW1[b]	134/15	53	46	35

[a]For PpSB1-LOV and PpSB2-LOV, values are derived from three CD measurements of three independent preparations.[25,26] For all other proteins, two measurements of two independent preparations were used for spectral deconvolution using the CCA+ tool.[50] For deconvolution, a set of five pure components was used as described previously.[25,51] [b]Secondary structure content derived from the crystal structure of full-length PpSB1-LOV.[7] The first 20 amino acids comprising the N-terminal His tag and a thrombin cleavage site as well as the last 12 C-terminal amino acids are lacking electron density in the crystal structure and are thus likely disordered.[7] This accounts for the difference between the CD-derived random coiled content of PpSB1-LOV in solution and the value derived from analysis of the crystal structure.

All studied "short" LOV proteins display very similar β-strand/turn and random-coil content. However, significant differences are found in their α-helix content. In particular, for the proteins with a longer C-terminal extension (Pf01-LOV, SBW25-LOV, and Pf5-LOV), the CD-derived α-helix content is increased compared to that of PpSB1-LOV.

Effect of N- and C-Terminal Truncations on the Soluble Expression of PpSB1-LOV and PpSB2-LOV in *E. coli*. To gain more insight into the structural role of the N-terminal cap (N-cap) and the C-terminal Jα-helix present outside the LOV core domain in the Pseudomonadaceae "short" LOV protein family, we generated a set of truncated protein variants of the two prototype proteins PpSB1-LOV and PpSB2-LOV. Using molecular biological means, constructs were generated lacking either the N-cap (ΔNcap), the Jα-helix (ΔJα), or both structural elements (ΔNcap-ΔJα). All constructs were expressed in *E. coli* in a manner identical to

that of the corresponding full-length proteins. Cells were lysed, and insoluble material was separated by centrifugation. The resulting protein fractions (insoluble pellet and soluble protein-containing supernatant) were separated by SDS−PAGE and transferred to a PVDF membrane. The respective LOV protein was detected immunologically using polyclonal antisera raised against either PpSB1-LOV or PpSB2-LOV (Figure 4). This

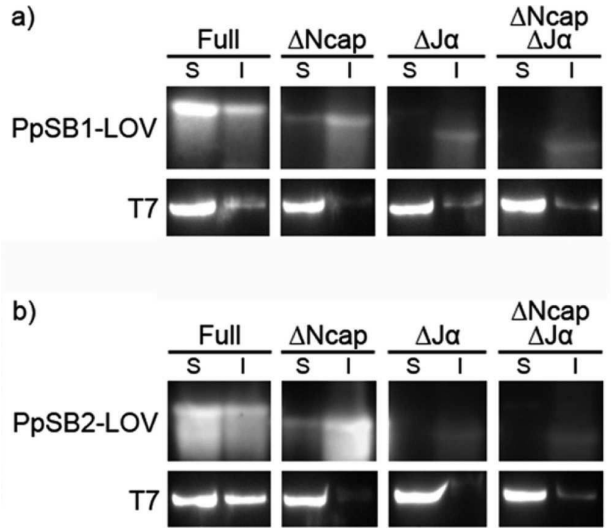

Figure 4. Immunoblot analysis illustrating the effect of N-terminal (N-cap) and C-terminal (Jα-helix) truncations of PpSB1-LOV (a) and PpSB2-LOV (b) on the accumulation of soluble and insoluble LOV protein in *E. coli* BL21(DE3). The respective full-length genes (Full), the N-terminally truncated construct (ΔNcap), the C-terminally truncated construct (ΔJα), and constructs lacking both structural elements (ΔNcapΔJα) were expressed using autoinduction medium in *E. coli* BL21(DE3) under identical conditions. After cell lysis, the soluble protein was separated from protein aggregates, inclusion bodies, and cell debris by centrifugation. Similar amounts of the resulting soluble (S) and insoluble (I) protein fraction were analyzed by immunoblotting. As a loading control, T7 RNA polymerase was expressed in *E. coli* BL21(DE3) by autoinduction and quantified in soluble and insoluble fractions.

strategy allows specific detection of even trace amounts of both proteins and the corresponding variants. Much to our surprise, removal of either structural element severely compromised the soluble expression of the respective truncated variants (Figure 4).

Whereas both full-length proteins are present predominately in the soluble fraction (solubility of ≥60%), removal of the N-cap results in an increased level of accumulation of the respective variants in the form of insoluble aggregates (solubility of ≤20%). Removal of the C-terminal Jα-helix or of both the N-cap and the Jα-helix has a much more detrimental effect on the production of the soluble protein. The respective truncated constructs accumulated exclusively in the form of insoluble aggregates; no soluble protein was detectable. As a loading control, T7 RNA polymerase (T7Pol) was quantified in the soluble and insoluble fractions after lactose-induced expression of the *T7pol* gene in *E. coli* BL21(DE3) (Figure 4a,b, bottom panels). In the autoinduction expression system employed here, *T7pol* gene expression was induced depending on growth and the metabolic state of the cell.[52] Hereby, depletion of glucose and the onset of utilization of lactose and/or glycerol resulted in T7 RNA polymerase gene expression from the lactose-inducible P_{lacUV5} promoter, which in turn facilitates target gene expression under control of the strong P_{T7} promoter. All samples of the soluble cell fraction contained very similar amounts of T7 RNA polymerase, thus verifying similar loading levels for the respective soluble samples (Figure 4). Please note that T7Pol is usually expressed in soluble form in *E. coli* BL21(DE3). Thus, T7Pol signals seen in the insoluble fraction most probably arise from the presence of a certain fraction of aggregated protein and/or incomplete cell lysis. We subsequently tried to purify both N-cap truncated variants of PpSB1-LOV and PpSB2-LOV as a small but detectable amount of soluble protein could be obtained. We were able to obtain milligram amounts of the purified protein, which however lacked bound FMN or rapidly lost the chromophore during desalting and concentration steps (data not shown). Taken together, the data indicate that removal of both auxiliary structural elements outside the LOV core (N-cap and Jα-helix) severely compromises the structural integrity of the two studied "short" LOV proteins.

Far-UV CD Spectroscopy To Probe Thermal Unfolding of the PpSB1-Jα and PpSB2-Jα Peptides. Coiled coils are widespread, many times independently folding, interaction motifs present in many structurally different proteins.[53] Therefore, we asked the question of whether the Jα-helix extension of PpSB1-LOV and PpSB2-LOV can fold in a manner that is independent of the rest of the protein. Given the short length of the Jα-helix extensions, we obtained both protein segments (PpSB1-Jα and PpSB2-Jα) as custom-synthesized N-terminally acetylated peptides.

To study the folding and secondary structure of both peptides, we used far-UV CD spectroscopy. Initially, CD spectra were recorded at 20 °C. At this temperature, clear spectral evidence of the presence of α-helical secondary structure could be obtained for only PpSB2-Jα (data not shown). Therefore, spectra were recorded at 1 °C and deconvoluted assuming the presence of two pure components (α-helix and random coil). The CD-predicted secondary structure content of the two peptides at 1 °C is given in Table 2. The far-UV CD spectra used for deconvolution are depicted in Figure 2 of the Supporting Information (black line). At 1 °C, both peptides are partially α-helical with 41 and 56% α-helical content for PpSB1-Jα and PpSB2-Jα, respectively. We studied thermal unfolding by collecting CD spectra for the two

Table 2. CD Spectroscopic Studies of PpSB1-Jα and PpSB2-Jα

	melting curve-derived thermodynamic parameters[a]			
peptide	T_m (°C)	ΔH (kcal mol^{-1})	ΔS (kcal K^{-1} mol^{-1})	ΔG (kcal mol^{-1})[b]
PpSB1-Jα (23 amino acids)	4	9.3	0.0336	0.26
PpSB2-Jα (29 amino acids)	16	14.3	0.0494	0.87

	CD-derived secondary structure content (%)[b] (no. of amino acids)	
	α-helix	random coil
PpSB1-Jα (23 amino acids)	41 (9)	59 (14)
PpSB2-Jα (29 amino acids)	56 (16)	44 (13)

[a]CD spectra of both peptides were determined in thermal equilibrium. Heating was performed from 1 to 65 °C until complete unfolding had been observed. [b]Derived from spectra recorded at 1 °C.

dx.doi.org/10.1021/bi400311r | *Biochemistry* 2013, 52, 4460−4473

peptide samples equilibrated at 1 °C and subsequently heating the samples stepwise to >65 °C with a constant ramp rate of 1 °C/min. When the samples were heated, a clear loss of negative ellipticity at 222 and 208 nm could be detected, suggestive of the loss of α-helical secondary structure (Figure 2 of the Supporting Information). Eventually, heating results in the formation of a spectral species with a blue-shifted minimum, resembling the CD spectra of random-coil model peptides.[54] The presence of one isodichroic point at 203 nm is supportive of a two-state transition. Interestingly, the thermal unfolding process is fully reversible for both peptides, with both the unfolding and folding transition displaying the same transition behavior (Figure 5). Under the premise of complete

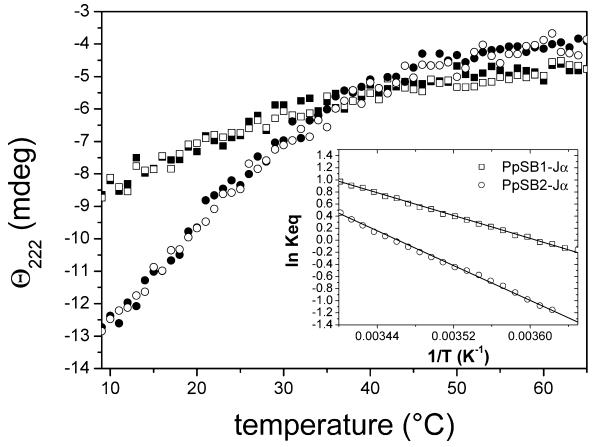

Figure 5. Unfolding (filled symbols) and refolding (empty symbols) curves recorded for PpSB1-Jα (squares) and PpSB2-Jα (circles). The depicted curves were extracted from the respective far-UV CD spectra by plotting Θ_{222} vs incubation temperature. Samples were equilibrated at 1 °C. Subsequently, CD spectra were recorded for the same sample heated stepwise to >65 °C using a constant ramp rate of 1 °C/min. After complete unfolding had been achieved, CD spectra were recorded for the same samples cooled stepwise to 1 °C using the same ramp rate that was used for heating. The inset depicts the van't Hoff plot (eq 3) for the unfolding−refolding transition of PpSB1-Jα (□) and PpSB2-Jα (○) that was used to derive the thermodynamic parameters listed in Table 2.

reversibility while assuming a two-state transition, thermodynamic parameters for the PpSB1-Jα and PpSB2-Jα unfolding−folding equilibrium can be extracted from CD data[55] (Table 2).

With an estimated melting temperature (T_m) of 16 °C, PpSB2-Jα appears to be slightly more stable against thermal unfolding than the PpSB1-Jα peptide (T_m = 4 °C). At 1 °C, PpSB1-LOV is marginally stabilized against unfolding with a Gibbs free energy of unfolding (ΔG) of 0.26 kcal mol^{-1} (ΔH = 9.3 kcal mol^{-1}, and ΔS = 0.0336 kcal K^{-1} mol^{-1}). For the thermally more stable peptide, PpSB2-Jα, the Gibbs free energy of unfolding (ΔG) is increased to 0.87 kcal mol^{-1} (ΔH = 14.3 kcal mol^{-1}, and ΔS = 0.0494 kcal K^{-1} mol^{-1}). This renders both isolated Jα peptides rather thermally unstable. However, the data nevertheless prove that both peptides are able to spontaneously adopt α-helical structures even when studied in isolated form in aqueous (buffer) solution.

NMR Solution Structure of the C-Terminal PpSB1-LOV and PpSB2-LOV Jα-Helix Extensions. The structure of both Jα-helix peptides was probed via solution NMR spectroscopy. Initially, 2D ^{1}H−^{1}H TOCSY spectra were collected at 1 °C for both peptides. However, at this temperature, severe line broadening was observed, yielding spectra that could not be interpreted. Spectra recorded at 25 °C were fully resolved. However, at this temperature, both peptides are already partially or completely unfolded. Therefore, we used the helix-stabilizing agent 2,2,2-trifluoroethanol (TFE) to stabilize α-helical peptide conformations at 25 °C. TFE is not a helix-inducing solvent in the sense that it will induce helix formation in a manner independent of the sequence. It is rather a helix-enhancing cosolvent that stabilizes helices in regions with some α-helical propensity.[56] To verify proper folding at 25 °C in the presence of minimal amounts of TFE, we recorded CD spectra for the peptide samples at 25 °C while sequentially increasing the TFE concentration (data not shown). In this way, the minimal concentration of TFE needed to promote complete folding of the respective peptide was determined. For the two peptides, addition of 10% (v/v) TFE (PpSB1-Jα) and 25% (v/v) TFE (PpSB2-Jα) was necessary to stabilize peptide folding at 25 °C. Under those buffer conditions, 2D (^{1}H−^{1}H) TOCSY spectra and 2D (^{1}H−^{1}H) NOESY spectra were recorded for the PpSB1-Jα and PpSB2-Jα peptides. Sequential assignment of the proton resonances was achieved considering sequential $H^N_{(i)}$−$H^N_{(i+1)}$, $H^\alpha_{(i)}$−$H^N_{(i+1)}$, and $H^\beta_{(i)}$−$H^N_{(i+1)}$ NOE correlations. Structures were calculated using CNS by utilizing 537 (PpSB1-Jα) and 749 (PpSB2-Jα) NOE-derived distance restraints, of which 485 (PpSB1-Jα) and 721 (PpSB2-Jα) were unambiguous. Structure quality, distance restraint, and violation statistics for the ensemble of the 10 lowest-energy structures are listed in Table 3.

The final ensemble of 10 structures was selected on the basis of energy from the ensemble of 250 calculated structures and subjected to a refinement in explicit water. The rmsd of the backbone atoms for the refined ensemble from the mean structure was 0.053 Å for PpSB1-Jα (ordered region of residues 121−134) and 0.191 Å for PpSB2-Jα (ordered region of residues 121−142). No NOE violations greater than 0.3 Å were observed. Figure 6 depicts the overlay of the 10 ensemble structures (Cα trace as a ribbon drawing) superimposed over the respective helical portion (as a transparent cartoon).

Please note that NMR structural models derived from NOE-based structure calculations inevitably overestimate the real secondary structure content of the ensemble. To quantify the α-helical secondary structure content directly from NMR chemical shift data, we used the secondary structure propensity score (SSP) developed by Marsh and co-workers.[41] An SSP score at a given residue of 1 or −1 is indicative of fully formed α- or β-structure, respectively. A score of 0.5 indicates that 50% of the conformers in the disordered state ensemble are helical at that position.[41] Figure 3 of the Supporting Information depicts the residue-wise SSP score for PpSB1-Jα (panel A) and PpSB2-Jα (panel B). For both peptides, most residue SSP scores are positive, indicative of a certain degree of α-helical propensity. Exceptions include R135 (PpSB1-Jα) and K147 (PpSB2-Jα), which show negative values. Average SSP scores for the ordered region of PpSB1-Jα (residues 121−134) and PpSB2-Jα (residues 121−142) are 0.48 and 0.44, respectively. This suggests that on average 48 and 44% of the conformers in the respective regions are α-helical in the disordered state ensemble. While SSP scores provide a more realistic measure of the true α-helical propensity of the sample, they unfortunately do not allow a clear-cut estimation of, for example, the percentage of residues in an α-helical conformation. Given the average SSP scores of 0.48 and 0.44 for the ordered region of

dx.doi.org/10.1021/bi400311r | Biochemistry 2013, 52, 4460−4473

Table 3. Structural, Distance Restraint, and Violation Statistics for the 10 Lowest-Energy Structures of PpSB1-Jα and PpSB2-Jα

	PpSB1-Jα (residues 120−142)	PpSB2-Jα (residues 120−148)
no. of experimental restraints		
total NOE distance restraints	537	749
unambiguous	485	721
intraresidue	190	321
interresidue	295	400
sequential	159	195
short range (2−3)	108	157
medium range (4−5)	28	48
long range (>5)	0	0
ambiguous	52	28
no. of NOE upper bound violations		
violations of >0.5 Å	0	0
violations of >0.3 Å	0	0
violations of >0.1 Å	12.1 ± 1.7	19.4 ± 2.0
rmsd from idealized covalent geometry		
bonds (Å)	0.004 ± 0.0001	0.004 ± 0.0001
angles (deg)	0.519 ± 0.0157	0.583 ± 0.0146
impropers (deg)	0.965 ± 0.1498	1.247 ± 0.1199
rmsd from experimental restraints		
NOE restraints (Å)	0.028 ± 0.002	0.027 ± 0.000
Ramachandran plot (ensemble)		
favored region	95.9%	95.4%
allowed region	100%	100%
disallowed region	0%	0%
ensemble rmsd (Å)		
core residues	121−134	121−142
backbone	0.053	0.191
heavy atoms	1.003	0.789

both peptides discussed above, we can set an arbitrary minimum threshold for the propensity of defining a residue in α-helical conformation of ∼0.4. Assuming this arbitrary SSP threshold, 9 of 23 residues for PpSB1-Jα (40%) and 16 of 29 residues for PpSB2-Jα (55%) possess a strong tendency for α-helical secondary structure. This translates roughly to three and five helical turns in structure for PpSB1-Jα and PpSB2-Jα, respectively. Additionally, evidence of the presence of an α-helical conformation of both peptide samples is provided by the observed NOE pattern typical for α-helices (Figure 3 of the Supporting Information).

The numbers of amino acid residues showing chemical shifts and NOE patterns typical for α-helical secondary structure are in good agreement with CD and bioinformatic predictions (Table 2 and Figure 3). Moreover, the CD and NMR data are coherent, as both methods predict that PpSB2-Jα is extended compared to PpSB1-Jα. This is in accordance with alignment analyses, where a conserved seven-residue insertion is observed for a subset of Pseudomonadaceae "short" LOV protein Jα-helix sequences (Figure 3).

DISCUSSION

Phylogenetic Analyses and Mutually Conserved Photocycle Kinetic Parameters Hint at a Conserved Physiological Role of Fast- and Slow-Reverting Pseudomonadaceae "Short" LOV Proteins. A comprehensive sequence database search was performed and a phylogenetic tree inferred from the retrieved sequences to provide a basis for the identification of prokaryotic PpSB1-LOV- and PpSB2-LOV-like "short" LOV proteins. Sequence alignment data (Figure 1 of the Supporting Information) as well as phylogenetic analyses (Figure 1) revealed a division of prokaryotic "short" LOV proteins into at least two subclasses. Hereby, it appears that "short" LOV proteins are solely present in proteobacteria. Sequences bearing the canonical LOV sequence motif G(X)-NCRFLQG are separated from PpSB1-LOV- and PpSB2-LOV-like sequences comprising a noncanonical Y(Q/R)DCRFLQG motif. While the latter class is restricted to γ-proteobacterial lineages, proteins of the first class are dispersed throughout α-, β-, and γ-proteobacteria. This observation suggests a niche specific conservation of "short" LOV protein architectures and thus hints at distinct blue light responses in those bacterial lineages. Moreover, the evolutionary conservation of fast- and slow-reverting LOV photoreceptors in *P. putida* (strains KT2440 and W619) suggests the functional importance of evolutionarily conserved recovery-kinetic properties. We previously identified residues R61 and R66 as the key determinants for the slow dark recovery of PpSB1-LOV.[7,25] In the X-ray structure of PpSB1-LOV, R61 and R66 together with two conserved arginines in all LOV proteins (R54 and R70, PpSB1-LOV numbering) form an unusual cluster of charged residues coordinating the FMN phosphate.[7] Interchange of those two residues with their counterparts in the fast-reverting PpSB2-LOV protein (H61 and I66) resulted in an acceleration of the dark recovery by a factor of ∼280.[7] This dark recovery-determining structural feature is likely conserved in the two *P. putida* W619 LOV proteins, as the respective positions are occupied by either two arginines in the slow-reverting W619_1-LOV protein or a histidine and a leucine residue in the fast-reverting W619_2-LOV protein (highlighted

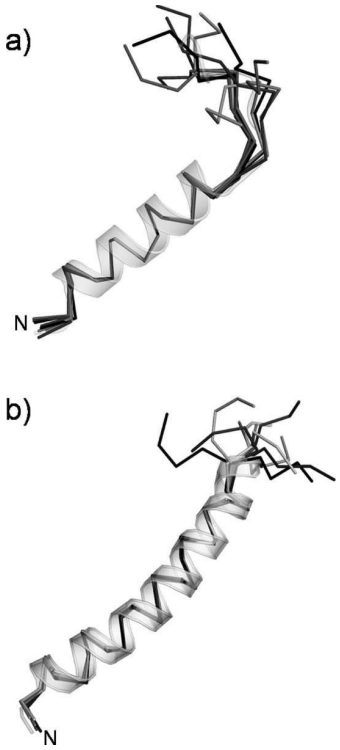

Figure 6. Ensemble of the 10 NMR-derived structures of PpSB1-Jα (a) and PpSB2-Jα (b) selected on the basis of energy from an ensemble of 250 structures. The polypeptide backbone of the 10 lowest-energy structures is shown as a ribbon (gray to black). The energy-minimized average structure is superimposed on the ensemble (colored white, transparent cartoon representation).

in red in Figure 1a of the Supporting Information). The other very slow-reverting LOV proteins (SBW25-LOV and Pf0-1-LOV) invariably contain an arginine at the position corresponding to R61 of PpSB1-LOV. Interestingly, in the two very-slow-reverting *P. fluorescens* LOV proteins, the position corresponding to R66 in PpSB1-LOV is occupied by a nonpolar leucine residue (see Figure 1a of the Supporting Information). Thus, additional structural features seem to contribute to the very slow dark recovery of the two *P. fluorescens* LOV proteins.

While the physiological role of both *P. putida* KT2240 LOV proteins remains elusive, experimental evidence of a functional role of a bacterial "short" LOV protein was recently provided for the "short" LOV protein RsLOV of *R. sphaeroides* 2.4.1.[24] Although small physiological similarities exist between the anoxygenic phototroph *R. sphaeroides* and the saprotrophic chemotroph *P. putida*, the study nevertheless proves that bacterial LOV proteins lacking fused effector domains can act as genuine blue light sensors, probably transducing the signal via protein−protein interactions with as yet unidentified downstream regulators. As a mode of signal transduction, changed surface properties caused by blue light-induced conformational changes in the LOV protein would provide a feasible mechanism for altering protein−protein interactions. A similar mechanism has been suggested for the fungal "short" LOV protein VVD of *Neurospora*.[57]

Conserved C-Terminal Jα-Helices Play an Essential Role in the Folding and Solubility of Pseudomonadaceae "Short" LOV Proteins. The CD spectroscopic data for the five Pseudomonadaceae "short" LOV proteins presented here as well as CD and NMR data for the two Jα-helix peptides suggest an evolutionary conservation and thus conserved structural role of the two N- and C-terminal auxiliary structural elements. For both PpSB1-LOV and PpSB2-LOV, the two elements need to be present to yield a soluble functional protein in *E. coli*. Hereby, the C-terminal Jα-helix seems to be more important, because its removal resulted in a nearly complete loss of solubility. This is in contrast to multidomain LOV photoreceptors, where both structural elements can be readily removed without the loss of protein solubility.[58−60] Hence, they appear to be integral for the functionality of the LOV sensory system. Thus, it is tempting to speculate that in the case of the Pseudomonadaceae "short" LOV proteins, the protruding C-terminal Jα-helices represent candidate structural elements whose coiled-coil-like interaction in the dimeric protein might be altered to modulate surface properties and thus could promote or impede protein−protein interactions in a given conformational state (light or dark).

CD and NMR Spectroscopic Studies Reveal Robust Folding of the Isolated Jα-Helix Peptides and Suggest a Certain Degree of Quaternary Structural Flexibility That Might Allow Signal Transduction. CD spectra as well as the solution NMR data presented here indicate α-helical secondary structure for the isolated PpSB1-Jα and PpSB2-Jα peptides at 1 °C in aqueous solution or at 25 °C in the presence of minimal amounts of the helix-stabilizing agent TFE. Both peptide CD spectra recorded at 1 °C in aqueous solution show minima at 222 and 208 nm as well as a maximum at ∼190 nm. These are signature features of helical secondary structure representing the n → π* transition (∼222 nm) and π → π* exciton split transition (∼190 and ∼208 nm) of peptide bonds.[61] The ellipticity ratio $[\Theta_{222}]/[\Theta_{208}]$ has previously been used as an indicator of coiled-coil formation of peptides.[62,63] Hereby, noncoiled helices show a ratio of ∼0.8, whereas coiled-coil structures yield values close to 1.[62] Mechanistically, this is due to the fact that in coiled coils the parallel polarized amide π → π* transition becomes less dichroic, which effectively reduces the negativity of $[\Theta_{208}]$. Because $[\Theta_{222}]$ is not affected, the $[\Theta_{222}]/[\Theta_{208}]$ ratio increases to ∼1. For PpSB1-Jα and PpSB2-Jα, $[\Theta_{222}]/[\Theta_{208}]$ ratios are ∼0.67 and ∼0.89, respectively. Thus, coiled-coil formation is not apparent from CD spectra recorded for the two isolated Jα-helix peptides studied in aqueous solution, even at low temperatures.

The superimposition of the NMR-derived peptide structure of PpSB1-Jα with the respective structural element in the full-length crystal structure (PDB entry 3SW1) yields backbone and all-atom rmsd values of 0.362 and 0.919 Å, respectively. Thus, while the general folding is conserved in both crystal and solution, the Jα-helix structural elements apparently possess a certain degree of quaternary structural flexibility. They exist as an isolated helix in solution or packed as a tight coiled coil in the context of the full-length protein in the crystal. Please note that we cannot rule out completely that Jα-helix coiled-coil formation as observed in the PpSB1-LOV crystal structure is an artifact related to crystal packing. While the data for truncated PpSB1-LOV and PpSB2-LOV protein constructs presented here as well as size-exclusion chromatographic data[25] argue against this scenario, the issue could be resolved unequivocally only by obtaining high-resolution NMR structures of the PpSB1-LOV protein. More likely, the conformational flexibility observed for the Jα-helix element in solution and the crystal structure is related to coiled-coil instability imposed by the

short sequence length of the PpSB1-LOV and PpSB2-LOV Jα-helices. Thus, it appears that the Jα-helix coiled coil observed in the crystal is not sufficiently stable to promote coiled-coil formation in solution. Anchoring of the Jα-helix at the C-terminus of the LOV core in the full-length protein might impose dynamic and distance restraints on the orientation of the Jα-helices and thus might promote coiled-coil formation as observed in the crystal structure. Please note that direct interactions between the PpSB1-LOV core subunits are absent in the dimeric crystal structure. In the full-length protein, subunit association is solely stabilized by contacts mediated by the C-terminal Jα-helix and the N-terminal cap (A′α-helix).[7] Thus, both structural elements seem to be crucial for dimer formation of the full-length protein, and hence, Jα-helix coiled-coil formation as seen in the crystal structure might be possible only in the presence of the dimer contact-mediating N-cap.

C-Terminal Jα-Helices as the Potential "Missing" Effector Domain of the Pseudomonadaceae "Short" LOV Protein Family: Implications for the Design of LOV-Based Optogenetic Tools. Given the structural features discussed above, the protruding C-terminal Jα-helices could well represent the missing effector domain of the Pseudomonadaceae "short" LOV protein family whose interaction with, as yet unidentified, downstream signaling partners could be modulated by blue light. Recently, a dimer arrangement similar to that seen in the PpSB1-LOV crystal structure has been suggested for the *B. subtilis* YtvA photoreceptor,[9,64] PAS domains of histidine kinase chemosensory two-component systems (TCS),[21,65−67] and has been implied for artificially constructed LOV-based optogenetic switches.[19,21] The data presented here as well as recently published X-ray crystallographic evidence[7] highlight the possibility of using "short" LOV proteins as sensory switches for the construction of LOV-based optogenetic tools. Hereby, they could be used either in *cis*, by fusion of an artificial effector domain module,[19−21] or in *trans*, employing an as yet unidentified regulatory protein[68] or even by using *de novo* designed binding proteins as regulatory modules.[69]

■ CONCLUSIONS

Our study provides a solely sequence-based criterion for differentiation of PpSB1-LOV- and PpSB2-LOV-like sequences from the vast variety of other ("short") LOV proteins found in databases.[70] At the same time, we provide evidence of the conservation of recovery kinetic properties supporting a classification into slow- and fast-reverting Pseudomonadaceae "short" LOV proteins and show that N- and C-terminal helical structural elements are conserved features of this class of LOV photoreceptors. Given the structural similarity of PAS-based chemosensory TCS as well as the proposed structure of recently developed LOV-based optogenetic tools used for the control of gene expression,[19−21] the adaptability of Pseudomonadaceae "short" LOV proteins as sensory modules for the design of LOV-based optogenetic switches can be anticipated. Moreover, given their diverse photochemical properties with respect to fast and slow dark recovery reactions, their different signaling state stabilities could be utilized to construct switches with tunable sensitivities and response times.[71]

■ ASSOCIATED CONTENT

Supporting Information

Oligonucleotides used in this study, sequence information for all bacterial "short" LOV protein sequences depicted in Figure 1, HPLC−SEC and HPLC chromophore acceptance analyses, amino acid sequence alignment of bacterial "short" LOV proteins, CD spectroscopic analysis of PpSB1-Jα and PpSB2-Jα thermal unfolding, and NOE pattern and residue-wise secondary structure propensity scores (SSP) for PpSB1-Jα and PpSB2-Jα. This material is available free of charge via the Internet at http://pubs.acs.org.

Accession Codes

NMR chemical shift information for PpSB1-Jα and PpSB2-Jα has been deposited in the Biological Magnetic Resonance Databank as entries 18159 and 18160 and the Protein Databank Europe as entries 2YON and 2YOM, respectively.

■ AUTHOR INFORMATION

Corresponding Author

*E-mail: u.krauss@fz-juelich.de. Phone: ++49 2461 61 2939. Fax: ++49 2461 61 2490.

Author Contributions

R.R. and K.J. contributed equally to this work.

Funding

This work was supported by the NRW Research School BioStruct and the "Fit for Excellence"-Fonds of the Heinrich-Heine-Universität Düsseldorf.

Notes

The authors declare no competing financial interest.

■ ACKNOWLEDGMENTS

We thank Dr. Wojtek Augustyniak (Conformetrix Ltd., Manchester, U.K.) for his initial help with peptide NMR assignments and Dr. Melanie Schwarten (Institut de Biologie Structurale Jean Pierre Ebel, Grenoble, France) for her help with peptide NMR assignments and valuable support and suggestions during the initial phase of the project. K.-E.J. and U.K. acknowledge the excellent technical support provided by Esther Knieps-Grünhagen, Maja Piqueray, and Astrid Wirtz.

■ ABBREVIATIONS

LOV, light, oxygen, voltage; FMN, flavin mononucleotide; phot, phototropin; rmsd, root-mean-square deviation; CD, circular dichroism.

■ REFERENCES

(1) Herrou, J., and Crosson, S. (2011) Function, structure and mechanism of bacterial photosensory LOV proteins. *Nat. Rev. Microbiol. 9*, 713−723.

(2) Krauss, U., Minh, B. Q., Losi, A., Gärtner, W., Eggert, T., von Haeseler, A., and Jaeger, K. E. (2009) Distribution and phylogeny of light-oxygen-voltage-blue-light-signaling proteins in the three kingdoms of life. *J. Bacteriol. 191*, 7234−7242.

(3) Möglich, A., Ayers, R. A., and Moffat, K. (2009) Structure and signaling mechanism of Per-ARNT-Sim domains. *Structure 17*, 1282−1294.

(4) Zoltowski, B. D., and Gardner, K. H. (2011) Tripping the light fantastic: Blue-light photoreceptors as examples of environmentally modulated protein-protein interactions. *Biochemistry 50*, 4−16.

(5) Losi, A., and Gärtner, W. (2008) Bacterial bilin- and flavin-binding photoreceptors. *Photochem. Photobiol. Sci. 7*, 1168−1178.

(6) Möglich, A., Yang, X., Ayers, R. A., and Moffat, K. (2010) Structure and function of plant photoreceptors. *Annu. Rev. Plant Biol. 61*, 21−47.

(7) Circolone, F., Granzin, J., Jentzsch, K., Drepper, T., Jaeger, K. E., Willbold, D., Krauss, U., and Batra-Safferling, R. (2012) Structural

basis for the slow dark recovery of a full-length LOV protein from *Pseudomonas putida*. *J. Mol. Biol. 417*, 362−374.
(8) Halavaty, A. S., and Moffat, K. (2007) N- and C-terminal flanking regions modulate light-induced signal transduction in the LOV2 domain of the blue light sensor phototropin 1 from *Avena sativa*. *Biochemistry 46*, 14001−14009.
(9) Möglich, A., and Moffat, K. (2007) Structural basis for light-dependent signaling in the dimeric LOV domain of the photosensor YtvA. *J. Mol. Biol. 373*, 112−126.
(10) Nash, A. I., McNulty, R., Shillito, M. E., Swartz, T. E., Bogomolni, R. A., Luecke, H., and Gardner, K. H. (2011) Structural basis of photosensitivity in a bacterial light-oxygen-voltage/helix-turn-helix (LOV-HTH) DNA-binding protein. *Proc. Natl. Acad. Sci. U.S.A. 108*, 9449−9454.
(11) Vaidya, A. T., Chen, C. H., Dunlap, J. C., Loros, J. J., and Crane, B. R. (2011) Structure of a light-activated LOV protein dimer that regulates transcription. *Sci. Signaling 4*, ra50.
(12) Crosson, S., and Moffat, K. (2001) Structure of a flavin-binding plant photoreceptor domain: Insights into light-mediated signal transduction. *Proc. Natl. Acad. Sci. U.S.A. 98*, 2995−3000.
(13) Crosson, S., and Moffat, K. (2002) Photoexcited structure of a plant photoreceptor domain reveals a light-driven molecular switch. *Plant Cell 14*, 1067−1075.
(14) Fedorov, R., Schlichting, I., Hartmann, E., Domratcheva, T., Fuhrmann, M., and Hegemann, P. (2003) Crystal structures and molecular mechanism of a light-induced signaling switch: The Phot-LOV1 domain from *Chlamydomonas reinhardtii*. *Biophys. J. 84*, 2474−2482.
(15) Drepper, T., Krauss, U., Meyer zu Berstenhorst, S., Pietruszka, J., and Jaeger, K. E. (2011) Lights on and action! Controlling microbial gene expression by light. *Appl. Microbiol. Biotechnol. 90*, 23−40.
(16) Krauss, U., Drepper, T., and Jaeger, K. E. (2011) Enlightened enzymes: Strategies to create novel photoresponsive proteins. *Chemistry 17*, 2552−2560.
(17) Krauss, U., Lee, J., Benkovic, S. J., and Jaeger, K. E. (2010) LOVely enzymes: Towards engineering light-controllable biocatalysts. *Microb. Biotechnol. 3*, 15−23.
(18) Möglich, A., and Moffat, K. (2010) Engineered photoreceptors as novel optogenetic tools. *Photochem. Photobiol. Sci. 9*, 1286−1300.
(19) Möglich, A., Ayers, R. A., and Moffat, K. (2009) Design and signaling mechanism of light-regulated histidine kinases. *J. Mol. Biol. 385*, 1433−1444.
(20) Ohlendorf, R., Vidavski, R. R., Eldar, A., Moffat, K., and Möglich, A. (2012) From dusk till dawn: One-plasmid systems for light-regulated gene expression. *J. Mol. Biol. 416*, 534−542.
(21) Möglich, A., Ayers, R. A., and Moffat, K. (2010) Addition at the molecular level: Signal integration in designed Per-ARNT-Sim receptor proteins. *J. Mol. Biol. 400*, 477−486.
(22) Zoltowski, B. D., Schwerdtfeger, C., Widom, J., Loros, J. J., Bilwes, A. M., Dunlap, J. C., and Crane, B. R. (2007) Conformational switching in the fungal light sensor Vivid. *Science 316*, 1054−1057.
(23) Hendrischk, A. K., Moldt, J., Frühwirth, S. W., and Klug, G. (2009) Characterization of an unusual LOV domain protein in the α-proteobacterium *Rhodobacter sphaeroides*. *Photochem. Photobiol. 85*, 1254−1259.
(24) Metz, S., Jäger, A., and Klug, G. (2012) Role of a short light, oxygen, voltage (LOV) domain protein in blue light- and singlet oxygen-dependent gene regulation in *Rhodobacter sphaeroides*. *Microbiology 158*, 368−379.
(25) Jentzsch, K., Wirtz, A., Circolone, F., Drepper, T., Losi, A., Gärtner, W., Jaeger, K. E., and Krauss, U. (2009) Mutual exchange of kinetic properties by extended mutagenesis in two short LOV domain proteins from *Pseudomonas putida*. *Biochemistry 48*, 10321−10333.
(26) Krauss, U., Losi, A., Gärtner, W., Jaeger, K.-E., and Eggert, T. (2005) Initial characterization of a blue-light sensing, phototropin-related protein from *Pseudomonas putida*: A paradigm for an extended LOV construct. *Phys. Chem. Chem. Phys. 7*, 2804−2811.
(27) Studier, F. W. (2005) Protein production by auto-induction in high-density shaking cultures. *Protein Expression Purif. 41*, 207−234.
(28) Jentzsch, K., Wirtz, A., Circolone, F., Drepper, T., Losi, A., Gärtner, W., Jaeger, K. E., and Krauss, U. (2009) Mutual exchange of kinetic properties by extended mutagenesis in two short LOV domain proteins from *Pseudomonas putida*. *Biochemistry 48*, 10321−10333.
(29) Sambrook, J., Russel, D. W. (2001), Molecular cloning: a laboratory manual. Cold Spring Harbor Laboratory Press, Plainview, NY.
(30) Laemmli, U. (1970) Cleavage of structural proteins during the assembly of the head of bacteriophage T4. *Nature 227*, 680−685.
(31) Bradford, M. M. (1976) A rapid and sensitive method for the quantitation of microgram quantities of protein utilizing the principle of protein-dye binding. *Anal. Biochem. 72*, 248−254.
(32) Buttani, V., Losi, A., Eggert, T., Krauss, U., Jaeger, K.-E., Cao, Z., and Gärtner, W. (2007) Conformational analysis of the blue-light sensing protein YtvA reveals a competitive interface for LOV-LOV dimerization and interdomain interactions. *Photochem. Photobiol. Sci. 6*, 41−49.
(33) Delaglio, F., Grzesiek, S., Vuister, G. W., Zhu, G., Pfeifer, J., and Bax, A. (1995) NMRPipe: A multidimensional spectral processing system based on UNIX pipes. *J. Biomol. NMR 6*, 277−293.
(34) Vranken, W. F., Boucher, W., Stevens, T. J., Fogh, R. H., Pajon, A., Llinas, M., Ulrich, E. L., Markley, J. L., Ionides, J., and Laue, E. D. (2005) The CCPN data model for NMR spectroscopy: Development of a software pipeline. *Proteins 59*, 687−696.
(35) Brunger, A. T. (2007) Version 1.2 of the Crystallography and NMR system. *Nat. Protoc. 2*, 2728−2733.
(36) Linge, J. P., and Nilges, M. (1999) Influence of non-bonded parameters on the quality of NMR structures: A new force field for NMR structure calculation. *J. Biomol. NMR 13*, 51−59.
(37) Koradi, R., Billeter, M., and Wüthrich, K. (1996) MOLMOL: A program for display and analysis of macromolecular structures. *J. Mol. Graphics 14*, 29−32 , 51−55.
(38) *PyMol* (2010) Schrödinger, LLC.
(39) Vriend, G. (1990) WHAT IF: A molecular modeling and drug design program. *J. Mol. Graphics 8*, 29 , 52−56.
(40) Davis, I. W., Leaver-Fay, A., Chen, V. B., Block, J. N., Kapral, G. J., Wang, X., Murray, L. W., Arendall, W. B., III, Snoeyink, J., Richardson, J. S., and Richardson, D. C. (2007) MolProbity: All-atom contacts and structure validation for proteins and nucleic acids. *Nucleic Acids Res. 35*, W375−W383.
(41) Marsh, J. A., Singh, V. K., Jia, Z., and Forman-Kay, J. D. (2006) Sensitivity of secondary structure propensities to sequence differences between α- and γ-synuclein: Implications for fibrillation. *Protein Sci. 15*, 2795−2804.
(42) Krieger, E., Koraimann, G., and Vriend, G. (2002) Increasing the precision of comparative models with YASARA NOVA: A self-parameterizing force field. *Proteins 47*, 393−402.
(43) Altschul, S. F., and Koonin, E. V. (1998) Iterated profile searches with PSI-BLAST: A tool for discovery in protein databases. *Trends Biochem. Sci. 23*, 444−447.
(44) Schultz, J., Milpetz, F., Bork, P., and Ponting, C. P. (1998) SMART, a simple modular architecture research tool: Identification of signaling domains. *Proc. Natl. Acad. Sci. U.S.A. 95*, 5857−5864.
(45) Notredame, C., Higgins, D. G., and Heringa, J. (2000) T-COFFEE: A novel method for fast and accurate multiple sequence alignment. *J. Mol. Biol. 302*, 205−217.
(46) Nicholas, K., Nicholas, H. J., and Deerfield, D. (1997) GeneDoc: Analysis and Visualization of Genetic Variation. *EMBNEWS 4*, 14.
(47) Stamatakis, A., Ludwig, T., and Meier, H. (2005) RAxML-III: A fast program for maximum likelihood-based inference of large phylogenetic trees. *Bioinformatics 21*, 456−463.
(48) Gruber, M., Soding, J., and Lupas, A. N. (2006) Comparative analysis of coiled-coil prediction methods. *J. Struct. Biol. 155*, 140−145.
(49) Kyte, J., and Doolittle, R. F. (1982) A simple method for displaying the hydropathic character of a protein. *J. Mol. Biol. 157*, 105−132.

(50) Perczel, A., Hollosi, M., Tusnady, G., and Fasman, G. D. (1991) Convex constraint analysis: A natural deconvolution of circular dichroism curves of proteins. *Protein Eng. 4*, 669−679.
(51) Buttani, V., Losi, A., Eggert, T., Krauss, U., Jaeger, K.-E., Cao, Z., and Gärtner, W. (2007) Conformational analysis of the blue-light sensing protein YtvA reveals a competitive interface for LOV-LOV dimerization and interdomain interactions. *Photochem. Photobiol. Sci. 6*, 41−49.
(52) Studier, F. W. (2005) Protein production by auto-induction in high-density shaking cultures. *Protein Expression Purif. 41*, 207−234.
(53) Robson Marsden, H., and Kros, A. (2010) Self-assembly of coiled coils in synthetic biology: Inspiration and progress. *Angew. Chem., Int. Ed. 49*, 2988−3005.
(54) Brahms, S., and Brahms, J. (1980) Determination of protein secondary structure in solution by vacuum ultraviolet circular dichroism. *J. Mol. Biol. 138*, 149−178.
(55) Greenfield, N. J. (2006) Using circular dichroism collected as a function of temperature to determine the thermodynamics of protein unfolding and binding interactions. *Nat. Protoc. 1*, 2527−2535.
(56) Sonnichsen, F. D., Van Eyk, J. E., Hodges, R. S., and Sykes, B. D. (1992) Effect of trifluoroethanol on protein secondary structure: An NMR and CD study using a synthetic actin peptide. *Biochemistry 31*, 8790−8798.
(57) Vaidya, A. T., Chen, C. H., Dunlap, J. C., Loros, J. J., and Crane, B. R. (2011) Structure of a light-activated LOV protein dimer that regulates transcription. *Sci. Signaling 4*, ra50.
(58) Buttani, V., Losi, A., Eggert, T., Krauss, U., Jaeger, K. E., Cao, Z., and Gärtner, W. (2007) Conformational analysis of the blue-light sensing protein YtvA reveals a competitive interface for LOV-LOV dimerization and interdomain interactions. *Photochem. Photobiol. Sci. 6*, 41−49.
(59) Fedorov, R., Schlichting, I., Hartmann, E., Domratcheva, T., Fuhrmann, M., and Hegemann, P. (2003) Crystal structures and molecular mechanism of a light-induced signaling switch: The Phot-LOV1 domain from *Chlamydomonas reinhardtii*. *Biophys. J. 84*, 2474−2482.
(60) Möglich, A., and Moffat, K. (2007) Structural Basis for Light-dependent Signaling in the Dimeric LOV Domain of the Photosensor YtvA. *J. Mol. Biol. 373*, 112−126.
(61) Han, S., and Hill, A. F. (2008) Analysis of PrP conformation using circular dichroism. *Methods Mol. Biol. 459*, 145−159.
(62) Dutta, K., Alexandrov, A., Huang, H., and Pascal, S. M. (2001) pH-induced folding of an apoptotic coiled coil. *Protein Sci. 10*, 2531−2540.
(63) Muhle-Goll, C., Gibson, T., Schuck, P., Schubert, D., Nalis, D., Nilges, M., and Pastore, A. (1994) The dimerization stability of the HLH-LZ transcription protein family is modulated by the leucine zippers: A CD and NMR study of TFEB and c-Myc. *Biochemistry 33*, 11296−11306.
(64) Ogata, H., Cao, Z., Losi, A., and Gärtner, W. (2009) Crystallization and preliminary X-ray analysis of the LOV domain of the blue-light receptor YtvA from *Bacillus amyloliquefaciens* FZB42. *Acta Crystallogr. F65*, 853−855.
(65) Cheung, J., Bingman, C. A., Reyngold, M., Hendrickson, W. A., and Waldburger, C. D. (2008) Crystal structure of a functional dimer of the PhoQ sensor domain. *J. Biol. Chem. 283*, 13762−13770.
(66) Reinelt, S., Hofmann, E., Gerharz, T., Bott, M., and Madden, D. R. (2003) The structure of the periplasmic ligand-binding domain of the sensor kinase CitA reveals the first extracellular PAS domain. *J. Biol. Chem. 278*, 39189−39196.
(67) Zhang, Z., and Hendrickson, W. A. (2010) Structural characterization of the predominant family of histidine kinase sensor domains. *J. Mol. Biol. 400*, 335−353.
(68) Yazawa, M., Sadaghiani, A. M., Hsueh, B., and Dolmetsch, R. E. (2009) Induction of protein-protein interactions in live cells using light. *Nat. Biotechnol. 27*, 941−945.
(69) Karanicolas, J., Corn, J. E., Chen, I., Joachimiak, L. A., Dym, O., Peck, S. H., Albeck, S., Unger, T., Hu, W., Liu, G., Delbecq, S., Montelione, G. T., Spiegel, C. P., Liu, D. R., and Baker, D. (2011) A de novo protein binding pair by computational design and directed evolution. *Mol. Cell 42*, 250−260.
(70) Pathak, G. P., Losi, A., and Gärtner, W. (2012) Metagenome-based screening reveals worldwide distribution of LOV-domain proteins. *Photochem. Photobiol. 88*, 107−118.
(71) Strickland, D., Lin, Y., Wagner, E., Hope, C. M., Zayner, J., Antoniou, C., Sosnick, T. R., Weiss, E. L., and Glotzer, M. (2012) TULIPs: Tunable, light-controlled interacting protein tags for cell biology. *Nat. Methods 9*, 379−384.

5. Physiological studies on *Pseudomonas putida KT2440*

5.1 Involvement of the "short" LOV protein PpSB1-LOV in the iron-starvation/motility response of *Pseudomonas putida* KT2440

Katrin Jentzsch, Karl-Erich Jaeger and Ulrich Krauss

Involvement of the "short" LOV protein PpSB1-LOV in the iron-starvation/motility response of *Pseudomonas putida* KT2440

Katrin Jentzsch, Karl-Erich Jaeger and Ulrich Krauss*

Institut für Molekulare Enzymtechnologie, Heinrich-Heine Universität Düsseldorf, Forschungszentrum Jülich, Stetternicher Forst D-52426 Jülich, Germany

Abstract

The saprotrophic γ-proteobacterium *Pseudomonas putida* KT2440 harbours two unusual light, oxygen, voltage (LOV) photoreceptor proteins, PpSB1-LOV and PpSB2-LOV. While both potential photoreceptor proteins possess a characteristic LOV photocycle, as well as all canonical sequence features of a LOV domain, they both lack a fused effector domain (*1*). In recent years a plethora of different physiological responses have been reported to be associated with LOV photoreceptor systems in different phototrophic and chemotrophic bacteria. Effects include among others cell-cell and cell-surface adhesion, motility, regulatory responses to (photooxidative) stress as well as host persistence and virulence. One common cause associated with many of the aforementioned effects, i.e. in proteobacteria, is iron limitation during growth of the respective organism. In light of those reports, we here study iron limitation related phenotypic traits in the *P. putida* KT2440 wild-type strain and a PpSB1-LOV deletion mutant strain. Our genetic data hints at the involvement of the PpSB1-LOV protein in the general iron-starvation response, i.e. affecting swimming motility, growth under iron limitation and iron scavenger pyoverdin production in a correlated manner. While only net pyoverdin levels seem to be directly regulated by blue light, the remaining phenotypic effects of the deletion appear to be light independent.

Introduction

Light is a ubiquitous stimulus for most living beings including amongst others bacteria, fungi, plants and mammals (*2-5*). Thus, it is not surprising that dedicated photosensory systems are present in all three kingdoms of life (*6*), which sense the quantity, direction, duration as well as the quality of the incoming radiation (*2, 5, 7*). Most photoreceptors identified so far respond to the visible fraction of the solar spectrum (390 nm – 750 nm). In particular for the blue region (430 nm - 500 nm) of the spectrum several photosensory receptor families have been identified (*8, 9*) Those include the sensors of the blue-light using FAD (BLUF) family, cryptochromes (Cry) and the light, oxygen, voltage (LOV) family (*10-13*). The latter, representing one of the most widespread photoreceptor families found in nature. LOV photoreceptors can be identified in fungi, algae, green plants as well as in phototrophic and chemotrophic bacteria (*14*). Currently, almost 600 sequences encoding for potential LOV proteins can be detected in 10–15% of deposited prokaryotic genomes (*15*) . While the role of LOV photoreceptors is well understood in fungi and plants still little is known about the role of the structurally diverse LOV proteins found in a plethora of chemotrophic bacteria (*5, 6, 13, 16*). Only recently it could be demonstrated that the YtvA protein of *B. subtilis* acts in the general stress-response pathway, by modulating gene expression under control of the alternative sigma factor σB in a blue-light dependent manner (*17-19*). Related responses were demonstrated for a homologous, YtvA-like, protein of *Listeria monocytogenes* (*20*). Moreover, this protein was shown to be involved in controlling enterocyte invasiveness and swimming motility of the organim (*21*). A LOV-dependent histidine-kinase was shown to be involved in host persistence and virulence of the mammalian pathogen *Brucella abortus* (*22*). Furthermore, in the marine bacterium *Caulobacter crescentus*, an architecturally similar protein regulates cellular attachment (*23*). Thus, in recent years diverse blue-light dependent physiological responses have been implied for various blue-light photoreceptor systems in chemotrophic bacteria ((*24*) and citations therein). However, no general physiological theme has yet emerged to account for the importance of blue light and thus for the widespread appearance of LOV sensory systems in chemotrophic bacteria. So far responses, even for structurally related sensory systems (i.e. LOV histidine kinases, or YtvA-like architectures) seem variable and quite specific for the particular host. This suggests a divergent evolution of the LOV dependent sensory apparatus in bacteria, highlighting the adaptability of this class of sensory proteins to changed ecological conditions imposed by the different microbial habitats. Hence further studies are needed to broaden our knowledge about the role and importance of LOV photosensory systems in bacteria.

We recently described the isolation, characterization (*1, 25*) and crystal structure (*26*) of the LOV protein PpSB1-LOV of the plant

root colonizing γ-proteobacterium *Pseudomonas putida* KT2440. PpSB1-LOV is one of two highly similar LOV proteins present in the organism. Both PpSB1-LOV and its paralogous twin PpSB2-LOV are members of the "short" LOV family, lacking fused effector domains (*9, 27*). The two LOV proteins are highly similar in sequence (about 66% identical amino acids positions), but display significantly different photochemical characteristic with respect to dark-state recovery (*1*). While the photochemistry as well as structural features of PpSB1-LOV have been studied in great detail, little is yet known about the physiological role of those putative photoreceptors.

Therefore, we here studied the blue-light dependent physiological behavior of *P. putida* KT2440 and a mutant strain in which the PpSB1-LOV encoding gene has been disrupted by insertion of an antibiotics resistance cassette. The presented data suggests the involvement of the PpSB1-LOV protein in the general iron-starvation response, i.e. affecting swimming motility, growth under iron limitation and iron scavenger pyoverdin production. Interestingly, the most pronounced phenotypic effects of the deletion appeared to be light independent.

Materials and Methods

Bacterial strains and plasmids

All strains and plasmids used in the study are listed in Table 1.

Table 1: Strains and plasmids used in this study

Strain or plasmid	Relevant characteristics	Source or reference
E. coli		
DH5α	F-, φ80dlacZΔM15, Δ(lacZYA-argF)U169, deoR, recA1, endA1, hsdR17 (rK-,, mK+), phoA, supE44, λ-, thi-1, gyrA96, relA1 Host for Plasmid amplification	(*28*)
S17-1	RP4-2 (Tc::Mu) (Km::Tn*7*) integrated in the chromosome	(*29*)
P. putida		
KT2440	mt-2 wildtype strain	(*30*)
ΔPpSB1-LOV	Δ*PpSB1-LOV*::[Spc::Sm]	This work
Plasmids		
pUC18	Apr, *lac*Zα	(*31*)
pHP45Ω	Smr, Spcr, (aaadA+ gene) derived from R100.1 plasmid cloned into a modified pBR322 vector	(*32*)
pWK329B	Derivative of pSUP301 carrying a 2.6 kb *Eco*RI fragment encoding Gm resistance, cloned by using *Sph*I-*Eco*RI adapters from pUC19	(*33*)
pR459	derivative of plasmid pR424; Mob, origin of transfer, Cmr, Tcr	(*29, 34*)
pUCSB1-KO	Apr, *lac*Zα, Mob, *PpSB1-LOV*::Smr, Spcr,	This work
pUCSB2-KO	Apr, *lac*Zα, Mob, *PpSB2-LOV*::Gmr,	This work

Microbial media

E. coli strains were grown in Luria-Bertani (LB) broth supplemented with the appropriate antibiotics for maintenance of the respective plasmids. Antibiotic concentrations employed for plasmid maintenance in *E. coli* were as follows: Ampicillin (Amp, 100 µg/mL), Gentamycin (Gm, 30 µg/mL), Spectinomycin (Spc, 300 µg/mL), Streptomycin (Sm, 450 µg/mL), Tetracyclin (Tc, 30 µg/mL), Chloramphenicaol (Cm, 10 µg/mL). For growth and conjugation of *P. putida* strains EM-medium (20 g/L Bacto-Trypton, 5 g/L yeast extract, 5 g/L NaCl, 5 g/L glucose) and EM-agar (15 g/L Agar-Agar) was used. Antibiotic concentrations employed for isolation of the *P. putida* KT2440 PpSB1-LOV and PpSB2-LOV isogenic deletion mutant were as follows: Gm (30 µg/mL), Spc (300 µg/mL), Sm (450 µg/mL), Tc (30 µg/mL), and Cm (10 µg/mL).

For growth of *P. putida* KT2440 under iron limiting conditions either M9 minimal medium or PG medium (*35, 36*) was used. M9 medium consisted of 12.8 g/L $Na_2HPO_4.7H_2O$, 3 g/L KH_2PO_4 , 0.5 g/L NaCl, 1 g/L NH_4Cl, and contained 2 mM $MgSO_4$, 0.1 mM $CaCl_2$ and 0.4 % (w/v) glucose. Swarming plates contained 0.5 % (w/v) agarose, swimming plates were supplemented with 0.2 % (w/v) agarose as hardening agent. PG medium contained 5 g/L proteose peptone No.3 (Difco, Proteose-Peptone 212693), and 2 g/L glucose. Swarming agar plates were supplemented with 0.5 % (w/v) Bacto Agar (Difco, Bacto-Agar: 214050). Swimming plates contained 0.2 % (w/v) Bacto Agar (adapted from (*35*)).

General microbiological and molecular biological methods

Heat-shock transformation of *E. coli* strains, isolation of plasmid DNA, restriction endonuclease digestion, agarose gel-electrophoresis and ligation of DNA fragments was carried using standard laboratory methods (*37*).

Construction of suicide vectors for the disruption of PpSB1-LOV and PpSB2-LOV encoding genes in P. putida KT2440

For disruption of the PpSB1-LOV (Q88E39) encoding gene in *P. putida* KT2440 the genomic region 700 basepairs up-and downstream of a singular *Mun*I restriction site at the 5'- end of the PpSB1-LOV gene was PCR amplified using the oligonucleotides SB1-KO_fw: 5'-TTCTTGACTCACTTGCGTTGGGATATCGC G-3' and SB1-KO_rev: 5'-CGTCCTCTACCAGCTGCAGGGGAAAAC-3'. The resulting fragment was cloned as blunt-ended PCR product into the *Sma*I site of pUC18 (Fermentas/Thermo Scientific, St.Leon Roth, Germany) yielding the construct pUCSB1. An Ω-Spc/Sm-Ω resistance cassette containing transcription termination sites (Ω-hairpin) at both the 5'- and 3'- end was isolated form pHP45Ω (*32*) by digesting the plasmid with *Eco*RI. Subsequently, this cassette was inserted

into the singular *Mun*I restriction site of the PpSB1-LOV genomic region of pUCSB1 vector resulting in pUCSB1-ΩSpc. For construction of the corresponding PpSB2-LOV suicide vector, employed for disruption of the PpSB2-LOV encoding gene, a similar strategy was used. The respective PpSB2-LOV (Q88JB0) encoding genomic region was amplified using the oligonucleotides SB2-KO_fw: 5'-AACTGCTCGAAGTAGGCACGCAGGG-3' and SB2-KO_rev: 5'-TCGACCTGGTTCATCTGCAAGCGCAG-3'. The resulting fragment was cloned blunt-ended into pUC18 resulting in pUCSB2. To facilitate gene disruption a Gm resistance cassette isolated from the pWK329B vector (*33*) was cloned into a singular *Bcl*I-restriction site present at the 5'-end of the PpSB1-LOV encoding gene in pUCSB2. This results in the plasmid pUCSB2-Gm. Since pUC18 vectors cannot be replicated in *P. putida*, selection on appropriate antibiotics will enforce the stable integration of the respective antibiotics resistance cassette in the corresponding targeted gene region of *P. putida* genome via homologous recombination. This will result in disruption of the respective LOV-protein encoding genes.

To allow mobilization via diparental conjugal transfer of both suicide vectors into *P. putida*, a MOB cassette (*29*), containing the origin of transfer along with a tetracyclin resistance cassette, was isolated from pR459 (*34*) by digestion with the restriction endonuclease *Eco*RI. The resulting DNA fragment was inserted into similarly hydrolyzed pUCSB1-ΩSpc and pUCSB2-Gm vectors, resulting in the mobilizable suicide plasmids pUCSB1-KO and pUCSB2-KO.

Diparental conjugal transfer and isolation of PpSB1-LOV and PpSB2-LOV deletion mutant strains.

The suicide vectors pUCSB1-KO and pUCSB2-KO were transformed into *E. coli* S17-1 λ pir, which is a helper-strain for conjugal transfer into *P. putida* and other gram-negative bacteria (*29*). In brief, the helper strain as well as *P. putida KT2440* wild-type were grown in either LB or EM liquid medium at constant agitation (120 rpm) at 37 °C or 30 °C until exponential growth was reached. Similar amounts of cells of both cultures (corresponding to an OD600 of 1) were harvested by centrifugation. The resulting pellet was carefully washed twice with fresh EM medium lacking antibiotics. Subsequently, the pUCSB1-KO/pUC-SB2-KO containing *E. coli* S17-1 cells were mixed with equal amounts of *P. putida* KT2440 wild-type cells. 40µl of the combined cell suspensions were then carefully pipetted onto a nucleopore Membrane (HAW P02500, Merck Millipore, Billerica, MA, USA) centered on an EM agar plate without antibiotics and incubated over night at 30 °C. Conjugants, containing the Spc/Sm (pUCSB1-KO) or the Gm resistance cassette (pUCSB2-KO) integrated in the respecive genomic region were selected by using Spc/Sm or Gm, respectively (single crossing-over). Counterselection against *E. coli* was carried out using Cm. Conjugants were replica plated on EM-agar containing either Spc/Sm or Tc to identify mutants which have

lost the vector part containing the MOB-Tc cassette (double crossing-over).

Verification of PpSB1-LOV and PpSB2-LOV isogenic deletion mutants by colony PCR

Potential double crossing-over mutants were verified using colony PCR. Taq Polymerase (Fermentas/Thermo Scientific, St. Leon Roth, Germany) was used for amplification according to the protocol described by Sheu and co-workers (Sheu et al. 2000). Oligonucleotides, binding at a genomic region immediately up-stream or down-stream of the genomic region used for homologous recombination were used to verify double crossing-over and thus clean disruption of the respective LOV-protein encoding gene. Sequences of the employed oligonucleotide primers were as follows: SB1-Out_fw: 5'-TGTACCAGCGCAGTTTCGTGCTCAACGACCGG-3', SB1-Out_rev: 5'-GCACGCCTTTGAAGGAAATCTCGCGCACCCACA-3',

SB2-Out_fw: 5'-CGCCAATGCAGGCAGCTGCAGCCTTGCAGCGTGATCGG-3', and SB2-Out_rev:- 5' -CGATGCGTTGTCGCTCGCTGCTCAACAGCAGC – 3'.

Illumination of shaken liquid cultures and agar plates

Illumination of agar plates and shaken liquid cultures was achieved using two custom-made blue-light (460 nm) LED-Panels (Firma Insta GmbH, Lüdenscheid, Germany) mounted perpendicular to a rotary shaker (IKA®Works, Staufen, Germany). Shaker and LED panels were placed in a temperature controllable incubation box (Certomat/Sartorius, Göttingen, Germany). Liquid cultures and agar plates were placed in the middle of the shaker platform to achieve even illumination. To conduct dark experiments plates and culture flask were wrapped in aluminium and placed at the perimeter of the shaker platform.

Swimming and swarming motility experiments

Swimming and swarming motility experiments were conducted using M9 or PG agar plates respectively. Motility plates were inoculated with 5 µl of a cell suspension containing similar amounts of fresh overnight grown cells (OD600 = ~3). The respective agar plates were incubated at 25 °C in the dark or under constant blue light.

Swarming plates were incubated for up to 3 days, while swimming plates were incubated overnight (16 hours). All plates were inspected visually every day, under dim red safety-light. All plates were photographed under ambient light as well as under a blue-light excitation (365 nm) to visualize pyoverdin production by the cells. At least 10 independent experiments were performed.

Growth of P. putida KT2440 wild-type and P. putida ΔPpSB1-LOV in different media

In order to assess the effect of the PpSB1-LOV gene disruption on growth of *P. putida* under iron-limiting conditions, the wild-type and deletion mutant strain were grown in LB, M9 and PG medium, either in the dark or under constant illumination as described above. The two strains were grown in 25 ml cultures of the respective medium containing the appropriate antibiotics. Cultures were inoculated with 20 µl of similar amounts of cells (OD600) from a fresh over night grown culture. After inoculation, samples were taken either every hour for up to 10 hours or were first left to grow over night and subsequently sampled every hour. For growth comparison the turbidity of the sample expressed as OD600 was measured for appropriately diluted samples.

Quantification of pyoverdin production

For comparison of pyoverdin production levels under iron limitation the wild-type *P. putida* strain as well as the PpSB1-LOV deletion mutant were grown in M9 minimal medium. 20 ml of medium were inoculated with 20 µl of a freshly grown overnight culture of the respective strain. All cultures were incubated at 30 °C at constant agitation (120 rpm), for 3 days either wrapped in aluminum foil to maintain constant darkness while shaking or exposed to constant blue-light illumination. For quantification of pyoverdin excretion to the culture medium cells were removed from the respective culture by centrifufation. The spent-cell free culture medium was spectrofluorimetrically analyzed to quantify pyoverdine production. To account for statistic variatons 10 independent experiments were performed for each strain. In each of those independent growth experiments, 4 cultures were grown under blue light while 4 cultures were kept in the dark under otherwise identical conditions.

Fluorimetric quantification of pyoverdin in spent culture medium

For all measurements a temperature controlled T-format Fluorolog-3 spectrofluorimeter (Horiba, Jobin Yvon GmbH, Bensheim, Germany) was used. Samples (in 10 mm quartz cuvettes) were excited at 350 nm and pyoverdin emission was detected from 380 nm -580 nm. Emission and excitation bandwidths were set at 5 nm and 1 nm, respectively. For data analysis the Origin-based software FluorEssence™ (v3.5) (Horiba, Jobin Yvon GmbH, Bensheim, Germany) was employed. Pyoverdin levels are expressed in terms of fluorescence emission at 485 nm normalized to the OD600 of the harvested culture from which the supernatant was derived.

Quantitative ICP-MS elementary analysis M9- and PG medium

For elementary analysis Inductively Coupled Plasma – Mass Spectrometry (ICP-MS) was used. The analyses were carried out at the ZCH (Zentralabteilung für Chemische Analysen) of the Research Centre Jülich using an Elan 6100 ICP mass-spectrometer. Additionally, iron was quantitatively determined applying a microwave extraction prior to analysing the sample on an Agilent 7500ce ICP-MS system.

Results

Isolation of the P. putida KT2440 ΔPpSB1-LOV and ΔPpSB2-LOV mutant strains

In order to disrupt the PpSB1-LOV and PpSB2-LOV encoding genes in the genome of *P. putida* KT2440 suitable suicide vectors (pUCSB1-KO and pUCSB2-KO) were constructed which allow the integration of an antibiotics cassette flanked by transcription termination sites into the respective LOV-protein encoding gene. Figure 1b, d depict the genomic region surrounding the PpSB1-LOV and PpSB2-LOV encoding genes, respectively. The fragments used for homologous recombination, as well as the respective singular restriction endonuclease recognition sites at the 5'- end of the PpSB1-LOV and PpSB2-LOV encoding ORF are highlighted. Oligonucleotide primers used for amplification of the respective genomic region are marked, as is the position of the respective "outside" oligonucleotides used for verification of successful gene disruption. A pUC18 vector-backbone was employed for construction of the pUCSB1-KO and pUCSB2-KO vectors, as pUC18 is stably maintained in *E. coli* but cannot be replicated in *P. putida* and other Gram-negative bacteria (*38*). Employing an appropriate helper strain, pUCSB1-KO and pUCSB2-KO vectors were transferred to *P. putida* KT2440 wild-type by diparental conjugation and potential trans-conjugants were selected using the strategy described in materials and methods section. Potential double crossing-over mutants were verified by colony PCR (Figure 1a, c). Identification of PpSB1-LOV deletion mutants was straight-forward. A mutant for that an appropriately sized PCR product (about 3800 bp) could be obtained using colony PCR was readily identified (Figure 1a). The size is hereby due to integration of the Ω-Spc/Sm cassette (2440 bp) into the PpSB1-LOV encoding gene region (1400 bp) (Figure 1c). Even though a large set of potential mutants showing the correct antibiotics resistance profile were found, no clean double crossing-over variants could be identified for the PpSB2-LOV encoding gene using colony PCR (data not shown). Therefore, different conditions were tested for isolations of PpSB2-LOV deletion mutant strains. For example conjugation plates were incubated in the dark or under constant blue-light or white-light illumination. Alternatively, trans-conjugants were selected on iron-supplemented agar plates under the above illumination scheme. Overall 350 potential variants were tested by colony PCR. Unfortunately, all attempts to obtain a PpSB2-LOV deletion mutant strain remained unsuccessful.

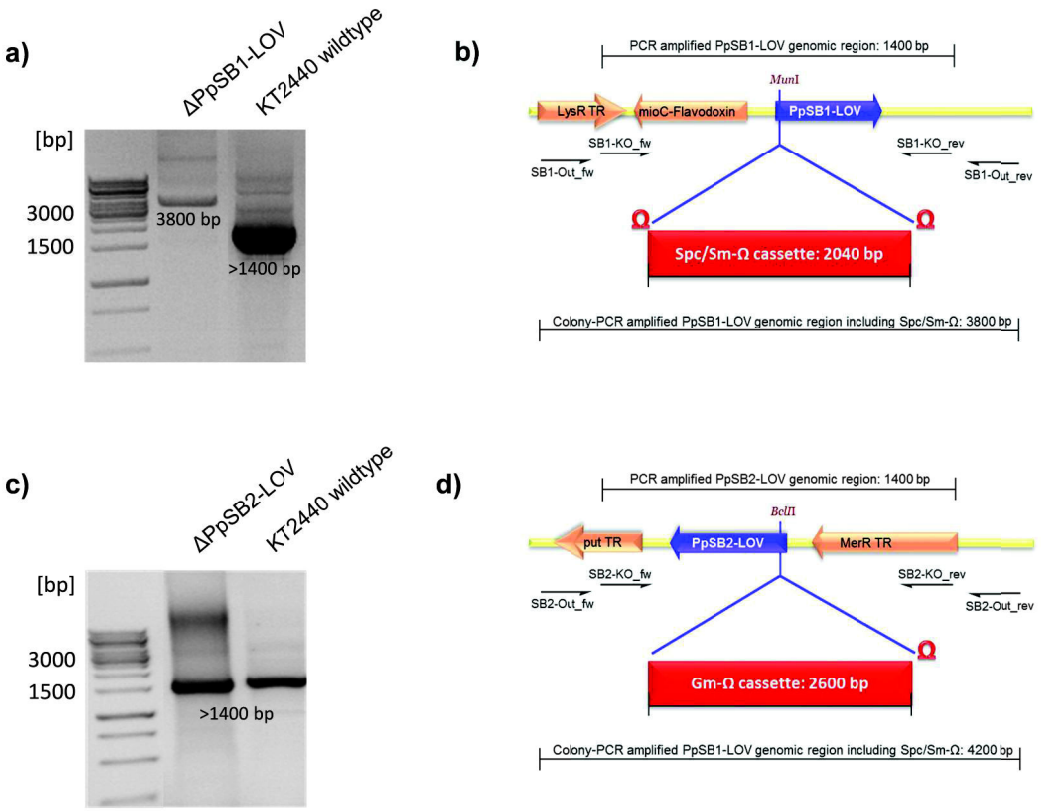

Figure 1: Strategy for the generation and PCR identification of *PpSB1-LOV* and *PpSB2-LOV* deletion mutant strains. a) Exemplary agarose gel illustrating colony PCR identification of *P. putida* strains bearing a successful *PpSB1-LOV* gene disruption. In case of successful integration of the Ω-Spc/Sm cassette into the PpSB1-LOV encoding gene, PCR amplification using the SB1-Out_fw and SB1-Out_rev oligonucleotides yields a fragment of about 3800 bp. For comparison PCR-amplification using the same oligonucleotides but the *P. putida* KT2440 wild-type strain yields a fragment of >1400 bp. b) Strategy for the disruption of the PpSB1-LOV encoding gene in *P. putida* KT2440. Oligonucleotide primers used for amplification of the respective genomic region as well as colony PCR primers are shown as black arrow below the genomic region. LysR TR: LysR type transcriptional regulator. mioC: flavodoxin. c) Exemplary agarose gel illustrating colony PCR identification of *P. putida* strains lacking a *PpSB2-LOV* gene disruption. In case of successful integration of the Gm cassette into the PpSB2-LOV encoding gene, PCR amplification using the SB2-Out_fw and SB2-Out_rev oligonucleotides should yield a fragment of about 4200 bp. For comparison PCR-amplification using the same oligonucleotides but the *P. putida* KT2440 wildt-ype strain yields a fragment of >1400 bp. d) Strategy for the disruption of the PpSB2-LOV encoding gene in *P. putida* KT2440. Oligonucleotide primers used for amplification of the respective genomic region as well as colony PCR primers are shown as black arrow below the genomic region: putTR: putative transcriptional regulator. MerR TR: MerR type transcriptional regulator.

Influence of the PpSB1-LOV disruption on cell motility

In order to test the effect of the PpSB1-LOV deletion with respect to iron-starvation associated phenotypic traits, several growth/motility experiments were conducted. When grown on swarming agar plates, the PpSB1-LOV deletion mutant strain displayed similar behaviour as the wild-type (data not shown). On both M9 and PG plates, clear

differences were observable between the wild-type strain and the PpSB1-LOV deletion mutant strain (Figure 2). While the PpSB1-LOV deletion mutant showed strongly reduced swimming on M9 plates, no growth (and thus swimming) was observed on PG plates. The same holds for pyoverdin production, which is strongly reduced on M9 medium and absent on PG plates (Figure 2). Both phenotypes seem independent of illumination (Figure 2).

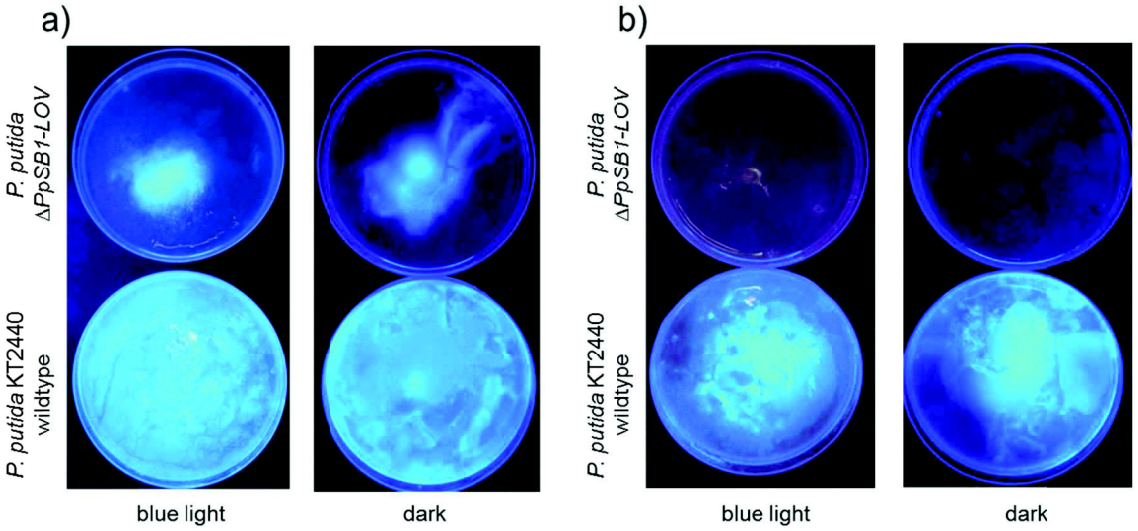

Figure 2: Swimming motility plates a) *P. putida* KT 2440 wildt-ype (bottom) and PpSB1-LOV deletion mutant (top) grown for 16 hours on M9 swimming plates. Plates were either incubated in the dark (right panel) or under constant blue-light illumination (left panel) b) *P. putida* KT 2440 wild-type (bottom) and PpSB1-LOV deletion mutant (top) grown for 30 hours on PG swimming plates. Plates were either incubated in the dark (right panel) or under constant blue-light illumination (left panel). Both figures (a) and b) represent the trend of at least 10 independent experiments.

Growth of P. putida KT2440 wildtype and P. putida ΔPpSB1-LOV on different media

In order to evaluate, whether the observed differences in swimming behaviour are related to differences in growth, the wild-type and the corresponding PpSB1-LOV deletion mutant strain were cultured in different liquid media. No significant growth differences were visible when both strains were grown on LB medium (Figure 3a). The same is true for growth on M9 medium, where both strains grow equally well (Figure 3b). In contrast, while *P. putida* wild-type did grow well on M9 and PG medium (Figure 3b and c), no growth could be observed for the PpSB1-LOV deletion mutant on PG medium (Figure 3c). One possible explanation for the observed medium dependent growth differences might be found in different iron levels of the PG medium compared to M9. Therefore, iron was supplemented at defined time-points during growth of the PpSB1-LOV deletion mutant on PG medium (Figure 3d). Supplying, iron to the medium at defined time points does restore growth of the deletion mutant strain to some extent. Immediately after supplying iron to the medium a rapid increase in

growth can be observed. This initial burst however, levels off, again resulting in intermediate stagnation of growth. If iron is again supplied another burst in growth can be observed. Like in agar plate swimming experiments, the observed growth differences are independent of illumination.

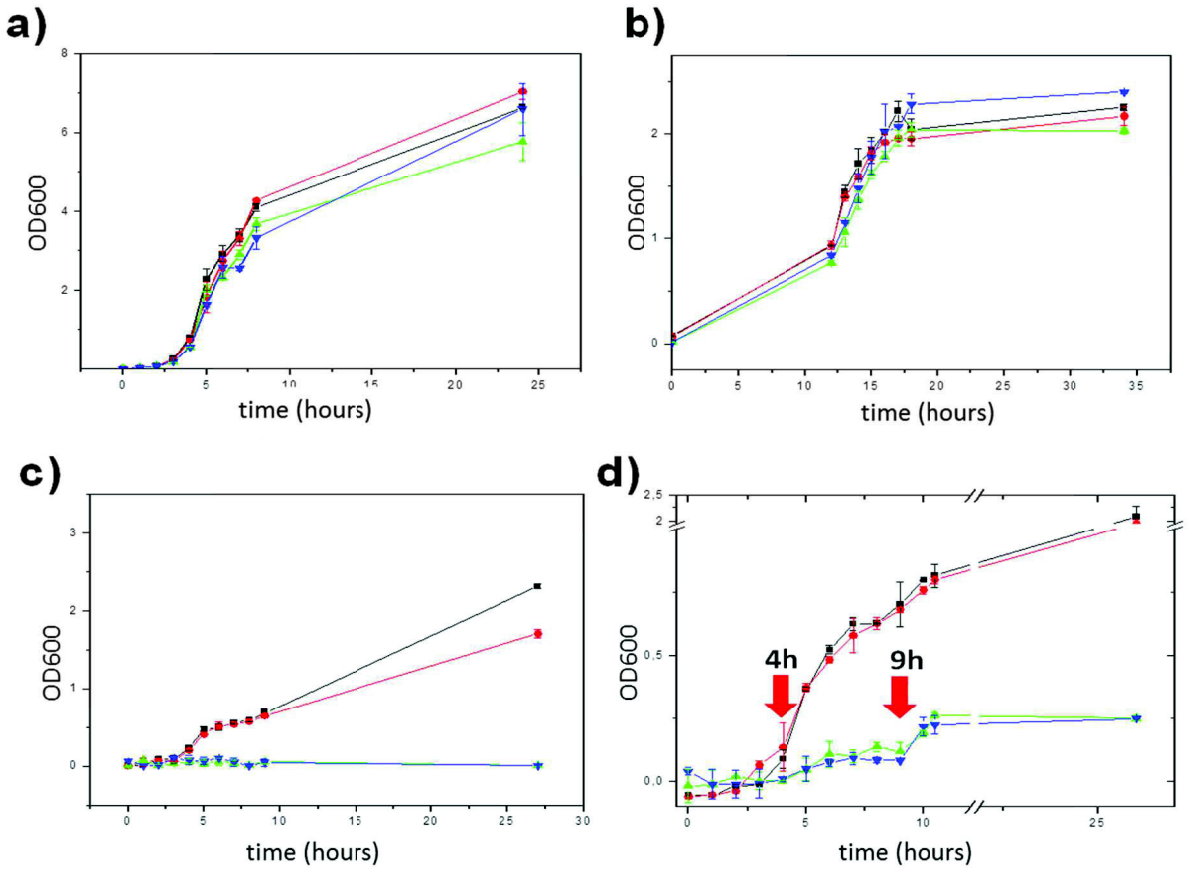

Figure 3: Growth of *P. putida* KT2440 wild-type (red squares and black squares) and the *P. putida* Δ*PpSB1-LOV* (blue and green triangles) on different media. Growth is expressed as OD600 plotted version time. The following media were used a) nutrient rich (undefined) LB medium b) M9 minimal medium and c) nutrient-rich (defined) PG medium. Error bars are derived from OD600 values of four independent cultures. d) *P. putida* KT2440 wildtype and *P. putida* Δ*PpSB1-LOV were* grown on PG medium over a total of 25 hours at 30°C. At indicated times (red arrows) 40 µM Fe_2SO_4 was added to the *P. putida ΔPpSB1-LOV* cultures.

Quantitative elementary analysis M9- and PG medium

In order to quantify potential differences in the elementary composition, which might result in the observed growth differences in the two media, ICP-MS was used to analyze the two growth media. Table 2 shows the results of the elementary analysis. While, the iron content of both media is equally low (< 200 µg/ml) major differences are found in potassium, zinc, rubidium and phosphate levels.

Table 2: Concentrations of trace elements in M9 and PG medium determined using ICP-MS.

Element	M9 medium	PG medium	Concentration Unit
K	1105	95	mg/L
Na	760	400	mg/L
Mg	7.4	0.6	mg/L
Al	0.4	0.08	mg/L
P	130	0.2	mg/L
Ca	1.2	n.d.	mg/L
Mn	< 0.05	< 0.05	mg/L
Fe	146	187	µg/L
Zn	< 2	145	µg/L
Cu	< 2	< 2	µg/L
Rb	6	115	µg/L
Sr	3	3	µg/L
Mo	2.4	5	µg/L

Influences of the PpSB1-LOV disruption on pyoverdin production

In order to detect quantitative differences between the *P. putida* wild-type strain and PpSB1-LOV deletion mutant with respect to pyoverdin production/excretion/uptake, the two strains were grown on M9 medium in the dark or under continuous blue-light illumination. Cells were removed and the spent culture medium was analyzed spectrofluorimetrically with respect to its pyoverdin content (Figure 4). The here observed pyoverdin levels detectable at a given time in

culture supernatants are the result of cellular processes such as pyoverdin production, excretion and uptake. As those processes cannot be assessed independently from each other, we will in the following only compare net pyoverdin levels quantified spectrofluorimetrically by quantifying pyoverdin specific fluorescence emission. No significant differences in pyoverdin levels were detectable for the wild-type strain grown in the dark and under constant illumination (One way-Anova, P = 0.0001, Dunnetts posttest for comparison to the wildtype, P< 0.001). Generally, net pyoverdin levels detected for the *PpSB1-LOV* deletion mutant strain are significantly reduced compared to net pyoverdin levels observed for the wild-type strain under both dark and light conditions (Dunnets-Post test for comparison to the wildtype, P=0.001). Moreover, significant differences in net pyoverdin levels were observed for the dark and light grown deletion mutant strain (Student t-test, 99% confidence interval). Hereby, growth of the deletion mutant under constant illumination resulted in increased net pyoverdin levels, compared to a culture of the same strain grown in the dark. (Figure 4d).

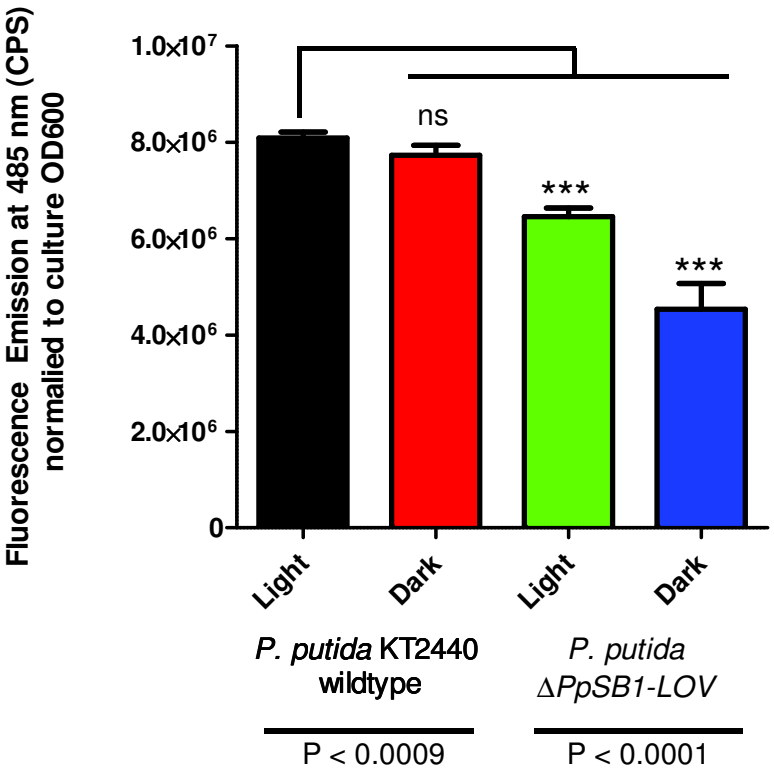

Figure 4: Pyoverdin concentration in spent culture supernatants of *P. putida* KT2440 wild-type and *P. putida* Δ*PpSB1-LOV*. Pyoverdin production was assayed by means pyoverdin specific fluorescence emission. Samples were excited at 350 nm and emission spectra were recorded from 380 nm to 580 nm. To account for growth differences of the tested strains, fluorescence emission data was normalized to the OD600 of the respective culture. Data represents the means ± standard deviation of the means (SD) from two independent experiments with 4 replica cultures per analyzed strain (n = 8; one-way ANOVA, P < 0.0001; Dunnett's posttest for comparison to wild type, P

< 0.001, ***, ns: not significant). Statistical significance of the differences in pyoverdin levels between light and dark grown *P. putida* KT2440 wild-type and *P. putida* Δ*PpSB1-LOV* was tested using the student t-test (99% confidence interval, n=8). The respective P values are given below the compared columns.

Discussion

The presented data suggests the involvement of the PpSB1-LOV encoding gene in the iron-starvation response of *P. putida* KT2440. Clear phenotypic differences between the two strains were detectable in growth experiments, i.e. for growth on PG medium, swimming motility and pyoverdine production. The observed differences for the PpSB1-LOV deletion mutant with regard to swimming behaviour on PG agar plates (Figure 2b) are most probably related to the growth impairment of the strain on this medium (Figure 3c). In contrast, growth of the deletion mutant is not impaired on M9 liquid medium. Therefore, the observed differences in swimming behaviour on M9 plates apparently relate to decreased motility of the deletion mutant strain. Interestingly, both growth-related phenotypes of the deletion mutant, i.e. loss of growth on PG liquid medium and reduced swimming motility on M9 plates are independent of light. When comparing the net levels of excreted pyoverdin between blue-light and dark-growth experiments (Figure 4), differences between light and dark incubations are apparent. It appears that during growth of the PpSB1-LOV deletion mutant strain under constant blue-light more pyoverdin is produced or excreted than when the same strain is grown in the dark. Moreover, net pyoverdin levels produced by the PpSB1-LOV deletion mutant are significantly lower than for the corresponding wild-type strain. Thus, it seems likely that the observed reduced motility for the deletion mutant on M9 plates is directly linked to a reduction in pyoverdin production/excretion. In a recent study Matilla *et. al* (*35*), provided direct physiologcial evidence for a link between pyoverdin production and swimming/swarming motility of *P. putida* KT2440. Our study thus supports this notion and moreover provides a direct link between the potential blue-light photoreceptor PpSB1-LOV and production/excretion of the iron-scavenger pyoverdin under iron limiting conditions. A potential biological mechanism for the importance of blue-light sensing under iron limiting conditions might be found in the observation that blue light can excite iron free porphyrin derivatives such as the heme precursor protoporphyrin IX (PPIX), with high yields to the corresponding triplet state. In the presence of molecular oxygen, this in turn can result in the generation of reactive oxygen species (ROS) and thus oxidative damage to cellular components (*39*). Such an effect might be particularly severe under growth condition where iron supply is limited within the cell. Thus, the ability to sense the presence of blue light, i.e. under growth conditions were iron is scarce, might represent a valid stress response mechanism. Here, up-regulation of pyoverdin excretion or production would alleviate the

stress imposed on the cell by increasing the intracellularily available iron pool thus limiting the amount of available photosenzitizers such as PPIX.

The absence of a significant blue-light dependent physiological effect observable for the *P. putida* KT2440 wild-type strain could have different reasons. One possibility might be related to the presence of the second LOV-photoreceptor PpSB2-LOV in *P. putida* KT2440. In fact, for the PpSB1-LOV deletion mutant strain a significant effect of blue-light illumination during growth under iron limitation is observable. Here, blue-light seems to regulate/influence the net pyoverdin production of the strain. When the deletion mutant strain is grown under blue-light illumination significantly higher pyoverdin concentrations are detectable in the respective culture supernatant. This might suggest that both PpSB1-LOV and PpSB2-LOV are involved in the same cellular response, acting in an agonist/antagonist like fashion. Thus only in the absence of one of the photoreceptor proteins, the effect of blue light would become apparent. Unfortunately, all attempts to disrupt the gene encoding for the PpSB2-LOV protein failed. Another possibility, which we cannot rule out, is that the environmental cellular signal sensed by PpSB1-LOV is not light, but some other cellular parameter. In a recent study using the plant pathogen *Xanthomonas axonopodis* pv. citri, several physiological aspects related to host colonization such as swarming and twitching motility, EPS production and adhesion to biotic and abiotic surfaces showed a clear dependence on one of three *lov* photoreceptor genes of the organism, while several of them did not have an apparent light regulation (*40*). Regarding this observation, it was shown that the photoactivity of some LOV and BLUF proteins can be regulated by the redox balance of the bacterial cytoplasm (*41*) or by temperature (*42*) .

The most striking phenotype of the PpSB1-LOV deletion mutant was the complete loss of the ability of the strain to grow on PG medium. Quantitative ICP-MS analyses revealed certain differences in the elementary composition of M9 and PG media, that might account for this observation. In light of the observed phenotypes of the PpSB1-LOV deletion mutant, the most likely explanation for lack of growth on PG medium would have been a different iron content of the two media. However, no evidence for such differences is provided by ICP-MS analyses. One striking difference between M9 and PG medium are the differences in their zinc (Zn) and rubidium (Rb) content. Hereby, 70 and 20-fold increased Zn and Rb levels were detected in PG medium compared to M9. Thus, it is tempting to speculate that PpSB1-LOV might be involved in the regulation of Zn and Rb detoxification in *P. putida*. In this regard several bacteria possess periplasmic Cu,Zn- superoxide dismutases (SODs) which can confer protection from extracellular reactive oxygen species (*43*). Moreover, this class of enzymes, together with catalases are reportedly involved in Zn detoxification in eukaryotes such as yeast (*44*). Unfortunately, no gene annotated as encoding

for a Cu/Zn superoxide dismutase can be found in the genome of *P. putida* KT2440. In contrast, the organism possesses two related enzymes, namely one Fe-SOD and a Mn-SOD (*45*) both of which have not been characterized genetically or biochemically. Another major difference can be found in the strongly limited supply of phosphate in PG medium compared to M9 (650-fold reduced). Under such phosphate starved growth conditions, increased superoxide production has been detected in stationary-phased cells of *E. coli* (*46*).

Conclusions

Although further studies are needed to elaborate on the potential role of the two LOV photoreceptors encoded in the genome of *P. putida* KT2240, this study nevertheless sheds some light on potential physiological functions of one of the two proteins. All experiments clearly indicate that PpSB1-LOV is involved in iron-starvation related physiological responses which would i.e. represent the organism a mean to cope with (photo)oxidative stress and cellular changes imposed to the cell by lack of environmental iron. In particular complementation studies would be needed to unequivocally prove the involvement of the PpSB1-LOV encoding gene, in the observed responses. Those studies could pave the way for the understanding of inter and intra- molecular LOV photoreceptor signal-transduction mechanisms as site-specific substitution mutant PpSB1-LOV proteins could be used in complementation studies. Likewise, proteomic and transcriptomic analyses, using the wild-type and the PpSB1-LOV deletion mutant, would particularly be helpful to clearly define the role of the PpSB1-LOV gene in the iron-starvation regulatory response of *P. putida* KT2440.

Acknowledgements

We thank Dr. PD Sabine Becker (Zentralabteilung für Chemische Analysen, ZCH, FZ-Jülich) for carrying out quantitative elementary analyses (ICP-MS).

References

1. Jentzsch, K., Wirtz, A., Circolone, F., Drepper, T., Losi, A., Gärtner, W., Jaeger, K.-E., and Krauss, U. (2009) Mutual Exchange of Kinetic Properties by Extended Mutagenesis in Two Short LOV Domain Proteins from *Pseudomonas putida*, *Biochemistry 48*, 10321-10333.

2. Dunlap J, C. (1999) Molecular bases for circadian clocks, *Cell 96*, 271-290.

3. Purschwitz, J., Müller, S., Kastner, C., and Fischer, R. (2006) Seeing the rainbow: light sensing in fungi, *Current Opinion in Microbiology 9*, 566-571.

4. Gyula, P., Schäfer, E., and Nagy, F. (2003) Light perception and signalling in higher plants, *Current Opinion in Plant Biology 6*, 446-452.

5. Losi, A. (2004) The bacterial counterparts of plant phototropins, *Photochem Photobiol Sci 3*, 566-574.

6. Krauss, U., Minh, B. Q., Losi, A., Gärtner, W., Eggert, T., von Haeseler, A., and Jaeger, K.-E. (2009) Distribution and Phylogeny of Light-Oxygen-Voltage-Blue-Light-Signaling Proteins in the Three Kingdoms of Life, *Journal of Bacteriology 191*, 7234-7242.

7. Lin, C. (2002) Phototropin Blue Light Receptors and Light-Induced Movement Responses in Plants, *Sci. STKE 2002*, pe5-14.

8. Pathak, G. P., Ehrenreich, A., Losi, A., Streit, W. R., and Gärtner, W. (2009) Novel blue light-sensitive proteins from a metagenomic approach, *Environmental Microbiology 11*, 2388-2399.

9. Losi, A. (2007) Flavin-based Blue-light Photosensors: A Photobiophysics Update, *Photochemistry and Photobiology 83*, 1283-1300.

10. Gomelsky, M., and Klug, G. (2002) BLUF: a novel FAD-binding domain involved in sensory transduction in microorganisms, *Trends Biochem Sci 27*, 497-500.

11. Brudler, R., Hitomi, K., Daiyasu, H., Toh, H., Kucho, K.-i., Ishiura, M., Kanehisa, M., Roberts, V. A., Todo, T., Tainer, J. A., and Getzoff, E. D. (2003) Identification of a New Cryptochrome Class: Structure, Function, and Evolution, *Molecular Cell 11*, 59-67.

12. Christie, J. M., Salomon, M., Nozue, K., Wada, M., and Briggs, W. R. (1999) LOV (light, oxygen, or voltage) domains of the blue-light photoreceptor phototropin (nph1): Binding sites for the chromophore flavin mononucleotide *Proceedings of the National Academy of Sciences of the United States of America 96* 8779-8783

13. Crosson, S. (2005) LOV-Domain Structure, Dynamics, and Diversity, In *Handbook of Photosensory Receptors*, pp 323-336, Wiley-VCH Verlag GmbH & Co. KGaA.

14. Kumauchi, M., and Ebrey, T. G. (2005) Visual Pigments as Photoreceptors, In *Handbook of Photosensory Receptors*, pp 43-76, Wiley-VCH Verlag GmbH & Co. KGaA.

15. Pathak, G. P., Losi, A., and Gärtner, W. (2012) Metagenome-based Screening Reveals Worldwide Distribution of LOV-Domain Proteins, *Photochemistry and Photobiology 88*, 107-118.

16. Swartz, T. E., and Bogomolni, R. A. (2005) LOV-Domain Photochemistry, In *Handbook of Photosensory Receptors*, pp 305-321, Wiley-VCH Verlag GmbH & Co. KGaA.

17. Avila-Perez, M., Hellingwerf, K. J., and Kort, R. (2006) Blue Light Activates the σB-Dependent Stress Response of *Bacillus subtilis* via YtvA, *J. Bacteriol. 188*, 6411-6414.

18. Gaidenko, T. A., Kim, T.-J., Weigel, A. L., Brody, M. S., and Price, C. W. (2006) The Blue-Light Receptor YtvA Acts in the Environmental Stress Signaling Pathway of *Bacillus subtilis*, *J. Bacteriol. 188*, 6387-6395.

19. Suzuki, N., Takaya, N., Hoshino, T., and Nakamura, A. (2007) Enhancement of a sigmaB-dependent stress response in *Bacillus subtilis* by light via YtvA photoreceptor, *J Gen Appl Microbiol 53*, 81 - 88.

20. Martinez, L., Reeves, A., and Haldenwang, W. (2010) Stressosomes Formed in *Bacillus subtilis* from the RsbR Protein of *Listeria monocytogenes* Allow σB Activation following Exposure to either Physical or Nutritional Stress, *Journal of Bacteriology 192*, 6279-6286.

21. Ondrusch, N., and Kreft, J. (2011) Blue and Red Light Modulates SigB-Dependent Gene Transcription, Swimming Motility and Invasiveness in *Listeria monocytogenes*, *PLoS ONE 6*, e16151.

22. Swartz, T., Tseng, T., Frederickson, M., Paris, G., Comerci, D., Rajashekara, G., Kim, J., Mudgett, M., Splitte, G., Ugalde, R., Goldbaum, F., Briggs, W., and Bogomolni, R. (2007) Blue-light-activated histidine kinases: two-component sensors in bacteria, *Science 317*, 1090 - 1093.

23. Purcell, E. B., Siegal-Gaskins, D., Rawling, D. C., Fiebig, A., and Crosson, S. (2007) A photosensory two-component system regulates bacterial cell attachment, *PNAS 104*, 18241-18246.

24. Herrou, J., and Crosson, S. (2011) Function, structure and mechanism of bacterial photosensory LOV proteins, *Nat Rev Micro 9*, 713-723.

25. Krauss, U., Losi, A., Gärtner, W., Jaeger, K.-E., and Eggert, T. (2005) Initial characterization of a blue-light sensing, phototropin-related protein from *Pseudomonas putida*: a paradigm for an extended LOV construct, *Physical Chemistry Chemical Physics 7*, 2804-2811.

26. Circolone, F., Granzin, J., Jentzsch, K., Drepper, T., Jaeger, K. E., Willbold, D., Krauss, U., and Batra-Safferling, R. (2012) Structural basis for the slow dark recovery of a full-length LOV protein from *Pseudomonas putida*, *J Mol Biol 417*, 362-374.

27. Losi, A., and Gärtner, W. (2011) Old Chromophores, New Photoactivation Paradigms, Trendy Applications: Flavins in Blue Light-Sensing Photoreceptors†, *Photochemistry and Photobiology 87*, 491-510.

28. Hanahan, D. (1983) Studies on transformation of *Escherichia coli* with plasmids, *Journal of Molecular Biology 166*, 557-580.

29. Simon, R., Priefer, U., and Puhler, A. (1983) A Broad Host Range Mobilization System for In Vivo Genetic Engineering: Transposon Mutagenesis in Gram Negative Bacteria, *Nat Biotech 1*, 784-791.

30. Nelson, K. E., Weinel, C., Paulsen, I. T., Dodson, R. J., Hilbert, H., Martins dos Santos, V. A. P., Fouts, D. E., Gill, S. R., Pop, M., Holmes, M., Brinkac, L., Beanan, M., DeBoy, R. T., Daugherty, S., Kolonay, J., Madupu, R., Nelson, W., White, O., Peterson, J., Khouri, H., Hance, I., Lee, P. C., Holtzapple, E., Scanlan, D., Tran, K., Moazzez, A., Utterback, T., Rizzo, M., Lee, K., Kosack, D., Moestl, D., Wedler, H., Lauber, J., Stjepandic, D., Hoheisel, J., Straetz, M., Heim, S., Kiewitz, C., Eisen, J., Timmis, K. N., Düsterhöft, A., Tümmler, B., and Fraser, C. M. (2002) Complete genome sequence and comparative analysis of the

metabolically versatile *Pseudomonas putida* KT2440, *Environmental Microbiology 4*, 799-808.

31. Messing, J., and Vieira, J. (1982) A new pair of M13 vectors for selecting either DNA strand of double-digest restriction fragments, *Gene 19*, 269-276.

32. Prentki, P., and Krisch, H. M. (1984) In vitro insertional mutagenesis with a selectable DNA fragment, *Gene 29*, 303-313.

33. Miksch, G., Arnold, W., Lentzsch, P., Priefer, U. B., and Pühler, A. (1994) A 4.6 kb DNA region of *Rhizobium meliloti* involved in determining urease and hydrogenase activities carries the structural genes for ureas (ureaA, ureB, ureC) interrupted by other open reading frames, *Molecular and General Genetics MGG 242*, 539-550.

34. Chastanet, A., Prudhomme, M., Claverys, J.-P., and Msadek, T. (2001) Regulation of *Streptococcus pneumoniae* clp Genes and Their Role in Competence Development and Stress Survival, *Journal of Bacteriology 183*, 7295-7307.

35. Matilla, M. A., Ramos, J. L., Duque, E., De Dios Alchè, J., Espinosa-Urgel, M., and Ramos-Gonzalez, M. a. I. (2007) Temperature and pyoverdine-mediated iron acquisition control surface motility of *Pseudomonas putida*, *Environmental Microbiology 9*, 1842-1850.

36. Anderson, E. H. (1946) Growth Requirements of Virus-Resistant Mutants of *Escherichia coli* Strain "B", *Proceedings of the National Academy of Sciences 32*, 120-128.

37. Maniatis, T., Fritsch, E. F., and Sambrook, J. (1989) *Molecular Cloning: A Laboratory Manual*, 2 ed., Cold Spring Harbor Laboratory Press, New York.

38. Herrero, M., de Lorenzo, V., and Timmis, K. N. (1990) Transposon vectors containing non-antibiotic resistance selection markers for cloning and stable chromosomal insertion of foreign genes in gram-negative bacteria, *Journal of Bacteriology 172*, 6557-6567.

39. Ryter, S. W., Kim, H. P., Hoetzel, A., Park, J. W., Nakahira, K., Wang, X., and Choi, A. M. (2007) Mechanisms of cell death in oxidative stress, *Antioxidants & Redox Signaling 9*, 49-89.

40. Kraiselburd, I., Alet, A. I., Tondo, M. L., Petrocelli, S., Daurelio, L. D., Monzón, J., Ruiz, O. A., Losi, A., and Orellano, E. G. (2012) A LOV Protein Modulates the Physiological Attributes of *Xanthomonas axonopodis* pv. citri Relevant for Host Plant Colonization, *PLoS ONE 7*, e38226.

41. Purcell, E. B., McDonald, C. A., Palfey, B. A., and Crosson, S. (2010) An Analysis of the Solution Structure and Signaling Mechanism of LovK, a Sensor Histidine Kinase Integrating Light and Redox Signals, *Biochemistry 49*, 6761-6770.

42. Mussi, M. A., Gaddy, J. A., Cabruja, M., Arivett, B. A., Viale, A. M., Rasia, R., and Actis, L. A. (2010) The Opportunistic Human Pathogen *Acinetobacter baumannii* Senses and Responds to Light, *J. Bacteriol. 192*, 6336-6345.

43. Pacello, F., Ceci, P., Ammendola, S., Pasquali, P., Chiancone, E., and Battistoni, A. (2008) Periplasmic Cu,Zn superoxide dismutase and cytoplasmic Dps concur in protecting *Salmonella enterica* serovar Typhimurium from extracellular reactive oxygen species, *Biochimica et Biophysica Acta (BBA) - General Subjects 1780*, 226-232.

44. Tarhan, C., Pekmez, M., Karaer, S., Arda, N., and Sarikaya, A. T. (2007) The effect of superoxide dismutase deficiency on zinc toxicity in

Schizosaccharomyces pombe, *Journal of Basic Microbiology 47*, 506-512.

45. Heim, S., Ferrer, M., Heuer, H., Regenhardt, D., Nimtz, M., and Timmis, K. N. (2003) Proteome reference map of *Pseudomonas putida* strain KT2440 for genome expression profiling: distinct responses of KT2440 and *Pseudomonas aeruginosa* strain PAO1 to iron deprivation and a new form of superoxide dismutase, *Environmental Microbiology 5*, 1257-1269.

46. Korshunov, S., and Imlay, J. A. (2006) Detection and Quantification of Superoxide Formed within the Periplasm of *Escherichia coli*, *Journal of Bacteriology 188*, 6326-6334.

6. General Discussion

6.1 The short LOV-proteins of *Pseudomonas putida* – two uneven twins

In *P. putida* KT2440, a typical saprotrophic γ-proteobacterium, two genes encoding for the "short" LOV proteins, PpSB1-LOV and PpSB2-LOV have been identified in previous studies (see chapter 2.1) (*179, 180*). Both proteins consist of a conserved LOV-core domain flanked N- and C-terminally by short α-helical extensions but lack a fused effector domain (see chapter 4.1). With about 13 %, "short" LOV proteins, found throughout the bacterial kingdom, represent the third largest prokaryotic LOV-protein family (*42, 115*). Both proteins undergo a typical LOV photocycle upon illumination with blue light. Although they are very similar in sequence (66 % sequence identity), they exhibit dramatically different dark recovery kinetics (chapter 2.1, (*179*)). While PpSB1-LOV is the slowest so far identified bacterial LOV protein (τ_{rec} = 37 h at 20 °C), PpSB2-LOV represents one of the fastest reverting ones (τ_{rec} = 114 s at 20 °C) (chapter 2.1). Parts of this study (chapter 2.1 and chapter 3.1.) addressed the mechanism underlying the slow and fast dark recovery reactions of the two LOV proteins. Based on a sequence comparison between the fast reverting PpSB2-LOV and the slow reverting PpSB1-LOV protein, amino acid positions were identified that differ between the two proteins. Moreover, the corresponding positions in plant phototropin (fast reverting) (*181*) and FKF1-LOV domains (slow reverting) (*182*) were taken into consideration and only amino acid positions differing between the fast and slow reverting as well as plant and bacterial systems were chosen for site-directed mutagenesis (chapter 2.1). Overall 12 amino acid positions as well as the PpSB1-LOV and PpSB2-LOV C -terminal Jα-extensions were interchanged between the two proteins. Effects of the mutations were analyzed, especially with respect to altered dark recovery kinetic properties. In particular two amino acid positions, i.e. at position 61 and position 66, turned out to be of special importance for the dark recovery process. The mutation at position 66 accelerated the recovery of PpSB1-LOV (R66I) from 2471 minutes to about 23 minutes (74 fold acceleration), while the reverse mutation (I66R) in PpSB2-LOV slowed the dark recovery of the protein down by a factor of 6, from ~2 minutes to ~16 minutes. Likewise, the mutation at position 61 in PpSB1-LOV (R61H) accelerated the dark recovery by a factor of about 2 (from 2471 min to 765 min), whereas the corresponding H61R mutation in PpSB2-LOV slows the recovery down by a factor of 3 from ~2 minutes to ~10 minutes.

6.1.1 On the mechanisms of the slow and fast recovery of PpSB1-LOV and PpSB2-LOV

Intricate FMN-phosphate-protein interactions are the main driving force that determine the dark recovery process in PpSB1-LOV and PpSB2-LOV

In chapter 2.2 the effect of two key arginines (R61, R66 in PpSB1-LOV), identified in chapter 2.1, was further investigated by generating the corresponding double-mutant of PpSB1-LOV (R66I/R61H). This mutant showed a further acceleration of the dark recovery reaction (approx. 280-fold) compared to the wild-type protein. Furthermore, the mutations led to a PpSB2-LOV-like chromophore acceptance binding both FMN and riboflavin in a 70:30 ratio, which could not be observed for the respective single mutants. The data obtained in both chapters revealed that the dark recovery reaction of PpSB1-LOV is cooperatively affected by two arginine residues, which then mutated to the corresponding residues found in the fast reverting PpSB2-LOV protein, accelerate the recovery process by three orders of magnitude.

Initially, homology modeling studies (Figure 9 shown in transparent) suggested that one of the two arginine residues (R66) might directly interact with the FMN phosphate via a salt-bridge contact (chapter 2.1.). In the subsequently determined PpSB1-LOV light-state crystal structure (PDB ID: 3SW1) (chapter 3.1) (Figure 9, shown in blue), both R61 and R66 were found to be part of a unique network of four arginine residues tightly coordinating the FMN-phosphate moiety (see chapter 3.1 (Fig. 4a)). In particular, the tight coordination, between R61 and the FMN-phosphate, results in a bending of the Eα-Fα loop toward the FMN chromophore (chapter 3.1 (Fig. 3a)). This unusual bent-in conformation of the Eα-Fα loop (Figure 9) is absent in all other LOV-protein X-ray structures and appears to be a unique structural feature of PpSB1-LOV.

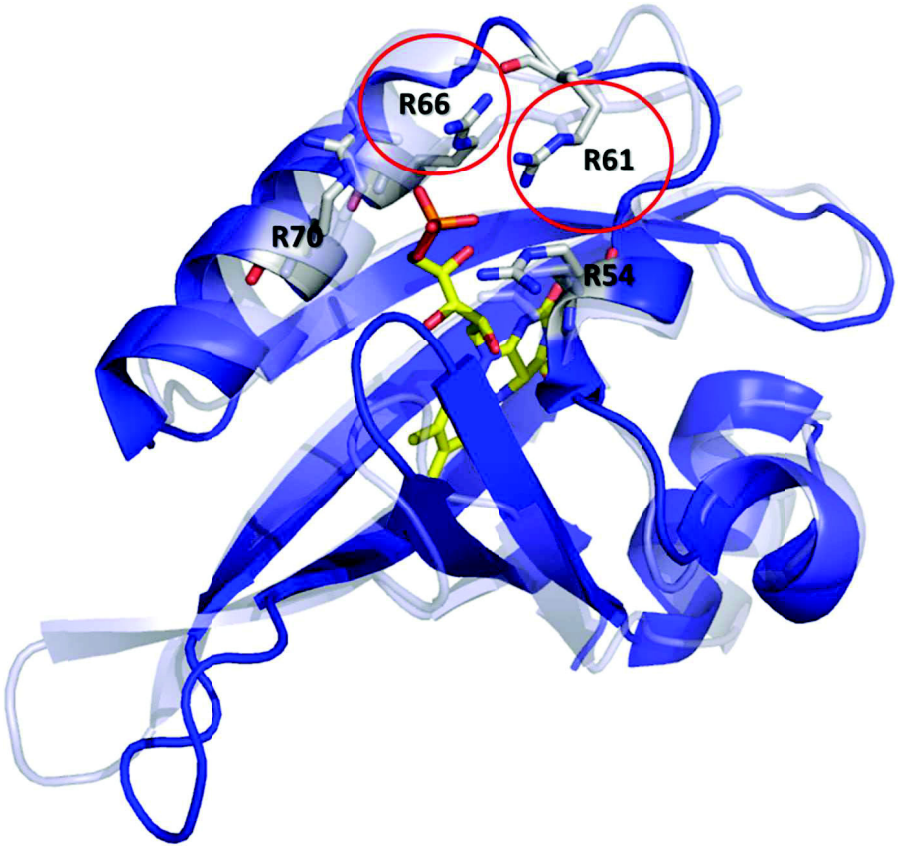

Fig. 9: **Cartoon representation of a PpSB1-LOV homology model** (light grey) and the later determined PpSB1-LOV light-state crystal structure (PDB ID: 3SW1) (blue) (*183*). FMN in the chromophore binding pocket is shown in stick representation and is colored by element: carbon, yellow; nitrogen, blue; oxygen, red; phosphorus, orange. The two arginine residues (R61 and R66 in both the model and the actual structure) that coordinate the FMN-phosphate are circled in red and shown in stick representation. Additionally, the two, in all LOV domains conserved arginines (R54 and R70 in PpSB1-LOV) are shown as sticks colored by element: carbon in grey, nitrogen in blue, oxygen in red.

Mechanistically, tuning of the dark recovery could be realized by either direct stabilization of the light-state conformation for example, by constraining the orientation of the phosphate group and possibly of the whole FMN molecule in the light-state geometry, or by selectively destabilizing the dark state over the light state, i.e. by steric effects.

In order to address this issue, the photoadduct formation was investigated using microsecond transient absorption spectroscopy (chapter 2.2). All transient absorption measurements were performed during a lab exchange visit in the group of Prof. Bernhard Dick at the University of Regensburg. Comparative studies were performed for PpSB1-LOV, PpSB2-LOV and the variants in position 61 and 66 are described in chapter 2.1. None of the introduced mutations had a significant impact on the triplet decay and thus adduct formation kinetics. This essentially rules out that structural differences in the FMN binding-pocket are selectively realized in the dark

state of PpSB1-LOV and PpSB2-LOV. This is in contrast to previous studies of Christie and co-workers, who showed that for the oat phototropin1 LOV2 domain (AsLOV2) steric support imposed in the dark state on the photoactive cystein residue (Cys39 in AsLOV2) by nearby Ile16 impacts on both the light-initiated forward (adduct formation) and dark recovery (adduct decay) reaction (*155*). While mutation of Ile16 to valine accelerated the dark recovery reaction 10-fold, adduct formation was slowed down by a factor of 2 (*155*). For the two *P. putida* proteins, solely the two PpSB2-LOV variants (H61R and I66R) showed a 1.2 and 1.5-fold slower triplet decay. However, in contrast to the study of Christie *et. al* (*155*) the two PpSB2-LOV variants, which showed marginally slower adduct formation kinetics, also displayed slowed dark recovery kinetics.

Given those findings, it seems more likely that the adduct state instability, correlated to faster dark recovery in PpSB2-LOV, is tuned by the constrain imposed on the system by adduct formation and anchoring of the FMN phosphate at the proximal end of the flavin-ribityl chain to R66 and R61. In conclusion, the stability of this strained conformation is affected by introducing the respective mutations in PpSB2-LOV. Likewise, in the slow reverting PpSB1-LOV protein the presence of the two FMN-phosphate anchoring arginine residues increases adduct stability probably by relieving strain imposed on the FMN-protein adduct by ideally supporting the observed light-state geometry. A good illustration of the suggested mechanism is represented by a spring under strain: When being embedded in the hydrogen-bonding/salt-bridge network, stabilized by the strengthened interaction of R66/R61 and the FMN phosphate (PpSB1-LOV and the respective PpSB2-LOV I66R and H61R mutants), the “spring” (i.e represented here by the FMN-protein adduct) is “relaxed” and thus the dark recovery is (very) slow. The opposite is the case in PpSB2-LOV and the respective faster reverting PpSB1-LOV variants, where the “spring” (representing the FMN-protein adduct) is “stretched/compressed” and thus under more strain. Hence, without the stabilizing effect of the FMN-phosphate R61 and R66 interaction, it readily bounces back into its initial conformation (adduct decay) in a much shorter time.

The only other very slow reverting LOV proteins of the FKF1/LKP2/ZTL LOV family (τ_{rec} = 62.5 h at room temperature) (*182*) contain a valine at the position corresponding to R66 in PpSB1-LOV. Thus the very slow recovery of the FKF1-LOV proteins must result from a different mechanism as suggested here for PpSB1-LOV. In their work Zikihara and co-workers speculated that the slow reversion of FKF1 may result from a nine amino acid insertion identified between helix Eα and Fα of the protein. Interestingly, substitution of the respective

loop (Tyr96-Val108) by four residues of the *A. thaliana* phototropin2 LOV2 domain (Gly431-Thr434) resulted in a 3-fold accelerated dark recovery reaction (*184*).

Thus, while the structural consequences of the R61-FMN phosphate interaction appear to be a unique feature of the PpSB1-LOV protein, the general mechanism of tuning the dark recovery via FMN-phosphate-protein interactions appears to be a conserved mechanism present in all LOV systems.

Base-catalyzed adduct rupture cannot fully account for the observed dark recovery differences

For plant LOV domains, it was suggested that surface-exposed histidine residues can act as base catalysts, abstracting the proton from the FMN-N5 atom in the light state, resulting in a catalyzed adduct rupture. This mechanistic assumption was mainly based on the accelerating effect, which addition of the base form of imidazole had on the dark recovery process (*153*). Additionally, the authors chemically modified the two conserved surface-exposed histidine residues of AsLOV2 (His1011 and His1035, phy3LOV2 numbering) by incubating the protein with an excess of the histidine-specific modification reagent diethyl pyrocarbonate (DEPC). The resulting preparation showed a 2-fold slower dark recovery reaction (*153*). Interestingly, while the fast reverting PpSB2-LOV protein contains 4 histidines, no histidines are present in PpSB1-LOV.

Arguably, the magnitude of the effect of the H61R mutation in PpSB2-LOV, which slowed down the recovery only about 3- to 4-fold, could be deduced to base-catalysis as proposed by Alexandre and co-workers (*153*). In PpSB2-LOV one histidine in question, H61, is located about 6 Å away from the FMN-N5 atom. In AsLOV2 the two histidines are located even further away, in a distance of about 12 Å from the chromophore (*153*). While base-catalysis driven from surface-exposed histidine residues could account in part for the fast recovery of PpSB2-LOV, its effect on the recovery reaction appears to be much less prominent, compared to the tuning of the dark recovery by the FMN phosphate-protein interaction.

Interchange of the C-terminal Jα extensions of PpSB1-LOV and PpSB2-LOV mutually affects the dark recovery process.

In the light-state X-ray structure (chapter 3.1) two PpSB1-LOV molecules were found in the asymmetric unit related by a 2-fold symmetry, thus forming a parallel homodimer. Hereby, the

dimer interface is constituted by residues from three major regions of each subunit, namely, the N-terminal cap (N-cap), the central LOV domain β-scaffold and the C-terminal Jα-helix. The N-terminal cap densely packs against the hydrophobic central part of the β-scaffold of the opposite subunit and interacts with its counterpart of the second molecule in the asymmetric unit. Limited interactions with the β-scaffold of the same subunit could also be identified. The protruding C-terminal Jα-helices pack against each other in the dimer, stabilized by a coiled-coil like interaction (see also chapter 4.1) ("helix-out" conformation) (Figure 6).

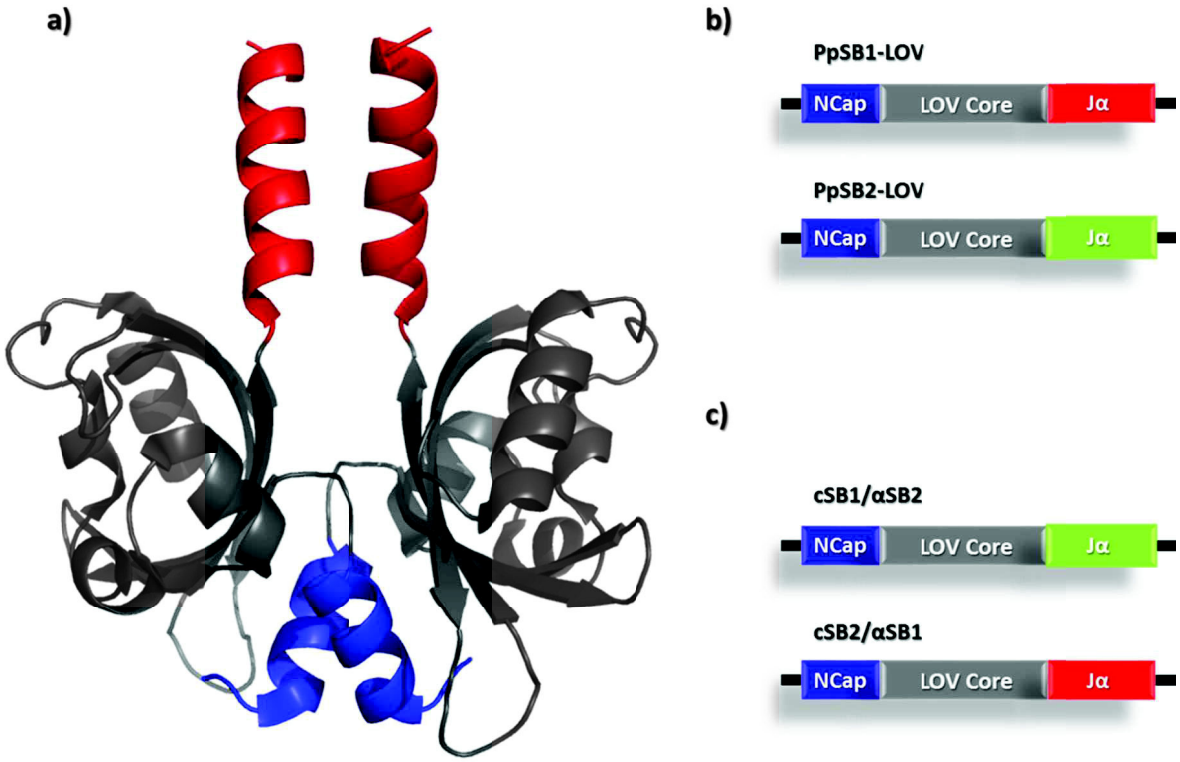

Fig. 10: Interchange of the C-terminal Jα extensions of PpSB1-LOV and PpSB2-LOV. **a)** Dimeric crystal structure of the full length PpSB1-LOV protein (PDB: 3SW1). LOV-core region: grey; C-terminal extension (Jα): red; N-terminal extension (N-Cap): blue. **b)** PpSB1- and PpSB2-LOV domain architecture, coloring adapted from a), Jα of PpSB2-LOV: green. **c)** LOV domain architecture after interchange of Jα.

In contrast, in AsLOV2, the Jα-helix packs against the central β-scaffold of the LOV domain in the dark displaying a "helix-in" conformation in which hydrophobic residues on the β-scaffold are shielded from the solvent by the Jα-helix (*185*). Interestingly, the exchange of the C-terminal Jα-helix segments between PpSB1-LOV and PpSB2-LOV had a pronounced correlated effect on the recovery of the respective variants. The recovery of the cSB1/αSB2 variant, consisting of the PpSB1-LOV core and the PpSB2-Jα-helix, was accelerated by a factor of about 2. Likewise, the

recovery of cSB2/αSB1, consisting of the PpSB2-LOV core and the PpSB1-Jα-helix, was slowed down by a factor of about 3 with respect to the corresponding wild-type proteins (chapter 2.1).

The effect of interchanging the C-terminal Jα extensions on the dark recovery process, as well as the influence of the interchange of the sole Trp residue (W94) of both proteins on the spectral properties (Figure 3, chapter 2.1), is clear evidence for an interaction of the respective C-terminal extensions with residues that directly or indirectly interact with the FMN chromophore and/or the LOV-core domain. The latter result moreover indicates that the respective extensions are located close to W94 in both proteins. Figure 10 depicts the close-up view of the PpSB1-LOV light-state X-ray structure illustrating the observed interactions between W94, the Jα-helix and residues on the central β-scaffold, which directly interact with the FMN chromophore.

In particular the effect of the Jα-helix interchange on the emission properties of W94 might be explained by altered Jα-helix LOV-core interactions. The Jα-helix of PpSB2-LOV contains a threonine at the position corresponding to Ser120 of PpSB1-LOV. The exchange S120T as realized in the respective cSB1/αSB2 variant results in the introduction of an unpolar methyl-function (of the Thr side-chain) in close proximity to W94. This alters the chemical microenvironment around W94 and could account for the observed blue-shift of the Trp emission maximum (chapter 2.1, Fig. 3). Correspondingly, removal of this methyl-group by introducing a T120S mutation, as realized in the reverse cSB2/αSB1 variant, results in a concomitant red-shift of the emission maximum (chapter 2.1, Fig. 3). In contrast, from structural analyses it is not directly obvious, why the Jα-helix interchange between the two proteins mutually affects the dark recovery reaction. In order to influence adduct rupture, the respective Jα-region should be structurally coupled to the LOV-core and/or residues directly contacting the FMN chromophore. In PpSB1-LOV the only directly apparent contact between the Jα-helix and the LOV core exists between the S120 Oγ atom and the backbone amide of W94. Since no X-ray structure of PpSB2-LOV exists, it is unclear how the introduced threonine side-chain present in position 120 in the respective Jα-helix interchange variant, will be oriented. However, due to the similar structural and chemical properties of serine and threonine, it can be expected that structural effects would be rather limited in nature.

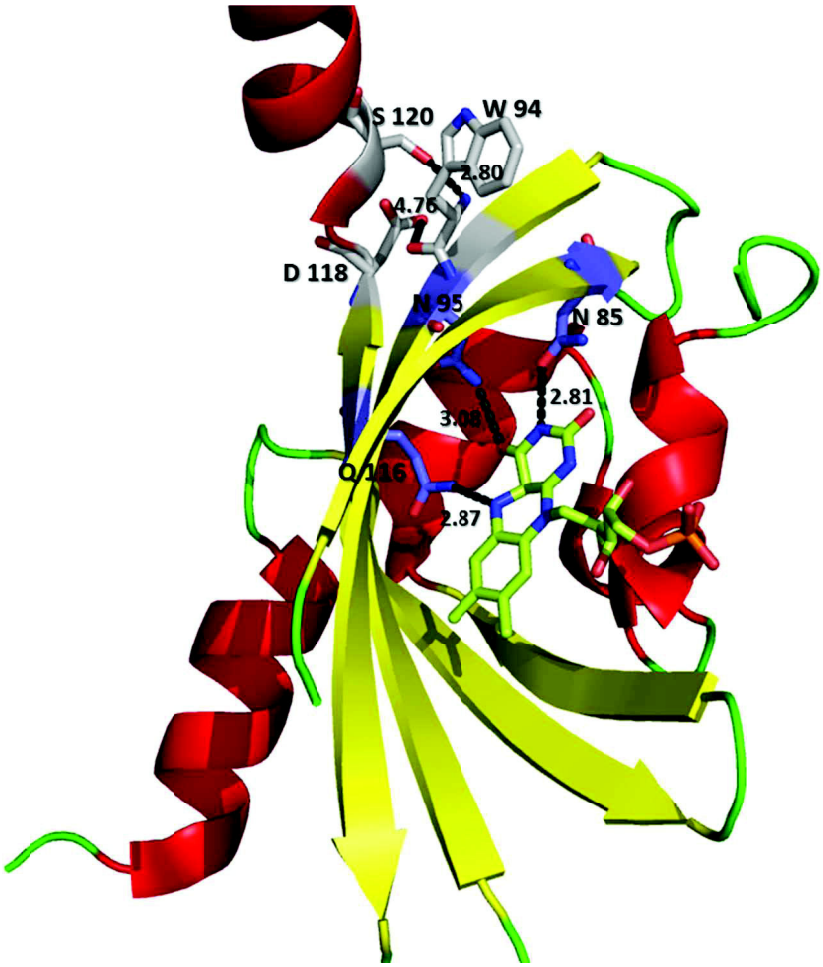

Fig.10: Cartoon representation of one subunit of the PpSB1-LOV light-state crystal structure (PDB ID: 3SW1) (β-sheets: yellow, loops: green, helices: red)(*183*). FMN in the chromophore binding pocket is shown in stick representation and is colored by element: carbon, yellow; nitrogen, blue; oxygen, red; phosphorus, orange. Residues within hydrogen bonding-distance to the FMN-chromophore are shown as sticks colored by element: carbon: steel-blue, nitrogen: dark blue, oxygen: red. (N85, N95, Q116). Hydrogen bonds are given as dashed lines with labels depicting the relevant interatomic distance in Angstrom. Additionally, residues located on the LOV-core (W94, D118) and at the C-terminal end of the PpSB1-LOV Jα-helix (S120) that could be responsible for Jα-based kinetic changes observed for the Jα-interchange mutants (cSB1/αSB2 and cSB2/αSB1) are shown in stick representation. Carbons are shown in grey, nitrogens in blue, oxygens in red.

Thus, another hypothesis has to be considered that can account for the observed influence of the Jα-helix interchange on the dark recovery reaction. Here, altered recovery kinetic reaction velocities might relate to an rearrangement of the Jα-helices in the light state compared to the dark state. Under this assumption the different dark recovery reaction kinetics seen for the Jα-helix interchange mutants could derive from altered Jα-interaction stabilities introduced by the interchange.

In conclusion, it appears that more than one amino acid is involved in tuning the dark recovery reaction kinetics in the two wild-type proteins. Thus, the observed differences in their full extent might be traced back to a cumulative effect of several amino acids and not just a single point mutation, nevertheless clear tendencies are observed that can account for the observed differences. Moreover, it is interesting to note, that the slow-reverting PpSB1-LOV protein can be effectively accelerated by just two mutations (R61H and R66I), while it appears much more difficult to effectively slow down the recovery of the fast reverting PpSB2-LOV protein to a level similar to PpSB1-LOV.

6.2 Conservation of dark recovery kinetic properties and structural features among the *Pseudomonadaceae* "short" LOV family

As already discussed in chapter 2.1, the presence of two highly similar LOV proteins, with very different dark recovery kinetic properties, in the same organism raises the question whether these differences bear any functional importance. If so, evolution should have retained slow and fast reverting "short" LOV proteins also in other related organisms. To address this issue, several *Pseudomonadaceae* "short" LOV proteins were studied in chapter 4.1. Hereby, it appears that "short" LOV proteins are solely present in Proteobacteria. Notably, in at least one other *P. putida* strain (*P. putida* W619) invariably two "short" LOV proteins are present. In contrast a set of *P. fluorescens* strains (PfO-1, Pf-5 and SBW25) possess only one "short" LOV protein.

Not surprisingly, the two *P. putida* W619 proteins display remarkably different kinetic properties. Hereby, their kinetic properties resemble the *P. putida* KT2440 twin LOV proteins. While one of the proteins (W619-1_LOV) reverts slow with a τ_{rec} of 54 min (at 37 °C) the other one (W619-2_LOV) shows a rapid dark reversion (τ_{rec} = 1 min (at 37 °C). At the same temperature PpSB1-LOV and PpSB2-LOV revert with a τ_{rec} of 127 and 0.3 minutes, respectively. The three *P. fluorescens* LOV-proteins show variably slow dark recovery velocities ranging from fairly fast for Pf-5-LOV (τ_{rec} = 4 min) over medium slow (PfO-1-LOV, τ_{rec} = 880 min) to extremely slow in case of the Pf-SBW25-LOV (τ_{rec} = 1260 min). Based on the presented data, it thus appears that indeed different dark recovery velocities have been conserved in different "short" LOV proteins of various *Pseudomonas* species, which hints at a functional importance of this LOV-protein property for the *in vivo* functional response.

Figure A1 in the appendix shows a multiple sequence alignment of several members of the the *Pseudomonadaceae* „short“ LOV protein family. Highlighted in red are the seven *Pseudomonas* proteins that were characterized in this study. Additionally, the two arginine residues (R61 and R66) which were identified in PpSB1-LOV as the key elements that facilitate slow recovery of the protein are highlighted in yellow.

Based on the above mentioned alignment a phylogenetic tree was reconstructed for several *Pseudomonadaceae* “short” LOV proteins (Figure 11). This tree supports the classification into PpSB1-LOV and PpSB2-LOV-like clades and thus highlights the possibility of retaining fast (PpSB2-LOV) and slow reverting (PpSB1-LOV) proteins in one organism at a time. Hereby, it is tempting to speculate that the slow reverting LOV proteins of *P. fluorescens* such as PfO-1-LOV and SBW25-LOV could represent the functional ancestors of the fast reverting “short” LOV proteins. In such a scenario, at first a slow and strictly thermally reverting photoreceptor protein, such as the ones of *P. fluorescens* and the slow reverting *P. putida* proteins, were present, which later, after gene duplication, freely evolved accompanied by an acceleration of the dark recovery reaction.

Though a total of seven examples of the structurally conserved “short” LOV protein family have now been characterized, their biological function(s) remain(s) elusive and leave room for speculation. Moreover, though fast and slow reverting “short” LOV proteins have apparently been conserved throughout evolution, the question remains why a single a non-phototrophic organism like *P. putida* needs a set of two highly similar LOV domains with such different kinetic properties? The situation is even more extreme for by *P. fluorescens* SBW25 which possess only a single “short“ LOV protein that however would need several days to revert back into the dark state after illumination at its ambient environmental living-temperature (i.e. 15 - 20 °C). Similarly slow reverting proteins are found in plants (*150*) and other bacterial species such as *Brucella* which appeared to even completely fail to revert back to the dark state after illumination (*151*). One possible explanation might relate to sensing light of different intensities. Hereby, a slow reverting system will inevitable by “pushed” into the light state even at very low intensities, while a fast reverting system needs higher or continuous illumination for sensing (*186*). Likewise, a slow reverting sensory system could adapt the celluar physiology to anticipated changes in environmental light-conditions (i.e. entrainment or light presence) while a faster reverting one would enable more modulated responses, i.e. also sensing the short term absence of light.

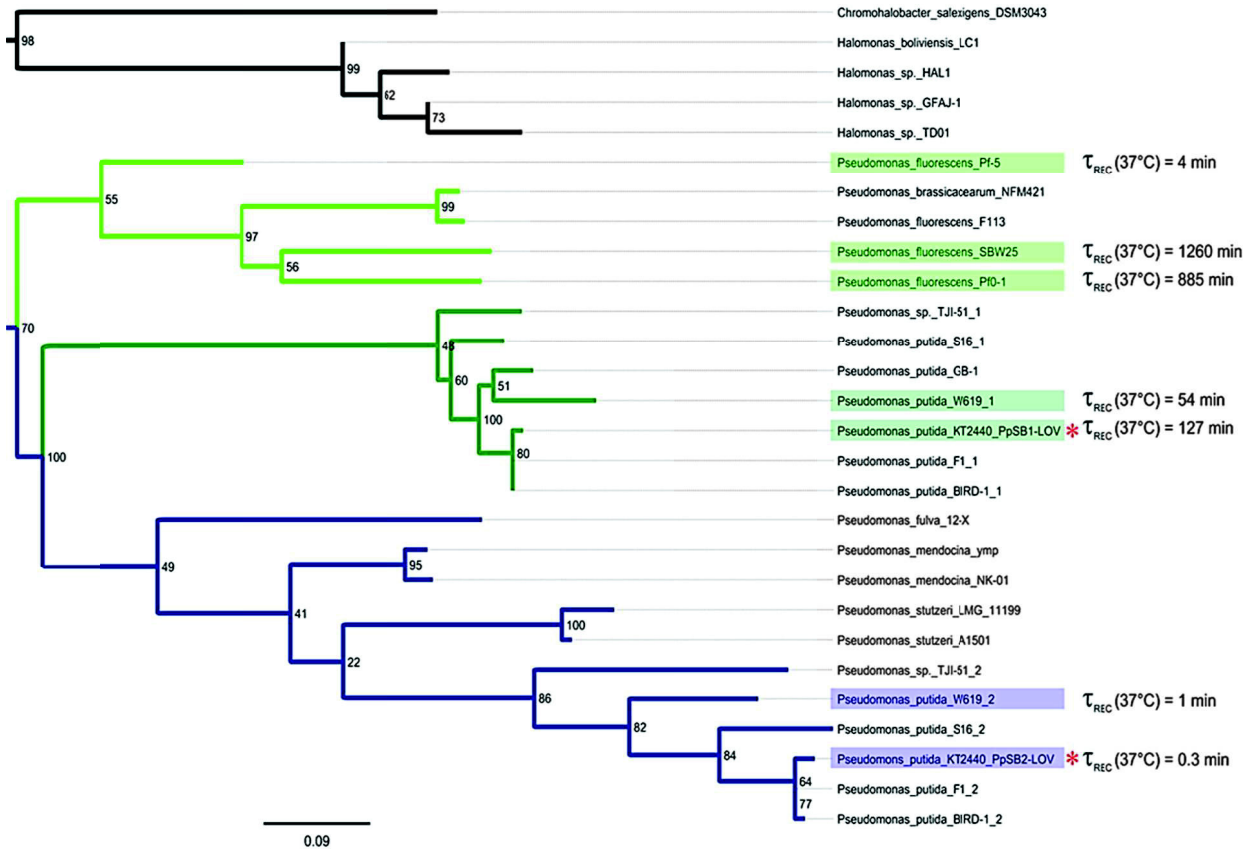

Fig. 11: Phylogenetic tree reconstructed for the "short" LOV protein family. At the right hand side of the tree, the respective dark recovery time constants measured at 37 °C are given. PpSB1-LOV and PpSB2-LOV sequences are marked by an asterisk. Accession numbers for the respective protein sequences used for tree reconstruction are summarized in the appendix (Table A.1)

6.2.1 Structural implications for the intra- and intermolecular signal-propagation mechanism

The lack of a fused effector domain in the PpSB1-LOV protein implies that the only way for signal transduction within the cell is by a light-induced alteration of protein-protein interactions between the photoreceptor and a yet unknown effector protein in *trans*.

The in chapter 4.1 presented CD spectroscopic data for the five *Pseudomonadaceae* "short" LOV proteins as well as CD and NMR data on the two Jα-peptides suggest a evolutionary conservation and thus conserved structural role of the two N- and C-terminal helical elements (N-cap and Jα-helix).

In most recent studies on other LOV photosensory systems, the importance of those N- and C-terminal auxiliary structural elements for the signal-transduction mechanisms was stressed (*127, 161, 162, 185*). In the following some of those examples will be reviewed and placed into the context of possible "short" LOV protein signalling mechanisms.

VVD, one of the few other known LOV photoreceptor proteins that lack a fused effector domain, is part of such a protein-protein-interaction-based signal-transduction cascade. Hereby, the LOV photoreceptor VVD interacts with the white-collar complex (WCC) in an antagonistic light-dependent fashion to allow the photoadaptation response of *N. crassa* (*187*). VVD is present as a symmetric dimer in the crystal in both, dark and the light states (*188*). In contrast, in solution dimer formation seems to be light dependent (*189*). Hereby, the monomer/dimer equillibrium appears to be affected by a structural rearrangement of the VVD N-cap (*189*). Obviously, the monomeric and dimeric forms of VVD will display different surface properties, which would enable/inhibit protein-protein interactions with the WCC in an antagonistic manner (*187*).

For bacterial LOV and PAS sensory systems such as YtvA-LOV (*165*) and FixL-PAS (*190*) it was suggested that signal perception (light absorption in case of YtvA and presence of oxygen in case of FixL) results in a rotation of the C-terminal Jα-helices transmitting a "torque"-like movement from the sensor to the spatially separated effector modules (STAS in case of YtvA and a histidine kinase in case of FixL). In turn, such a rotation would entail a change of the molecular surface of the whole protein (including the effector domain), thus enabling or locking downstream protein-protein communication, i.e. with the stressosome of *B. subtilis* (*117*). In this scenario, the N-terminal extension of the protein could either act as a pivotal point for the rotational movement or actively support the structural rearrangements as suggested for fungal VVD (*188*).

In analogy PpSB1-LOV signal-transduction might involve a light-induced change of the molecular surface of the protein, i.e. mediated by subunit and/or N-cap, Jα-helix rotation which would in turn enable/inhibit possible protein-protein-interaction-based signalling responses in the cell. The importance of the N-cap and Jα-helix is further corroborated by the data presented in chapter 4.1. Using truncated constructs, it was shown, that both elements are essential for the structural integrity of PpSB1-LOV and PpSB2-LOV. Hereby, the C-terminal Jα-helix seems to be more important, since its removal caused near complete loss of solubility. This is in contrast to multi-domain LOV photoreceptors, were both structural elements can be readily removed

without loss of protein solubility (*139, 165, 191*). Moreover,the Jα-helix coiled-coil like interaction pattern suggested to stabilize dimer association of both *P. putida* proteins (chapter 4.1, Figure 6), might hint at the Jα-helices as a kind of "missing" effector domain, whose quaternary structural rearrangement (i.e. rotation or dissolution) could be part of the light-induced structural signal. Such a rearrangement could well cause changes in the molecular surface properties of those proteins which in turn would enable/inhibit downstream signalling responses, as outlined above.

6.3 Initial studies on the physiological role of PpSB1-LOV in *P. putida* KT2440

In the following chapters microbial physiological and genetic studies carried out to assess the function of the two *P. putida* KT2440 "short" LOV proteins will be discussed and placed into the broader context of microbial photosensory biology.

6.3.1 General concepts and evolutionary paradigms related to niche adapation

In the three kingdoms of life, adaption of a certain species to specific lifestyles and environmental niches is of paramount importance. Based on a comparative genomic analysis of several *P. putida* genomes, Wu et al. (*192*) pointed out conclusively that horizontal gene transfer must have played an important role in the process of acquisition of certain functions and regulatory pathways in this organismal clade, as many of the niche-specific adaptions were found to be encoded on clearly defined genomic islands or on regions with lost synteny between closely related strains (*192*). They mentioned that some features might be acquired rather than being part of the respective core genome, and that the presence of various complete and many incomplete pathways as well as duplication of pathways on the genomes of different *P. putida* strains is striking. Furthermore it indicates, that these strains, before adapting to their current biotopes, have a lush history of colonizing various habitats each of which with specific requirements and means of adaption that were facilitated by the acquisition and re-shuffling of new pathways (*192*). Dedicated management of incoming systems to avoid functional redundancy for example, under stress when resources are scarce, optimization and economical comprehension between the various pathway genes supported by a large diversity of regulators are also crucial for adaption of the "right" functionalities (*192*). In light of those observations it

is not surprising that many chemotrophic bacteria carry genes encoding for various photoreceptor proteins among which LOV photoreceptors are one of the most abundant and diverse. Hereby, a given organism might have encountered various light conditions during its evolutionary history so that certain key photoreceptor functions might have been retained even though today's habitants vary significantly from the ancient primordial ones that shaped the respective genome.

6.3.1 Phenotypic effects of the PpSB1-LOV deletion

In chapter 5.1, 3.1 and 2.1 the two paralogous LOV photoreceptor proteins PpSB1-LOV and PpSB2-LOV from *P. putida* KT2440 have been extensively characterized regarding their biochemical, photochemical and structural properties. However, their physiological role remained elusive. Therefore attempts were undertaken to disrupt the PpSB1-LOV and PpSB2-LOV encoding genes in the genome of *P. putida* KT2440, by insertion of an antibiotic resistance cassette flanked by appropriate transcriptional termination sites into the respective open reading frame (chapter 5.1, Figure 1). The resulting "short" LOV photoreceptor deficient *P. putida* KT2440 strains could then be studied with respect to altered physiological properties. The PpSB1-LOV encoding gene could be readily disrupted resulting in a PpSB1-LOV deficient *P. putida* strain (ΔPpSB1-LOV). In contrast, we were not able to obtain a *P. putida* KT2440 PpSB2-LOV deficient strain, even though several hundreds of potential mutant strains were screened by colony PCR (chapter 5.1).

Extensive analysis of the genomic context (esp. neighboring genes) of the two "short" LOV encoding genes in *P. putida* KT2440 and other *Pseudomonadaceae* genomes revealed a clustering of genes annotated to be involved in the iron-limitation response (*178*). In particular, several iron-siderophore sensors and receptors (Q88E56, Q88E62) as well as a ferric iron receptor (Q88E55) are found in the wider genomic context of the PpSB1-LOV encoding gene in the genome of *P. putida* KT2440 (*178*), hinting at the involvement of the respective LOV protein encoding genes in the iron-starvation response. Hereby, a visually easy to study phenotypic trait associated with iron limitation of fluorescent Pseudomonads is the excretion of the fluorescent pigment pyoverdin (*172, 193*). Various representatives of fluorescent *Pseudomonas* species, such as the root colonizing *P. putida* (*194*), the pathogen *P. aeruginosa* (*195*), the plant pathogen *P.*

syringae pv. *syringae* (*196*) and the plant commensal *P. fluorescens* Pf5 (*197*) produce, under iron-limiting growth conditions, so-called pyoverdines, a structurally conserved group of siderophores. Siderophores are iron-chelating molecules that scavenge trace amounts of iron from the environment. The iron-loaded form of the pigment is subsequently taken up by the cell in order to replenish the intracellular iron-pool. Additional iron-limitation associated phenotypic effects are motility responses and biofilm formation (*198, 199*).

Therefore, in this study the effect of PpSB1-LOV gene disruption on several of those iron-limitation associated phenotypic traits was studied in chapter 5.1 (Figures 2-4). The most prominent and striking phenotype of the PpSB1-LOV deletion mutant was the complete loss of the ability of the strain to grow on a defined iron-deficient full medium (PG medium) (chapter 5.1, Figure 2a). In contrast, the strain grew well on an iron-deficient minimal M9 medium (chapter 5.1, Figure 2b).

Additionally, the PpSB1-LOV deficient mutant strain showed altered swimming motility on M9 agar and was affected in its ability to produce pyoverdine. Apparently, most of the observed ΔPpSB1-LOV phenotypes, such as growth deficiency on PG medium and reduced swimming motility of M9 agar were light independent. Interestingly, a significant light-dependent difference in excreted pyoverdine levels was observed. Hereby, the PpSB1-LOV deficient strain accumulated higher amounts of pyoverdine in the light compared to a dark grown strain. In a recent study Matilla et. al (*200*), provided direct physiologcial evidence for a link between pyoverdin production and swimming/swarming motility of *P. putida* KT2440. The data presented in this thesis supports this notion and moreover provides a direct link between the potential blue-light photoreceptor PpSB1-LOV and production/excretion of the iron-scavenger pyoverdin under iron-limiting conditions. Given those observations, the immediate question arises, regarding the physiological impact of blue light on *P. putida*, i.e. under iron-limiting growth conditions.

A potential biological mechanism that could account for the importance of blue-light sensing under iron limiting conditions might be found in the observation that blue light can excite iron-free porphyrin derivatives such as the heme precursor protoporphyrin IX (PPIX), with high yields to the corresponding triplet state. In the presence of molecular oxygen, this in turn can result in the generation of reaction oxygen species (ROS) and thus oxidative damage to cellular components (*201*). Thus, the ability to sense or “see” the presence of blue light, i.e. under growth

conditions were iron is scarce, might represent a valid stress response mechanism. Here, up-regulation of pyoverdin excretion or initiation of its production would alleviate the stress imposed on the cell by increasing the intracellularily available iron pool and in turn limiting the amount of available photosensitizers such as PPIX.

Moreover, several recent studies, i.e. for the *B. subtilis* LOV photoreceptor YtvA (*117-119*) and the "short" LOV protein *Rs*LOV from *R. sphaeroides* (*202, 203*) revealed the role of LOV photoreceptors in the general stress- and oxidative damage response. Typically, such physiological studies are being carried out in defined minimal media that more closely mimic the nutrient limited habitats of the respective bacteria or provoke stress responses, i.e. for YtvA a salt-deprived medium was used for β-Galactosidase essays (*118*) or in case of *R. sphaeroides* malate-minimal medium combined with microaerobic growth conditons was employed (*202*). Although, many times not considered explicitly, those media are often limiting with respect to iron and/or trace-element supply. As discussed above (6.3.1), limited iron supply and the presence of light (i.e. blue light) might represent a general stress factor, which eventually triggers transcriptional responses that allow the organism to adapt to those potentially harmful environmental conditions.

6.3.2 The conservation of "short" LOV protein encoding genome regions in several *Pseudomonas* strains hints at potential downstream signaling partners

Figure 12 depicts the respective "short" LOV protein encoding genome region. The analysis emphasizes the presence and conservation of genes encoding for helix-turn-helix (HTH) DNA-binding transcriptional regulators (TRs) in operon-like structures, organized together with the respective "short" LOV-protein coding genes.

In 2010, comparative genomic and functional analysis of nice-specific adaption in different *P. putida* strains was conducted, revealing, that within the complex regulatory networks of the oxidative stress response system (*204*), a LysR-type HTH-transcriptional regulator (called *PerR* in *B. subtilis* (*205*)) regulates the expression of the ferric uptake regulator Fur in *P. putida* W619. When iron is limited, the unloaded Fur protein is inactive as a repressor. This results in de-repressed transcription of genes involved in siderophore synthesis and consequently high-affinity iron uptake. When iron is plentiful, the ferrous-iron-bound Fur protein binds to its DNA targets

to repress transcription of the respective transport genes. This allows elevated production of iron-containing proteins and several iron storage proteins (*206*). Those studies stress the importance of HTH-TRs in controlling transcriptional responses linked to iron-limitation associated stress and highlight the possibility of similar possibly light-driven responses in *P. putida* KT2440.

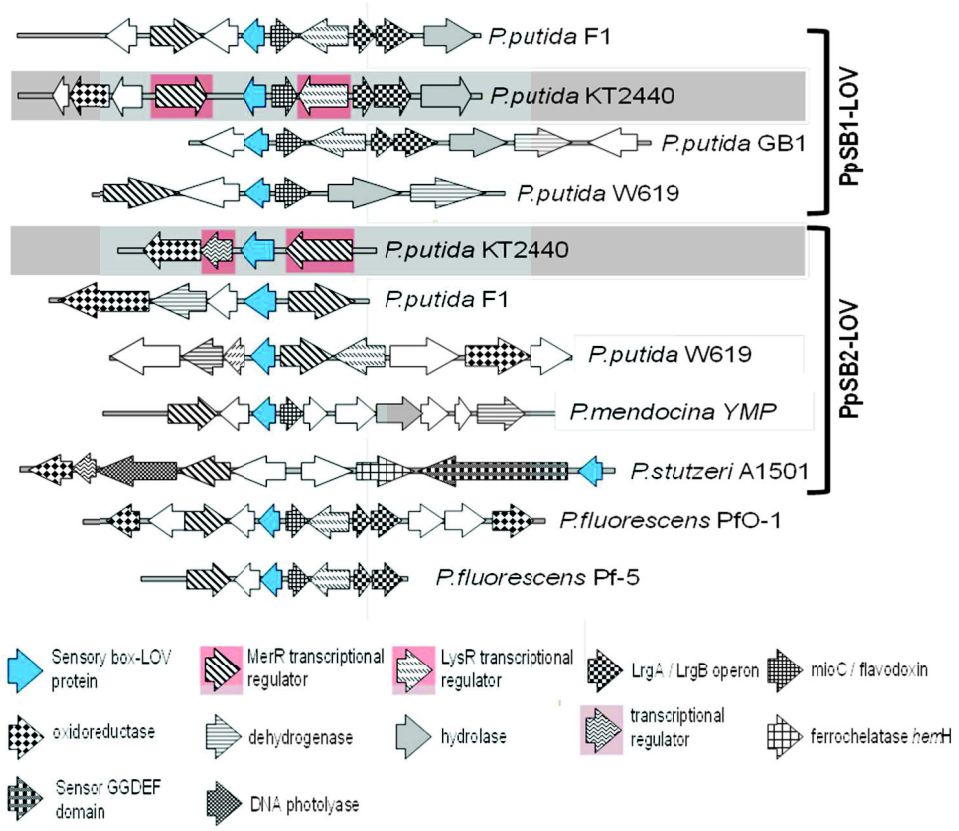

Fig. 12: Conserved operon-like structures and phylogenetic sub-classification for the different "short" LOV proteins found in several *Pseudomonas* species, highlighted in red are the helix-turn-helix (HTH) transcriptional regulators present in *P. putida* KT2440.

Given the conservation of several HTH-TRs in operon-like structures together with "short" LOV-proteins in several *Pseudomonas* strains, it is tempting to speculate, that one of the TRs might represent the down-stream target that interacts with the respective LOV-protein in a light dependent manner. This would allow for the light-dependent control of gene expression (i.e. of iron-limitation associated genes) in *P. putida*. As part of this study, a set of three HTH transcriptional regulators found in the PpSB1-LOV and PpSB2-LOV genome region in close proximity to the respective LOV sensor protein, were cloned and expressed in *E. coli*.

Unfortunately, all TRs accumulated as insoluble inclusion bodies, and thus could not be obtained in purified form for further studies (data not shown). Extensive optimization of expression and purification condition as well as the use of alternative purification tags (His-tag, Strep-tag and Maltose-binding-protein (MBP)-tag) did not yield TR soluble protein (data not shown). Future studies could focus on the *in vivo* detection of potential LOV-protein / HTH-TR interactions, e.g. by using yeast-two hybrid techniques (*207*).

Concluding remarks

The in this study presented biochemical, photochemical and structural data sheds new light onto the mechanisms that tune the dark state recovery of bacterial LOV sensor systems. In particular for the here studied *Pseudomonadaceae* "short" LOV protein family, key residues could be identified, that tune the dark recovery reaction over several orders of magnitude. Interestingly, adduct rupture (i.e. breaking of the covalent FMN-C4a cysteinyl-thioladduct) can apparently be influenced by residues found at the opposite end of the FMN chromophore, i.e. by altering the FMN-phosphate-protein interaction. Related studies for other slow reverting plant and bacterial LOV photoreceptors such as FKF1 (*182, 184*) and YtvA (*208*), suggest that anchoring of the FMN-phosphate to the protein plays an important role for adduct and thus signaling state stability. Thus, the here presented work, on the one hand provides new insights into the LOV photocycle mechanism and at the same time suggests design principles that allow the tuning of LOV signaling state stabilities over several orders of magnitude. The corresponding mutations might thus be of interest for the rapidly growing field of LOV-based optogenetics, where LOV domains are used as the sensory module in artificially constructed photoreceptor proteins, that allow the control of biological functions both *in vivo* and *in vitro* (*209-213*) and citations therein). Hereby, mutation of the respective LOV domain would result in variants possessing variable signaling state stabilities, which would result in sensory systems with variable sensitivities and response times.

Moreover, the presented physiological studies broaden our knowledge about the photobiology of chemotrophic microorganisms. Although, further experimental work is necessary to unequivocally address the function of the two *P. putida* KT2440 "short" LOV proteins, the here presented data nevertheless represents a starting point on which further experiments could be based. In the future, proteomic and transcriptomic analyses, using the wild-type and the PpSB1-LOV deletion mutant, could be conducted to clearly define the role of the PpSB1-LOV gene in

the iron-starvation regulatory response of *P. putida* KT2440. Moreover complementation studies would be needed to unequivocally prove the involvement of the PpSB1-LOV encoding gene, in the so far observed responses. Furthermore, such studies could pave the way for the understanding of inter- and intra- molecular LOV photoreceptor signal-transduction mechanisms as site-specific mutant PpSB1-LOV proteins could be used in complementation studies.

7. References

1. Jung, E. G. (2007) Sonne und Sonnenkult Eine kleine Kulturgeschichte der Haut, (Jung, E. G., Ed.), pp 108-112, Steinkopff.

2. Bible *The holy Bible. Authorized King James version*, Oxford University Press., [S.l.].

3. Bakalis, N. (2005) *Handbook of Greek Philosophy: From Thales to the Stoics Analysis and Fragments*.

4. Burnet, J. (1908) *Early Greek philosophy*.

5. Lucretius Carus, T., Melville, R., Fowler, D., and Fowler, P. (1997) On the nature of the Universe, Oxford University Press, New York.

6. Drake, S. (1953, revised in 1967) Galieo Galilei: *Dialogue concerning the two chief world systems, Ptolemaic & Copernican*. University of California Press

7. Romer, M., and Cohen, I. B. (1940) Roemer and the First Determination of the Velocity of Light (1676), *Isis 31*, 327-379.

8. Newton, I. (1671) *A letter of Mr. Isaac Newton ... containing his new theory about light and colors*. Philosophical Transactions of the Royal Society, No. 80 (19 Feb. 1671/2), pp. 3075-3087

9. Perkowitz, S. (1998) *Eine kurze Geschichte des Lichts: Die Erforschung eines Mysteriums*. Deutscher Taschenbuchverlag München 1998.

10. Maxwell, J. C. (2011, first published in 1873) *A treatise on electricity and magnetism*. Cambridge University Press, USA.

11. Planck, M. (1906) *The theory of heat radiation*. Published 1914 by P. Blakiston's Son & Co. in Philadelphia

12. Einstein, A. (1904) On the general molecular theory of heat, *Annalen der Physik 14*, 68.

13. Planck, M. (1927) Die physikalische Realität der Lichtquanten, *Naturwissenschaften 15*, 529-531.

14. Einstein, A. (1916) Die Grundlage der allgemeinen Relativitätstheorie, *Annalen der Physik 354*, 769-822.

15. Demmig-Adams, B., and Adams, W. W. (1992) Photoprotection and Other Responses of Plants to High Light Stress, *Annual Review of Plant Physiology and Plant Molecular Biology 43*, 599-626.

16. Pigllucci, M. (1996) How organisms respond to environmental changes: from phenotypes to molecules (and vice versa), *Trends in Ecology & Evolution 11*, 168-173.

17. Gomelsky, M., and Hoff, W. D. (2011) Light helps bacteria make important lifestyle decisions, *Trends in Microbiology 19*, 441-448.

18. Ruberti, I., Sessa, G., Ciolfi, A., Possenti, M., Carabelli, M., and Morelli, G. (2012) Plant adaptation to dynamically

changing environment: The shade avoidance response, *Biotechnology Advances 30*, 1047-1058.

19. Kirk, J. T. O. (1994) *Light and photosynthesis in aquatic ecosystems; The nature of the underwater light field*, 2 ed., Cambridge University Press, Canberra.

20. Hall, D. O., and Hall. (1978) Solar energy conversion through biology—could it be a practical energy source?, *Fuel 57*, 322.

21. Losi, A. (2004) The bacterial counterparts of plant phototropins, *Photochem Photobiol Sci 3*, 566-574.

22. Wu, Y. P., and Krogmann, D. W. (1997) The orange carotenoid protein of Synechocystis PCC 6803, *Biochimica et Biophysica Acta (BBA) - Bioenergetics 1322*, 1-7.

23. Ryter, S. W., Kim, H. P., Hoetzel, A., Park, J. W., Nakahira, K., Wang, X., and Choi, A. M. K. (2007) Mechanisms of Cell Death in Oxidative Stress, *Antioxidants & Redox Signaling 9*, 49-89.

24. Pattison, D. I., and Davies, M. J. (2006) Actions of ultraviolet light on cellular structures, *EXS.* 2006;96:131–157.

25. Christie, J. M., Arvai, A. S., Baxter, K. J., Heilmann, M., Pratt, A. J., O'Hara, A., Kelly, S. M., Hothorn, M., Smith, B. O., Hitomi, K., Jenkins, G. I., and Getzoff, E. D. (2012) Plant UVR8 Photoreceptor Senses UV-B by Tryptophan-Mediated Disruption of Cross-Dimer Salt Bridges, *Science 335*, 1492-1496.

26. Di, W., Hu, Q., Yan, Z., Chen, W., Yan, C., Huang, X., Zhang, J., Yang, P., Deng, H., Wang, J., Deng, X., and Shi, Y. (2012) Structural basis of ultraviolet-B perception by UVR8, *Nature 484*, 214-219.

27. Quail, P. H. (1998) The phytochrome family: dissection of functional roles and signalling pathways among family members, *Philosophical Transactions of the Royal Society of London. Series B: Biological Sciences 353*, 1399-1403.

28. Kort, R., Hoff, W. D., Van West, M., Kroon, A. R., Hoffer, S. M., Vlieg, K. H., Crielaand, W., Van Beeumen, J. J., and Hellingwerf, K. J. (1996) The xanthopsins: a new family of eubacterial blue-light photoreceptors, *The EMBO Journal 15*, 3209-3218.

29. Spudich, J. L., Yang, C.-S., Jung, K.-H., and Spudich, E. N. (2000) Retinylidene Proteins: Structures and Functions from Archaea to Humans, *Annual Review of Cell and Developmental Biology 16*, 365-392.

30. Berera, R., van Stokkum, I. H. M., Gwizdala, M., Wilson, A., Kirilovsky, D., and van Grondelle, R. (2012) The Photophysics of the Orange Carotenoid Protein, a Light-Powered Molecular Switch, *The Journal of Physical Chemistry B 116*, 2568-2574.

31. Ahmad, M., and Cashmore, A. R. (1993) HY4 gene of A. thaliana encodes a protein with characteristics of a blue-light photoreceptor, *366*, 162-166.

32. Gomelsky, M., and Klug, G. (2002) BLUF: a novel FAD-binding domain involved in sensory transduction in microorganisms, *Trends Biochem Sci 27*, 497-500.

33. Jung, A., Domratcheva, T., Tarutina, M., Wu, Q., Ko, W.-h., Shoeman, R. L., Gomelsky, M., Gardner, K. H., and Schlichting, I. (2005) Structure of a bacterial BLUF photoreceptor: Insights into blue light-mediated signal transduction, *Proceedings of the National Academy of Sciences of the*

United States of America 102, 12350-12355.

34. Christie, J. M., Salomon, M., Nozue, K., Wada, M., and Briggs, W. R. (1999) LOV (light, oxygen, or voltage) domains of the blue-light photoreceptor phototropin (nph1): Binding sites for the chromophore flavin mononucleotide *Proceedings of the National Academy of Sciences of the United States of America 96* 8779-8783

35. Borthwick, H. A., Hendricks, S. B., Parker, M. W., Toole, E. H., and Toole, V. K. (1952) A Reversible Photoreaction Controlling Seed Germination, *Proceedings of the National Academy of Sciences of the United States of America 38*, 662-666.

36. Butler, W. L., Norris, K. H., Siegelman, H. W., and Hendricks, S. B. (1959) Detection, Assay and Preliminary Purifcation of the Pigment Controlling Photoresponsive Development of Plants, *Proceedings of the National Academy of Sciencesof the United States of America 45*, 1703-1708.

37. Fankhauser, C., Yeh, K.-C., Clark , J., Lagarias, Zhang, H., Elich, T. D., and Chory, J. (1999) PKS1, a Substrate Phosphorylated by Phytochrome That Modulates Light Signaling in Arabidopsis *Science 284* 1539-1541.

38. Briggs, W. R., Beck, C. F., Cashmore, A. R., Christie, J. M., Hughes, J., Jarillo, J. A., Kagawa, T., Kanegae, H., Liscum, E., Nagatani, A., Okada, K., Salomon, M., Rudiger, W., Sakai, T., Takano, M., Wada, M., and Watson, J. C. (2001) The Phototropin Family of Photoreceptors, *Plant Cell 13*, 993-997.

39. Christie, J. M., Reymond, P., Powell, G. K., Bernasconi, P., Raibekas, A. A., Liscum, E., and Briggs, W. R. (1998) Arabidopsis NPH1: a flavoprotein with the properties of a photoreceptor for phototropism, *Science 282*, 1698-1701.

40. Hughes, J., Lamparter, T., Mittmann, F., Hartmann, E., Gärtner, W., Wilde, A., and Borner, T. (1997) A prokaryotic phytochrome, *386*, 663.

41. Mathews, S. (2006) Phytochrome-mediated development in land plants: red light sensing evolves to meet the challenges of changing light environments, *Molecular Ecology 15*, 3483-3503.

42. Losi, A., and Gärtner, W. (2008) Bacterial bilin- and flavin-binding photoreceptors, *Photochemical & Photobiological Sciences 7*, 1168-1178.

43. Lamparter, T., Mittmann, F., Gärtner, W., Börner, T., Hartmann, E., and Hughes, J. (1997) Characterization of recombinant phytochrome from the cyanobacterium Synechocystis, *Proceedings of the National Academy of Sciences 94*, 11792-11797.

44. Goodner, B., Hinkle, G., Gattung, S., Miller, N., Blanchard, M., Qurollo, B., Goldman, B. S., Cao, Y., Askenazi, M., Halling, C., Mullin, L., Houmiel, K., Gordon, J., Vaudin, M., Iartchouk, O., Epp, A., Liu, F., Wollam, C., Allinger, M., Doughty, D., Scott, C., Lappas, C., Markelz, B., Flanagan, C., Crowell, C., Gurson, J., Lomo, C., Sear, C., Strub, G., Cielo, C., and Slater, S. (2001) Genome Sequence of the Plant Pathogen and Biotechnology Agent Agrobacterium tumefaciens C58, *Science 294*, 2323-2328.

45. Davis, S. J., Vener, A. V., and Vierstra, R. D. (1999) Bacteriophytochromes: Phytochrome-Like Photoreceptors from Nonphotosynthetic Eubacteria, *Science 286*, 2517-2520.

46. Pattanaik, B., Whitaker, M. J., and Montgomery, B. L. (2012) Light quantity affects the regulation of cell shape in Fremyella diplosiphon, *Frontiers in Microbiology 3*.

47. Gärtner, W. (2012) Kurt Schaffner: from organic photochemistry to photobiology, *Photochemical & Photobiological Sciences 11*, 872-880.

48. Raymond, J. C., and Sistrom, W. R. (1967) The isolation and preliminary characterization of a halophilic photosynthetic bacterium, *Archives of Microbiology 59*, 255-268.

49. Raymond, J. C., and Sistrom, W. R. (1969) *Ectothiorhodospira halophila*: A new species of the genus *Ectothiorhodospira*, *Archives of Microbiology 69*, 121-126.

50. Meyer, T. E. (1985) Isolation and characterization of soluble cytochromes, ferredoxins and other chromophoric proteins from the halophilic phototrophic bacterium Ectothiorhodospira halophila, *Biochimica et Biophysica Acta (BBA) - Bioenergetics 806*, 175-183.

51. McRee, D. E., Meyer, T. E., Cusanovich, M. A., Parge, H. E., and Getzoff, E. D. (1986) Crystallographic characterization of a photoactive yellow protein with photochemistry similar to sensory rhodopsin, *Journal of Biological Chemistry 261*, 13850-13851.

52. Kyndt, J. A., Meyer, T. E., and Cusanovich, M. A. (2004) Photoactive yellow protein, bacteriophytochrome, and sensory rhodopsin in purple phototrophic bacteria, *Photochemical & Photobiological Sciences 3*, 519-530.

53. Sprenger, W. W., Hoff, W. D., Armitage, J. P., and Hellingwerf, K. J. (1993) The eubacterium Ectothiorhodospira halophila is negatively phototactic, with a wavelength dependence that fits the absorption spectrum of the photoactive yellow protein, *Journal of Bacteriology 175*, 3096-3104.

54. Oesterhelt, D. (1998) The structure and mechanism of the family of retinal proteins from halophilic archaea, *Curr Opin Struct Biol 8*, 489-500.

55. Schegk, E. S., and Oesterhelt, D. (1988) Isolation of a prokaryotic photoreceptor: sensory rhodopsin from halobacteria. EMBO J.; 7(9): 2925–2933

56. Stoeckenius, W. (1985) The rhodopsin-like pigments of halobacteria: light-energy and signal transducers in an archaebacterium, *Trends in Biochemical Sciences 10*, 483-486.

57. Spudich, J. L., and Jung, K.-H. (2005) Microbial Rhodopsins: Phylogenetic and Functional Diversity, In *Handbook of Photosensory Receptors*, pp 1-23, Wiley-VCH Verlag GmbH & Co. KGaA.

58. Béjà, O., Aravind, L., Koonin, E. V., Suzuki, M. T., Hadd, A., Nguyen, L. P., Jovanovich, S. B., Gates, C. M., Feldman, R. A., Spudich, J. L., Spudich, E. N., and DeLong, E. F. (2000) Bacterial Rhodopsin: Evidence for a New Type of Phototrophy in the Sea, *Science 289*, 1902-1906.

59. Jung, K.-H., Trivedi, V. D., and Spudich, J. L. (2003) Demonstration of a sensory rhodopsin in eubacteria, *Molecular Microbiology 47*, 1513-1522.

60. Bieszke, J. A., Braun, E. L., Bean, L. E., Kang, S., Natvig, D. O., and Borkovich, K. A. (1999) The nop-1 gene of Neurospora crassa encodes a seven transmembrane helix retinal-binding protein homologous to archaeal rhodopsins, *Proceedings of the National Academy of*

Sciences of the United States of America 96, 8034-8039.

61. Sineshchekov, O. A., Jung, K.-H., and Spudich, J. L. (2002) Two rhodopsins mediate phototaxis to low- and high-intensity light in Chlamydomonasreinhardtii *Proceedings of the National Academy of Sciences of the United States of America 99* 8689-8694.

62. Stoeckenius, W. (1999) Bacterial rhodopsins: Evolution of a mechanistic model for the ion pumps, *Protein Science 8*, 447-459.

63. Bogomolni, R. A., and Spudich, J. L. (1982) Identification of a third rhodopsin-like pigment in phototactic Halobacterium halobium, *Proceedings of the National Academy of Sciences 79*, 6250-6254.

64. Spudich, J. L., and Bogomolni, R. A. (1984) Mechanism of colour discrimination by a bacterial sensory rhodopsin, *Nature 312*, 509-513.

65. Wilson, A., Punginelli, C., Gall, A., Bonetti, C., Alexandre, M., Routaboul, J.-M., Kerfeld, C. A., van Grondelle, R., Robert, B., Kennis, J. T. M., and Kirilovsky, D. (2008) A photoactive carotenoid protein acting as light intensity sensor, *Proceedings of the National Academy of Sciences 105*, 12075-12080.

66. Horton, P., Ruban, A. V., and Walters, R. G. (1996) Regulation of Light Harvesting in Green Plants, *Annual Review of Plant Physiology and Plant Molecular Biology 47*, 655-684.

67. Rizzini, L., Favory, J.-J., Cloix, C., Faggionato, D., O'Hara, A., Kaiserli, E., Baumeister, R., Schäfer, E., Nagy, F., Jenkins, G. I., and Ulm, R. (2011) Perception of UV-B by the Arabidopsis UVR8 Protein, *Science 332*, 103-106.

68. Kliebenstein, D. J., Lim, J. E., Landry, L. G., and Last, R. L. (2002) Arabidopsis UVR8 Regulates Ultraviolet-B Signal Transduction and Tolerance and Contains Sequence Similarity to Human Regulator of Chromatin Condensation 1, *Plant Physiology 130*, 234-243.

69. Cloix, C., and Jenkins, G. I. (2008) Interaction of the Arabidopsis UV-B-Specific Signaling Component UVR8 with Chromatin, *Molecular Plant 1*, 118-128.

70. Huala, E., Oeller, P. W., Liscum, E., Han, I.-S., Larsen, E., and Briggs, W. R. (1997) Arabidopsis NPH1: A Protein Kinase with a Putative Redox-Sensing Domain *Science 278* 2120-2123.

71. Suetsugu, N., Mittmann, F., Wagner, G., Hughes, J., and Wada, M. (2005) A chimeric photoreceptor gene, NEOCHROME, has arisen twice during plant evolution, *Proceedings of the National Academy of Sciences of the United States of America 102*, 13705-13709.

72. Takahashi, F., Yamagata, D., Ishikawa, M., Fukamatsu, Y., Ogura, Y., Kasahara, M., Kiyosue, T., Kikuyama, M., Wada, M., and Kataoka, H. (2007) AUREOCHROME, a photoreceptor required for photomorphogenesis in stramenopiles *Proceedings of the National Academy of Sciences 104* 19625-19630.

73. Losi, A. (2007) Flavin-based Blue-light Photosensors: A Photobiophysics Update, *Photochemistry and Photobiology 83*, 1283-1300.

74. Cheng, P., He, Q., Yang, Y., Wang, L., and Liu, Y. (2003) Functional conservation of light, oxygen, or voltage

domains in light sensing, *Proceedings of the National Academy of Sciences 100*, 5938-5943.

75. He, Q., Cheng, P., Yang, Y., Wang, L., Gardner, K. H., and Liu, Y. (2002) White Collar-1, a DNA Binding Transcription Factor and a Light Sensor, *Science 297*, 840-843.

76. Briggs, W. R., and Christie, J. M. (2002) Phototropins 1 and 2: versatile plant blue-light receptors, *Trends in Plant Science 7*, 204-210.

77. Briggs, W. R., and Huala, E. (1999) Blue-Light Photoreceptors in Higher Plants, *Annual Review of Cell and Developmental Biology 15*, 33-62.

78. Lin, C. (2002) Blue Light Receptors and Signal Transduction, *Plant Cell 14*, S207-225.

79. Lin, C., and Shalitin, D. (2003) Cryptochrome structure and signal transduction, *Annu Rev Plant Biol 54*, 469-496.

80. Liscum, E., Hodgson, D. W., and Campbell, T. J. (2003) Blue Light Signaling through the Cryptochromes and Phototropins. So That's What the Blues Is All About, *Plant Physiology 133*, 1429-1436.

81. Wada, M., Kagawa, T., and Sato, Y. (2003) Chloroplast Movement, *Annual Review of Plant Biology 54*, 455-468.

82. Lin, C., and Todo, T. (2005) The cryptochromes, *Genome Biology 6*, 220.

83. Cashmore, A. R. (2003) Cryptochromes: Enabling Plants and Animals to Determine Circadian Time, *Cell 114*, 537-543.

84. Sancar, A. (2003) Structure and Function of DNA Photolyase and Cryptochrome Blue-Light Photoreceptors, *Chemical Reviews 103*, 2203-2238.

85. van der Horst, M. A., and Hellingwerf, K. J. (2003) Photoreceptor Proteins, "Star Actors of Modern Times": A Review of the Functional Dynamics in the Structure of Representative Members of Six Different Photoreceptor Families, *Accounts of Chemical Research 37*, 13-20.

86. Hitomi, K., Okamoto, K., Daiyasu, H., Miyashita, H., Iwai, S., Toh, H., Ishiura, M., and Todo, T. (2000) Bacterial cryptochrome and photolyase: characterization of two photolyase-like genes of Synechocystis sp. PCC6803 *Nucleic Acids Research 28* 2353-2362.

87. Worthington, E. N., Kavakli, I. H., Berrocal-Tito, G., Bondo, B. E., and Sancar, A. (2003) Purification and characterization of three members of the photolyase/cryptochrome family blue-light photoreceptors from Vibrio cholerae, *J Biol Chem 278*, 39143-39154.

88. Brudler, R., Hitomi, K., Daiyasu, H., Toh, H., Kucho, K.-i., Ishiura, M., Kanehisa, M., Roberts, V. A., Todo, T., Tainer, J. A., and Getzoff, E. D. (2003) Identification of a New Cryptochrome Class: Structure, Function, and Evolution, *Molecular Cell 11*, 59-67.

89. Selby, C. P., and Sancar, A. (2006) A cryptochrome/photolyase class of enzymes with single-stranded DNA-specific photolyase activity *Proceedings of the National Academy of Sciences 103* 17696-17700.

90. Masuda, S., and Bauer, C. E. (2002) AppA is a blue light photoreceptor that antirepresses photosynthesis gene expression in Rhodobacter sphaeroides, *Cell 110*, 613-623.

91. Iseki, M., Matsunaga, S., Murakami, A., Ohno, K., Shiga, K., Yoshida, K., Sugai, M., Takahashi, T., Hori, T., and Watanabe, M. (2002) A blue-light-activated adenylyl cyclase mediates photoavoidance in *Euglena gracilis*, *Nature 415*, 1047-1051.

92. Anderson, S., Dragnea, V., Masuda, S., Ybe, J., Moffat, K., and Bauer, C. (2005) Structure of a Novel Photoreceptor, the BLUF Domain of AppA from Rhodobacter sphaeroides , *Biochemistry 44*, 7998-8005.

93. Grinstead, J. S., Hsu, S.-T. D., Laan, W., Bonvin, A. M. J. J., Hellingwerf, K. J., Boelens, R., and Kaptein, R. (2006) The Solution Structure of the AppA BLUF Domain: Insight into the Mechanism of Light-Induced Signaling, *Chembiochem 7*, 187-193.

94. Yuan, H., Anderson, S., Masuda, S., Dragnea, V., Moffat, K., and Bauer, C. (2006) Crystal Structures of the Synechocystis Photoreceptor Slr1694 Reveal Distinct Structural States Related to Signaling, *Biochemistry 45*, 12687-12694.

95. Kita, A., Okajima, K., Morimoto, Y., Ikeuchi, M., and Miki, K. (2005) Structure of a Cyanobacterial BLUF Protein, Tll0078, Containing a Novel FAD-binding Blue Light Sensor Domain, *Journal of Molecular Biology 349*, 1-9.

96. Jung, A., Reinstein, J., Domratcheva, T., Shoeman, R. L., and Schlichting, I. (2006) Crystal Structures of the AppA BLUF Domain Photoreceptor Provide Insights into Blue Light-mediated Signal Transduction, *Journal of Molecular Biology 362*, 717-732.

97. Kennis, J. T. M., Crosson, S., Gauden, M., van Stokkum, I. H. M., Moffat, K., and van Grondelle, R. (2003) Primary Reactions of the LOV2 Domain of Phototropin, a Plant Blue-Light Photoreceptor, *Biochemistry 42*, 3385-3392.

98. Crosson, S., and Moffat, K. (2001) Structure of a flavin-binding plant photoreceptor domain: Insights into light-mediated signal transduction, *Proceedings of the National Academy of Sciences 98*, 2995-3000.

99. Zeiger, E., and Zhu, J. (1998) Role of zeaxanthin in blue light photoreception and the modulation of light-CO2 interactions in guard cells, *Journal of Experimental Botany 49*, 433-442.

100. Guo, H., Duong, H., Ma, N., and Lin, C. (1999) The Arabidopsis blue light receptor cryptochrome 2 is a nuclear protein regulated by a blue light-dependent post-transcriptional mechanism, *The Plant Journal 19*, 279-287.

101. Smith, H. (1995) Physiological and Ecological Function within the Phytochrome Family, *Annual Review of Plant Physiology and Plant Molecular Biology 46*, 289-315.

102. Fankhauser, C., and Chory, J. (1997) Light Control of Plant Development, *Annual Review of Cell and Developmental Biology 13*, 203-229.

103. Christie, J. M. (2007) Phototropin Blue-Light Receptors, *Annual Review of Plant Biology 58*, 21-45.

104. Tsuboi, H., Suetsugu, N., Kawai-Toyooka, H., and Wada, M. (2007) Phototropins and Neochrome1 Mediate Nuclear Movement in the Fern Adiantum capillus-veneris, *Plant and Cell Physiology 48*, 892-896.

105. Takahashi, F., Yamagata, D., Ishikawa, M., Fukamatsu, Y., Ogura, Y., Kasahara, M., Kiyosue, T., Kikuyama, M., Wada, M., and Kataoka, H. (2007)

AUREOCHROME, a photoreceptor required for photomorphogenesis in stramenopiles, *Proceedings of the National Academy of Sciences 104*, 19625-19630.

106. Toyooka, T., Hisatomi, O., Takahashi, F., Kataoka, H., and Terazima, M. (2011) Photoreactions of Aureochrome-1, *Biophysical Journal 100*, 2801-2809.

107. Banerjee, R., and Batschauer, A. (2005) Plant blue-light receptors, *Planta 220*, 498-502.

108. Mizoguchi, T. (2000) ZEITLUPE and FKF1: novel connections between flowering time and circadian clock control, *Trends in Plant Science 5*, 409.

109. Somers, D. E., Schultz, T. F., Milnamow, M., and Kay, S. A. (2000) ZEITLUPE Encodes a Novel Clock-Associated PAS Protein from Arabidopsis, *Cell 101*, 319-329.

110. Baudry, A., Ito, S., Song, Y. H., Strait, A. A., Kiba, T., Lu, S., Henriques, R., Pruneda-Paz, J. L., Chua, N.-H., Tobin, E. M., Kay, S. A., and Imaizumi, T. (2010) F-Box Proteins FKF1 and LKP2 Act in Concert with ZEITLUPE to Control Arabidopsis Clock Progression, *The Plant Cell Online 22*, 606-622.

111. Ballario, P., Vittorioso, P., Magrelli, A., Talora, C., Cabibbo, A., and Macino, G. (1996) White collar-1, a central regulator of blue light responses in Neurospora, is a zinc finger protein, *Embo J 15*, 1650-1657.

112. Schwerdtfeger, C., and Linden, H. (2003) VIVID is a flavoprotein and serves as a fungal blue light photoreceptor for photoadaptation, *Embo J 22*, 4846-4855.

113. Crosson, S., Rajagopal, S., and Moffat, K. (2002) The LOV Domain Family: Photoresponsive Signaling Modules Coupled to Diverse Output Domains *Biochemistry 42*, 2-10.

114. Gärtner, W., and Losi, A. (2003) Crossing the borders: archaeal rhodopsins go bacterial, *Trends in Microbiology 11*, 405-407.

115. Krauss, U., Minh, B. Q., Losi, A., Gärtner, W., Eggert, T., von Haeseler, A., and Jaeger, K.-E. (2009) Distribution and Phylogeny of Light-Oxygen-Voltage-Blue-Light-Signaling Proteins in the Three Kingdoms of Life, *Journal of Bacteriology 191*, 7234-7242.

116. Herrou, J., and Crosson, S. (2011) Function, structure and mechanism of bacterial photosensory LOV proteins, *Nat Rev Micro 9*, 713-723.

117. Ávila-Pérez, M., Hellingwerf, K. J., and Kort, R. (2006) Blue Light Activates the σB-Dependent Stress Response of Bacillus subtilis via YtvA, *Journal of Bacteriology 188*, 6411-6414.

118. Gaidenko, T. A., Kim, T.-J., Weigel, A. L., Brody, M. S., and Price, C. W. (2006) The Blue-Light Receptor YtvA Acts in the Environmental Stress Signaling Pathway of Bacillus subtilis, *J. Bacteriol. 188*, 6387-6395.

119. Suzuki, N., Takaya, N., Hoshino, T., and Nakamura, A. (2007) Enhancement of a sigmaB-dependent stress response in Bacillus subtilis by light via YtvA photoreceptor, *J Gen Appl Microbiol 53*, 81 - 88.

120. Ondrusch, N., and Kreft, J. (2011) Blue and Red Light Modulates SigB-Dependent Gene Transcription, Swimming Motility and Invasiveness in *Listeria monocytogenes*, *PLoS ONE 6*, e16151.

121. Swartz, T. E., Tseng, T. S., Frederickson, M. A., Paris, G., Comerci, D. J., Rajashekara, G., Kim, J. G., Mudgett, M. B., Splitter, G. A., Ugalde, R. A., Goldbaum, F. A., Briggs, W. R., and Bogomolni, R. A. (2007) Blue-light-activated histidine kinases: two-component sensors in bacteria, *Science 317*, 1090-1093.

122. Purcell, E. B., Siegal-Gaskins, D., Rawling, D. C., Fiebig, A., and Crosson, S. (2007) A photosensory two-component system regulates bacterial cell attachment, *Proceedings of the National Academy of Sciences of the United States of America 104*, 18241-18246.

123. Cao, Z., Livoti, E., Losi, A., and Gärtner, W. (2010) A Blue Light-inducible Phosphodiesterase Activity in the Cyanobacterium Synechococcus elongatus, *Photochemistry and Photobiology 86*, 606-611.

124. Parkinson, J. S. (1993) Signal transduction schemes of bacteria, *Cell 73*, 857-871.

125. Cao, Z., Buttani, V., Losi, A., and Gärtner, W. (2008) A Blue Light Inducible Two-Component Signal Transduction System in the Plant Pathogen Pseudomonas syringae pv. tomato, *Biophysical Journal 94*, 897-905.

126. Crosson, S., and Moffat, K. (2002) Photoexcited Structure of a Plant Photoreceptor Domain Reveals a Light-Driven Molecular Switch, *Plant Cell 14*, 1067-1075.

127. Rinaldi, J., Gallo, M., Klinke, S., Paris, G., Bonomi, H. R., Bogomolni, R. A., Cicero, D. O., and Goldbaum, F. A. (2012) The β-Scaffold of the LOV Domain of the Brucella Light-Activated Histidine Kinase Is a Key Element for Signal Transduction, *Journal of Molecular Biology 420*, 112-127.

128. West, A. H., and Stock, A. M. (2001) Histidine kinases and response regulator proteins in two-component signaling systems, *Trends in biochemical sciences 26*, 369-376.

129. Foreman, R., Fiebig, A., and Crosson, S. (2012) The LovK-LovR Two-Component System Is a Regulator of the General Stress Pathway in *Caulobacter crescentus*, *Journal of Bacteriology 194*, 3038-3049.

130. Chan, C., Paul, R., Samoray, D., Amiot, N. C., Giese, B., Jenal, U., and Schirmer, T. (2004) Structural basis of activity and allosteric control of diguanylate cyclase, *Proceedings of the National Academy of Sciences of the United States of America 101*, 17084-17089.

131. Galperin, M. Y., Nikolskaya, A. N., and Koonin, E. V. (2001) Novel domains of the prokaryotic two-component signal transduction systems, *FEMS Microbiology Letters 203*, 11-21.

132. Römling, U., Gomelsky, M., and Galperin, M. Y. (2005) C-di-GMP: the dawning of a novel bacterial signalling system, *Molecular Microbiology 57*, 629-639.

133. Quin, Maureen B., Berrisford, John M., Newman, Joseph A., Baslé, A., Lewis, Richard J., and Marles-Wright, J. (2012) The Bacterial Stressosome: A Modular System that Has Been Adapted to Control Secondary Messenger Signaling, *Structure 20*, 350-363.

134. Aravind, L., Anantharaman, V., Balaji, S., Babu, M. M., and Iyer, L. M. (2005) The many faces of the helix-turn-helix domain: Transcription regulation and beyond, *FEMS Microbiology Reviews 29*, 231-262.

135. (2012) Correction for Nash et al., Structural basis of photosensitivity in a bacterial light-oxygen-voltage/helix-turn-helix (LOV-HTH) DNA-binding protein, *Proceedings of the National Academy of Sciences 109*, 5904.

136. Nash, A. I., McNulty, R., Shillito, M. E., Swartz, T. E., Bogomolni, R. A., Luecke, H., and Gardner, K. H. (2011) Structural basis of photosensitivity in a bacterial light-oxygen-voltage/helix-turn-helix (LOV-HTH) DNA-binding protein, *Proceedings of the National Academy of Sciences 108*, 9449-9454.

137. Aravind, L., and Ponting, C. P. (1997) The GAF domain: an evolutionary link between diverse phototransducing proteins, *Trends in Biochemical Sciences 22*, 458-459.

138. Hefti, M. H., Françoijs, K.-J., de Vries, S. C., Dixon, R., and Vervoort, J. (2004) The PAS fold, *European Journal of Biochemistry 271*, 1198-1208.

139. Fedorov, R., Schlichting, I., Hartmann, E., Domratcheva, T., Fuhrmann, M., and Hegemann, P. (2003) Crystal Structures and Molecular Mechanism of a Light-Induced Signaling Switch: The Phot-LOV1 Domain from *Chlamydomonas reinhardtii*, *Biophysical Journal 84*, 2474-2482.

140. Crosson, S., and Moffat, K. (2001) Structure of a flavin-binding plant photoreceptor domain: Insights into light-mediated signal transduction *Proceedings of the National Academy of Sciences of the United States of America 98* 2995-3000.

141. Pellequer, J.-L., Wager-Smith, K. A., Kay, S. A., and Getzoff, E. D. (1998) Photoactive yellow protein: A structural prototype for the three-dimensional fold of the PAS domain superfamily, *Proceedings of the National Academy of Sciences of the United States of America 95*, 5884-5890.

142. Crews, S. T., Thomas, J. B., and Goodman, C. S. (1988) The Drosophila single-minded gene encodes a nuclear protein with sequence similarity to the per gene product, *Cell 52*, 143-151.

143. Hill, S., Austin, S., Eydmann, T., Jones, T., and Dixon, R. (1996) Azotobacter vinelandii NIFL is a flavoprotein that modulates transcriptional activation of nitrogen-fixation genes via a redox-sensitive switch *Proceedings of the National Academy of Sciences of the United States of America 93* 2143-2148

144. Hoff, W. D., Dux, P., Hard, K., Devreese, B., Nugteren-Roodzant, I. M., Crielaard, W., Boelens, R., Kaptein, R., Beeumen, J. V., and Hellingwerf, K. J. (1994) Thiol ester-linked p-coumaric acid as a new photoactive prosthetic group in a protein with rhodopsin-like photochemistry, *Biochemistry 33*, 13959-13962.

145. Gong, W., Hao, B., Mansy, S. S., Gonzalez, G., Gilles-Gonzalez, M. A., and Chan, M. K. (1998) Structure of a biological oxygen sensor: A new mechanism for heme-driven signal transduction *Proceedings of the National Academy of Sciences of the United States of America 95* 15177-15182.

146. Losi, A., Quest, B., and Gärtner, W. (2003) Listening to the blue: the time-resolved thermodynamics of the bacterial blue-light receptor YtvA and its isolated LOV domain, *Photochemical & photobiological sciences 2*, 759-766.

147. Salomon, M., Eisenreich, W., Duerr, H., Schleicher, E., Knieb, E., Massey, V., Ruediger, W., Mueller, F., Bacher, A., and Richter, G. (2001) An

optomechanical transducer in the blue light receptor phototropin from Avena sativa *Proceedings of the National Academy of Sciences of the United States of America 98* 12357-12361.

148. Salomon, M., Christie, J. M., Knieb, E., Lempert, U., and Briggs, W. R. (2000) Photochemical and Mutational Analysis of the FMN-Binding Domains of the Plant Blue Light Receptor Phototropin, *Biochemistry 39*, 9401-9410.

149. Kasahara, M., Swartz, T. E., Olney, M. A., Onodera, A., Mochizuki, N., Fukuzawa, H., Asamizu, E., Tabata, S., Kanegae, H., Takano, M., Christie, J. M., Nagatani, A., and Briggs, W. R. (2002) Photochemical Properties of the Flavin Mononucleotide-Binding Domains of the Phototropins from Arabidopsis, Rice, and *Chlamydomonas reinhardtii*, *Plant Physiology 129*, 762-773.

150. Imaizumi, T., Tran, H. G., Swartz, T. E., Briggs, W. R., and Kay, S. A. (2003) FKF1 is essential for photoperiodic-specific light signalling in Arabidopsis, *Nature 426*, 302-306.

151. Swartz, T. E., Tseng, T.-S., Frederickson, M. A., Paris, G., Comerci, D. J., Rajashekara, G., Kim, J.-G., Mudgett, M. B., Splitter, G. A., Ugalde, R. A., Goldbaum, F. A., Briggs, W. R., and Bogomolni, R. A. (2007) Blue-Light-Activated Histidine Kinases: Two-Component Sensors in Bacteria, *Science 317*, 1090-1093.

152. Möglich, A., Yang, X., Ayers, R. A., and Moffat, K. (2010) Structure and Function of Plant Photoreceptors, *Annual Review of Plant Biology 61*, 21-47.

153. Alexandre, M. T. A., Arents, J. C., van Grondelle, R., Hellingwerf, K. J., and Kennis, J. T. M. (2007) A Base-Catalyzed Mechanism for Dark State Recovery in the Avena sativa Phototropin-1 LOV2 Domain, *Biochemistry 46*, 3129-3137.

154. Swartz, T. E., Corchnoy, S. B., Christie, J. M., Lewis, J. W., Szundi, I., Briggs, W. R., and Bogomolni, R. A. (2001) The photocycle of a flavin-binding domain of the blue light photoreceptor phototropin, *J Biol Chem 276*, 36493-36500.

155. Christie, J. M., Corchnoy, S. B., Swartz, T. E., Hokenson, M., Han, I.-S., Briggs, W. R., and Bogomolni, R. A. (2007) Steric Interactions Stabilize the Signaling State of the LOV2 Domain of Phototropin1 *Biochemistry 46*, 9310-9319.

156. Losi, A., and Gärtner, W. (2011) Old Chromophores, New Photoactivation Paradigms, Trendy Applications: Flavins in Blue Light-Sensing Photoreceptors, *Photochemistry and Photobiology 87*, 491-510.

157. Song, S.-H., Freddolino, P. L., Nash, A. I., Carroll, E. C., Schulten, K., Gardner, K. H., and Larsen, D. S. (2011) Modulating LOV Domain Photodynamics with a Residue Alteration outside the Chromophore Binding Site, *Biochemistry 50*, 2411-2423.

158. Veetil, S. K., Mittal, C., Ranjan, P., and Kateriya, S. (2011) A conserved isoleucine in the LOV1 domain of a novel phototropin from the marine alga Ostreococcus tauri modulates the dark state recovery of the domain, *Biochimica et Biophysica Acta (BBA) - General Subjects 1810*, 675-682.

159. Salomon, M., Christie, J. M., Knieb, E., Lempert, U., and Briggs, W. R. (2000) Photochemical and Mutational Analysis of the FMN-Binding Domains of the Plant Blue Light Receptor, Phototropin, *Biochemistry 39*, 9401-9410.

160. Harper, S. M., Neil, L. C., and Gardner, K. H. (2003) Structural Basis of a

Phototropin Light Switch, *Science 301*, 1541-1544.

161. Harper, S. M., Christie, J. M., and Gardner, K. H. (2004) Disruption of the LOVJα Helix Interaction Activates Phototropin Kinase Activity, *Biochemistry 43*, 16184-16192.

162. Yamamoto, A., Iwata, T., Sato, Y., Matsuoka, D., Tokutomi, S., and Kandori, H. (2009) Light Signal Transduction Pathway from Flavin Chromophore to the Jα Helix of Arabidopsis Phototropin1, *Biophysical Journal 96*, 2771-2778.

163. Zayner, J. P., Antoniou, C., and Sosnick, T. R. (2012) The Amino-Terminal Helix Modulates Light-Activated Conformational Changes in AsLOV2, *Journal of Molecular Biology 419*, 61-74.

164. Vaidya, A. T., Chen, C.-H., Dunlap, J. C., Loros, J. J., and Crane, B. R. (2011) Structure of a Light-Activated LOV Protein Dimer That Regulates Transcription, *Sci. Signal. 4*, ra50-.

165. Möglich, A., and Moffat, K. (2007) Structural Basis for Light-dependent Signaling in the Dimeric LOV Domain of the Photosensor YtvA, *Journal of Molecular Biology 373*, 112-126.

166. Möglich, A., Ayers, R. A., and Moffat, K. (2009) Design and Signaling Mechanism of Light-Regulated Histidine Kinases, *Journal of Molecular Biology 385*, 1433-1444.

167. Palleroni, N. J. (2010) Pseudomonas, In *Topley & Wilson's Microbiology and Microbial Infections*, John Wiley & Sons, Ltd.

168. Espinosa-Urgel, M., Salido, A., and Ramos, J.-L. (2000) Genetic Analysis of Functions Involved in Adhesion of Pseudomonas putida to Seeds, *Journal of Bacteriology 182*, 2363-2369.

169. Ward, P. G., Goff, M., Donner, M., Kaminsky, W., and O'Connor, K. E. (2006) A Two Step Chemo-biotechnological Conversion of Polystyrene to a Biodegradable Thermoplastic, *Environmental Science & Technology 40*, 2433-2437.

170. Wackett, L. P., and Gibson, D. T. (1988) Degradation of trichloroethylene by toluene dioxygenase in whole-cell studies with Pseudomonas putida F1, *Applied and Environmental Microbiology 54*, 1703-1708.

171. Aalam, S., Pauss, A., and Lebeault, J.-M. (1993) High efficiency styrene biodegradation in a biphasic organic/water continuous reactor, *Applied Microbiology and Biotechnology 39*, 696-699.

172. Nelson, K. E., Weinel, C., Paulsen, I. T., Dodson, R. J., Hilbert, H., Martins dos Santos, V. A. P., Fouts, D. E., Gill, S. R., Pop, M., Holmes, M., Brinkac, L., Beanan, M., DeBoy, R. T., Daugherty, S., Kolonay, J., Madupu, R., Nelson, W., White, O., Peterson, J., Khouri, H., Hance, I., Lee, P. C., Holtzapple, E., Scanlan, D., Tran, K., Moazzez, A., Utterback, T., Rizzo, M., Lee, K., Kosack, D., Moestl, D., Wedler, H., Lauber, J., Stjepandic, D., Hoheisel, J., Straetz, M., Heim, S., Kiewitz, C., Eisen, J., Timmis, K. N., Düsterhöft, A., Tümmler, B., and Fraser, C. M. (2002) Complete genome sequence and comparative analysis of the metabolically versatile Pseudomonas putida KT2440, *Environmental Microbiology 4*, 799-808.

173. Raghavan, P. U. M., and Vivekanandan, M. (1999) Bioremediation of oil-spilled sites through seeding of naturally adapted Pseudomonas putida, *International Biodeterioration & Biodegradation 44*, 29-32.

174. Nwachukwu, S. U. (2001) Bioremediation of Sterile Agricultural Soils Polluted with Crude Petroleum by Application of the Soil Bacterium, Pseudomonas putida, with Inorganic Nutrient Supplementations, *Current Microbiology 42*, 231-236.

175. Compeau, G., Al-Achi, B. J., Platsouka, E., and Levy, S. B. (1988) Survival of rifampin-resistant mutants of *Pseudomonas fluorescens* and *Pseudomonas putida* in soil systems., *Appl. Environ. Microbiol. 54*, 2432-2438.

176. Heim, S., Ferrer, M., Heuer, H., Regenhardt, D., Nimtz, M., and Timmis, K. N. (2003) Proteome reference map of *Pseudomonas putida* strain KT2440 for genome expression profiling: distinct responses of KT2440 and *Pseudomonas aeruginosa* strain PAO1 to iron deprivation and a new form of superoxide dismutase, *Environmental Microbiology 5*, 1257-1269.

177. Martìnez-Bueno, M. A., Tobes, R., Rey, M., and Ramos, J.-L. (2002) Detection of multiple extracytoplasmic function (ECF) sigma factors in the genome of *Pseudomonas putida* KT2440 and their counterparts in Pseudomonas aeruginosa PA01, *Environmental Microbiology 4*, 842-855.

178. Krauss, U. (2008) Bakterielle Blaulicht-Rezeptoren der LOV-Familie. Dissertation

179. Krauss, U., Losi, A., Gärtner, W., Jaeger, K.-E., and Eggert, T. (2005) Initial characterization of a blue-light sensing, phototropin-related protein from Pseudomonas putida: a paradigm for an extended LOV construct, *Physical Chemistry Chemical Physics 7*, 2804-2811.

180. Jentzsch, K., Wirtz, A., Circolone, F., Drepper, T., Losi, A., Gaì^rtner, W., Jaeger, K.-E., and Krauss, U. (2009) Mutual Exchange of Kinetic Properties by Extended Mutagenesis in Two Short LOV Domain Proteins from Pseudomonas putida, *Biochemistry 48*, 10321-10333.

181. Losi, A., Kottke, T., and Hegemann, P. (2004) Recording of Blue Light-Induced Energy and Volume Changes within the Wild-Type and Mutated Phot-LOV1 Domain from Chlamydomonas reinhardtii, *Biophysical Journal 86*, 1051-1060.

182. Zikihara, K., Iwata, T., Matsuoka, D., Kandori, H., Todo, T., and Tokutomi, S. (2006) Photoreaction Cycle of the Light, Oxygen, and Voltage Domain in FKF1 Determined by Low-Temperature Absorption Spectroscopy *Biochemistry 45*, 10828-10837.

183. Circolone, F., Granzin, J., Jentzsch, K., Drepper, T., Jaeger, K. E., Willbold, D., Krauss, U., and Batra-Safferling, R. (2012) Structural basis for the slow dark recovery of a full-length LOV protein from Pseudomonas putida, *J Mol Biol 417*, 362-374.

184. Nakasone, Y., Zikihara, K., Tokutomi, S., and Terazima, M. (2010) Kinetics of Conformational Changes of the FKF1-LOV Domain upon Photoexcitation, *Biophysical Journal 99*, 3831-3839.

185. Halavaty, A. S., and Moffat, K. (2007) N- and C-Terminal Flanking Regions Modulate Light-Induced Signal Transduction in the LOV2 Domain of the Blue Light Sensor Phototropin 1 from Avena sativa, *Biochemistry 46*, 14001-14009.

186. van der Horst, M. A., Key, J., and Hellingwerf, K. J. (2007) Photosensing in chemotrophic, non-phototrophic bacteria: let there be light sensing too, *Trends in Microbiology 15*, 554-562.

187. Chen, C.-H., DeMay, B. S., Gladfelter, A. S., Dunlap, J. C., and Loros, J. J. (2010) Physical interaction between VIVID and white collar complex regulates photoadaptation in Neurospora *Proceedings of the National Academy of Sciences 107* 16715-16720.

188. Zoltowski, B. D., Schwerdtfeger, C., Widom, J., Loros, J. J., Bilwes, A. M., Dunlap, J. C., and Crane, B. R. (2007) Conformational Switching in the Fungal Light Sensor Vivid, *Science 316*, 1054-1057.

189. Zoltowski, B. D., and Crane, B. R. (2008) Light Activation of the LOV Protein Vivid Generates a Rapidly Exchanging Dimer, *Biochemistry 47*, 7012-7019.

190. Möglich, A., Ayers, R. A., and Moffat, K. (2009) Structure and Signaling Mechanism of Per-ARNT-Sim Domains, *Structure 17*, 1282-1294.

191. Buttani, V., Losi, A., Eggert, T., Krauss, U., Jaeger, K.-E., Cao, Z., and Gärtner, W. (2007) Conformational analysis of the blue-light sensing protein YtvA reveals a competitive interface for LOV-LOV dimerization and interdomain interactions., *Photochemical & Photobiological Sciences 6*, 41-49.

192. Wu, X., Monchy, S. b., Taghavi, S., Zhu, W., Ramos, J., and Van Der Lelie, D. (2010) Comparative genomics and functional analysis of niche-specific adaptation in Pseudomonas putida, *FEMS Microbiology Reviews*, Volume 35, Issue 2, pages 299–323.

193. Visca, P., Imperi, F., and Lamont, I. L. (2007) Pyoverdine siderophores: from biogenesis to biosignificance, *Trends in Microbiology 15*, 22-30.

194. Boukhalfa, H., Reilly, S. D., Michalczyk, R., Iyer, S., and Neu, M. P. (2006) Iron(III) Coordination Properties of a Pyoverdin Siderophore Produced by Pseudomonas putida ATCC 33015, *Inorganic Chemistry 45*, 5607-5616.

195. Meyer, J.-M., Stintzi, A., De Vos, D., Cornelis, P., Tappe, R., Taraz, K., and Budzikiewicz, H. (1997) Use of Siderophores to Type Pseudomonads: The Three Pseudomonas Aeruginosa Pyoverdine Systems, *Microbiology 143*, 35-43.

196. Cody, Y. S., and Gross, D. C. (1987) Characterization of Pyoverdinpss, the Fluorescent Siderophore Produced by Pseudomonas syringae pv. syringae, *Applied and Environmental Microbiology 53*, 928-934.

197. Paulsen, I. T., Press, C. M., Ravel, J., Kobayashi, D. Y., Myers, G. S. A., Mavrodi, D. V., DeBoy, R. T., Seshadri, R., Ren, Q., Madupu, R., Dodson, R. J., Durkin, A. S., Brinkac, L. M., Daugherty, S. C., Sullivan, S. A., Rosovitz, M. J., Gwinn, M. L., Zhou, L., Schneider, D. J., Cartinhour, S. W., Nelson, W. C., Weidman, J., Watkins, K., Tran, K., Khouri, H., Pierson, E. A., Pierson, L. S., Thomashow, L. S., and Loper, J. E. (2005) Complete genome sequence of the plant commensal Pseudomonas fluorescens Pf-5, *Nat Biotech 23*, 873-878.

198. Patriquin, G. M., Banin, E., Gilmour, C., Tuchman, R., Greenberg, E. P., and Poole, K. (2008) Influence of Quorum Sensing and Iron on Twitching Motility and Biofilm Formation in Pseudomonas aeruginosa, *Journal of Bacteriology 190*, 662-671.

199. Weinberg, E. D. (2004) Suppression of bacterial biofilm formation by iron limitation, *Medical Hypotheses 63*, 863-865.

200. Matilla, M. A., Ramos, J. L., Duque, E., De Dios Alchè, J., Espinosa-Urgel, M., and Ramos-Gonzàlez, M. a. I. (2007) Temperature and pyoverdine-mediated iron acquisition control surface motility of Pseudomonas putida, *Environmental Microbiology 9*, 1842-1850.

201. Ryter, S. W., Kim, H. P., Hoetzel, A., Park, J. W., Nakahira, K., Wang, X., and Choi, A. M. (2007) Mechanisms of cell death in oxidative stress, *Antioxidants & Redox Signaling 9*, 49-89.

202. Metz, S., Jaeger, A., and Klug, G. (2012) Role of a short light, oxygen, voltage (LOV) domain protein in blue light- and singlet oxygen-dependent gene regulation in Rhodobacter sphaeroides, *Microbiology 158*, 368-379.

203. Metz, S., Haberzettl, K., Frühwirth, S., Teich, K., Hasewinkel, C., and Klug, G. (2012) Interaction of two photoreceptors in the regulation of bacterial photosynthesis genes, *Nucleic Acids Research 40*, 5901-5909.

204. Storz, G., and Imlayt, J. A. (1999) Oxidative stress, *Current Opinion in Microbiology 2*, 188-194.

205. Mongkolsuk, S., and Helmann, J. D. (2002) Regulation of inducible peroxide stress responses, *Molecular Microbiology 45*, 9-15.

206. Hassett, D. J., Sokol, P. A., Howell, M. L., Ma, J. F., Schweizer, H. T., Ochsner, U., and Vasil, M. L. (1996) Ferric uptake regulator (Fur) mutants of Pseudomonas aeruginosa demonstrate defective siderophore-mediated iron uptake, altered aerobic growth, and decreased superoxide dismutase and catalase activities, *Journal of Bacteriology 178*, 3996-4003.

207. Walhout, A. J. M., and Vidal, M. (2001) High-Throughput Yeast Two-Hybrid Assays for Large-Scale Protein Interaction Mapping, *Methods 24*, 297-306.

208. Raffelberg, S., Mansurova, M., Gärtner, W., and Losi, A. (2011) Modulation of the Photocycle of a LOV Domain Photoreceptor by the Hydrogen-Bonding Network, *Journal of the American Chemical Society 133*, 5346-5356.

209. Scholz, K. E., Okrob, D., Kopka, B., Grünberger, A., Pohl, M., Jaeger, K.-E., and Krauss, U. (2012) Synthesis of Chiral Cyanohydrins by Recombinant *Escherichia coli* Cells in a Micro-Aqueous Reaction System, *Applied and Environmental Microbiology 78*, 5025-5027.

210. Hegemann, P., and Moglich, A. (2011) Channelrhodopsin engineering and exploration of new optogenetic tools, *Nat Meth 8*, 39-42.

211. Pathak, G. P., Vrana, J. D., and Tucker, C. L. (2012) Optogenetic Control of Cell Function Using Engineered Photoreceptors, *Biology of the Cell*, n/a-n/a.

212. Moglich, A., and Moffat, K. (2010) Engineered photoreceptors as novel optogenetic tools, *Photochemical & Photobiological Sciences 9*, 1286-1300.

213. Christie, J. M., Gawthorne, J., Young, G., Fraser, N. J., and Roe, A. J. (2012) LOV to BLUF: Flavoprotein Contributions to the Optogenetic Toolkit, *Molecular Plant 5*, 7-18.

Appendix

Tab.A1: Sequences of all primers used in chapter 2.1 given in 5'-3' direction.

SB1_A13H	forward CGATGGTCGATCATTCCAATGACGGCATCGTGGTTGCC reverse GGCAACCACGATGCCGTCATTGGAATGATCGACCATCG
SB1_K23Q	forward GCATCGTGGTTGCCGAACAGGAAGGCGA reverse TCGCCTTCCTGTTCGGCAACCACGATGC
SB1_E47D	forward GCCGTGACGATATTCTCTACCAGGATTGCCG reverse CGGCAATCCTGGTAGAGAATATCGTCACGGC
SB1_R61H	forward GCAGGGTGACGACCATGACCAGCTTGG reverse CCAAGCTGGTCATGGTCGTCACCCTGC
SB1_R66I	forward CGTGACCAGCTTGGCATTGCACGCATCCGCAAGG reverse CCTTGCGGATGCGTGCAATGCCAAGCTGGTCACG
SB1_K71E	forward GCACGCATCCGCGAAGCCATGGCCGAAGGCC reverse GGCCTTCGGCCATGGCTTCGCGGATGCGTGC
SB2_H13A	forward GATGGTCGAAGCGTCCAACGATGGCATCGTTGTCGC reverse GCGACAACGATGCCATCGTTGGACGCTTCGACCATC
SB2_Q23K	forward GCATCGTTGTCGCCGAGAAAGAAGGCAATGAGAGCATCC reverse GGATGCTCTCATTGCCTTCTTTCTCGGCGACAACGATGC
SB2_D47E	forward GCGCCGACGAAATTCTCTATCAGGACTGC reverse

	GGCAGTCCTGATAGAGAATTTCGTCGGCGC
SB2_H61R	forward GTTTTCTTCAGGGCGAGGATCGTGACCAGCCGG reverse CCGGCTGGTCACGATCCTCGCCCTGAAGAAAAC
SB2_I66R	forward GGATCACGACCAGCCGGGCCGTGCAATTATCCG reverse CGGATAATTGCACGGCCCGGCTGGTCGTGATCC
SB2_E71K	forward GCATCGCAATTATCCGCAAAGCGATCCGCGAAGGCC reverse GGCCTTCGCGGATCGCTTTGCGGATAATTGCGATGC
Zra I	forward TCCAGCGCGACGTCACAGCGCAAGTATTCG reverse CGAATACTTGCGCTGTGACGTCGCGCTGGA

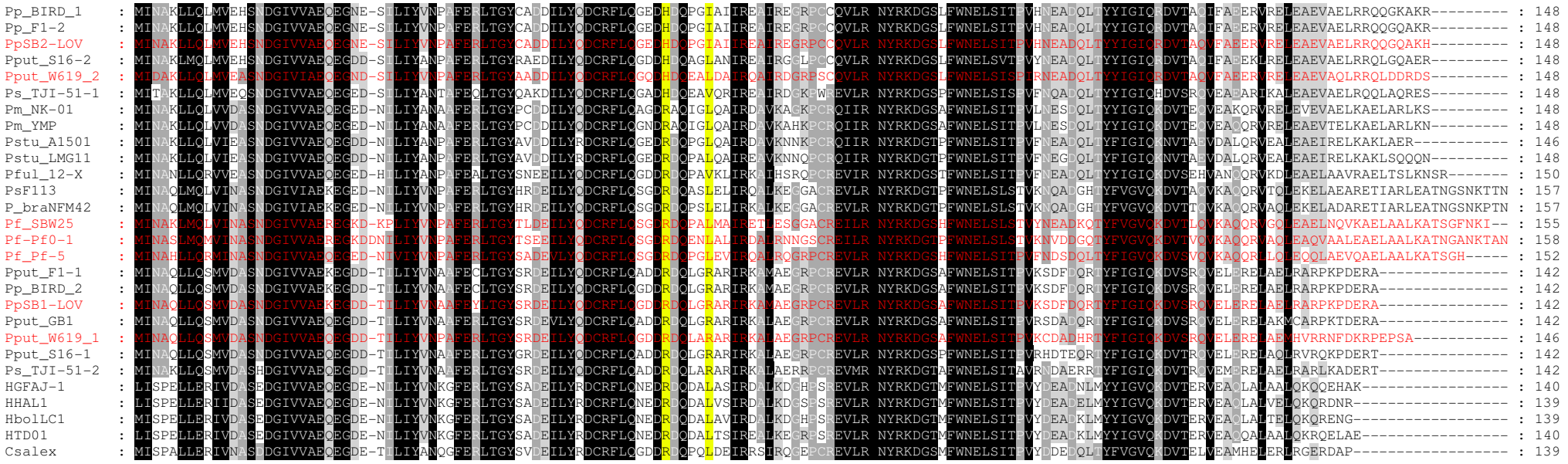

Fig. A1: Multiple sequence alignment of several members of the the *Pseudomonadaceae* „short“ LOV protein family. Highlighted in red are the seven *Pseudomonas* proteins that were characterized in this study. Additionally, the two arginine residues (R61 and R66) which were identified in PpSB1-LOV as the key elements that facilitate slow recovery of the protein are highlighted in yellow.

SUPPLEMENTARY TABLE 2a: „Short“ LOV proteins with Y(Q/R)DCRFLQG motif identified in the prokaryotic kingdom

Tree-ID	Organims	UniProt/Genbank	Subclass	Order
PpSB1-LOV	*Pseudomonas putida* KT2440	Q88E39	Gamma	*Pseudomonadales*
PpSB2-LOV	*Pseudomonas putida* KT2440	Q88JB0	Gamma	*Pseudomonadales*
Pput_F1-1	*Pseudomonas putida* F1	A5W8Z9	Gamma	*Pseudomonadales*
Pput_F1-2	*Pseudomonas putida* F1	A5W4T2	Gamma	*Pseudomonadales*
Pput_S16-1	*Pseudomonas putida* S16	F8G5Y7	Gamma	*Pseudomonadales*
Pput_S16-2	*Pseudomonas putida* S16	F8G2U7	Gamma	*Pseudomonadales*
Pput_W619_1	*Pseudomonas putida* W619	B1J385	Gamma	*Pseudomonadales*
PputW619_2	*Pseudomonas putida* W619	B1JAC4	Gamma	*Pseudomonadales*
Ps_TJI-51-1	*Pseudomonas* sp. TJI-51	ZP_08139218.1	Gamma	*Pseudomonadales*
Ps_TJI-51-2	*Pseudomonas* sp. TJI-51	ZP_08142158.1	Gamma	*Pseudomonadales*
Pp_BIRD_1	*Pseudomonas putida* BIRD-1	E4RI35	Gamma	*Pseudomonadales*
Pp_BIRD_2	*Pseudomonas putida* BIRD-1	E4R4W4	Gamma	*Pseudomonadales*
Pput_GB1	*Pseudomonas putida* GB1	B0KGV4	Gamma	*Pseudomonadales*
Pflu_Pf-5	*Pseudomonas fluorescens* Pf-5	Q4KI48	Gamma	*Pseudomonadales*
P_ful_12-X	*Pseudomonas fulva* 12-X	F6AEJ4	Gamma	*Pseudomonadales*
Pmend_YMP	*Pseudomonas mendocina* ymp	A4XXH1	Gamma	*Pseudomonadales*
Pmend_NK-01	*Pseudomonas mendocina* NK-01	F4DSG2	Gamma	*Pseudomonadales*
P_braNFM421	*Pseudomonas brassicacearum subsp. brassicacearum* NFM421	F2KL83	Gamma	*Pseudomonadales*
Pstu_A1501	*Pseudomonas stutzeri* A1501	A4VKZ3	Gamma	*Pseudomonadales*
Pstu_LMG11199	*Pseudomonas stutzeri* ATCC 17588 = LMG 11199	F8H9C5	Gamma	*Pseudomonadales*
Pflu_WH6	*Pseudomonas fluorescens* WH6	ZP_07777456.1	Gamma	*Pseudomonadales*
Pflu_SBW25	*Pseudomonas fluorescens* SBW25	C3K1W0	Gamma	*Pseudomonadales*
P_flu-Pf0-1	*Pseudomonas fluorescens* Pf0-1	Q3KHW7	Gamma	*Pseudomonadales*
PsF113	*Pseudomonas fluorescens* F113		Gamma	*Pseudomonadales*

Csalex	*Chromohalobacter salexigens* DSM 3043	Q1QU87	Gamma	*Oceanospirillales*
HTD01	*Halomonas* sp. TD01	ZP_08635475.1	Gamma	*Oceanospirillales*
HbolLC1	*Halomonas boliviensis* LC1	ZP_09188734.1	Gamma	*Oceanospirillales*
HGFAJ-1	*Halomonas* sp. GFAJ-1	ZP_09288308.1	Gamma	*Oceanospirillales*
HHAL1	*Halomonas* sp. HAL1	ZP_08961366.1	Gamma	*Oceanospirillales*
TcycDSM	*Thioalkalimicrobium cyclicum* (strain DSM 14477 / JCM 11371 / ALM1	F6D9J9	Gamma	*Thiotrichales*
Hnea_ATCC	*Halothiobacillus neapolitanus*	D0L135	Gamma	*Chromatiales*
T_K90mix	*Thioalkalivibrio* sp. (strain K90mix)	D3S9U5	Gamma	*Chromatiales*
T_EbGR7	*Thioalkalivibrio* sp. (strain HL-EbGR7)	B8GRG0	Gamma	*Chromatiales*

SUPPLEMENTARY TABLE 2b: „Short“ LOV proteins with GXNCRFLQG motif identified in the prokaryotic kingdom

Tree-ID	Organims	UniProt/Genbank	Subclass	Order
F9TYW6	*Marichromatium purpuratum* 984	F9TYW6	Gamma	*Chromatiales*
Q3J6W8	*Nitrosococcus oceani* (strain ATCC 19707 / NCIMB 11848)	Q3J6W8	Gamma	*Chromatiales*
B6C5R4	*Nitrosococcus oceani* AFC27	B6C5R4	Gamma	*Chromatiales*
D5BVD1	*Nitrosococcus halophilus*	D5BVD1	Gamma	*Chromatiales*
F9U8V4	*Thiocapsa marina* 5811	F9U8V4	Gamma	*Chromatiales*
G0A1Q1	*Methylomonas methanica* (strain MC09)	G0A1Q1	Gamma	*Methylococcales*
F8GDY9	*Nitrosomonas* sp. (strain Is79A3)	F8GDY9	Beta	*Nitrosomonadales*
Q2Y837	*Nitrosospira multiformis* (strain ATCC 25196 / NCIMB 11849)	Q2Y837	Beta	*Nitrosomonadales*
F9ZGQ1	*Nitrosomonas* sp. AL212	F9ZGQ1	Beta	*Nitrosomonadales*
C7RJT7	*Accumulibacter phosphatis* (strain UW-1)	C7RJT7	Beta	*unclassified*
Q0BT22	*Granulibacter bethesdensis* (strain ATCC BAA-1260 / CGDNIH1)	Q0BT22	Alpha	*Rhodospirillales*
F6ID38	*Novosphingobium* sp. PP1Y	F6ID38	Alpha	*Sphingomonadales*
C8X922	*Nakamurella multipartita* (strain ATCC 700099)	C8X922	Actino	*Actinomycetales*
D0CZ83	*Citreicella* sp. SE45	D0CZ83	Alpha	*Rhodobacterales*
A8LP63	*Dinoroseobacter shibae* (strain DFL 12)	A8LP63	Alpha	*Rhodobacterales*
B9QXI1	*Labrenzia alexandrii* DFL-11	B9QXI1	Alpha	*Rhodobacterales*
Q0FR10	*Pelagibaca bermudensis* HTCC2601	Q0FR10	Alpha	*Rhodobacterales*
Q3J4A0	*Rhodobacter sphaeroides* (strain ATCC 17023 / 2.4.1 / NCIB 8253 / DSM 158)	Q3J4A0	Alpha	*Rhodobacterales*
B9KPB3	*Rhodobacter sphaeroides* (strain KD131 / KCTC 12085)	B9KPB3	Alpha	*Rhodobacterales*
F5M2M2	*Rhodobacter sphaeroides* WS8N	F5M2M2	Alpha	*Rhodobacterales*
A3PI49	*Rhodobacter sphaeroides* (strain ATCC 17029 / ATH 2.4.9)	A3PI49	Alpha	*Rhodobacterales*
A4EHF4	*Roseobacter* sp. CCS2	A4EHF4	Alpha	*Rhodobacterales*
A4EIJ8	*Roseobacter* sp. CCS2	A4EIJ8	Alpha	*Rhodobacterales*
A3K7J8	*Sagittula stellata* E-37	A3K7J8	Alpha	*Rhodobacterales*
B1ZH86	*Methylobacterium populi* (strain ATCC BAA-705 / NCIMB 13946 / BJ001)	B1ZH86	Alpha	*Rhizobiales*
B1M4A2	*Methylobacterium radiotolerans* (strain ATCC 27329 / DSM 1819 / JCM 2831)	B1M4A2	Alpha	*Rhizobiales*
B1M516	*Methylobacterium radiotolerans* (strain ATCC 27329 / DSM 1819 / JCM 2831)	B1M516	Alpha	*Rhizobiales*
E8L553	*Methylocystis* sp. ATCC 49242	E8L553	Alpha	*Rhizobiales*
E8L19	*Methylocystis* sp. ATCC 49242	E8L19	Alpha	*Rhizobiales*

Acknowledgements

Firstly, I would like to thank Prof. Dr. Karl-Erich Jaeger (Institut für Molekulare Enzymtechnologie in Jülich) for providing me with this interesting and challenging topic and moreover for funding and encouragement to outgrow myself with this work. Also I am thankful for continuous help and guidance with the publication of the results of this thesis. Also I want to thank Prof. Dr. Martina Pohl (Institute of Bio- and Geosciences, IBG-1) for agreeing to take over the secondary examination of this thesis and for always helping out with criticism, ideas and encouragement.

I am very much indebted to my supervisor on-site, Dr. Ulrich Krauss. I hardly know where to start on summing up what I am thankful for. Very special thanks for the faith he put in my skills from the very start and even more when I myself did not know what I can do, thanks for the opportunity to work in a newly founded workgroup from the very beginning and of course for the many many helpful and encouraging discussions and debates. I am very grateful that he always left room for ideas, to pursue independent work but at the same time maintaining a critical view so I never got lost in trying over and over again but was able to move on and broaden my own view on the topic. Furthermore I am thankful for his guidance and patience and belief when I had a harder time keeping it up. He has certainly been a role model for me, which I can only hope to keep up with one day!

One ant can move a multiple of her own bodyweight, many ants can move a mountain. Herewith I would like to thank the following collaborators, supporters and hidden genies. Without them and their continuous work, dedication and support nothing of this would have been possible.

Many thanks go to Prof. Dr. Wolfgang Gärtner (Max Planck Institute for Bioinorganic Chemistry, Mülheim a.d.Ruhr) for initially introducing me to the field of bacterial photoreceptors and sending me off to Jülich. Thanks as well for encouragement and support throughout the last years. From the group of Prof. Dr. W. Gärtner I would like to thank Dr. Björn Zorn for help with laser-flash photolysis and data evaluation.

I also like to thank Dr. Roger-Jan Kutta from the University of Regensburg for inviting me to work with him on transient absorption spectroscopy and showing me how cool and interesting laser-stuff can be.

My next big “thank you” goes to the technicians of the IMET, Vera Svensson, Astrid Wirtz, Maja Piqueray, Esther Knieps-Grünhagen and Katharina Range for all kinds of support; technical, time-wise, psychological, physical…for help with analytics, media, buffers, for switching on and off shakers, chambers, blue-lights and what not.

Thank you very much also to Naomi Crawford from the University of Waikato in New Zealand for putting finishing language-touches to this work.

One of the most important factors to being able to finally finish this thesis were all other members of the AG Krauss and the whole IMET, who were workmates, comrades, collaborators, colleagues and most of all friends, sharing labs, offices, coffee, sweets, laughter, disappointment, frustration and everything else between heaven and hell. I want to name a few outstanding ones here: Marco Kaschner, Benita Kopka, Martin Diener, Raj Rani, Franco Circolone, Anita Loeschke and last but not least, Kathrin Emmi Scholz (neè Klein), Kathrin, most of all you have been a great friend over the last years, listening, laughing, sharing and caring. Thank you so much!

The best comes at the end: Last but never least I would like to thank my family, the one I share blood with and the one that I am bound to through friendship. Very special thanks to Micheal and Julia Carthy for years of friendship, support and soulfood. Thanks also to Discrims Dilletanten for encouraging words and support especially throughout the last year. I want to thank my family, grandparents, aunts, uncles, cousins for their love, support, faith and patience, for keeping the world away from me when I had to dig myself into this thesis and for digging me out when I got lost. Thanks to Mom and Dad and Timo; you always loved me, you always were my home, my solid rock in the storm, you never lost faith in me you always knew I could make it and look at me now : I DID IT!

Eigenständigkeitserklärung

Hiermit erkläre ich, dass ich diese Arbeit selbständig und ohne fremde Hilfe verfasst, andere als die von mir angegebenen Quellen und Hilfsmittel nicht benutzt und die den benutzten Werken wörtlich oder inhaltlich entnommenen Stellen als solche kenntlich gemacht habe.

Oberhausen, den xx.12.2012 Katrin Jentzsch

aus dem Institut für Molekulare Enzymtechnologie (IMET)
der Heinrich-Heine Universität Düsseldorf

Gedruckt mit der Genehmigung der
Mathematisch-Naturwissenschaftlichen Fakultät der
Heinrich-Heine-Universität Düsseldorf

Referent: Prof. Dr. Karl-Erich Jaeger
Korreferent: Prof. Dr. Martina Pohl

Tag der mündlichen Prüfung: 28.01.2013